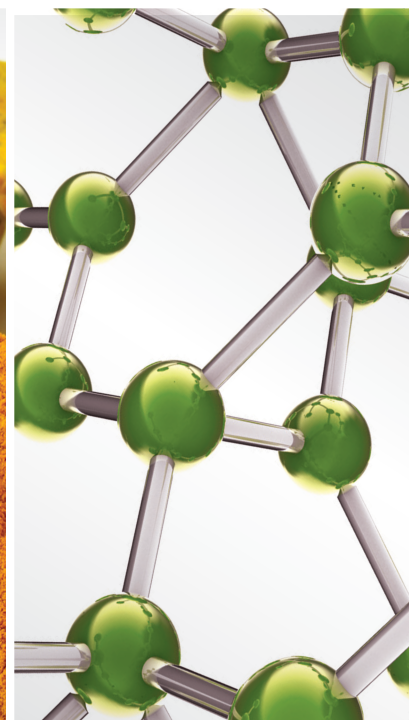
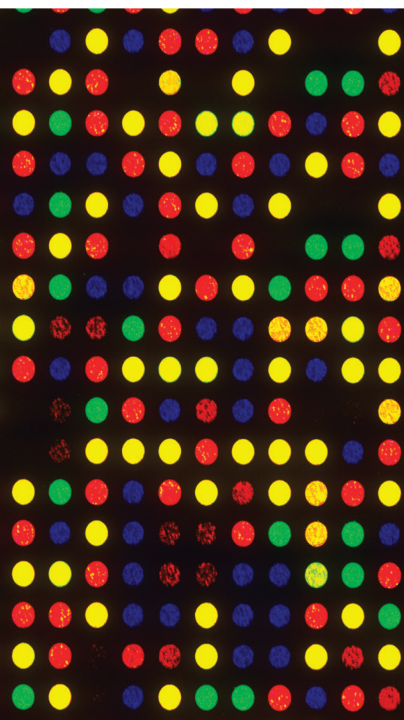


Natural Products Potentiate the Anticancer Effect of Chemotherapeutics

Lead Guest Editor: Mohammed El-Magd

Guest Editors: Badrul Hisham Yahaya and Yousef Hawsawi





Natural Products Potentiate the Anticancer Effect of Chemotherapeutics

Natural Products Potentiate the Anticancer Effect of Chemotherapeutics

Lead Guest Editor: Mohammed El-Magd

Guest Editors: Badrul Hisham Yahaya and Yousef
Hawsawi



Copyright © 2023 Hindawi Limited. All rights reserved.

This is a special issue published in "Evidence-Based Complementary and Alternative Medicine." All articles are open access articles distributed under the Creative Commons Attribution License, which permits unrestricted use, distribution, and reproduction in any medium, provided the original work is properly cited.

Chief Editor

Jian-Li Gao , China






Associate Editors

Hyunsu Bae , Republic of Korea
Raffaele Capasso , Italy
Jae Youl Cho , Republic of Korea
Caigan Du , Canada
Yuewen Gong , Canada
Hai-dong Guo , China
Kuzhuvelil B. Harikumar , India
Ching-Liang Hsieh , Taiwan
Cheorl-Ho Kim , Republic of Korea
Victor Kuete , Cameroon
Hajime Nakae , Japan
Yoshiji Ohta , Japan
Olumayokun A. Olajide , United Kingdom
Chang G. Son , Republic of Korea
Shan-Yu Su , Taiwan
Michał Tomczyk , Poland
Jenny M. Wilkinson , Australia

Academic Editors

Eman A. Mahmoud , Egypt
Ammar AL-Farga , Saudi Arabia
Smail Aazza , Morocco
Nahla S. Abdel-Azim, Egypt
Ana Lúcia Abreu-Silva , Brazil
Gustavo J. Acevedo-Hernández , Mexico
Mohd Adnan , Saudi Arabia
Jose C Adsuar , Spain
Sayeed Ahmad, India
Touqeer Ahmed , Pakistan
Basiru Ajiboye , Nigeria
Bushra Akhtar , Pakistan
Fahmida Alam , Malaysia
Mohammad Jahoor Alam, Saudi Arabia
Clara Albani, Argentina
Ulysses Paulino Albuquerque , Brazil
Mohammed S. Ali-Shtayeh , Palestinian Authority
Ekram Alias, Malaysia
Terje Alraek , Norway
Adolfo Andrade-Cetto , Mexico
Letizia Angiolella , Italy
Makoto Arai , Japan

Daniel Dias Rufino Arcanjo , Brazil
Duygu AĞAGÜNDÜZ , Turkey
Neda Baghban , Iran
Samra Bashir , Pakistan
Rusliza Basir , Malaysia
Jairo Kenupp Bastos , Brazil
Arpita Basu , USA
Mateus R. Beguelini , Brazil
Juana Benedí, Spain
Samira Boulbaroud, Morocco
Mohammed Bourhia , Morocco
Abdelhakim Bouyahya, Morocco
Nunzio Antonio Cacciola , Italy
Francesco Cardini , Italy
María C. Carpinella , Argentina
Harish Chandra , India
Guang Chen, China
Jianping Chen , China
Kevin Chen, USA
Mei-Chih Chen, Taiwan
Xiaojia Chen , Macau
Evan P. Cherniack , USA
Giuseppina Chianese , Italy
Kok-Yong Chin , Malaysia
Lin China, China
Salvatore Chirumbolo , Italy
Hwi-Young Cho , Republic of Korea
Jeong June Choi , Republic of Korea
Jun-Yong Choi, Republic of Korea
Kathrine Bisgaard Christensen , Denmark
Shuang-En Chuang, Taiwan
Ying-Chien Chung , Taiwan
Francisco José Cidral-Filho, Brazil
Daniel Collado-Mateo , Spain
Lisa A. Conboy , USA
Kieran Cooley , Canada
Edwin L. Cooper , USA
José Otávio do Amaral Corrêa , Brazil
Maria T. Cruz , Portugal
Huantian Cui , China
Giuseppe D'Antona , Italy
Ademar A. Da Silva Filho , Brazil
Chongshan Dai, China
Laura De Martino , Italy
Josué De Moraes , Brazil

Arthur De Sá Ferreira , Brazil
Nunziatina De Tommasi , Italy
Marinella De leo , Italy
Gourav Dey , India
Dinesh Dhamecha, USA
Claudia Di Giacomo , Italy
Antonella Di Sotto , Italy
Mario Dioguardi, Italy
Jeng-Ren Duann , USA
Thomas Effërth , Germany
Abir El-Alfy, USA
Mohamed Ahmed El-Esawi , Egypt
Mohd Ramli Elvy Suhana, Malaysia
Talha Bin Emran, Japan
Roger Engel , Australia
Karim Ennouri , Tunisia
Giuseppe Esposito , Italy
Tahereh Eteraf-Oskouei, Iran
Robson Xavier Faria , Brazil
Mohammad Fattahi , Iran
Keturah R. Faurot , USA
Piergiorgio Fedeli , Italy
Laura Ferraro , Italy
Antonella Fioravanti , Italy
Carmen Formisano , Italy
Hua-Lin Fu , China
Liz G Müller , Brazil
Gabino Garrido , Chile
Safoora Gharibzadeh, Iran
Muhammad N. Ghayur , USA
Angelica Gomes , Brazil
Elena González-Burgos, Spain
Susana Gorzalczany , Argentina
Jiangyong Gu , China
Maruti Ram Gudavalli , USA
Jian-You Guo , China
Shanshan Guo, China
Narcís Gusi , Spain
Svein Haavik, Norway
Fernando Hallwass, Brazil
Gajin Han , Republic of Korea
Ihsan Ul Haq, Pakistan
Hicham Harhar , Morocco
Mohammad Hashem Hashempur , Iran
Muhammad Ali Hashmi , Pakistan

Waseem Hassan , Pakistan
Sandrina A. Heleno , Portugal
Pablo Herrero , Spain
Soon S. Hong , Republic of Korea
Md. Akil Hossain , Republic of Korea
Muhammad Jahangir Hossen , Bangladesh
Shih-Min Hsia , Taiwan
Changmin Hu , China
Tao Hu , China
Weicheng Hu , China
Wen-Long Hu, Taiwan
Xiao-Yang (Mio) Hu, United Kingdom
Sheng-Teng Huang , Taiwan
Ciara Hughes , Ireland
Attila Hunyadi , Hungary
Liaqat Hussain , Pakistan
Maria-Carmen Iglesias-Osma , Spain
Amjad Iqbal , Pakistan
Chie Ishikawa , Japan
Angelo A. Izzo, Italy
Satveer Jagwani , USA
Rana Jamous , Palestinian Authority
Muhammad Saeed Jan , Pakistan
G. K. Jayaprakasha, USA
Kyu Shik Jeong, Republic of Korea
Leopold Jirovetz , Austria
Jeeyoun Jung , Republic of Korea
Nurkhalida Kamal , Saint Vincent and the
Grenadines
Atsushi Kameyama , Japan
Kyungsu Kang, Republic of Korea
Wenyi Kang , China
Shao-Hsuan Kao , Taiwan
Nasiara Karim , Pakistan
Morimasa Kato , Japan
Kumar Katragunta , USA
Deborah A. Kennedy , Canada
Washim Khan, USA
Bonglee Kim , Republic of Korea
Dong Hyun Kim , Republic of Korea
Junghyun Kim , Republic of Korea
Kyungho Kim, Republic of Korea
Yun Jin Kim , Malaysia
Yoshiyuki Kimura , Japan

Nebojša Kladar , Serbia
Mi Mi Ko , Republic of Korea
Toshiaki Kogure , Japan
Malcolm Koo , Taiwan
Yu-Hsiang Kuan , Taiwan
Robert Kubina , Poland
Chan-Yen Kuo , Taiwan
Kuang C. Lai , Taiwan
King Hei Stanley Lam, Hong Kong
Faniel Lampiao, Malawi
Ilaria Lampronti , Italy
Mario Ledda , Italy
Harry Lee , China
Jeong-Sang Lee , Republic of Korea
Ju Ah Lee , Republic of Korea
Kyu Pil Lee , Republic of Korea
Namhun Lee , Republic of Korea
Sang Yeoup Lee , Republic of Korea
Ankita Leekha , USA
Christian Lehmann , Canada
George B. Lenon , Australia
Marco Leonti, Italy
Hua Li , China
Min Li , China
Xing Li , China
Xuqi Li , China
Yi-Rong Li , Taiwan
Vuanghao Lim , Malaysia
Bi-Fong Lin, Taiwan
Ho Lin , Taiwan
Shuibin Lin, China
Kuo-Tong Liou , Taiwan
I-Min Liu, Taiwan
Suhuan Liu , China
Xiaosong Liu , Australia
Yujun Liu , China
Emilio Lizarraga , Argentina
Monica Loizzo , Italy
Nguyen Phuoc Long, Republic of Korea
Zaira López, Mexico
Chunhua Lu , China
Ângelo Luís , Portugal
Anderson Luiz-Ferreira , Brazil
Ivan Luzardo Luzardo-Ocampo, Mexico

Michel Mansur Machado , Brazil
Filippo Maggi , Italy
Juraj Majtan , Slovakia
Toshiaki Makino , Japan
Nicola Malafrente, Italy
Giuseppe Malfa , Italy
Francesca Mancianti , Italy
Carmen Mannucci , Italy
Juan M. Manzanque , Spain
Fatima Martel , Portugal
Carlos H. G. Martins , Brazil
Maulidiani Maulidiani, Malaysia
Andrea Maxia , Italy
Avijit Mazumder , India
Isac Medeiros , Brazil
Ahmed Mediani , Malaysia
Lewis Mehl-Madrona, USA
Ayikoé Guy Mensah-Nyagan , France
Oliver Micke , Germany
Maria G. Miguel , Portugal
Luigi Milella , Italy
Roberto Miniero , Italy
Letteria Minutoli, Italy
Prashant Modi , India
Daniel Kam-Wah Mok, Hong Kong
Changjong Moon , Republic of Korea
Albert Moraska, USA
Mark Moss , United Kingdom
Yoshiharu Motoo , Japan
Yoshiki Mukudai , Japan
Sakthivel Muniyan , USA
Saima Muzammil , Pakistan
Benoit Banga N'guessan , Ghana
Massimo Nabissi , Italy
Siddavaram Nagini, India
Takao Namiki , Japan
Srinivas Nammi , Australia
Krishnadas Nandakumar , India
Vitaly Napadow , USA
Edoardo Napoli , Italy
Jorddy Neves Cruz , Brazil
Marcello Nicoletti , Italy
Eliud Nyaga Mwaniki Njagi , Kenya
Cristina Nogueira , Brazil

Sakineh Kazemi Noureini , Iran
Rômulo Dias Novaes, Brazil
Martin Offenbaecher , Germany
Oluwafemi Adeleke Ojo , Nigeria
Olufunmiso Olusola Olajuyigbe , Nigeria
Luís Flávio Oliveira, Brazil
Mozaniel Oliveira , Brazil
Atolani Olubunmi , Nigeria
Abimbola Peter Oluyori , Nigeria
Timothy Omara, Austria
Chiagoziem Anariochi Otuechere , Nigeria
Sokcheon Pak , Australia
Antônio Palumbo Jr, Brazil
Zongfu Pan , China
Siyaram Pandey , Canada
Niranjan Parajuli , Nepal
Gunhyuk Park , Republic of Korea
Wansu Park , Republic of Korea
Rodolfo Parreira , Brazil
Mohammad Mahdi Parvizi , Iran
Luiz Felipe Passero , Brazil
Mitesh Patel, India
Claudia Helena Pellizzon , Brazil
Cheng Peng, Australia
Weijun Peng , China
Sonia Piacente, Italy
Andrea Pieroni , Italy
Haifa Qiao , USA
Cláudia Quintino Rocha , Brazil
DANIELA RUSSO , Italy
Muralidharan Arumugam Ramachandran,
Singapore
Manzoor Rather , India
Miguel Rebollo-Hernanz , Spain
Gauhar Rehman, Pakistan
Daniela Rigano , Italy
José L. Rios, Spain
Francisca Rius Diaz, Spain
Eliana Rodrigues , Brazil
Maan Bahadur Rokaya , Czech Republic
Mariangela Rondanelli , Italy
Antonietta Rossi , Italy
Mi Heon Ryu , Republic of Korea
Bashar Saad , Palestinian Authority
Sabi Saheed, South Africa









Mohamed Z.M. Salem , Egypt
Avni Sali, Australia
Andreas Sandner-Kiesling, Austria
Manel Santafe , Spain
José Roberto Santin , Brazil
Tadaaki Satou , Japan
Roland Schoop, Switzerland
Sindy Seara-Paz, Spain
Veronique Seidel , United Kingdom
Vijayakumar Sekar , China
Terry Selfe , USA
Arham Shabbir , Pakistan
Suzana Shahar, Malaysia
Wen-Bin Shang , China
Xiaofei Shang , China
Ali Sharif , Pakistan
Karen J. Sherman , USA
San-Jun Shi , China
Insop Shim , Republic of Korea
Maria Im Hee Shin, China
Yukihiro Shoyama, Japan
Morry Silberstein , Australia
Samuel Martins Silvestre , Portugal
Preet Amol Singh, India
Rajeev K Singla , China
Kuttulebbai N. S. Sirajudeen , Malaysia
Slim Smaoui , Tunisia
Eun Jung Sohn , Republic of Korea
Maxim A. Solovchuk , Taiwan
Young-Jin Son , Republic of Korea
Chengwu Song , China
Vanessa Steenkamp , South Africa
Annarita Stringaro , Italy
Keiichiro Sugimoto , Japan
Valeria Sulsen , Argentina
Zewei Sun , China
Sharifah S. Syed Alwi , United Kingdom
Orazio Tagliatalata-Scafati , Italy
Takashi Takeda , Japan
Gianluca Tamagno , Ireland
Hongxun Tao, China
Jun-Yan Tao , China
Lay Kek Teh , Malaysia
Norman Temple , Canada

Kamani H. Tennekoon , Sri Lanka
Seong Lin Teoh, Malaysia
Menaka Thounaojam , USA
Jinhui Tian, China
Zipora Tietel, Israel
Loren Toussaint , USA
Riaz Ullah , Saudi Arabia
Philip F. Uzor , Nigeria
Luca Vanella , Italy
Antonio Vassallo , Italy
Cristian Vergallo, Italy
Miguel Vilas-Boas , Portugal
Aristo Vojdani , USA
Yun WANG , China
QIBIAO WU , Macau
Abraham Wall-Medrano , Mexico
Chong-Zhi Wang , USA
Guang-Jun Wang , China
Jinan Wang , China
Qi-Rui Wang , China
Ru-Feng Wang , China
Shu-Ming Wang , USA
Ting-Yu Wang , China
Xue-Rui Wang , China
Youhua Wang , China
Kenji Watanabe , Japan
Jintanaporn Wattanathorn , Thailand
Silvia Wein , Germany
Katarzyna Winska , Poland
Sok Kuan Wong , Malaysia
Christopher Worsnop, Australia
Jih-Huah Wu , Taiwan
Sijin Wu , China
Xian Wu, USA
Zuoqi Xiao , China
Rafael M. Ximenes , Brazil
Guoqiang Xing , USA
JiaTuo Xu , China
Mei Xue , China
Yong-Bo Xue , China
Haruki Yamada , Japan
Nobuo Yamaguchi, Japan
Junqing Yang, China
Longfei Yang , China










Mingxiao Yang , Hong Kong
Qin Yang , China
Wei-Hsiung Yang, USA
Swee Keong Yeap , Malaysia
Albert S. Yeung , USA
Ebrahim M. Yimer , Ethiopia
Yoke Keong Yong , Malaysia
Fadia S. Youssef , Egypt
Zhilong Yu, Canada
RONGJIE ZHAO , China
Sultan Zahiruddin , USA
Armando Zarrelli , Italy
Xiaobin Zeng , China
Y Zeng , China
Fangbo Zhang , China
Jianliang Zhang , China
Jiu-Liang Zhang , China
Mingbo Zhang , China
Jing Zhao , China
Zhangfeng Zhong , Macau
Guoqi Zhu , China
Yan Zhu , USA
Suzanna M. Zick , USA
Stephane Zingue , Cameroon

Contents








Rutin and Hesperidin Revoke the Hepatotoxicity Induced by Paclitaxel in Male Wistar Rats *via* Their Antioxidant, Anti-Inflammatory, and Antiapoptotic Activities

Yasmine A. Ali , Hanan A. Soliman , Mohamed Abdel-Gabbar , Noha A. Ahmed , Kandil A. A. Attia , Fatma M. Shalaby , El-Shaymaa El-Nahass , and Osama M. Ahmed 
Research Article (17 pages), Article ID 2738351, Volume 2023 (2023)




Ginsenosides Rg1 and CK Control Temozolomide Resistance in Glioblastoma Cells by Modulating Cholesterol Efflux and Lipid Raft Distribution

Runze Qiu , Jingjing Zhang , Chun Ge , Yue Zhong , Suo Liu , Qingquan Li , Jianjun Zou , Hongwei Fan , and Yingbin Li 
Research Article (17 pages), Article ID 1897508, Volume 2022 (2022)




The Preventive Effects of Naringin and Naringenin against Paclitaxel-Induced Nephrotoxicity and Cardiotoxicity in Male Wistar Rats

Shimaa S. Khaled , Hanan A. Soliman, Mohammed Abdel-Gabbar , Noha A. Ahmed , Kandil Abdel Hai Ali Attia , Hesham A. Mahran , El-Shaymaa El-Nahass , and Osama M. Ahmed 
Research Article (11 pages), Article ID 8739815, Volume 2022 (2022)







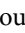

Antitumor Potential of Sericite Treatment Mediated by Cell Cycle Arrest in Triple-Negative MDA-MB231 Breast Cancer Cells

Seonhee Kim, Harsha Nagar, Ikjun Lee, Su-Jeong Choi, Shuyu Piao, Byeong Hwa Jeon, Shin Kwang Kang , Hee-Jung Song , and Cuk-Seong Kim 
Research Article (14 pages), Article ID 2885293, Volume 2022 (2022)






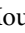





***Yifei sanjie* Pills Alleviate Chemotherapy-Related Fatigue by Reducing Skeletal Muscle Injury and Inhibiting Tumor Growth in Lung Cancer Mice**

Yingchao Wu , Dajin Pi, Yiliu Chen, Qian Zuo, Lizhu Lin , and Mingzi Ouyang 
Research Article (19 pages), Article ID 2357616, Volume 2022 (2022)

Grain-Sized Moxibustion Heightens the Anti-Tumor Effect of Cyclophosphamide in Hepa1-6 Bearing Mice

Tao Zhu , Yanzhu Ma , Jianyun Wang , Xiaolin Chen , Jianhao Li , Liqiang Meng , Yuduo Hou , and Yanting Cheng 
Research Article (12 pages), Article ID 3684899, Volume 2022 (2022)

Chemical Composition and the Anticancer, Antimicrobial, and Antioxidant Properties of *Acacia* Honey from the Hail Region: The *in vitro* and *in silico* Investigation

Walid Sabri Hamadou , Nouha Bouali , Riadh Badraoui , Ramzi Hadj Lajimi , Assia Hamdi , Mousa Alreshidi , Mitesh Patel , Mohd Adnan , Arif Jamal Siddiqui , Emira Noumi , Visweswara Rao Pasupuleti , and Mejdi Snoussi
Research Article (16 pages), Article ID 1518511, Volume 2022 (2022)









Cytotoxic Activity, Cell Cycle Inhibition, and Apoptosis-Inducing Potential of *Athyrium hohenackerianum* (Lady Fern) with Its Phytochemical Profiling

Abdelbaset Mohamed Elsbali , Waleed Abu Al-Soud , Ziad H. Al-Oanzi , Husam Qanash , Bandar Alharbi , Naif K. Binsaleh , Mousa Alreshidi , Mitesh Patel , and Mohd Adnan 

Research Article (13 pages), Article ID 2055773, Volume 2022 (2022)

Research Article

Rutin and Hesperidin Revoke the Hepatotoxicity Induced by Paclitaxel in Male Wistar Rats *via* Their Antioxidant, Anti-Inflammatory, and Antiapoptotic Activities

Yasmine A. Ali ¹, Hanan A. Soliman ¹, Mohamed Abdel-Gabbar ¹, Noha A. Ahmed ²,
Kandil A. A. Attia ^{3,4}, Fatma M. Shalaby ^{5,6}, El-Shaymaa El-Nahass ⁷,
and Osama M. Ahmed ²

¹Biochemistry Department, Faculty of Science, Beni-Suef University, P.O. Box 62521, Beni-Suef, Egypt

²Physiology Division, Zoology Department, Faculty of Science, Beni-Suef University, P.O. Box 62521, Beni-Suef, Egypt

³Clinical Nutrition Department, College of Applied Medical Sciences, Jazan University, P.O. Box 114, Jazan 45142, Saudi Arabia

⁴Department of Evaluation of Natural Resources, Environmental Studies and Research Institute, El-Sadat City University, El-Sadat City 32897, Egypt

⁵Biology Department, Faculty of Science, King Khalid University, Abha, Saudi Arabia

⁶Department of Zoology, Faculty of Science, Mansoura University, Mansoura, Egypt

⁷Department of Pathology, Faculty of Veterinary Medicine, Beni-Suef University, P.O. Box 62521, Beni-Suef, Egypt

Correspondence should be addressed to Osama M. Ahmed; osamamoha@yahoo.com

Received 20 July 2022; Revised 9 September 2022; Accepted 29 September 2022; Published 26 May 2023

Academic Editor: Mohammed El-Maghd

Copyright © 2023 Yasmine A. Ali et al. This is an open access article distributed under the Creative Commons Attribution License, which permits unrestricted use, distribution, and reproduction in any medium, provided the original work is properly cited.

Paclitaxel, one of the most effective chemotherapeutic drugs, is used to treat various cancers but it is exceedingly toxic when used long-term and can harm the liver. This study aimed to see if rutin, hesperidin, and their combination could protect male Wistar rats against paclitaxel (Taxol)-induced hepatotoxicity. Adult male Wistar rats were subdivided into 5 groups (each of six rats). The normal group was orally given the equivalent volume of vehicles for 6 weeks. The paclitaxel-administered control group received intraperitoneal injection of paclitaxel at a dose of 2 mg/Kg body weight twice a week for 6 weeks. Treated paclitaxel-administered groups were given paclitaxel similar to the paclitaxel-administered control group together with oral supplementation of rutin, hesperidin, and their combination at a dose of 10 mg/Kg body weight every other day for 6 weeks. The treatment of paclitaxel-administered rats with rutin and hesperidin significantly reduced paclitaxel-induced increases in serum alanine transaminase, aspartate transaminase, lactate dehydrogenase, alkaline phosphatase, and gamma-glutamyl transferase activities as well as total bilirubin level and liver lipid peroxidation. However, the levels of serum albumin, liver glutathione content, and the activities of liver superoxide dismutase and glutathione peroxidase increased. Furthermore, paclitaxel-induced harmful hepatic histological changes (central vein and portal area blood vessel congestion, fatty changes, and moderate necrotic changes with focal nuclear pyknosis, focal mononuclear infiltration, and Kupffer cell proliferation) were remarkably enhanced by rutin and hesperidin treatments. Moreover, the elevated hepatic proapoptotic mediator (caspase-3) and pro-inflammatory cytokine (tumor necrosis factor- α) expressions were decreased by the three treatments in paclitaxel-administered rats. The cotreatment with rutin and hesperidin was the most effective in restoring the majority of liver function and histological integrity. Therefore, rutin, hesperidin, and their combination may exert hepatic protective effects in paclitaxel-administered rats by improving antioxidant defenses and inhibiting inflammation and apoptosis.

1. Introduction

Paclitaxel, which stabilizes microtubules and inhibits their depolymerization during cell division, is one of the most

widely used chemotherapy drugs [1–4]. The active compound selection program founded by the National Cancer Institute in 1981 proved that paclitaxel was the only active biological ingredient that falls within this category and

meets the standard that could be effectively used to manage cancer, mainly from clinical trials [5, 6]. Paclitaxel is used to treat various cancers, including breast, prostate, bladder, cervical, and brain cancer [7–10]. Many different cancers are also treated with paclitaxel, such as aggressive and metastatic breast cancer, ovarian cancer, lung cancer, pancreatic cancer, and others [11]. However, its administration causes numerous adverse effects, including neuropathy, cardiotoxicity, and hepatotoxicity, as well as cancer cells' resistance to paclitaxel chemotherapy [12–14]. Paclitaxel has been widely known to stimulate apoptosis. Moreover, it has been recognized to produce reactive oxygen species (ROS) that trigger mitochondrial dysfunction to release cytochrome C into the cytoplasm and activate the caspase cascade and apoptosis stimulation [15, 16]. Paclitaxel promotes oxidative stress, decreases antioxidants, increases liver enzymes, and impairs renal function, which may be due to its mechanism of action and the oxidative stress that it caused [17]. Paclitaxel exacerbates liver damage during treatment and causes severe liver necrosis that may lead to mortality [18–20]. Paclitaxel has been reported to exert inflammatory actions. It also revealed a significant increase in pro-inflammatory cytokines, such as interleukin (IL)-17A, tumor necrosis factor- α (TNF- α), interferon- γ (IFN- γ), and keratinocyte, in paclitaxel-treated mice [21].

To reduce the toxicity of various organs from chemotherapeutic drugs, several studies have investigated the use of natural compounds that have antioxidant and anti-apoptotic effects [22–28]. Citrus species are considered to be among the most economically significant biological resources, as they contain a variety of plant nutrients and phytochemicals with promising therapeutic properties [29]. Flavonoids have various biological effects and may confer health benefits *via* different mechanisms through anti-inflammatory, antioxidant, antimicrobial, and anti-proliferative regulatory activities [30–32]. Several natural antioxidants have been experimentally tested for their potential to protect the liver, such as rutin [33] and hesperidin [34]. Combining rutin with other drugs can reduce drug resistance and side effects of chemotherapy [35]. Rutin has tremendous medicinal potential to regulate several cell signaling and apoptotic pathways implicated in cancer progression [36]. Additionally, it induces an important mechanism in inhibiting cell proliferation in neoplastic cells in the liver tissue by hepatocellular marker enzyme and tumor incursion suppression [37]. Rutin has shown remarkable protection against acrylamide-induced oxidative deoxyribonucleic acid (DNA) damage, which may be due to its antioxidant potential [38]. Hesperidin possesses chemopreventive potential against paclitaxel-induced hepatotoxicity probably by reducing oxidative stress, inflammation, apoptosis, and autophagy [39]. Furthermore, the pretreatment of hesperidin offers powerful protective effects against cisplatin-induced hepatic damage, which is achieved by its antioxidant, anti-inflammatory, and antiapoptotic activities [40]. Hesperidin's anticancer potential is controlled by ROS-dependent apoptotic pathways in certain cancer cells, despite the fact that it can be an excellent ROS

scavenger and could operate as a powerful antioxidant defense mechanism [41].

Chemotherapeutic drugs such as paclitaxel have several deleterious side effects including liver injury and we aim to minimize these effects by using plant constituents with antioxidant and anti-inflammatory activities. Therefore, this research aimed to scrutinize the preventative efficacy of rutin, hesperidin, and their combination on paclitaxel (Taxol)-induced liver toxicity, as well as to investigate the roles of inflammation, oxidative stress, and apoptosis modulations in preventative action.

2. Materials and Methods

2.1. Chemicals. The trade name drug, paclitaxel, or Taxol, in the formulation vehicle of cremophor® EL * (CrEL) (polyoxyethylated castor oil) (batch number: 7E05628), was obtained from Bristol-Myers Squibb global biopharmaceutical company (Princeton, USA). Rutin (batch number: 501) was obtained from Oxford Laboratory Company (Mumbai, India). Rutin is a light yellow crystalline powder with the empirical formula C₂₇H₃₀O₁₆ and a molecular weight of 610.5 and tastes slightly bitter. It has low solubility in water (125 mg/L), while it is highly soluble in polar solvents and melts at around 176–178°C. Hesperidin (lot number: # SLBT3541) was obtained from Sigma-Aldrich Company (St. Louis, MO, USA). Hesperidin is a light yellow crystalline powder with the empirical formula C₂₈H₃₄O₁₅ and a molecular weight of 610.6, odorless, and tasteless. It demonstrated poor, pH-independent, aqueous solubility, while it dissolves in dimethyl formamide and formamide at 60°C and slightly soluble in other polar solvents and melts at around 258–262°C. Alanine transaminase (ALT) reagent kit (catalog number: M11533c-21) and aspartate transaminase (AST) reagent kit (catalog number: M11531c-21) were purchased from Biosystem S.A. (Barcelona, Spain). The alkaline phosphatase (ALP) reagent kit and gamma-glutamyl transferase (GGT) reagent kit were purchased from Biosystem S.A. (Barcelona, Spain), with catalog numbers M11592-0610 and M11584c-11, respectively. A lactate dehydrogenase (LDH) reagent kit (catalog number: MX41214) was purchased from Spin React (Girona, Spain). Total bilirubin reagent kit (catalog number: 10742) and albumin reagent kit (catalog number: 10560) were purchased from HUMAN Gesellschaft für Biochemica und Diagnostica mbH (Wiesbaden, Germany). Chemicals of oxidative stress including trichloroacetic acid (TCA) (batch number: 50011689) obtained from PanReac AppliChem ITW Companies (Spain); thiobarbituric acid (TBA) (batch number: L 16A/1916/1212/13) was obtained from Sd Fine Chem Limited (SDFCL) Company (India); 1,1,3,3-tetramethoxy propane or malondialdehyde (MDA) (catalog number: T9889) was obtained from Sigma-Aldrich (MO, USA); metaphosphoric acid (batch number: M21519) was obtained from ALPHA CHEMIKA Company (India); 5,5-dithiobis nitrobenzoic acid (DTNB or Ellman's reagent) (batch number: 40K3652) was obtained from Sigma-Aldrich (MO, USA); Reduced glutathione (GSH) (batch number:

3W010085) was obtained from PanReac AppliChem ITW Companies (Spain); and pyrogallol (batch number: 1280B251114) was obtained from ResearchLab Company (India).

2.2. Experimental Animals. The experimental animals in this study were thirty adult male Wistar rats weighing 130–150 g and aged 7–8 weeks. They came from the National Research Center's Animal House in Dokki, Giza, Egypt. The animals were monitored for 15 days before the trial began to ensure that no inter competitive infections existed. The animals were kept in polypropylene cages with well-ventilated stainless steel lids at room temperature ($25 \pm 5^\circ\text{C}$) and on a 12-hourlight-dark cycle every day. The animals had unlimited access to water and were fed a well-balanced meal *ad libitum* daily. The Experimental Animal Ethics Committee's rules and guidelines were followed in all animal procedures. Faculty of Science, University of Beni-Suef, Egypt (Ethical Approval Number: BSU/FS/2017/8). Every effort has been made to reduce pain, distress, and discomfort among animals.

2.3. Experimental Design. Adult male Wistar rats were subdivided into 5 groups in this study (6 rats per group).

- (i) Normal group: rats in this group were orally administered with 5 mL 1% carboxymethylcellulose (CMC) (vehicle in which rutin and hesperidin are dissolved)/Kg body weight (b. wt) every other day and 2 mL isotonic saline (0.9% NaCl) (vehicle in which paclitaxel is dissolved)/Kg b. wt twice per week *via* the intraperitoneal (i.p.) route for 6 weeks.
- (ii) Paclitaxel-administered control group: this group of rats received paclitaxel at a dose of 2 mg/Kg b. wt (in 2 mL 0.9% NaCl) by i.p. injection [42] twice a week on the 2nd and 5th days of each week for 6 weeks, an equivalent dose of 1% CMC (5 mL/Kg b. wt) was also given orally every other day.
- (iii) Paclitaxel-administered group treated with rutin: this group of rats received paclitaxel as in the paclitaxel-administered control group, as well as rutin orally every other day at a dose of 10 mg/Kg b. wt [43] (dissolved in 5 mL of 1% CMC) for 6 weeks.
- (iv) Paclitaxel-administered group treated with hesperidin: this group of rats received paclitaxel as in the paclitaxel-administered control group, as well as hesperidin orally every other day at a dose of 10 mg/Kg b. wt [44] (dissolved in 5 mL of 1% CMC) for 6 weeks.
- (v) Paclitaxel-administered group treated with rutin and hesperidin combination: this group of rats received paclitaxel as in the paclitaxel-administered control group, as well as rutin and hesperidin combination orally every other day at a dose of 10 mg/Kg b. wt (dissolved in 5 mL of 1% CMC) for 6 weeks.

2.4. Blood and Liver Sampling. Under inhalation anesthesia [45], blood samples were collected from the jugular vein into gel and clot activator tubes after a 6-week treatment with the prescribed dosages. Blood samples were allowed to clot at room temperature and then centrifuged for 15 minutes at 3,000 rounds per minute (rpm). For various biochemical experiments, sera were quickly separated, split into four portions for each animal, and kept at -30°C . Following decapitation and dissection, livers were dissected for biochemical testing and histopathological examination, with each rat's liver tissue being quickly weighed and washed with isotonic saline (0.9% NaCl). A part of the liver was preserved in buffered formalin for 24 hours, then cut and placed in 70% alcohol for histopathologic analysis. The Teflon homogenizer (Glas-Col, Terre Haute, IND, USA) was used to homogenize approximately 0.5 g of each liver tissue into 5 mL 0.9% NaCl. The homogenates were then centrifuged for 15 minutes at 3,000 rpm, and the supernatants were aspirated and frozen at -30°C until employed in the assessment of oxidative stress marker-related biochemical and antioxidant parameters.

2.5. Determination of Liver Function Biomarkers in Serum. ALT and AST activities were assessed according to the method of Gella et al. [46]. The activities of GGT and ALP were assayed using the methods of Schumann et al. [47] and Schumann et al. [48], respectively. The activity of LDH was measured as previously described by Pesce [49]. The levels of serum albumin and total bilirubin were measured according to the procedures of Doumas et al. [50] and Jendrassik [51], respectively.

2.6. Liver Oxidative Stress and Antioxidant Biomarkers' Analysis. Chemical reagents prepared in the laboratory were used to evaluate liver oxidative stress and antioxidant biomarkers. The method provided by Preuss et al. [52] was used to estimate liver lipid peroxidation (LPO). Briefly, 0.15 mL 76% TCA was added to 1 mL liver homogenate to precipitate the protein. The isolated supernatant was then color-enhanced with 0.35 mL TBA. At 532 nm, the produced pale pink color was identified after 30 minutes in an 80°C water bath. The standard was MDA. On the other hand, GSH concentration in the liver was evaluated by adding 0.5 mL DTNB or Ellman's reagent (as a color-developing agent), and phosphate buffer solution (pH, 7) to homogenate supernatant after protein precipitation by centrifugation, as described by Beutler et al. [53]. At 412 nm, the generated yellow colors in the samples and GSH standard were measured and compared to a blank. The activity of liver GPx was determined using a modified version of the procedure described by Matkovic et al. [54]. The remaining GSH after it has been converted by the enzyme to GSSG (oxidized glutathione) and deducting the residual from the total is the basis of this approach. Briefly, 50 μL of homogenate supernatant was introduced to a Wasserman tube that already contained 350 μL of Tris buffer (pH 7.6), 50 μL of GSH solution (2 mM), and 50 μL of hydrogen peroxide (H_2O_2) (3.38 mM). The previously mentioned technique for

determining GSH was used to quantify the residual GSH content at 430 nm following a 10-minute incubation period. The standard test was made using 50 μL of dist. H_2O instead of 50 μL sample and the blank test was made with 100 μL of distilled water instead of 50 μL sample and 50 μL GSH solution. Following the discovery of residual GSH in the sample, the enzyme activity was measured by converting GSH to GSSG. The activity of the liver SOD was measured using the method of Marklund and Marklund [55]. SOD inhibits pyrogallol autoxidation, which is the basis for the reaction. Superoxide ions are necessary for the process to take place. One unit of enzyme is equivalent to the quantity of enzyme required to reduce extinction changes by 50% in one minute as compared to the control.

2.7. Histological Investigations. After the fast decapitation and dissection of each rat, 3 mm³ pieces of liver from all groups were preserved in 10% neutral phosphate-buffered formalin (pH 7.2) for 24 hours. The fixed livers were transferred to the Pathology Department of Beni-Suef University's Faculty of Veterinary Medicine in Egypt for additional processing, wax blocking, sectioning, and hematoxylin and eosin (H&E) staining [56]. Histological scores were determined by examining the stained liver sections. Six random fields were estimated for each section. The number of sections in each group is six. Degenerative change, fatty change, inflammatory cell infiltration, necrosis, vascular congestion, and Kupffer cell proliferation were among the graded lesions. Scoring of these hepatic lesions was calculated based on Khafaga et al. [57] and Wasef et al. [58] and graded as follows 0 = none; 1 = 25%; 2 = 26–50%; 3 = 51–75%; and 4 = 76–100%.

2.8. Immunohistochemical Investigations of Caspase-3 and TNF- α . The liver samples, secured with 10% neutral buffered formalin, were processed, blocked, and divided into 5- μm -thick sections that were fixed on positive-loaded slides (Fisher Scientific, Pittsburgh, PA, USA) at the National Cancer Institute's Pathology Department. The immunohistochemical reactions in the liver sections were investigated according to the method described by previous publications [59–63]. Briefly, after antigen retrieval, liver sections were incubated for 1 hour with diluted primary antibodies (dilution: 1–100 in phosphate buffer saline) for caspase-3 or TNF- α (Santa Cruz Biotechnology, Santa Cruz, CA, USA). Diluted biotinylated secondary antibodies (dilution: 1–200 in phosphate buffer saline) of DakoCytomation Kit were added and incubation was carried out for 15 minutes at 37°C. Then, using a DakoCytomation Kit, horseradish peroxidase conjugated with streptavidin was added and incubated for another 15 minutes. A reaction of 3,3'-diaminobenzidine (DAB) substrate was used to visualize the bound antibody complex, which was counterstained with hematoxylin. Immunostaining was comparable across all research groups since all liver slices were incubated under the same conditions with the same antibody dilutions and for the same period. A light microscope was used to examine the immunostained liver

sections and determine the degree of cell immunopositivity. A digital camera was used to capture photos of the liver section (Leica, DM2500M Leica, Wetzlar, Germany). ImageJ (1.51d), a free software program, was used to measure the area percentage of immune positivity for caspase-3 and TNF- α reactions according to Khafaga et al. [64] and El-Far et al. [65].

2.9. Statistical Analysis. The mean and standard error of the mean (SEM) were used to express all of the data. The Statistical Package for Social Sciences computer software (SPSS) (version 22, IBM software, Armonk, NY, USA) was used to perform the statistical analysis. A one-way analysis of variance (ANOVA) test was performed to clarify the significance among group means, followed by Tukey's post hoc test to compare-averaged aged results. At $p < 0.05$, differences were considered significant. Percentage changes were calculated using the formula: % change = [(Final value – Initial value)/Initial] \times 100 [66].

3. Results

3.1. Effects on Serum Parameters Related to Liver Function. The serum AST, ALT, GGT, LDH, and ALP activities, as well as the total bilirubin level, increased significantly ($p < 0.05$) after rats were given paclitaxel intraperitoneally for 6 weeks. When compared to the corresponding normal controls, paclitaxel administration resulted in a significant decrease in serum albumin level, with a documented percentage change of -37.37% . The treatment of paclitaxel-administered rats with rutin and/or hesperidin resulted in substantial decreases in increased serum AST, ALT, LDH, ALP, GGT, and total bilirubin levels when compared to the paclitaxel-administered control group. The treatment with rutin and its combination with hesperidin, on the other hand, resulted in a significant change in albumin levels, with recorded percentage changes of $+31.72$ and $+34.41\%$, respectively, whereas the treatment with hesperidin produced a nonsignificant improvement ($p > 0.05$). Moreover, compared with the paclitaxel-administered control group, the treatment of paclitaxel-administered rats with rutin and hesperidin combination was the most efficacious in improving the elevated serum AST, ALT, LDH, ALP, and total bilirubin levels, as well as the decreased albumin levels. Hesperidin treatment was the most effective in lowering GGT activity, with a recorded percentage change of -33.33% (Table 1).

3.2. Effects on Liver Oxidative Stress and Antioxidant Defense Parameters. Paclitaxel was given intraperitoneally to rats for six weeks, resulting in a highly significant rise in liver LPO and a highly significant decrease in liver GSH content, as well as SOD and GPx activities. The treatment of paclitaxel-administered rats with rutin, hesperidin, and their combination significantly decreased liver LPO. Hesperidin seemed to be the most effective in lowering the increased LPO product in the liver. In contrast to the paclitaxel-

TABLE 1: Effects of rutin and hesperidin on the activities of serum enzymes related to liver function in paclitaxel-injected rats.

Groups	Parameters													
	AST (U/L)	% Change	ALT (U/L)	% Change	GGT (U/L)	% Change	LDH (U/L)	% Change	ALP (U/L)	% Change	Total bilirubin (mg/dl)	% Change	Albumin (g/dl)	% Change
Normal	120.67 ± 4.56	—	41.17 ± 2.94	—	5.10 ± 0.45	—	565.50 ± 29.48	—	183.50 ± 6.89	—	0.23 ± 0.03	—	2.97 ± 0.16	—
Paclitaxel	185.00 ± 11.17 ^a	53.31	89.83 ± 2.68 ^a	118.19	10.80 ± 0.60 ^a	111.76	2327.50 ± 122.24 ^a	311.58	781.00 ± 34.58 ^a	325.61	0.76 ± 0.12 ^a	230.43	1.86 ± 0.10 ^a	-37.37
Paclitaxel + rutin	132.50 ± 6.01 ^b	-28.38	51.60 ± 2.23 ^{abc}	-42.56	7.80 ± 0.48 ^{ab}	-27.78	1681.67 ± 115.22 ^{ab}	-27.75	307.33 ± 21.87 ^{ab}	-60.65	0.33 ± 0.03 ^{bc}	-57.69	2.45 ± 0.14 ^b	31.72
Paclitaxel + hesperidin	145.13 ± 5.14 ^b	-21.55	61.80 ± 1.89 ^{abc}	-31.20	7.20 ± 0.48 ^{ab}	-33.33	1515.83 ± 167.47 ^{ab}	-34.87	368.67 ± 39.30 ^{ab}	-52.79	0.30 ± 0.02 ^{bc}	-61.54	2.43 ± 0.11	30.65
Paclitaxel + rutin + hesperidin	131.50 ± 9.10 ^b	-28.92	43.92 ± 2.22 ^b	-51.11	7.50 ± 0.18 ^{ab}	-30.56	988.33 ± 187.86 ^b	-57.54	284.67 ± 25.89 ^b	-63.55	0.25 ± 0.01 ^b	-67.95	2.50 ± 0.17 ^b	34.41

Data are expressed as Mean ± SEM ($n = 6$). ^a $p < 0.05$; significant compared with the normal group. ^b $p < 0.05$; significant compared with the paclitaxel-injected group. ^c $p < 0.05$; significant compared with the paclitaxel-injected group treated with both rutin and hesperidin. Percentage changes are calculated by comparing the paclitaxel-injected group with normal and paclitaxel-injected groups treated with rutin and hesperidin with the paclitaxel-injected group.

administered control group, paclitaxel-administered rats treated with rutin, hesperidin, or their combination showed a significant improvement in lowered liver SOD and GPx activities. The treatment of paclitaxel-administered rats with rutin and hesperidin caused a significant increase in the GSH content (Table 2).

3.3. Liver Histological Changes. Histopathological findings of the liver specimens from different experimental groups are presented in Figure 1 and Table 3. The normal group's liver sections revealed normal histological structures in the form of a thin-walled central vein and normal hepatocytes forming the hepatic cords radiating from the central vein toward the periphery and alternating with narrow blood spaces, the sinusoids, which are lined with single-layered Kupffer cells on histopathological analysis (Figure 1(a)). Conversely, the livers of the paclitaxel-administered group showed marked pathological changes in the form of central vein and portal area blood vessel congestion, marked degenerative changes, including fatty changes and moderate necrotic changes with focal nuclear pyknosis in certain areas, focal leukocytic infiltration (mainly mononuclear cells), and Kupffer cell proliferation (Figure 1(b)). These changes were altered to some extent in different paclitaxel-treated groups. These changes were amended to some extent by treatments of paclitaxel-administered groups. First, rats treated with paclitaxel/rutin showed severe degenerative and fatty changes associated with moderate necrotic changes and focal leukocytic infiltration associated with moderate proliferation of Kupffer cell activation (Figure 1(c)). Second, pathologic changes in the paclitaxel/hesperidin-treated group were relatively similar to those in the paclitaxel/rutin-treated group (Figure 1(d)). Finally, the treatment of paclitaxel/rutin/hesperidin produced a good improvement in liver histological changes compared with other treated rats. Moderate degenerative changes and mild necrotic changes accompanied by the mild Kupffer cell proliferation were noted (Figure 1(e)). The significantly elevated histological lesion scores of degenerative changes, fatty changes, necrosis, inflammatory cells, congestion, and activated Kupffer cell proliferation in the paclitaxel-injected group were significantly decreased by treatments with rutin, hesperidin, and their combination. The combinatory treatment was the most effective in improving the degenerative and fatty changes (Table 3).

3.4. Effects on Liver Caspase-3 and TNF- α . As demonstrated in Figures 2 and 3, immunohistochemical detection of expressed caspase-3 and TNF- α in the liver was performed. Caspases-3 and TNF- α immunohistochemistry reactivity was very feeble in the liver sections of normal control rats, indicating that their expression levels are very low. Caspase-3 and TNF- α staining in the livers of paclitaxel-administered rats was highly positive, as shown by a dense cytoplasmic brownish-yellow color that suggested their high expression, with percentage changes of +549.29% and +309.55%, respectively, in comparison to the control group. Rutin, hesperidin, and their combination significantly reduced the

enhanced caspase-3 activity and TNF- α concentration in paclitaxel-administered rats. The treatment of paclitaxel-administered rats with rutin and hesperidin combination was the most successful in lowering caspase-3 and TNF- α expressions.

4. Discussion

Paclitaxel is a drug that is commonly used to treat a variety of cancers. Its use may have a variety of adverse effects on several organs, including the liver, kidneys, and heart [67–70]. Despite remarkable progress in cancer research, compounds derived from natural resources are powerful candidates for cancer treatment [71]. Flavonoids and other reported phenolic components were discovered to have impressive antioxidative, cardioprotective, anticancer, antibacterial, antidiabetic, hypertensive, anti-inflammatory, and immune response enhancing effects as well as to protect skin from harmful ultraviolet radiation, making them outstanding drugs for pharmaceutical and medical use [72–74].

This study showed that the intraperitoneal injection of paclitaxel in the form of Taxol at a dose of 2 mg/Kg *b. wt* twice a week for 6 weeks caused hepatotoxicity, which was manifested biochemically by a significant increase in serum activities of cytosolic enzymes (ALT, AST, and LDH) due to their leakage into the bloodstream from injured hepatocytes [75]. Elevated serum ALT and AST levels in hepatocellular damage have been previously reported in paclitaxel-induced hepatotoxicity models [76–81]. Furthermore, the activity of LDH increased in paclitaxel-administered rats [82]. The LDH activity is elevated in patients with cancer and as a result of tissue damage; it is a common marker of toxicity. Additionally, we found a significant elevation in serum activities of membrane-bound enzymes (ALP and GGT) as a result of the increased rate of bile duct production and/or regurgitation in the blood after bile duct blockage [83]. These findings are similar to those reported by Ortega-Alonso et al. [84] who stated that the alteration of membrane permeability of liver cells and bile ducts triggers the release of their specific enzymes, notably GGT and ALP. Moreover, paclitaxel administration led to a significant increase in the total bilirubin content [85, 86], and this increase may be indicative of a specific liver injury and loss of function [87]. The serum albumin level was significantly reduced in paclitaxel-administered rats, which agrees with Wang et al. [88], who found that serum albumin concentration decreased significantly following chemotherapy. A decrease in albumin concentration, as observed in paclitaxel-administered rats, indicated insufficiency of albumin synthesis by the liver due to hepatopathy [89]. These biochemical parameter alterations strongly correlate with hepatic histopathological changes in the form of central vein and portal area blood vessel congestion, marked degenerative changes, including fatty changes and moderate necrotic changes with focal nuclear pyknosis in certain areas, focal leukocytic infiltration, and Kupffer cell proliferation. The current findings are congruent with those of Salahshoor et al. [80] who showed obvious changes and damage in the liver following paclitaxel treatment. Additionally,

TABLE 2: Effects of rutin and hesperidin on liver LPO, GSH content, and activities of SOD and GPx in paclitaxel-injected rats.

Groups	Parameters							
	LPO (nmol MDA/100 mg tissue/hour)	% Change	GSH (nmol/100 mg tissue)	% Change	SOD (U/g tissue)	% Change	GPx (mU/100 mg tissue)	% Change
Normal	11.10 ± 0.62	—	87.68 ± 3.32	—	19.05 ± 0.18	—	99.70 ± 1.80	—
Paclitaxel	23.30 ± 2.05 ^a	109.91	52.89 ± 1.96 ^a	-39.67	17.18 ± 0.13 ^a	-9.80	87.20 ± 1.20 ^a	-12.54
Paclitaxel + rutin	18.10 ± 0.64 ^{ab}	-22.32	75.83 ± 2.24 ^{abc}	43.37	18.16 ± 0.14 ^{ab}	5.70	93.90 ± 1.10 ^{ab}	7.68
Paclitaxel + hesperidin	12.10 ± 1.30 ^{bc}	-48.10	71.86 ± 0.85 ^{abc}	35.86	18.37 ± 0.09 ^{ab}	6.93	92.70 ± 0.80 ^{ab}	6.31
Paclitaxel + rutin + hesperidin	18.10 ± 0.96 ^{ab}	-22.32	54.17 ± 2.89 ^a	2.42	18.46 ± 0.12 ^{ab}	7.46	92.20 ± 0.60 ^{ab}	5.73

Data are expressed as Mean ± SEM ($n = 6$). ^a $p < 0.05$; significant compared with the normal group. ^b $p < 0.05$; significant compared with the paclitaxel-injected group. ^c $p < 0.05$; significant compared with the paclitaxel-injected group treated with both rutin and hesperidin. Percentage changes are calculated by comparing the paclitaxel-injected group with normal and paclitaxel-injected groups treated with rutin and hesperidin with the paclitaxel-injected group.

TABLE 3: Pathological hepatic lesion scores in different groups.

Groups	Parameters					
	Degenerative change	Fatty change	Necrosis	Inflammatory cells	Congestion	Activated Kupffer cell proliferation
Normal	0	0	0	0	0	0
Paclitaxel	3.83 ± 0.17 ^a	3.83 ± 0.17 ^a	2.17 ± 0.17 ^a	3.33 ± 0.21 ^a	3.17 ± 0.4 ^a	3.67 ± 0.21 ^a
Paclitaxel + rutin	2.50 ± 0.22 ^{abc}	3.00 ± 0.26 ^{abc}	1.00 ± 0.37 ^{ab}	1.83 ± 0.31 ^{ab}	1.50 ± 0.22 ^{ab}	2.67 ± 0.33 ^{ab}
Paclitaxel + hesperidin	3.00 ± 0.37 ^{abc}	2.83 ± 0.31 ^{abc}	1.67 ± 0.31 ^{ab}	2.00 ± 0.36 ^{ab}	1.67 ± 0.33 ^{ab}	2.50 ± 0.22 ^{ab}
Paclitaxel + rutin + hesperidin	1.67 ± 0.33 ^{ab}	2.00 ± 0.26 ^{ab}	1.33 ± 0.21 ^{ab}	1.50 ± 0.43 ^{ab}	1.00 ± 0.26 ^{ab}	2.17 ± 0.31 ^{ab}

Data are expressed as Mean ± SEM ($n = 6$). ^a $p < 0.05$: significant compared with the normal group. ^b $p < 0.05$: significant compared with the paclitaxel-injected group. ^c $p < 0.05$: significant compared with the paclitaxel-injected group treated with both rutin and hesperidin. Scoring of hepatic histological lesions was calculated and graded as follows 0 = none; 1 ≤ 25%; 2 = 26–50%; 3 = 51–75%; and 4 = 76–100%.

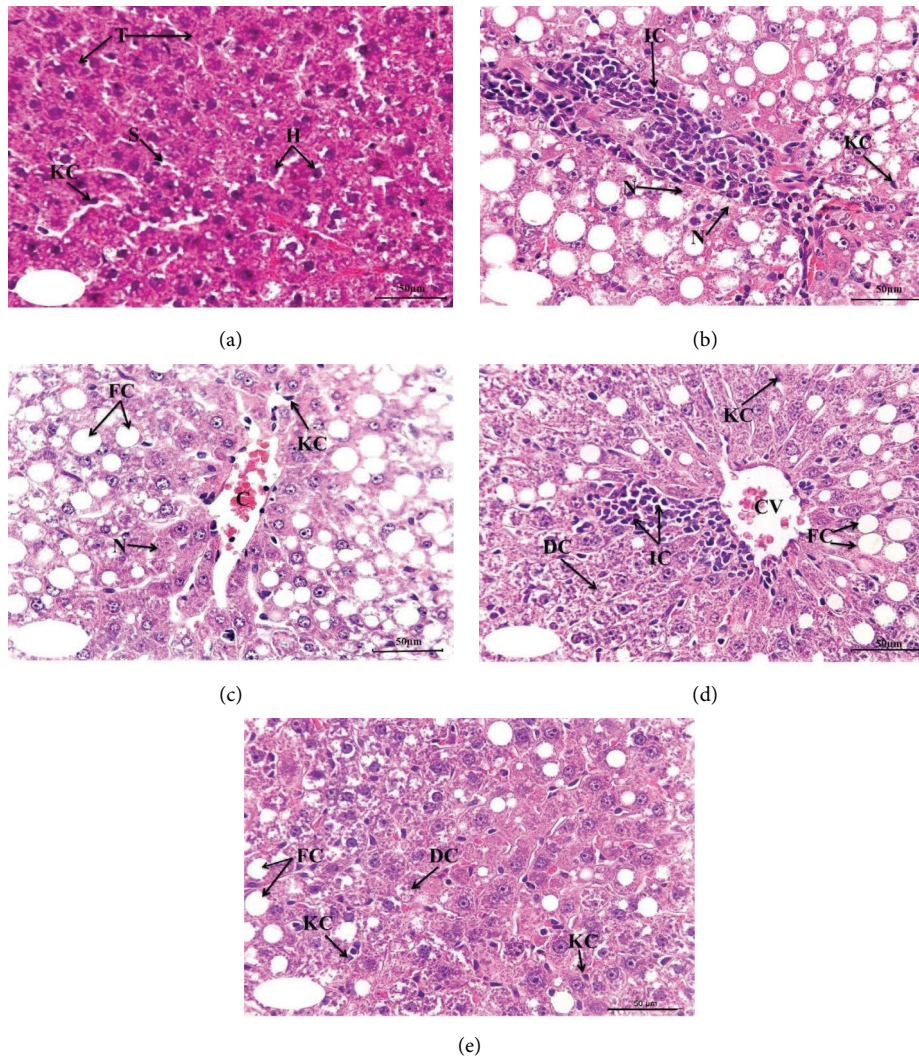


FIGURE 1: Photomicrographs of liver sections of the normal (a), paclitaxel-injected control group (b), and paclitaxel-injected groups treated with rutin (c), hesperidin (d), and their combination (e). (H) hepatocytes; (T) trabeculae; (S) sinusoids; and KC: Kupffer cells; (N) necrosis; IC: inflammatory cells infiltration; FC: fatty changes; (C) congestion; CV: central vein; DC: degenerative changes. (H&E; ×400).

hepatotoxic effects following paclitaxel therapy were observed [90, 91]. It has been also found a distinctive hepatocellular carcinoma in hepatic histological sections in all groups following paclitaxel treatment was observed [85].

Rutin and/or hesperidin treatment of paclitaxel-administered rats successfully reduced increased blood ALT, AST, LDH, ALP, and GGT activities, as well as serum total bilirubin levels, by stopping further paclitaxel-induced

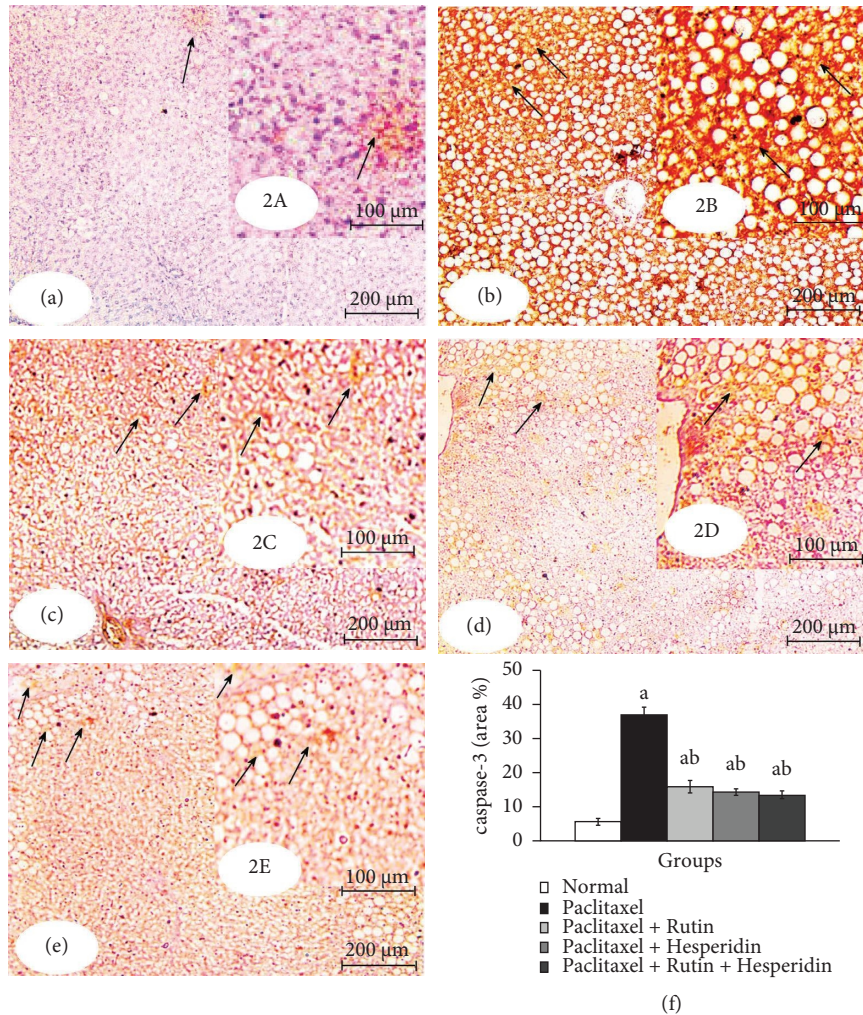


FIGURE 2: Photomicrographs of immunohistochemically stained liver sections for caspase-3 detection showing very weak expression in normal (2a and 2A), very strong expression in the paclitaxel-administered group (2b and 2B), and moderate expression in paclitaxel-administered groups treated with rutin (2c and 2C), hesperidin (2d and 2D), and their combination (2e and 2E). Arrows indicate positive reactivity. 2f indicates the image analysis result of caspase-3 of the tested groups. ^a $p < 0.05$: significant compared with the normal group. ^b $p < 0.05$: significant compared with the paclitaxel-injected group. Photomicrographs 2A–2E are magnified sectors of Photomicrographs 2a–2e respectively.

hepatocellular damage and stabilizing membrane activity, thereby decreasing the leakage of these enzymes into the general circulation. The treatments potentially increased the reduced serum albumin level. Moreover, most hepatic histopathological changes were effectively improved by these treatments. Similar observations have been reported by Hozayen et al. [92] who stated that the pretreatment with rutin, hesperidin, and their combination can protect the liver against the hepatotoxic effect of doxorubicin by ameliorating the elevated AST, ALT, ALP, and γ -GT activities. This is attributed to the hepatoprotective potential of rutin [33] and hesperidin [34]. It was found that hesperidin reduces the severity of sodium arsenate (SA)-induced liver damage [93]. Rutin administration restored the elevated ALT, LDH, AST, and ALP levels in 5-fluorouracil (FU)-treated rats and improved the hepatic structure to normal [24]. Furthermore, rutin treatment improved carfilzomib-induced elevated levels of direct bilirubin in rats [94].

Enzymatic and nonenzymatic antioxidant substances are components of antioxidant defense systems. GSH has a tripeptide structure and is a potent nonenzymatic antioxidant. SOD, catalase, and GPx are additional enzymatic antioxidants for ROS defense [95, 96]. Paclitaxel administration increases the formation of oxygen-free radicals, decreases antioxidants (SOD and GPx) and GSH content, and increases LPO, which results in liver damage. These results are consistent with those of Harisa [97] who reported that paclitaxel induces oxidative stress through decreased GSH content and increased MDA levels. In addition, it was reported that paclitaxel increases ROS and MDA concentrations and decreases SOD activity [82], indicating that paclitaxel induces changes in protein expression associated with apoptosis and ROS generation (Figure 4). ROS activates several mechanisms by damaging cell membranes and macromolecules in cells, resulting in inflammation and cell death [98]. Therefore, oxidative stress, which is caused by

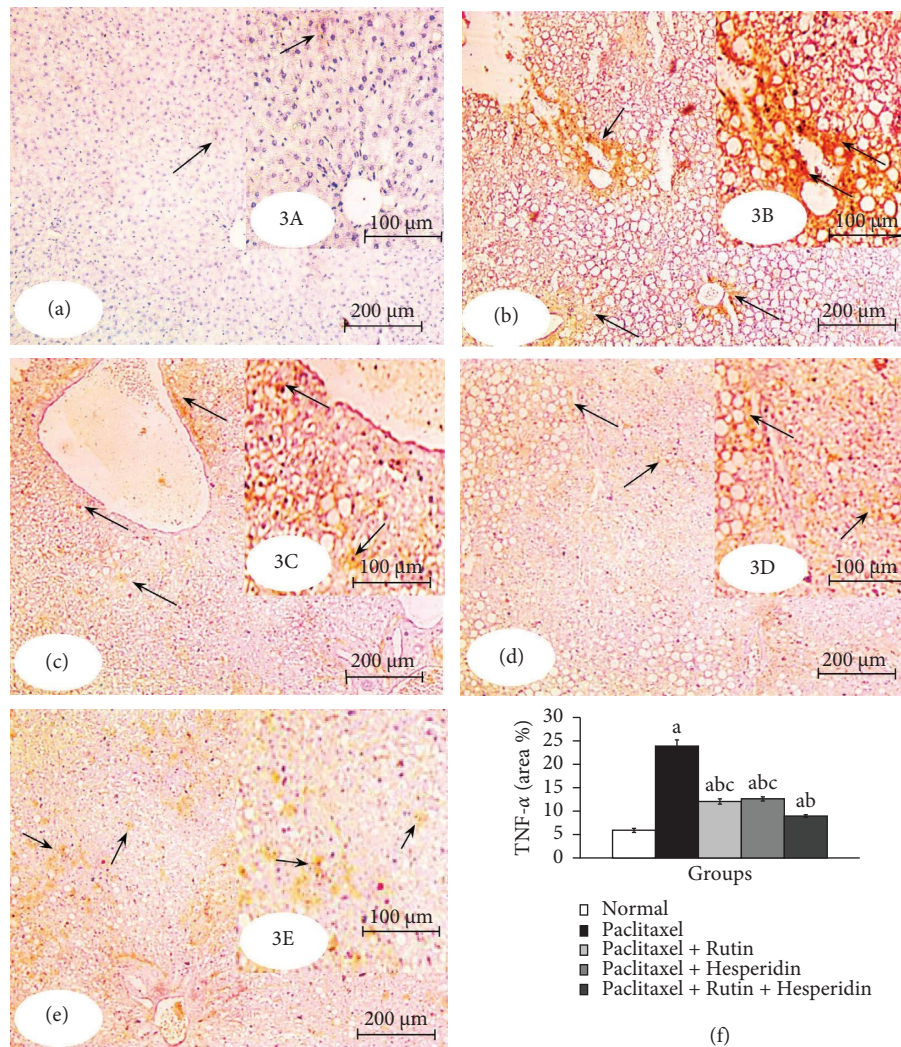


FIGURE 3: Photomicrographs of immunohistochemically stained liver sections for TNF- α detection showing very weak expression in normal (3a and 3A), strong expression in the paclitaxel-administered group (3b and 3B), and moderate expression in paclitaxel-administered groups treated with rutin (3c and 3C) and hesperidin (3d and 3D) and mild expression in the paclitaxel-administered group treated the combination of rutin and hesperidin (3e and 3E). Arrows indicate positive reactivity. 3f indicates the image analysis result of TNF- α of the tested groups. ^a $p < 0.05$: significant compared with the normal group. ^b $p < 0.05$: significant compared with the paclitaxel-injected group. ^c $p < 0.05$: significant compared with the paclitaxel-injected group treated with both rutin and hesperidin. Photomicrographs 3A–3E are magnified sectors of Photomicrographs 3a–3e respectively.

paclitaxel administration, may cause the production of active oxygen species, including pure oxygen, H_2O_2 and superoxide radicals, which destroy cells, DNA, proteins, and intracellular lipids, and finally liver damage [99]. According to the findings, rutin and hesperidin treatment remarkably reduced paclitaxel-induced oxidative stress by reducing LPO and improving GSH content along with the activities of antioxidant enzymes due to the ability of rutin to recover-free radicals by chelating metallic iron ions [100, 101] as well as the antioxidant activity and radical recovery properties of hesperidin [102, 103]. These findings are consistent with those of Hozayen et al. [92], who found that rutin and hesperidin significantly increased GSH and GPx levels in the liver and decreased the LPO level in doxorubicin-treated rats. Rutin treatment alleviated liver and kidney damage by reducing oxidative stress, endoplasmic reticulum stress,

inflammation, apoptosis, and autophagy caused by valproic acid [104]. Additionally, rutin has a hepatoprotective role in eliminating isoniazid-induced oxidative stress [33]. Hesperidin has been discovered to protect the brain, liver, kidneys, and oxidative damage caused by numerous toxins [105, 106]. In another way, thymoquinone and costunolide are also natural products that have been shown to have an apoptotic effect to rapidly eliminate the senescent cells induced by doxorubicin and induce apoptosis of proliferative cancer cell lines [107].

Immunohistochemical investigations showed a significant increase in the proapoptotic protein (caspase-3) activity and pro inflammatory cytokine (TNF- α) concentration in the liver of paclitaxel-administered rats. The findings of our investigation agree with those of Yardım et al. [108] who revealed that the mRNA levels of TNF- α and caspase-3 were

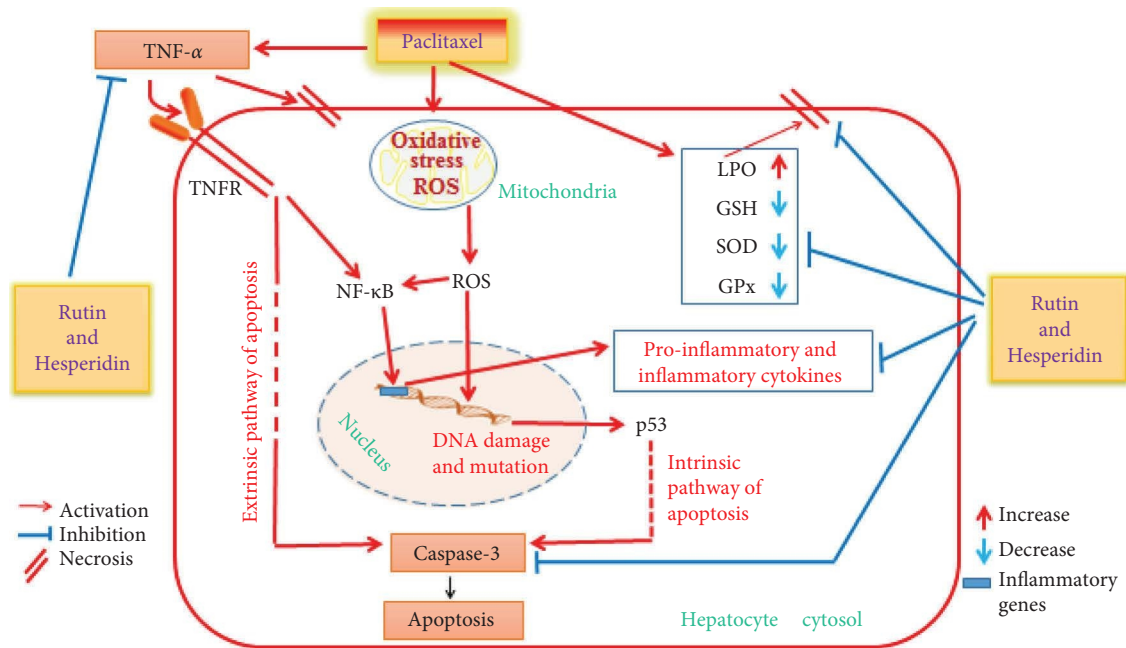


FIGURE 4: The effects of rutin and hesperidin on oxidative stress, inflammation, and apoptosis in the livers of paclitaxel-administered rats are depicted in a schematic diagram. The target effects of rutin and hesperidin on various mediators of oxidative stress, inflammation, and apoptosis are shown. The figure was designed by us using power point software.

higher in the paclitaxel group for the sciatic nerve and spinal cord, and the immunohistochemical expression of caspase-3 in the paclitaxel-induced bone marrow tissue was increased. Furthermore, taxanes, including paclitaxel, induced an increase in IL-1 β , IL-6, and TNF- α levels in patients with cancer [109–111]. It was also found that circulating IL-6 and TNF- α levels were increased 3 days after a 6-dose paclitaxel regimen [112]. TNF- α is a critical mediator of inflammation [113] that has been demonstrated to recruit and trigger more inflammatory cells in response to increased oxidative stress [114]. TNF- α can promote hepatocyte apoptosis *via* binding to TNF receptors (TNFR) and death receptors, triggering the extrinsic apoptosis pathway [115–117] (Figure 4). Through the permeability of the mitochondrial membrane or its transition pore apertures, paclitaxel releases apoptogenic components, including cytochrome C, into the cytosol, either directly or indirectly [118, 119]. Apoptosis is facilitated by cytochrome C active caspase-9, which stimulates various caspase enzymes, including caspase-3 and caspase-7, in the presence of apoptotic protease activating factor-1 [120, 121].

The treatment of paclitaxel-administered rats with rutin and/or hesperidin suppressed the activity of caspase-3, which is a common mediator of extrinsic and intrinsic apoptotic pathways and the level of TNF- α , which is a key regulator of inflammation (Figure 4). These results are consistent with those of Li and Schluesener [122] who reported that hesperidin suppressed oxidative/nitrative stress, inflammation, and apoptosis. Hesperidin reduced the caspase-3 activity and showed an anti-inflammatory effect by decreasing the levels of TNF- α , nuclear factor kappa B (NF- κ B), and IL1 β in the kidney and liver tissues of rats with SA-induced toxicity [93]. It also reduced the serum level of TNF- α in arthritic rats [123]. Hesperidin decreased the

elevated liver caspase-3 expression and altered serum TNF- α , IL-17, and IL-4 levels in diclofenac-administered rats [124]. Additionally, rutin may have potential protective benefits against hepatotoxicity induced by doxorubicin through reducing oxidative stress, inflammation, and apoptosis as well as altering the expression of the nuclear factor erythroid 2-related factor 2 (Nrf2) gene [125]. Rutin decreased the hepatic TNF- α and IL-6 levels of carbon tetrachloride-treated rats [126]. It was found that rutin significantly decreased caspase-3 immunopositivity in 5-FU-treated rats [24]. The therapeutic potential of rutin can be owed to its antioxidant, anti-inflammatory, antiallergic, and antiangiogenic properties [127, 128]. Based on our findings and past research studies, the intrinsic pathway, which is activated by high ROS levels, or extrinsic ligands of pathway receptors, such as TNF- α , can cause caspase-3, the apoptosis executor, to be activated in paclitaxel hepatotoxicity. Rutin and hesperidin may have reduced apoptosis by modulating both intrinsic and extrinsic apoptotic pathways by suppressing oxidative stress and significantly lowering increased TNF- α concentration (Figure 4). In addition, TNF- α (through canonical pathway) can activate NF- κ B, which promotes NF- κ B target genes involved in inflammatory responses [129]. Both rutin and hesperidin may produce their anti-inflammatory effects by affecting the canonical pathway of NF- κ B through the suppression of TNF- α levels and in turn inhibition of TNF- α receptors (TNFR) (Figure 4).

5. Conclusion

Oral administration of rutin, hesperidin, and their combination could counteract paclitaxel-induced liver damage and toxicity by strengthening the antioxidant defense system and

decreasing oxidative stress and apoptosis. Additionally, it was discovered that rutin and hesperidin combined therapy was the most effective at restoring liver function and histological integrity in paclitaxel-administered rat models. However, before rutin and hesperidin be used in humans, more clinical trials are necessary to evaluate their effectiveness and safety during paclitaxel administration. The Food and Drug Administration also needs to approve their use in human beings these evaluations. Moreover, further studies are required to scrutinize the effect on mediators of apoptosis other than caspase-3 and mediators of inflammation other TNF- α to identify other targets of rutin and hesperidin in paclitaxel-administered rats.

Abbreviations

ALP:	Alkaline phosphatase
ALT:	Alanine aminotransferase
ANOVA:	One-way analysis of variance
AST:	Aspartate aminotransferase
CMC:	Carboxymethylcellulose
DAB:	3,3'-Diaminobenzidine
DNA:	Deoxyribonucleic acid
GGT:	Gamma-glutamyl transferase
GPx:	Glutathione peroxidase
GSH:	Reduced glutathione
GSSG:	Oxidized glutathione
H&E:	Hematoxylin and eosin stain
H ₂ O ₂ :	Hydrogen peroxide
IFN- γ :	Interferon- γ
IL:	Interleukin
b:	Wt: Kilogram body weight
LDH:	Lactate dehydrogenase
LPO:	Lipid peroxidation
MDA:	Malondialdehyde or 1,1,3,3-tetramethoxypropane
mRNA:	Messenger ribonucleic acid
NF- κ B:	Nuclear factor kappa B
Nrf2:	The nuclear factor erythroid 2-related factor 2
O ²⁻ :	Superoxide radical
rpm.:	Round per minute
ROS:	Reactive oxygen species
SA:	Sodium arsenate
SEM:	Standard error of the mean
SPSS:	Statistical Package for Social Sciences
SOD:	Superoxide dismutase
TBA:	Thiobarbituric acid
TCA:	Trichloroacetic acid
TNFR:	TNF receptor
TNF- α :	Tumor necrosis factor-alpha.

Data Availability

All data are available from the corresponding author upon reasonable request.

Conflicts of Interest

The authors declare that they have no conflicts of interest.

Acknowledgments

The authors express their thanks to Jazan University, P.O. Box 114, Postal code 45142, Jazan, Saudi Arabia, for support.

References

- [1] A. M. Khalifa, M. A. Elsheikh, A. M. Khalifa, and Y. S. Elnaggar, "Current strategies for different paclitaxel-loaded nano-delivery systems towards therapeutic applications for ovarian carcinoma: a review article," *Journal of Controlled Release*, vol. 311, pp. 125–137, 2019.
- [2] I. Khan, M. Apostolou, R. Bnyan, C. Houacine, A. Elhissi, and S. S. Yousaf, "Paclitaxel-loaded micro or nano trans-fersome formulation into novel tablets for pulmonary drug delivery via nebulization," *International Journal of Pharmaceutics*, vol. 575, Article ID 118919, 2020.
- [3] F. Naaz, M. R. Haider, S. Shafi, and M. S. Yar, "Anti-tubulin agents of natural origin: targeting taxol, vinca, and colchicine binding domains," *European Journal of Medicinal Chemistry*, vol. 171, pp. 310–331, 2019.
- [4] A. M. Sofias, M. Dunne, G. Storm, and C. Allen, "The battle of "nano" paclitaxel," *Advanced Drug Delivery Reviews*, vol. 122, pp. 20–30, 2017.
- [5] A. G. Atanasov, S. B. Zotchev, V. M. Dirsch, and C. T. Supuran, "Natural products in drug discovery: advances and opportunities," *Nature Reviews Drug Discovery*, vol. 20, no. 3, pp. 200–216, 2021.
- [6] R. Renneberg, "Biotech History: yew trees, paclitaxel synthesis and fungi," *Biotechnology Journal*, vol. 2, no. 10, pp. 1207–1209, 2007.
- [7] F. Gelsomino, M. Tiseo, F. Barbieri et al., "Phase 2 study of NAB-paclitaxel in SensiTivE and refractory relapsed small cell lung cancer (SCLC) (NABSTER TRIAL)," *British Journal of Cancer*, vol. 123, no. 1, pp. 26–32, 2020.
- [8] A. Hernández-Prat, A. Rodriguez-Vida, N. Juanpere-Rodero et al., "Novel oral mTORC1/2 inhibitor TAK-228 has synergistic antitumor effects when combined with paclitaxel or PI3K α inhibitor TAK-117 in preclinical bladder cancer models," *Molecular Cancer Research*, vol. 17, no. 9, pp. 1931–1944, 2019.
- [9] A. Y. Kilcar, O. Yildiz, T. Dogan, E. Sulu, G. Takan, and F. Z. B. Muftuler, "Bitter melon (*Momordica charantia*) extract effect against 99mTc labeled paclitaxel: *in vitro* monitoring on breast cancer cells," *Anti-Cancer Agents in Medicinal Chemistry*, vol. 20, no. 12, pp. 1497–1503, 2020.
- [10] D. Qu, M. Jiao, H. Lin et al., "Anisamide-functionalized pH-responsive amphiphilic chitosan-based paclitaxel micelles for sigma-1 receptor targeted prostate cancer treatment," *Carbohydrate Polymers*, vol. 229, Article ID 115498, 2020.
- [11] I. Klein and H. C. Lehmann, "Pathomechanisms of paclitaxel-induced peripheral neuropathy," *Toxics*, vol. 9, no. 10, p. 229, 2021.
- [12] A. M. Cirrincione, A. D. Pellegrini, J. R. Dominy et al., "Paclitaxel-induced peripheral neuropathy is caused by epidermal ROS and mitochondrial damage through conserved MMP-13 activation," *Scientific Reports*, vol. 10, no. 1, pp. 3970–4012, 2020.
- [13] M. L. Costa, J. A. Rodrigues, J. Azevedo, V. Vasconcelos, E. Eiras, and M. G. Campos, "Hepatotoxicity induced by paclitaxel interaction with turmeric in association with a microcystin from a contaminated dietary supplement," *Toxicon*, vol. 150, pp. 207–211, 2018.

- [14] M. J. Gil-Gil, M. Bellet, S. Morales et al., "Pegylated liposomal doxorubicin plus cyclophosphamide followed by paclitaxel as primary chemotherapy in elderly or cardiotoxicity-prone patients with high-risk breast cancer: results of the phase II CAPRICE study," *Breast Cancer Research and Treatment*, vol. 151, no. 3, pp. 597–606, 2015.
- [15] V. Annamalai, M. Kotakonda, and V. Periyannan, "JAK1/STAT3 regulatory effect of β -caryophyllene on MG-63 osteosarcoma cells via ROS-induced apoptotic mitochondrial pathway by DNA fragmentation," *Journal of Biochemical and Molecular Toxicology*, vol. 34, no. 8, Article ID e22514, 2020.
- [16] A. W. Kwak, J. S. Choi, K. Liu et al., "Licochalcone C induces cell cycle G1 arrest and apoptosis in human esophageal squamous carcinoma cells by activation of the ROS/MAPK signaling pathway," *Journal of Chemotherapy*, vol. 32, no. 3, pp. 132–143, 2020.
- [17] D. T. AL-Gabri, A. J. Al-Naely, and H. A. Alghanmi, "Using of nanocomposite loading *klisinema persicum* for reducing the damage of the liver and kidneys in female rats caused by taxol (paclitaxel)," *Turkish Journal of Physiotherapy and Rehabilitation*, vol. 32, no. 3, 2021.
- [18] Z. N. Anber, "Effect of doxorubicin and cyclophosphamide regimen versus taxane on liver enzymes in Iraqi women with breast cancer," *Biomedical Research*, vol. 29, no. 21, pp. 3869–3873, 2018.
- [19] X. Guo, W. Li, J. Hu, E. C. Zhu, and Q. Su, "Hepatotoxicity in patients with solid tumors treated with PD-1/PD-L1 inhibitors alone, PD-1/PD-L1 inhibitors plus chemotherapy, or chemotherapy alone: systematic review and meta-analysis," *European Journal of Clinical Pharmacology*, vol. 76, no. 10, pp. 1345–1354, 2020.
- [20] H. Mandaliya, P. Baghi, A. Prawira, and M. K. George, "A rare case of paclitaxel and/or trastuzumab induced acute hepatic necrosis," *Case Reports in Oncological Medicine*, vol. 2015, Article ID 825603, 2 pages, 2015.
- [21] M. Caillaud, N. H. Patel, W. Toma et al., "A fenofibrate diet prevents paclitaxel-induced peripheral neuropathy in mice," *Cancers*, vol. 13, no. 1, p. 69, 2020.
- [22] V. Gelen and E. Şengül, "Hepatoprotective effect of naringin on 5-Fluorouracil (5-FU) toxicity in rats," *Chemistry Research Journal*, vol. 3, no. 1, pp. 127–130, 2018.
- [23] V. Gelen and E. Şengül, "Antioxidant, antiinflammatory and antiapoptotic effects of naringin on cardiac damage induced by cisplatin," *Indian Journal of Traditional Knowledge (IJTK)*, vol. 19, no. 2, pp. 459–465, 2020.
- [24] V. Gelen, E. Şengül, S. Gedikli, G. Atila, H. Uslu, and M. Makav, "The protective effect of rutin and quercetin on 5-FU-induced hepatotoxicity in rats," *Asian Pacific Journal of Tropical Biomedicine*, vol. 7, no. 7, pp. 647–653, 2017.
- [25] V. Gelen, E. Şengül, S. Gedikli, C. Gür, and S. Özkanlar, "Therapeutic effect of quercetin on renal function and tissue damage in the obesity induced rats," *Biomedicine & Pharmacotherapy*, vol. 89, pp. 524–528, 2017.
- [26] V. Gelen, E. Şengül, S. Yıldırım, and G. Atila, "The protective effects of naringin against 5-fluorouracil-induced hepatotoxicity and nephrotoxicity in rats," *Iranian Journal of Basic Medical Sciences*, vol. 21, no. 4, pp. 404–410, 2018.
- [27] V. Gelen, S. U. Gelen, F. Celebi, A. Cinar, S. Yildirim, and G. Eser, "The protective effect of *Lactobacillus rhamnosus*, *Lactobacillus fermentum* and *Lactobacillus brevis* against cisplatin-induced hepatic damage in rats," *Fresenius Environmental Bulletin*, vol. 28, pp. 7583–7592, 2019.
- [28] E. Şengül, V. Gelen, S. Gedikli et al., "The protective effect of quercetin on cyclophosphamide induced lung toxicity in rats," *Biomedicine & Pharmacotherapy*, vol. 92, pp. 303–307, 2017.
- [29] M. Addi, A. Elbouzidi, M. Abid, D. Tungmunnithum, A. Elamrani, and C. Hano, "An overview of bioactive flavonoids from citrus fruits," *Applied Sciences*, vol. 12, no. 1, p. 29, 2021.
- [30] K. Borowiec and A. Michalak, "Flavonoids from edible fruits as therapeutic agents in neuroinflammation: a comprehensive review and update," *Critical Reviews in Food Science and Nutrition*, vol. 62, no. 24, pp. 6742–6760, 2021.
- [31] C. Del Bo, S. Bernardi, M. Marino et al., "Systematic review on polyphenol intake and health outcomes: is there sufficient evidence to define a health-promoting polyphenol-rich dietary pattern?" *Nutrients*, vol. 11, no. 6, p. 1355, 2019.
- [32] R. K. Sharma, N. Sharma, U. Kumar, and S. S. Samant, "Antioxidant properties, phenolics and flavonoids content of some economically important plants from North-west Indian Himalaya," *Natural Product Research*, vol. 36, no. 6, pp. 1565–1569, 2021.
- [33] O. Abdel-Ghaf, S. T. Mahmoud, A. Ali Said, and F. Abdel-Azee, "Hepatoprotective effect of rutin against oxidative stress of isoniazid in albino rats," *International Journal of Pharmacology*, vol. 13, no. 6, pp. 516–528, 2017.
- [34] G. Zhang, J. Zhu, Y. Zhou et al., "Hesperidin alleviates oxidative stress and upregulates the multidrug resistance protein 2 in isoniazid and rifampicin-induced liver injury in rats," *Journal of Biochemical and Molecular Toxicology*, vol. 30, no. 7, pp. 342–349, 2016.
- [35] A. Satari, S. Ghasemi, S. Habtemariam, S. Asgharian, and Z. Lorigooini, "Rutin: a flavonoid as an effective sensitizer for anticancer therapy; insights into multifaceted mechanisms and applicability for combination therapy," *Evidence-based Complementary and Alternative Medicine*, vol. 2021, Article ID 9913179, 10 pages, 2021.
- [36] P. Pandey, F. Khan, H. A. Qari, and M. Oves, "Rutin (bioflavonoid) as cell signaling pathway modulator: prospects in treatment and chemoprevention," *Pharmaceuticals*, vol. 14, no. 11, p. 1069, 2021.
- [37] Y. P. Chandra and A. Viswanathswamy, "Chemopreventive effect of rutin against N-nitrosodiethylamine-induced and phenobarbital-promoted hepatocellular carcinoma in Wistar rats," *Indian Journal of Pharmaceutical Education and Research*, vol. 52, no. 1, pp. 78–86, 2018.
- [38] C. Uthra, M. S. Reshi, A. Jaswal et al., "Protective efficacy of rutin against acrylamide-induced oxidative stress, biochemical alterations and histopathological lesions in rats," *Toxicology Research*, vol. 11, no. 1, pp. 215–225, 2022.
- [39] C. Gur, F. M. Kandemir, C. Caglayan, and E. Satici, "Chemopreventive effects of hesperidin against paclitaxel-induced hepatotoxicity and nephrotoxicity via amendment of Nrf2/HO-1 and caspase-3/Bax/Bcl-2 signaling pathways," *Chemico-Biological Interactions*, vol. 365, p. 110073, 2022.
- [40] D. M. Aboraya, A. El Baz, E. F. Risha, and F. M. Abdelhamid, "Hesperidin ameliorates cisplatin induced hepatotoxicity and attenuates oxidative damage, cell apoptosis, and inflammation in rats," *Saudi Journal of Biological Sciences*, vol. 29, 2022.
- [41] M. S. Antunes, F. V. L. Ladd, A. A. B. L. Ladd, A. L. Moreira, S. P. Boeira, and L. Cattelan Souza, "Hesperidin protects against behavioral alterations and loss of dopaminergic neurons in 6-OHDA-lesioned mice: the role of mitochondrial dysfunction and apoptosis," *Metabolic Brain Disease*, vol. 36, no. 1, pp. 153–167, 2021.

- [42] A. Mangaiarkkarsi, S. Rameshkannan, and R. M. Ali, "Effect of gabapentin and pregabalin in rat model of taxol induced neuropathic pain," *Journal of Clinical and Diagnostic Research: Journal of Clinical and Diagnostic Research*, vol. 9, no. 5, pp. FF11–FF14, 2015.
- [43] S. L. Patil, H. Somashekarappa, and K. Rajashekhar, "Radiomodulatory role of rutin and quercetin in Swiss albino mice exposed to the whole body gamma radiation," *Indian Journal of Nuclear Medicine*, vol. 27, no. 4, pp. 237–242, 2012.
- [44] Y. Wang, C. Han, and A. Leng, "Pharmacokinetics of vitexin in rats after intravenous and oral administration," *African Journal of Pharmacy and Pharmacology*, vol. 6, no. 31, pp. 2368–2373, 2012.
- [45] O. M. Ahmed, S. R. Galaly, M. Raslan, and M. A. Mostafa, "Thyme oil and thymol abrogate doxorubicin-induced nephrotoxicity and cardiotoxicity in Wistar rats via repression of oxidative stress and enhancement of antioxidant defense mechanisms," *Biocell*, vol. 44, no. 1, pp. 41–53, 2020.
- [46] F. J. Gella, T. Olivella, M. C. Pastor et al., "A simple procedure for the routine determination of aspartate aminotransferase and alanine aminotransferase with pyridoxal phosphate," *Clinica Chimica Acta*, vol. 153, no. 3, pp. 241–247, 1985.
- [47] G. Schumann, R. Bonora, F. Ceriotti et al., "IFCC primary reference procedures for the measurement of catalytic activity concentrations of enzymes at 37°C. Part 6: reference procedure for the measurement of catalytic concentration of γ -Glutamyltransferase," *Clinical Chemistry and Laboratory Medicine*, vol. 40, pp. 734–738, 2002.
- [48] G. Schumann, R. Klauke, F. Canalias et al., "IFCC primary reference procedures for the measurement of catalytic activity concentrations of enzymes at 37 °C. Part 9: reference procedure for the measurement of catalytic concentration of alkaline phosphatase International Federation of Clinical Chemistry and Laboratory Medicine (IFCC) Scientific Division, Committee on Reference Systems of Enzymes (C-RSE) (1)," *Clinical Chemistry and Laboratory Medicine*, vol. 49, no. 9, pp. 1439–1446, 2011.
- [49] A. Pesce, "Lactate dehydrogenase," in *Clinical Chemistry*, pp. 1124–2117, The CV Mosby, St Louis, Toronto, Princeton, 1984.
- [50] B. T. Dumas, W. Ard Watson, and H. G. Biggs, "Albumin standards and the measurement of serum albumin with bromocresol green," *Clinica Chimica Acta*, vol. 31, no. 1, pp. 87–96, 1971.
- [51] L. Jendrassik and P. Grof, "Colorimetric method of determination of bilirubin," *Biochemische Zeitschrift*, vol. 297, pp. 81–82, 1938.
- [52] H. G. Preuss, S. T. Jarrell, R. Scheckenbach, S. Lieberman, and R. A. Anderson, "Comparative effects of chromium, vanadium and Gymnema sylvestre on sugar-induced blood pressure elevations in SHR," *Journal of the American College of Nutrition*, vol. 17, no. 2, pp. 116–123, 1998.
- [53] E. Beutler, O. Duron, and B. M. Kelly, "Improved method for the determination of blood glutathione," *The Journal of Laboratory and Clinical Medicine*, vol. 61, pp. 882–888, 1963.
- [54] B. Matkovic, M. Sasvári, M. Kotormán, I. S. Varga, D. Q. Hai, and C. Varga, "Further prove on oxidative stress in alloxan diabetic rat tissues," *Acta Physiologica Hungarica*, vol. 85, no. 3, pp. 183–192, 1997.
- [55] S. Marklund and G. Marklund, "Involvement of the superoxide anion radical in the autoxidation of pyrogallol and a convenient assay for superoxide dismutase," *European Journal of Biochemistry*, vol. 47, no. 3, pp. 469–474, 1974.
- [56] J. D. Bancroft, A. Stevens, and D. R. Turner, *Theory and Practice of Histological Techniques*, Churchill living stone, London, UK, 4 edition, 1996.
- [57] A. F. Khafaga, A. E. Noreldin, and A. E. Taha, "The adaptogenic anti-ageing potential of resveratrol against heat stress-mediated liver injury in aged rats: role of HSP70 and NF-kB signalling," *Journal of Thermal Biology*, vol. 83, pp. 8–21, 2019.
- [58] L. Wasef, A. M. K. Nassar, Y. S. El-Sayed et al., "The potential ameliorative impacts of cerium oxide nanoparticles against fipronil-induced hepatic steatosis," *Scientific Reports*, vol. 11, no. 1, pp. 1310–1315, 2021.
- [59] O. M. Ahmed and R. R. Ahmed, "Anti-proliferative and apoptotic efficacies of ulvan polysaccharides against different types of carcinoma cells *in vitro* and *in vivo*," *Journal of Cancer Science & Therapy*, vol. 6, pp. 202–208, 2014.
- [60] O. M. Ahmed and R. R. Ahmed, "Anti-proliferative and apoptotic efficacy of diallyl disulfide on Ehrlich ascites carcinoma," *Hepatoma Research*, vol. 1, no. 2, pp. 67–74, 2015.
- [61] S. R. Galaly, O. M. Ahmed, and A. M. Mahmoud, "Thymoquinone and curcumin prevent gentamicin-induced liver injury by attenuating oxidative stress, inflammation and apoptosis," *Journal of Physiology & Pharmacology: An Official Journal of the Polish Physiological Society*, vol. 65, no. 6, pp. 823–832, 2014.
- [62] A. M. Hussein and O. M. Ahmed, "Regioselective one-pot synthesis and anti-proliferative and apoptotic effects of some novel tetrazolo [1, 5-a] pyrimidine derivatives," *Bioorganic & Medicinal Chemistry*, vol. 18, no. 7, pp. 2639–2644, 2010.
- [63] F. Varghese, A. B. Bukhari, R. Malhotra, and A. De, "IHC profiler: an open source plugin for the quantitative evaluation and automated scoring of immunohistochemistry images of human tissue samples," *PLoS One*, vol. 9, no. 5, Article ID e96801, 2014.
- [64] A. F. Khafaga, S. E. El-Kazaz, and A. E. Noreldin, "*Boswellia serrata* suppress fipronil-induced neuronal necrosis and neurobehavioral alterations via promoted inhibition of oxidative/inflammatory/apoptotic pathways," *Science of the Total Environment*, vol. 785, Article ID 147384, 2021.
- [65] A. H. El-Far, M. A. Lebda, A. E. Noreldin et al., "Quercetin attenuates pancreatic and renal D-Galactose-induced aging-related oxidative alterations in rats," *International Journal of Molecular Sciences*, vol. 21, no. 12, p. 4348, 2020.
- [66] A. M. Zaazaa, "Studying the anticancer properties of bone marrow-derived mesenchymal stem cells against hepatocellular carcinoma induced by n-nitrosodiethylamine in male rats," *Biointerface Research in Applied Chemistry*, vol. 13, no. 1, pp. 1–13, 2022.
- [67] A. Grigorian and C. B. O'Brien, "Hepatotoxicity secondary to chemotherapy," *Journal of Clinical and Translational Hepatology*, vol. 2, no. 2, pp. 95–102, 2014.
- [68] P. D. King and M. C. Perry, "Hepatotoxicity of chemotherapy," *The Oncologist*, vol. 6, no. 2, pp. 162–176, 2001.
- [69] N. Lameire, "Nephrotoxicity of recent anti-cancer agents," *Clinical Kidney Journal*, vol. 7, no. 1, pp. 11–22, 2014.
- [70] G. Miolo, N. La Mura, P. Nigri et al., "The cardiotoxicity of chemotherapy: new prospects for an old problem," *Radiology and Oncology*, vol. 40, no. 3, pp. 149–161, 2006.
- [71] K. Hayat, J. Khan, A. Khan et al., "Ameliorative effects of exogenous proline on photosynthetic attributes, nutrients uptake, and oxidative stresses under cadmium in pigeon pea (*Cajanus cajan* L.)," *Plants*, vol. 10, no. 4, p. 796, 2021.

- [72] M. Działo, J. Mierziak, U. Korzun, M. Preisner, J. Szopa, and A. Kulma, "The potential of plant phenolics in prevention and therapy of skin disorders," *International Journal of Molecular Sciences*, vol. 17, no. 2, p. 160, 2016.
- [73] O. M. Ahmed, "Natural flavonoids: chemistry, therapeutic potentials, therapeutic targets and mechanisms of actions," *Current Pharmaceutical Design*, vol. 27, no. 4, p. 455, 2021.
- [74] O. M. Ahmed, S. F. AbouZid, N. A. Ahmed, M. Y. Zaky, and H. Liu, "An up-to-date review on citrus flavonoids: chemistry and benefits in health and diseases," *Current Pharmaceutical Design*, vol. 27, no. 4, pp. 513–530, 2021.
- [75] M. Salahshoor, S. Mohamadian, S. Kakabaraei, S. Roshankhah, and C. Jalili, "Curcumin improves liver damage in male mice exposed to nicotine," *Journal of Traditional and Complementary Medicine*, vol. 6, no. 2, pp. 176–183, 2016.
- [76] T. Bai, L. H. Lian, Y. L. Wu, Y. Wan, and J. X. Nan, "Thymoquinone attenuates liver fibrosis via PI3K and TLR4 signaling pathways in activated hepatic stellate cells," *International Immunopharmacology*, vol. 15, no. 2, pp. 275–281, 2013.
- [77] D. G. Dastidar, A. Das, S. Datta et al., "Paclitaxel-encapsulated core-shell nanoparticle of cetyl alcohol for active targeted delivery through oral route," *Nanomedicine*, vol. 14, no. 16, pp. 2121–2150, 2019.
- [78] L. A. Ermolaeva, T. Y. Dubskaya, T. I. Fomina, T. V. Vetoshkina, and V. E. Gol'dberg, "Toxic effect of an antitumor drug paclitaxel on morphofunctional characteristics of the liver in rats," *Bulletin of Experimental Biology and Medicine*, vol. 145, no. 2, pp. 263–265, 2008.
- [79] M. Jiko, I. Yano, M. Okuda, and K. I. Inui, "Altered pharmacokinetics of paclitaxel in experimental hepatic or renal failure," *Pharmaceutical Research*, vol. 22, no. 2, pp. 228–234, 2005.
- [80] C. Jalili, M. Salahshoor, and S. Roshankhah, "Antioxidative properties of *Thymus vulgaris* on liver rats induced by paclitaxel," *Pharmacognosy Research*, vol. 11, no. 3, pp. 315–320, 2019.
- [81] Y. Song, H. Cai, T. Yin et al., "Paclitaxel-loaded redox-sensitive nanoparticles based on hyaluronic acid-vitamin E succinate conjugates for improved lung cancer treatment," *International Journal of Nanomedicine*, vol. 13, pp. 1585–1600, 2018.
- [82] X. Ren, B. Zhao, H. Chang, M. Xiao, Y. Wu, and Y. Liu, "Paclitaxel suppresses proliferation and induces apoptosis through regulation of ROS and the AKT/MAPK signaling pathway in canine mammary gland tumor cells," *Molecular Medicine Reports*, vol. 17, no. 6, pp. 8289–8299, 2018.
- [83] O. M. Ahmed, S. R. Abdel-Aleem, and N. M. Mossa, "Chemopreventive effect of diallyl disulphide on CCl₄-induced liver injury in albino rats," *Journal of The Egyptian-German Society of Zoology*, vol. 56A, pp. 25–62, 2008.
- [84] A. Ortega-Alonso, C. Stephens, M. I. Lucena, and R. J. Andrade, "Case characterization, clinical features and risk factors in drug-induced liver injury," *International Journal of Molecular Sciences*, vol. 17, no. 5, p. 714, 2016.
- [85] H. Choudhury, B. Gorain, R. K. Tekade, M. Pandey, S. Karmakar, and T. K. Pal, "Safety against nephrotoxicity in paclitaxel treatment: oral nanocarrier as an effective tool in preclinical evaluation with marked *in vivo* antitumor activity," *Regulatory Toxicology and Pharmacology*, vol. 91, pp. 179–189, 2017.
- [86] M. Joerger, A. D. R. Huitema, M. T. Huizing et al., "Safety and pharmacology of paclitaxel in patients with impaired liver function: a population pharmacokinetic-pharmacodynamic study," *British Journal of Clinical Pharmacology*, vol. 64, no. 5, pp. 622–633, 2007.
- [87] K. M. Field, C. Dow, and M. Michael, "Part I: liver function in oncology: biochemistry and beyond," *The Lancet Oncology*, vol. 9, no. 11, pp. 1092–1101, 2008.
- [88] X. Yao, X. Wang, H. Han, Q. Duan, U. Khan, and Y. Hu, "Changes of serum albumin level and systemic inflammatory response in inoperable non-small cell lung cancer patients after chemotherapy," *Journal of Cancer Research and Therapeutics*, vol. 10, no. 4, pp. 1019–1023, 2014.
- [89] J. E. Okokon, J. O. Simeon, and E. E. Umoh, "Hepatoprotective activity of the extract of *Homalium letestui* stem against paracetamol-induced liver injury," *Avicenna Journal of Phytomedicine*, vol. 7, no. 1, pp. 27–36, 2017.
- [90] D. Karaduman, B. Eren, and O. N. Keles, "The protective effect of beta-1, 3-D-glucan on taxol-induced hepatotoxicity: a histopathological and stereological study," *Drug and Chemical Toxicology*, vol. 33, no. 1, pp. 8–16, 2010.
- [91] S. O. Rabah, S. S. Ali, S. M. Alsagoff, and N. N. Ayuob, "Acute taxol toxicity: the effects on bone marrow mitotic index and the histology of mice hepatocytes," *Journal of Applied Animal Research*, vol. 38, no. 2, pp. 201–207, 2010.
- [92] W. G. Hozayen, H. S. Abou Seif, and S. Amin, "Protective effects of rutin and/or hesperidin against doxorubicin-induced hepatotoxicity," *International Journal of Clinical Nutrition*, vol. 2, no. 1, pp. 11–17, 2014.
- [93] E. Turk, F. M. Kandemir, S. Yildirim, C. Caglayan, S. Kucukler, and M. Kuzu, "Protective effect of hesperidin on sodium arsenite-induced nephrotoxicity and hepatotoxicity in rats," *Biological Trace Element Research*, vol. 189, no. 1, pp. 95–108, 2019.
- [94] N. O. Al-Harbi, F. Imam, M. M. Al-Harbi et al., "Rutin inhibits carfilzomib-induced oxidative stress and inflammation via the NOS-mediated NF- κ B signaling pathway," *Inflammopharmacology*, vol. 27, no. 4, pp. 817–827, 2019.
- [95] N. S. El-Shenawy, "Effects of insecticides fenitrothion, endosulfan and abamectin on antioxidant parameters of isolated rat hepatocytes," *Toxicology in Vitro*, vol. 24, no. 4, pp. 1148–1157, 2010.
- [96] A. Yardim, C. Gur, S. Comakli et al., "Investigation of the effects of berberine on bortezomib-induced sciatic nerve and spinal cord damage in rats through pathways involved in oxidative stress and neuro-inflammation," *NeuroToxicology*, vol. 89, pp. 127–139, 2022.
- [97] G. I. Harisa, "Blood viscosity as a sensitive indicator for paclitaxel induced oxidative stress in human whole blood," *Saudi Pharmaceutical Journal*, vol. 23, no. 1, pp. 48–54, 2015.
- [98] C. Gur, O. Kandemir, and F. M. Kandemir, "Investigation of the effects of hesperidin administration on abamectin-induced testicular toxicity in rats through oxidative stress, endoplasmic reticulum stress, inflammation, apoptosis, autophagy, and JAK2/STAT3 pathways," *Environmental Toxicology*, vol. 37, no. 3, pp. 401–412, 2022.
- [99] T. Zhou, X. Luo, C. Yu et al., "Transcriptome analyses provide insights into the expression pattern and sequence similarity of several taxol biosynthesis-related genes in three *Taxus* species," *BMC Plant Biology*, vol. 19, no. 1, pp. 33–10, 2019.
- [100] R. Huang, Z. Shi, L. Chen, Y. Zhang, J. Li, and Y. An, "Rutin alleviates diabetic cardiomyopathy and improves cardiac function in diabetic ApoE knockout mice," *European Journal of Pharmacology*, vol. 814, pp. 151–160, 2017.

- [101] J. Yang, J. Guo, and J. Yuan, "In vitro antioxidant properties of rutin," *LWT--Food Science and Technology*, vol. 41, no. 6, pp. 1060–1066, 2008.
- [102] J. M. Choi, B. S. Yoon, S. K. Lee, J. K. Hwang, and R. Ryang, "Antioxidant properties of neohesperidin dihydrochalcone: inhibition of hypochlorous acid-induced DNA strand breakage, protein degradation, and cell death," *Biological and Pharmaceutical Bulletin*, vol. 30, no. 2, pp. 324–330, 2007.
- [103] K. B. Kalpana, M. Srinivasan, and V. P. Menon, "Evaluation of antioxidant activity of hesperidin and its protective effect on H₂O₂ induced oxidative damage on pBR322 DNA and RBC cellular membrane," *Molecular and Cellular Biochemistry*, vol. 323, no. 1-2, pp. 21–29, 2009.
- [104] F. M. Kandemir, M. Ileriturk, and C. Gur, "Rutin protects rat liver and kidney from sodium valproate-induced damage by attenuating oxidative stress, ER stress, inflammation, apoptosis and autophagy," *Molecular Biology Reports*, vol. 49, no. 7, pp. 6063–6074, 2022.
- [105] M. M. Abdel-Daim and R. H. Abdou, "Protective effects of diallyl sulfide and curcumin separately against thallium-induced toxicity in rats," *Cell Journal (Yakhteh)*, vol. 17, no. 2, pp. 379–388, 2015.
- [106] A. E. Elhelaly, G. AlBasher, S. Alfarraj et al., "Protective effects of hesperidin and diosmin against acrylamide-induced liver, kidney, and brain oxidative damage in rats," *Environmental Science and Pollution Research*, vol. 26, no. 34, pp. 35151–35162, 2019.
- [107] A. H. El-Far, K. Godugu, A. E. Noreldin et al., "Thymoquinone and costunolide induce apoptosis of both proliferative and doxorubicin-induced-senescent colon and breast cancer cells," *Integrative Cancer Therapies*, vol. 20, 2021.
- [108] A. Yardim, F. M. Kandemir, S. Çomaklı et al., "Protective effects of curcumin against paclitaxel-induced spinal cord and sciatic nerve injuries in rats," *Neurochemical Research*, vol. 46, no. 2, pp. 379–395, 2021.
- [109] R. T. Penson, K. Kronish, Z. Duan et al., "Cytokines IL-1beta, IL-2, IL-6, IL-8, MCP-1, GM-CSF and TNFalpha in patients with epithelial ovarian cancer and their relationship to treatment with paclitaxel," *International Journal of Gynecological Cancer*, vol. 10, no. 1, pp. 33–41, 2000.
- [110] L. Pusztai, T. R. Mendoza, J. M. Reuben et al., "Changes in plasma levels of inflammatory cytokines in response to paclitaxel chemotherapy," *Cytokine*, vol. 25, no. 3, pp. 94–102, 2004.
- [111] N. C. M. P. D. Tsavaris, C. Kosmas, M. Vadiaka, P. Kanelopoulos, and D. Boulamatsis, "Immune changes in patients with advanced breast cancer undergoing chemotherapy with taxanes," *British Journal of Cancer*, vol. 87, no. 1, pp. 21–27, 2002.
- [112] K. A. Sullivan, C. V. Grant, K. R. Jordan, S. S. Vickery, and L. M. Pyter, "Voluntary wheel running ameliorates select paclitaxel chemotherapy-induced sickness behaviors and associated melanocortin signaling," *Behavioural Brain Research*, vol. 399, Article ID 113041, 2021.
- [113] G. Sethi, M. K. Shanmugam, L. Ramachandran, A. P. Kumar, and V. Tergaonkar, "Multifaceted link between cancer and inflammation," *Bioscience Reports*, vol. 32, no. 1, pp. 1–15, 2012.
- [114] C. R. Gardner, J. D. Laskin, D. M. Dambach et al., "Reduced hepatotoxicity of acetaminophen in mice lacking inducible nitric oxide synthase: potential role of tumor necrosis factor- α and interleukin-10," *Toxicology and Applied Pharmacology*, vol. 184, no. 1, pp. 27–36, 2002.
- [115] O. M. Ahmed, H. I. Fahim, H. Y. Ahmed et al., "The preventive effects and the mechanisms of action of navel Orange Peel Hydroethanolic extract, naringin, and naringenin in N-Acetyl- p-aminophenol- induced liver injury in Wistar rats," *Oxidative Medicine and Cellular Longevity*, vol. 2019, Article ID 2745352, 19 pages, 2019.
- [116] O. M. Ahmed, H. Ebaïd, E.-S. El-Nahass, M. Ragab, and I. M. Alhazza, "Nephroprotective effect of *Pleurotus ostreatus* and *Agaricus bisporus* extracts and carvedilol on ethylene glycol-induced urolithiasis: roles of NF- κ B, p53, Bcl-2, Bax and Bak," *Biomolecules*, vol. 10, no. 9, p. 1317, 2020.
- [117] B. E. Jones, C. R. Lo, H. Liu et al., "Hepatocytes sensitized to tumor necrosis factor- α cytotoxicity undergo apoptosis through caspase-dependent and caspase-independent pathways," *Journal of Biological Chemistry*, vol. 275, no. 1, pp. 705–712, 2000.
- [118] A. L. Blajeski, T. J. Kottke, and S. H. Kaufmann, "A multistep model for paclitaxel-induced apoptosis in human breast cancer cell lines," *Experimental Cell Research*, vol. 270, no. 2, pp. 277–288, 2001.
- [119] Z. Pan, A. Avila, and L. Gollahon, "Paclitaxel induces apoptosis in breast cancer cells through different calcium-regulating mechanisms depending on external calcium conditions," *International Journal of Molecular Sciences*, vol. 15, no. 2, pp. 2672–2694, 2014.
- [120] S. V. Bava, V. T. Puliappadamba, A. Deepti, A. Nair, D. Karunakaran, and R. J. Anto, "Sensitization of taxol-induced apoptosis by curcumin involves down-regulation of nuclear factor- κ B and the serine/threonine kinase Akt and is independent of tubulin polymerization," *Journal of Biological Chemistry*, vol. 280, no. 8, pp. 6301–6308, 2005.
- [121] Y. P. Dang, X. Y. Yuan, R. Tian, D. G. Li, and W. Liu, "Curcumin improves the paclitaxel-induced apoptosis of HPV-positive human cervical cancer cells via the NF- κ B-p53-caspase-3 pathway," *Experimental and Therapeutic Medicine*, vol. 9, no. 4, pp. 1470–1476, 2015.
- [122] C. Li and H. Schluesener, "Health-promoting effects of the citrus flavanone hesperidin," *Critical Reviews in Food Science and Nutrition*, vol. 57, no. 3, pp. 613–631, 2017.
- [123] O. Ahmed, H. Fahim, A. Mahmoud, and E. Ahmed, "Bee venom and hesperidin effectively mitigate complete Freund's adjuvant-induced arthritis via immunomodulation and enhancement of antioxidant defense system," *Archives of Rheumatology*, vol. 33, no. 2, pp. 198–212, 2018.
- [124] R. A. Hassan, W. G. Hozayen, H. T. Abo Sree, H. M. Al-Muzafar, K. A. Amin, and O. M. Ahmed, "Naringin and hesperidin counteract diclofenac-induced hepatotoxicity in male Wistar rats via their antioxidant, anti-inflammatory, and antiapoptotic activities," *Oxidative Medicine and Cellular Longevity*, vol. 2021, Article ID 9990091, 14 pages, 2021.
- [125] O. M. Ahmed, M. H. Elkomy, and H. I. Fahim, "Rutin and quercetin counter doxorubicin-induced liver toxicity in Wistar rats via their modulatory effects on inflammation, oxidative stress, apoptosis, and Nrf2," *Oxidative Medicine and Cellular Longevity*, vol. 2022, Article ID 2710607, 19 pages, 2022.
- [126] C. C. Lee, S. R. Shen, Y. J. Lai, and S. C. Wu, "Rutin and quercetin, bioactive compounds from tartary buckwheat, prevent liver inflammatory injury," *Food & Function*, vol. 4, no. 5, pp. 794–802, 2013.
- [127] S. E. Park, K. Sapkota, J. H. Choi et al., "Rutin from *Dendropanax moribifera* Leveille protects human dopaminergic cells against rotenone induced cell injury through inhibiting JNK and p38 MAPK signaling," *Neurochemical Research*, vol. 39, no. 4, pp. 707–718, 2014.

- [128] H. Yoo, S. K. Ku, Y. D. Baek, and J. S. Bae, "Anti-inflammatory effects of rutin on HMGB1-induced inflammatory responses *in vitro* and *in vivo*," *Inflammation Research*, vol. 63, no. 3, pp. 197–206, 2014.
- [129] A. Khalil, B. H. Elesawy, T. M. Ali, and O. M. Ahmed, "Bee venom: from venom to drug," *Molecules*, vol. 26, no. 16, p. 4941, 2021.

Research Article

Ginsenosides Rg1 and CK Control Temozolomide Resistance in Glioblastoma Cells by Modulating Cholesterol Efflux and Lipid Raft Distribution

Runze Qiu ¹, Jingjing Zhang ¹, Chun Ge ^{1,2}, Yue Zhong ³, Suo Liu ², Qingquan Li ⁴,
Jianjun Zou ^{1,2}, Hongwei Fan ^{1,2} and Yingbin Li ⁴

¹Department of Clinical Pharmacology Lab, Nanjing First Hospital, Nanjing Medical University, Nanjing 210006, China

²Department of Pharmacy, School of Basic Medicine and Clinical Pharmacy, China Pharmaceutical University, Nanjing 210009, China

³Center of Drug Discovery, State Key Laboratory of Natural Medicines, China Pharmaceutical University, Nanjing 210009, China

⁴Department of Neurosurgery, The Second Affiliated Hospital of Nanjing Medical University, Nanjing 210011, China

Correspondence should be addressed to Hongwei Fan; fanhongwei178@njmu.edu.cn and Yingbin Li; yingbinli65@sina.com

Runze Qiu and Jingjing Zhang contributed equally to this work.

Received 30 May 2022; Revised 16 August 2022; Accepted 26 August 2022; Published 10 October 2022

Academic Editor: Mohammed El-Magd

Copyright © 2022 Runze Qiu et al. This is an open access article distributed under the Creative Commons Attribution License, which permits unrestricted use, distribution, and reproduction in any medium, provided the original work is properly cited.

Background. Cholesterol efflux and lipid raft redistribution contribute to attenuating temozolomide resistance of glioblastoma. Ginsenosides are demonstrated to modify cholesterol metabolism and lipid raft distribution, and the brain distribution and central nervous effects of whose isoforms Rb1, Rg1, Rg3, and CK have been identified. This study aimed to reveal the role of Rb1, Rg1, Rg3, and CK in the drug resistance of glioblastoma. **Methods.** The effects of ginsenosides on cholesterol metabolism in temozolomide-resistant U251 glioblastoma cells were evaluated by cholesterol content and efflux assay, confocal laser, qRT-PCR, and Western blot. The roles of cholesterol and ginsenosides in temozolomide resistance were studied by CCK-8, flow cytometry, and Western blot, and the mechanism of ginsenosides attenuating resistance was confirmed by inhibitors. **Results.** Cholesterol protected the survival of resistant U251 cells from temozolomide stress and upregulated multidrug resistance protein (MDR)1, which localizes in lipid rafts. Resistant cells tended to store cholesterol intracellularly, with limited cholesterol efflux and LXR α expression to maintain the distribution of lipid rafts. Ginsenosides Rb1, Rg1, Rg3, and CK reduced intracellular cholesterol and promoted cholesterol efflux in resistant cells, causing lipid rafts to accumulate in specific regions of the membrane. Rg1 and CK also upregulated LXR α expression and increased the cytotoxicity of temozolomide in the presence of cholesterol. We further found that cholesterol efflux induction, lipid raft redistribution, and temozolomide sensitization by Rg1 and CK were induced by stimulating LXR α . **Conclusions.** Ginsenosides Rg1 and CK controlled temozolomide resistance in glioblastoma cells by regulating cholesterol metabolism, which are potential synergists for temozolomide therapy.

1. Introduction

Glioblastoma (GBM) is the most frequent and most malignant (WHO IV) central nervous system (CNS) tumor. According to the latest statistics [1], the proportion was 54.4% among CNS tumor patients ≥ 20 years old, which rises with age. In the past 40 years, the treatment of GBM has not made significant progress, and the 5-year survival rate of

patients has only increased from 4% to 7%. DNA alkylating agent temozolomide (TMZ) is the first-line drug for GBM, used in conjunction with radiotherapy and further adjuvant therapy after maximal safe surgical resection [2]. It has completed oral absorption, depressed plasma protein binding, metabolism not affected by liver and kidney status, and easy penetration of the blood-brain barrier (BBB) [3]. Nonetheless, drug resistance developed in about half of the

patients [4]. They relapsed within 6 months of TMZ standard treatment and had to start a second-line treatment with deficient standards, higher toxicity, and less benefit [5]. O6-methylguanine-DNA methyltransferase (MGMT) and drug efflux transporters such as multidrug resistance protein 1 (MDR1, also known as ATP-binding cassette (ABC)B1 or P-glycoprotein) and ABCG2, are still independent risk factors for TMZ resistance [6–8]. Strategies to address resistance need to be established.

In traditional medicine, the herbs of the *Panax* genus, *Araliaceae*, including ginseng (*Panax ginseng* C.A. Mey.), American ginseng (*Panax quinquefolius* L.), and pseudoginseng (*Panax notoginseng* (Burkill) F.H. Chen), which can “nourish vitality” and “disperse stasis” [9], were used to combat the pathogenesis of glioma [10]. They exhibited therapeutic activities against tumors including GBM and have been commonly used in East Asia as adjuvant drugs [10, 11]. Ginsenosides containing numerous subtypes (Figure 1) are active ingredients with high content in *Panax* genus [11], and their saponin structure makes them amphipathic and BBB permeability, which have been confirmed by generally reported CNS effects. For instance, the oral pharmacokinetics of total ginsenosides indicated high concentrations of subtype Rg1 and compound K (CK) in brain tissues [12, 13]. Rb1, the precursor of CK, can enter the brain through glucose transporter member 1 (GLUT1) [14]. Moreover, Rg3 was identified to attenuate the TMZ resistance of GBM *in vivo* and *in vitro* [15].

As the most cholesterol-rich organ [16], the brain provides a unique microenvironment for GBM. GBM cells not only retain the ability of glial cells to synthesize cholesterol *de novo* but also increase cholesterol uptake mediated by low-density lipoprotein receptor (LDLR) [17]. Stimulating the liver X receptor (LXR) to promote ABCA1-mediated cholesterol efflux and degradation of LDLR induced GBM cell death [18–20]. It seems that the enormous demand for cholesterol from GBM cells is not just for the production of organelles. The increase in cholesterol and LDL levels promotes resistance of various tumors to chemotherapy, and it is also an independent risk factor for poor prognosis of GBM under standard TMZ treatment [21, 22]. Although cholesterol-induced drug resistance has not been confirmed in CNS tumors, elevated cholesterol in malignant ascites was proved to induce chemotherapy resistance by upregulating the drug efflux proteins ABCG1 and MDR1 [23]. MDR1 is located and stably expressed in lipid rafts composed of cholesterol, sphingolipid, and proteins on the plasma membrane [24]. When lipid rafts were induced to accumulate in specific parts of the membrane, MDR1 expression was confined, and tumor cells were less resistant [25]. Moreover, additionally added cholesterol restored the homogenous (broad and low-density) distribution of lipid rafts and upregulated MDR1 [25]. Conversely, lipid rafts were depleted when cholesterol was scavenged, and chemotherapy resistance was correspondingly diminished [26].

Both ginsenosides and cholesterol have steroid core structures (Figure 1), and ginsenosides can regulate cholesterol metabolism in tumor cells. Rg3 and CK hindered cholesterol synthesis by inhibiting β -hydroxy-

β -methylglutaryl coenzyme A (HMG-CoA) [27, 28], and CK also promoted cholesterol efflux by stimulating LXR α [29, 30] to synergistically decrease intracellular cholesterol. Rh2 revealed lipid raft depleting activity [31, 32]. More direct evidence indicates that the ginsenoside derivative Rp1 decreased MDR1 activity by redistributing lipid rafts and attenuated the cholesterol-dependent resistance [25]. Consequently, ginsenosides are potential agents for the treatment of tumor resistance as regulators of cellular cholesterol metabolism. However, the differential roles of ginsenoside subtypes that govern cholesterol metabolism and drug resistance in CNS tumors remain undisclosed. In this study, we certified the role of cholesterol in TMZ resistance of glioblastoma U251 cells and investigated the effects of several ginsenosides with BBB penetration on TMZ resistance of U251 cells in the presence of cholesterol. We further studied the roles of ginsenosides on cholesterol metabolism and lipid raft distribution and the mechanisms controlling TMZ resistance. Our work suggests that ginsenosides Rg1 and CK are potential drugs to control TMZ resistance, providing references for adjuvant therapy of GBM.

2. Materials and Methods

2.1. Chinese Glioma Genome Atlas (CGGA) RNA-seq Analysis. From the CGGA database (<https://www.cgga.org.cn/>, China), which is a professional clinical transcriptome database of glioma, the mRNA-seq_693 dataset [33] was downloaded to attain the clinical information and sequencing data of samples. Among the 693 glioma patients, those who were known to be ≥ 18 years old, diagnosed with WHO grades III to IV, and treated by TMZ were screened. To eliminate the interference from the data of surviving patients with a short observation period, we excluded the surviving patients with less than 6 months of overall survival (OS). The mRNA-seq data were used to evaluate the correlation between OS, tumor tissue MGMT methylation status, fragments per kilobase transcriptome per million (FPKM) fragments of drug resistance gene *MDR1*, and FPKM of cholesterol metabolism genes including *LDLR*, *SREBF2*, *HMGCR*, *NRIH3*, *ABCA1*, and *ABCG1* via the Pearson correlation test.

2.2. Cell Culture, Resistance Induction, and Treatment. U251 human GBM cells (U251 MG, KeyGEN, #KG050) were cultured in high-glucose DMEM (KeyGEN, #KGM12800-500) containing penicillin, streptomycin, and fetal bovine serum (Gibco, #30044333), with a constant ambient temperature of 37°C, saturated humidity, and 5% CO₂. After stable growth, the TMZ-resistant U251 cells were induced by the dose escalation [34]. The escalating doses of TMZ (MCE, #HY-17364) were 0.645, 1.29, 2.58, 5.16, 10.32, 20.64, 41.28, and 82.56 μ M. When the cells treated with the previous dose had grown to a confluency >50% and were stably passaged 2–3 times, the treatment was continued with the next dose. Induction of TMZ resistance was accomplished when cells were stably grown at 82.56 μ M TMZ. The Jiangsu KeyGEN BioTECH was commissioned to identify

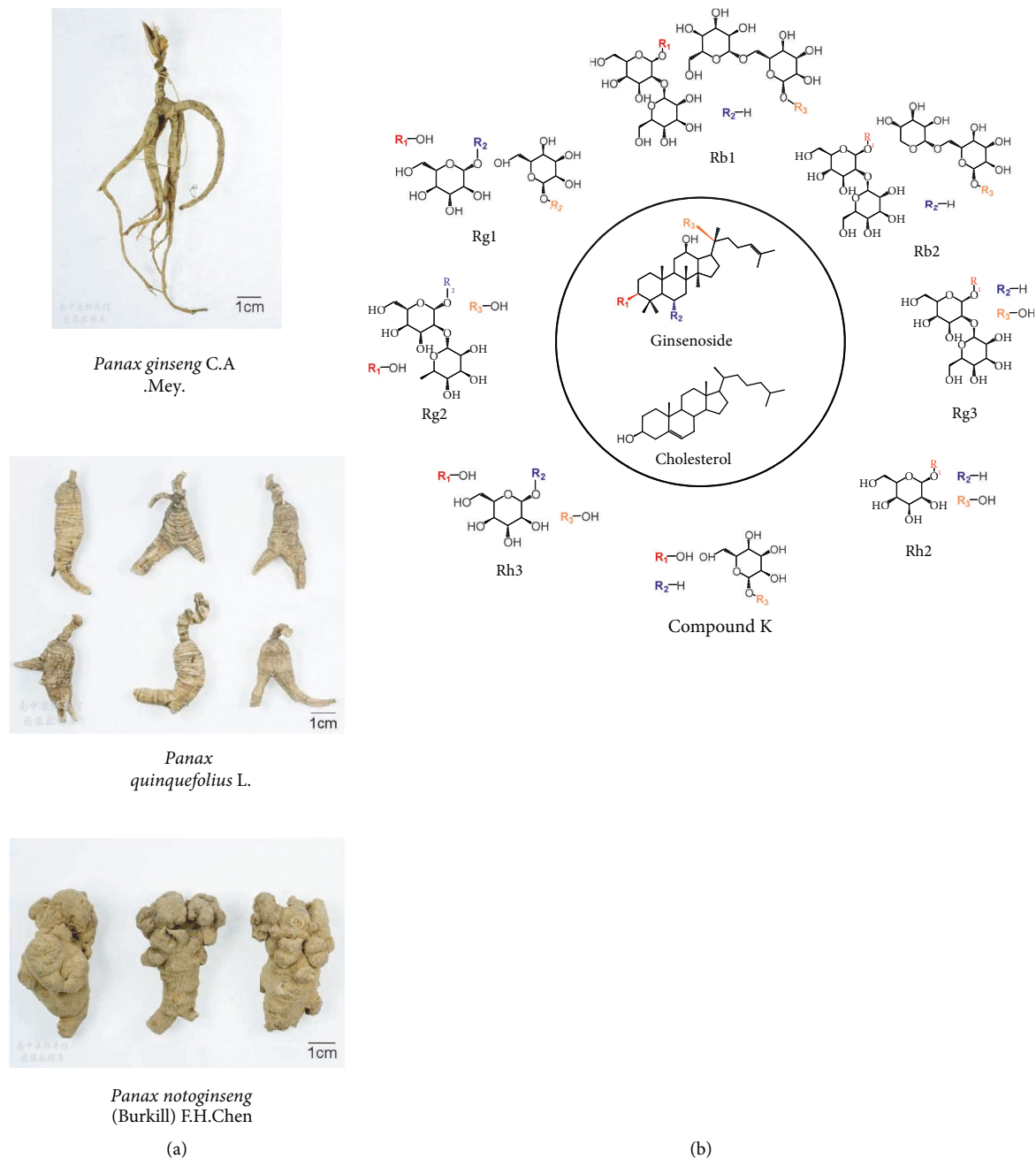


FIGURE 1: *Acanthaceae*, *Panax* genus, and ginsenosides. (a) The photographs of 3 representative *Panax* genus plants from the Chinese medicine specimen center of Nanjing University of Chinese Medicine (<https://zybb.njucm.edu.cn/>). (b) The structure of ginsenosides and cholesterol. The core steroid structure of ginsenosides is similar to cholesterol.

the genetic stability of the constructed TMZ-resistant cells by comparing the alleles on short tandem repeat (STR) and Amelogenin locus of the resistant cells with the data of parental U251 cells (Supplementary Figures S1 and Table S1). TMZ-resistant and wild-type U251 cells were treated with 0.78, 1.56, 3.13, 6.25, 12.5, 25, 25, 50, and 100 μM TMZ with DMSO as a control, and IC_{50} and resistance index were calculated by Cell Counting Kit (CCK)-8 (KeyGEN, #KGA317).

Cells were collected when rapidly grown to 60–80% density after passaging and treated with 5 $\mu\text{g}/\text{ml}$ cholesterol

(dissolved in anhydrous ethanol, Solarbio, #C8280) for 24 h depending on the grouping needs, and an equal volume of anhydrous ethanol was used as control. After the cells were washed, 200 μM TMZ was added to continue treatment for 72 h, and an equal volume of DMSO was used as the control. Referring to the dose reported in GBM cells [15], 100 μM ginsenosides Rb1 (Yuanye, #B21050), Rg1 (Yuanye, #B2105), Rg3 (Yuanye, #B21059), and CK (Yuanye, #B21045), and 100 nM LXR inhibitor GSK2033 (MCE, #HY-108688) were used to treat cells alone or concurrently with TMZ for 72 h, with an equal volume of DMSO as the control.

2.3. Cell Proliferation and Cytotoxicity Assay. The cells were cultured in 96-well plates and treated according to the above protocol. CCK-8 reagent (KeyGEN, #KGA317) was added in plates 3 h before the end of administration, and the cells continued to incubate in the original culture environment. After 3 h, the plates were shaken and placed into the microplate reader (BioTek ELx800, USA), and the optical density (OD) value was read at 450 nm to calculate the inhibition rate. Inhibition rate = $(1 - \text{OD}_{\text{Test well}} / \text{OD}_{\text{Control well}}) \times 100\%$.

2.4. Flow Cytometry for Apoptosis and Cell Cycle Analysis. After 72 h of administration, cells were digested and collected with 0.25% EDTA-free trypsin (KeyGEN, #KGM27250), washed, and resuspended with PBS containing 2% BSA. Annexin V-FITC Apoptosis Detection Kit (KeyGEN, #KGA105) and Cell Cycle Detection Kit (KeyGEN, #KGA511) were used for flow cytometry. For apoptosis staining, cells were mixed with Annexin V-FITC and propidium iodide (PI) reagents and were incubated for 10 min at room temperature in the dark. After fixation in 70% cold ethanol at 4°C for 12 h, PI containing RNase A was added into the resuspended cells for 45 min at room temperature in the dark for cell cycle assay. Flow cytometer (Beckman Coulter CytoFLEX, USA) was used to detect FITC and PI. Annexin V⁺ populations were considered as apoptotic cells, including PI⁻ early apoptotic cells and PI⁺ late apoptotic cells. The flow cytometry data were processed by FlowJo vX.0.7 (BD, USA) to evaluate apoptosis and cell cycle.

2.5. Western Blotting for Protein Expression. The total cell protein was extracted with cold RIPA lysis buffer containing phenylmethylsulfonyl fluoride (PMSF) (Whole Cell Lysis Assay Kit, KeyGEN, #KGP250). The protein concentration of the extracts was determined by BCA Protein Quantitation Assay Kit (KeyGEN, #KGP902) using a microplate reader. Then, SDS-PAGE loading buffer (KeyGEN, #KGP101) was added to denature the protein at 100°C in thermostat. The prepared protein samples and prestained protein mass marker (KeyGEN, #KGM441) were added to a 10% SDS-polyacrylamide gel with equal mass for electrophoresis (Bio-Rad Power Supplies Basic, USA). Then, the protein transfer system (Bio-Rad Trans-Blot Turbo, USA) was used to transfer the separated proteins from the gel to a polyvinylidene fluoride (PVDF) membrane, and 5% skim milk was used to eliminate nonspecific binding. Under the instruction of the prestained marker, the PVDF membranes were cut according to the protein mass and were incubated with primary antibodies overnight in a shaker at 4°C, including rabbit monoclonal to MGMT (Abcam, #ab108630, dilution ratio 1:1000), rabbit monoclonal to P glycoprotein (MDR1, Abcam, #ab168337, dilution ratio 1:1000), rabbit monoclonal to LXR α (Abcam, #ab176323, dilution ratio 1:2000), and mouse monoclonal to GAPDH (Abcam, #ab8245, dilution ratio 1:2000). After washing the PVDF membranes combined with primary antibodies, goat anti-rabbit IgG-HRP (for rabbit antibody, KeyGEN, #KGAA35, dilution ratio 1:10000) or goat anti-mouse IgG-HRP (for mouse antibody, KeyGEN, #KGAA37, dilution ratio 1:

10000) was added to continue incubating. The electrochemiluminescence reagent (KeyGEN, #KGP1121) was dripped on the PVDF membrane after antibody labeling, and a gel imaging system (Syngene G:BOX Chemi XR5, UK) was used to photograph the blots. The raw images of the immunoblot bands are presented in Supplementary Figure S2. The images were subjected to background removal and gray value (integrated density) determination via ImageJ 1.51j8 (National Institutes of Health, USA). The integrated density of (sample target blot/control target blot)/(sample GAPDH blot/control GAPDH blot) was considered as the relative expression of the target proteins.

2.6. Cholesterol Content Detection. Free cholesterol in the collected cells was removed by centrifugation. BCA Protein Quantitation Assay Kit (KeyGEN, #KGP902) was used to determine protein concentration. Cells were treated with isopropanol and sonicated in the ice bath to prepare cell lysates. The total cholesterol content detection kit (Solarbio, #BC1985) was used to detect the cholesterol concentration in the lysates. The samples, standard, and control solutions were treated with a reaction solution containing cholesterol ester hydrolase, cholesterol oxidase, and peroxidase at 37°C for 15 min, and OD values at 500 nm were measured with a microplate reader (MD SpectraMax M3, USA). After subtracting the OD value of the blank wells, the total cholesterol concentrations of the samples were calculated by the standard curve, and the total cholesterol concentration/protein concentration was calculated as the total cholesterol content.

2.7. Cholesterol Efflux Assay. For cholesterol tracking, 10 $\mu\text{g}/\text{mL}$ 25-NBD cholesterol (Sigma-Aldrich, #810250P) was added to the cells in serum-free medium. After 24 h, the 25-NBD cholesterol that had not entered the cell was washed away. 6h before the end of drug treatment, 1 mM sodium taurocholate (NaTC, Solarbio, #YZ-110815) was added as a receptor for ABCA1-mediated cholesterol efflux, which acts similarly to apolipoprotein A-I [35, 36]. After 6 h, the culture supernatant and pelleted cells were collected separately. Cells were lysed by 0.1 M NaOH for 30 min. The entire process was protected from light. A fluorescence microplate reader (BioTek ELx800, USA) was used to measure the fluorescence intensity (FI) at 469/537 nm of Abs/Em, and the cholesterol efflux rate was calculated. Cholesterol efflux rate = $(\text{FI}_{\text{supernatant}} / (\text{FI}_{\text{supernatant}} + \text{FI}_{\text{cell}})) \times 100\%$.

2.8. Lipid Raft Labeling and Confocal Laser Scanning. After the cells were fixed with 4% formaldehyde for 15 min at 4°C, the Vybrant Alexa Fluor 594 Lipid Raft Labeling Kit (Invitrogen, #V34405) was used to label lipid rafts by cholera toxin subunit B (CT-B). After incubating with Alexa Fluor 594-conjugated CT-B for 10 min at 4°C, the cells were centrifuged and resuspended in anti-CT-B antibody solution and kept at 4°C for 15 min in the dark. After lipid raft labeling, the cells were washed and treated with 4',6-diamidino-2-phenylindole (DAPI, KeyGEN, #KGA215-50) for 10 min to stain the nucleus.

After washing, cells were resuspended in cold PBS and photographed using a confocal laser scanning microscope (Olympus FV3000, Japan) at Ex/Em = 594/618 nm for Alexa Fluor 594 and Ex/Em = 359/461 nm for DAPI.

2.9. Quantitative Real-Time PCR (qRT-PCR) for mRNA Expression. Total cell RNA was extracted with TRIzol reagent (Invitrogen, #15596–026). RNA concentration (OD260) and purity (OD260/280) were determined by UV spectrophotometer (Shimadzu UV-2450, Japan), and RNA with satisfactory purity (OD260/280 1.8–2.1) was quantified to 200 ng/ μ l. RT Master Mix (Takara, #RR036B) reagent and thermal cycler (ABI Veriti, USA) were used to reverse transcribe the RNA samples into cDNA. cDNA samples, primers, and PCR Master Mix containing SYBR Green (Takara, #RR086B) were added to the PCR plate to detect the Ct values (amplification cycles) of *SREBF2*, *NRIH3*, *ABCA1*, and *GAPDH* mRNA through a qRT-PCR system (ABI StepOnePlus, USA). The relative expression of target mRNAs was calculated as $2^{-\Delta\Delta Ct}$ $\{\Delta\Delta Ct = (Ct(\text{target RNA in sample well}) - Ct(\text{GAPDH in sample well})) - (Ct(\text{target RNA in control well}) - Ct(\text{GAPDH in control well}))\}$. The primers (Table 1) were designed by KeyGEN BioTECH (China) using Primer 6.0 (Premier, Canada) and purified by PAGE. The amplification efficiency of primers was detected by cDNA standards prepared from U251 cells. The total RNA of U251 cells was quantified to 80 ng/ μ l and mixed with a Total-Transcriptome cDNA Synthesis Reagent (ABM, #G904) for reverse transcription by a thermal cycler (Bio-Rad C1000 Touch, USA), and five 10-fold concentration gradient cDNA standards were prepared. A qRT-PCR system (ABI QuantStudio 5, USA) was used to detect Ct values of cDNA standards after mixing with primers and BlasTaq 2X qPCR MasterMix Reagent (ABM, #G891). Linear regression was executed according to the gene copies and Ct values of the standards, and the amplification efficiency (E) was calculated by the slope, $E = (10^{-1/\text{slope}} - 1) \times 100\%$ (Table 1, Supplementary Figure S3).

2.10. Statistics and Graphs. GraphPad Prism 8.3.0 (GraphPad Software, USA) was used to perform statistical tests and data graphing. The RNA-seq data from CGGA were analyzed by the two-way ANOVA, Person correlation test, linear regression, and residual test. To calculate IC_{50} , a variable slope nonlinear regression was performed. Other data were analyzed by the one-way ANOVA and passed the Brown–Forsythe test of variance homogeneity. $P < 0.05$ was considered statistically significant.

3. Results

3.1. Cholesterol Promoted the Resistance of GBM Cells to TMZ. We first analyzed the correlation between drug resistance and cholesterol metabolism through the CGGA database. By comparing the levels of cholesterol metabolism genes in high-grade glioma (HGG, WHO III-IV) tissues of patients receiving TMZ therapy with OS less than half a year and 5 years (Supplementary Figure S4(a)), we found that the level of *NRIH3* (transcribing *LXR α*) mRNA that mediates

cholesterol efflux in patients with longer survival is higher than that with shorter survival. The clinical response of GBM patients to TMZ is related to the methylation status of *MGMT* and the expression of *MDR1* [6, 8], but the levels of cholesterol metabolism genes displayed a correlation with *MDR1* expression rather than *MGMT* methylation (Supplementary Figures S4(b) and S4(c)). *LDLR* that mediates cholesterol uptake and *SREBF2* and *HMGCR* that mediate cholesterol synthesis were positively correlated with the level of *MDR1*, and *NRIH3* that mediates cholesterol release was negatively correlated. These findings imply that cholesterol is related to *MDR1*-related TMZ resistance and the prognosis of GBM patients.

To explore whether cholesterol affects the TMZ resistance of GBM cells, we induced TMZ-resistant U251 GBM cells (resistance index = 8.784, Supplementary Figure S5 and Table S2). The levels of viable wild-type and resistant cells were similar, and TMZ inhibited the survival of both cell lineages, but the inhibition of TMZ on the resistant cells was considerably weaker than wild type (Figure 2(a)). The reaction of resistant strains to TMZ was further attenuated after cholesterol addition and was even comparable to that of the untreated resistant strains (Figure 2(b)). We further verified the protective effects of cholesterol on resistant U251 cells from TMZ pressure through flow cytometry. Compared with Annexin V⁺ apoptosis cells generally induced by TMZ in wild-type U251 cells (Figures 2(c) and 2(d)), including PI⁻ early apoptosis and PI⁺ late apoptosis, the level of apoptosis in resistant strains was moderate. The addition of cholesterol decreased apoptotic resistant cells in each phase, which was similar to untreated resistant cells. As a non-cell cycle-specific drug, TMZ displayed a slight effect on the cell cycle (Figures 2(e) and 2(f)). We only observed the shortening of S phase in wild-type cells, while cholesterol showed no further effect on the cell cycle. The above results demonstrated that cholesterol supports TMZ resistance of U251 cells.

As the most cholesterol-rich organ [16], the brain provides a unique microenvironment for GBM. GBM cells not only retain the ability of glial cells to synthesize cholesterol de novo but also increase cholesterol uptake mediated by low-density lipoprotein receptor (*LDLR*) [17]. Stimulating the liver X receptor (*LXR*) to promote *ABCA1*-mediated cholesterol efflux and degradation of *LDLR* induced GBM cell death [18–20]. It seems that the enormous demand for cholesterol from GBM cells is not just for the production of organelles. The increase in cholesterol and LDL levels promotes resistance of various tumors to chemotherapy, and it is also an independent risk factor for poor prognosis of GBM under standard TMZ treatment [21, 22]. Although cholesterol-induced drug resistance has not been confirmed in CNS tumors, elevated cholesterol in malignant ascites was proved to induce chemotherapy resistance by upregulating the drug efflux proteins *ABCG1* and *MDR1* [23]. *MDR1* is located and stably expressed in lipid rafts composed of cholesterol, sphingolipid, and proteins on the plasma membrane [24]. When lipid rafts were induced to accumulate in specific parts of the membrane, *MDR1* expression was confined, and tumor cells were less resistant

TABLE 1: Primer parameters for qRT-PCR.

Gene	NCBI ID	Forward primer	Reverse primer	Efficiency (%)
<i>SREBF2</i>	6721	5'-TTGTCGGGTGTCATGGGC-3'	5'-ACAAATTGCAGCATCTCGTCG-3'	108.88
<i>NR1H3</i>	10062	5'-TCTGGACAGGAAACTGCACC-3'	5'-ACATCTCTTCCTGGAGCCCT-3'	113.12
<i>ABCA1</i>	19	5'-GGGTCTGTCCCCAGCATAAC-3'	5'-TCTGCATTCCACCTGACAGC-3'	101.44
<i>GAPDH</i>	2597	5'-AGATCATCAGCAATGCCTCCT-3'	5'-TGAGTCCTTCCACGATACCAA-3'	110.17

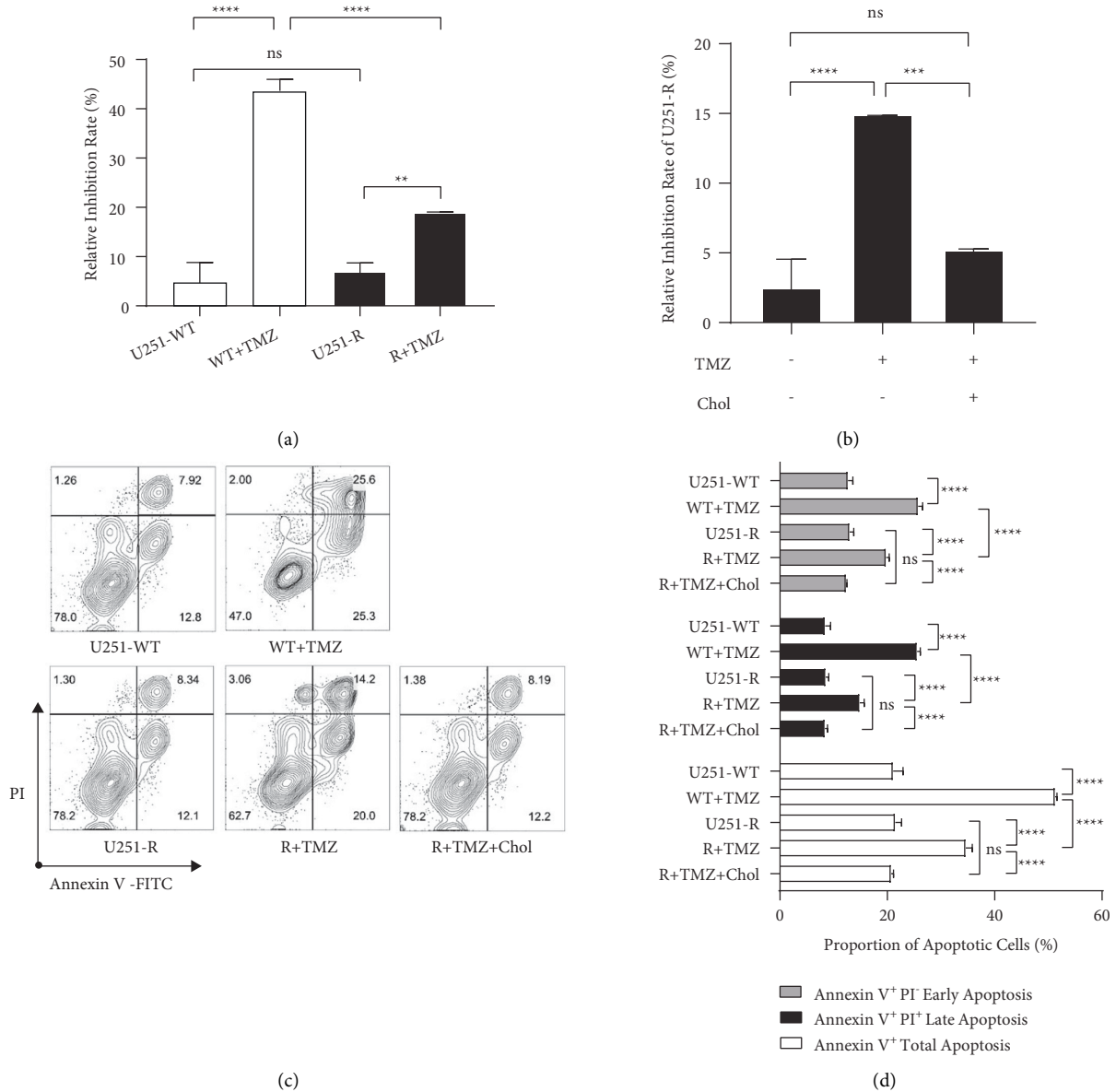


FIGURE 2: Continued.

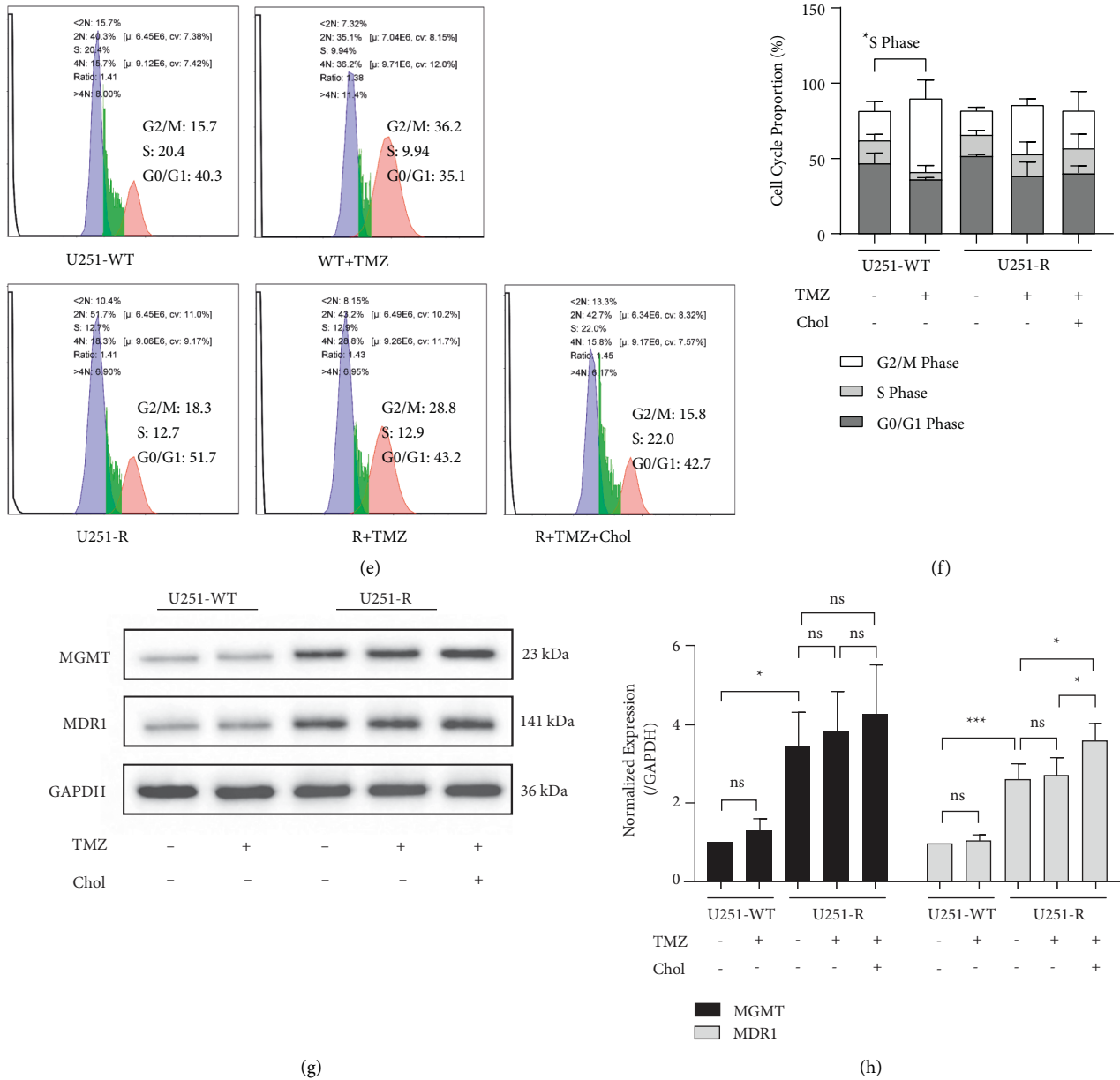


FIGURE 2: Cholesterol promoted temozolomide (TMZ) resistance of U251 cells. (a) Inhibition rate of 200 μ M TMZ or DMSO on U251 wild-type (U251-WT) and TMZ-resistant U251 (U251-R) cells evaluated by CCK-8. (b) Inhibition rate of 200 μ M TMZ on U251-R cells treated with 5 μ g/ml cholesterol (Chol) or DMSO. (c, d) The apoptosis proportion of U251-WT and U251-R cells treated with DMSO, 200 μ M TMZ alone, or combined with 5 μ g/ml Chol. (e, f) The cell cycle of U251-WT and U251-R cells treated with DMSO, 200 μ M TMZ alone, or combined with 5 μ g/ml Chol. (g, h) The protein expression of MGMT and MDR1 (integrated density referred to GAPDH) in DMSO, 200 μ M TMZ, or additional 5 μ g/ml Chol-treated U251-WT and U251-R cells. The histograms show the mean, and the error bars indicate SD. The percentage of cells (%) is displayed in the flow cytometry chart. $P^* < 0.05$, $P^{**} < 0.01$, $P^{***} < 0.001$, $P^{****} < 0.0001$; ns, no significant.

[25]. Moreover, additionally added cholesterol restored the homogenous (broad and low-density) distribution of lipid rafts and upregulated MDR1 [25]. Conversely, lipid rafts were depleted when cholesterol was scavenged, and chemotherapy resistance was correspondingly diminished [26].

Both ginsenosides and cholesterol have steroid core structures (Figure 1), and ginsenosides can regulate cholesterol metabolism in tumor cells. Rg3 and CK hindered cholesterol synthesis by inhibiting β -hydroxy- β -methylglutaryl coenzyme A (HMG-CoA) [27, 28], and CK also

promoted cholesterol efflux by stimulating LXR α [29, 30] to synergistically decrease intracellular cholesterol. Rh2 revealed lipid raft depleting activity [31, 32]. More direct evidence indicates that the ginsenoside derivative Rp1 decreased MDR1 activity by redistributing lipid rafts and attenuated the cholesterol-dependent resistance [25]. Consequently, ginsenosides are potential agents for the treatment of tumor resistance as regulators of cellular cholesterol metabolism. However, the differential roles of ginsenoside subtypes that govern cholesterol metabolism

and drug resistance in CNS tumors remain undisclosed. In this study, we certified the role of cholesterol in TMZ resistance of glioblastoma U251 cells and investigated the effects of several ginsenosides with BBB penetration on TMZ resistance of U251 cells in the presence of cholesterol. We further studied the roles of ginsenosides on cholesterol metabolism and lipid raft distribution and the mechanisms controlling TMZ resistance. Our work suggests that ginsenosides Rg1 and CK are potential drugs to control TMZ resistance, providing references for adjuvant therapy of GBM.

3.2. Cholesterol Metabolism and Lipid Raft Distribution in TMZ-Resistant GBM Cells Were Significantly Different from Wild Type. As cholesterol attenuated the cytotoxicity of TMZ to resistant U251 cells and increased the expression of MDR1, we studied the cholesterol metabolism characteristics of TMZ-resistant U251 cells, to assess the potential of resistant cells to utilize cholesterol. When exposed to cholesterol, TMZ-resistant U251 cells preserved higher levels of intracellular cholesterol than wild type (Figure 3(a)), which may be due to cytotoxicity-mediated disruption of membrane integrity. We subsequently treated two cell lines with 25-NBD cholesterol to assay the cholesterol efflux provoked by the extracellular receptor NaTC [35, 36]. We found that the cholesterol efflux level of resistant U251 cells was markedly lower than wild type (Figure 3(b)). In addition, TMZ slightly reduced the content of intracellular cholesterol in both wild-type and resistant cells and promoted cholesterol efflux, implying that TMZ has a weak activity on cholesterol metabolism, which may also be related to its cytotoxic effect. The results reveal that TMZ-resistant GBM cells tend to retain more cholesterol and are associated with their resistance to chemotherapy.

MDR1 expression positively correlated with the homogenous distribution (broad and low density) of lipid rafts, which was attenuated upon the accumulation of lipid rafts and restored to a homogenous distribution after cholesterol uptake [25]. To confirm this phenomenon in GBM cells, we used fluorescently coupled CT-B to label lipid rafts [37, 38]. Under laser confocal microscopy, the CT-B signal of wild-type U251 cells was concentrated in a small area of the plasma membrane, while CT-B bound to TMZ-resistant strains tended to be distributed widely, homogeneously, and moderately (Figure 3(c)).

3.3. Ginsenosides Attenuated Cholesterol Accumulation and Redistributed Lipid Rafts in TMZ-Resistant GBM Cells. Since the heterogeneous cholesterol metabolism properties of TMZ-resistant U251 cells, we studied the effects of brain tissue-permeable ginsenosides Rb1, Rg1, Rg3, and CK [12–14, 39] on cholesterol accumulation and efflux. All four ginsenosides decreased cholesterol content in resistant U251 cells (Figure 3(d)) and promoted NaTC-mediated cholesterol efflux (Figure 3(e)). Rg3 and CK exhibited the most pronounced effects.

Next, we studied the impact of ginsenosides on the distribution of lipid rafts. We found that the CT-B-binding lipid raft areas of the ginsenoside-treated TMZ-resistant strains exhibited different degrees of redistribution (Figure 3(c)). Among the resistant U251 cells, lipid rafts were significantly concentrated in partial areas after Rb1 and CK treatment, while the CT-B-labeled regions of the cells treated with Rg1 and Rg3 increased in density only in part of the plasma membrane, but were still widely distributed. Consequently, ginsenosides Rb1, Rg1, Rg3, and CK can redistribute lipid rafts, which are potentially associated with a decline in MDR1 expression. Among them, Rb1 and CK can redistribute lipid rafts more markedly.

3.4. Ginsenosides Increased LXR α Expression in TMZ-Resistant GBM Cells. To study how ginsenosides regulate cholesterol aggregation and efflux, we assayed the expression of metabolism genes, including *NR1H3* (LXR α) that activates cholesterol efflux, cholesterol efflux transporter *ABCA1*, and *SREBF2*, which mediates the de novo synthesis of cholesterol. Compared with wild-type U251 cells, the transcription of *NR1H3* considerably diminished in TMZ-resistant cells, but ginsenosides Rg1, Rg3, and CK reversed this phenomenon to varying degrees (Figure 4(a)). Unexpectedly, the *ABCA1* transcription in the TMZ-resistant U251 cells was higher than the wild type. Although Rb1 displayed no effect on *NR1H3* mRNA, Rb1 and Rg1 both further upregulated *ABCA1* mRNA in resistant cells. In addition, compared with the wild-type cells, the expression of *SREBF2* mRNA in TMZ-resistant strains was almost undetectable. The expression of *SREBF2* mRNA in resistant cells treated with these ginsenosides was restored to a certain extent, but the upregulation mediated by Rg1, Rg3, and CK was subdued.

Due to the gene expression results, the effects of ginsenosides on intracellular cholesterol content may depend on cholesterol efflux mediated by LXR α , rather than attenuating SREBF2-mediated cholesterol synthesis. To verify this conjecture, we next identified the expression of LXR α on the protein level and found the reduced expression of LXR α in TMZ-resistant U251 cells (Figures 4(b) and 4(c)). Similarly, ginsenosides Rb1, Rg1, Rg3, and CK upregulated the protein expression of LXR α , particularly Rg1 and CK. The results disclose that ginsenosides Rb1, Rg1, Rg3, and CK may decrease the intracellular cholesterol content and promote cholesterol efflux in TMZ-resistant GBM cells by upregulating LXR α .

3.5. Ginsenosides Rg1 and CK Improved Cholesterol Efflux and Inhibited TMZ Resistance in GBM Cells by Upregulating LXR α . Given that Rg1 and CK showed better upregulation of LXR α among the four ginsenoside subtypes (Figures 4(b) and 4(c)), we consider that these two ginsenosides have more potential to control the TMZ resistance of GBM cells in the presence of cholesterol. The results indicated that resistant U251 cells were more resistant to TMZ stress than wild type in the presence of cholesterol. The cells were nearly uninhibited (Figure 5(a)), and the level of apoptosis was lower at all stages,

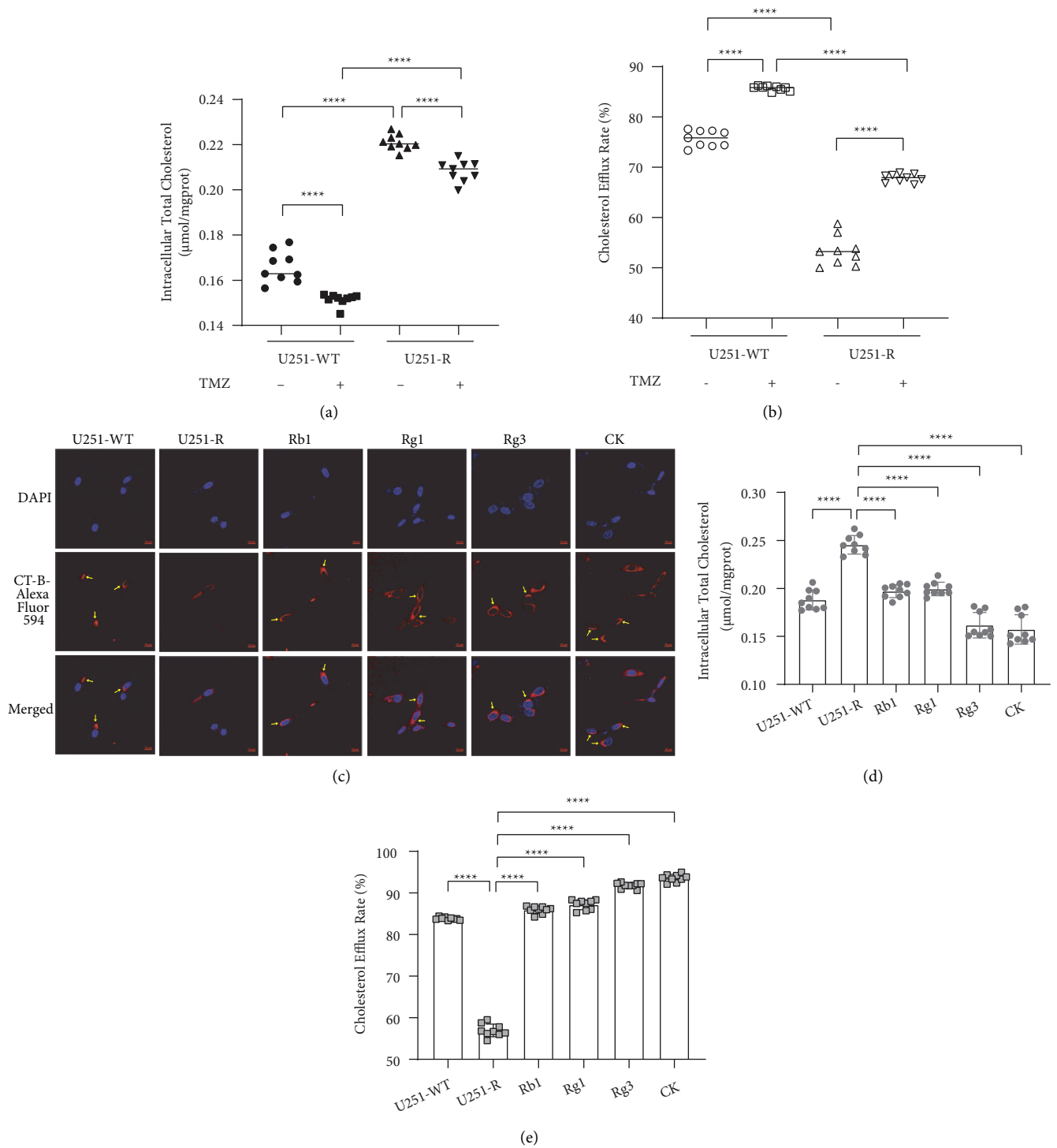


FIGURE 3: Ginsenosides Rb1, Rg1, Rg3, and compound K (CK) regulated cholesterol accumulation, efflux, and lipid raft distribution in temozolomide (TMZ)-resistant U251 (U251-R) cells. (a) Intracellular cholesterol concentrations of U251 wild-type (U251-WT) and resistant cells treated with 200 µM TMZ or DMSO. (b) NaTC-induced 25-NBD cholesterol (10 µg/mL) efflux rate of U251-WT and U251-R cells treated with 200 µM TMZ or DMSO. (c) Intracellular cholesterol concentration of U251-WT cells treated with DMSO and U251-R cells treated with 100 µM ginsenoside or DMSO. All cells were pretreated with 5 µg/ml cholesterol. (d) NaTC-induced cholesterol efflux rate in U251-WT and U251-R cells. The cells were incubated with 10 µg/mL 25-NBD cholesterol and treated with DMSO or 100 µM ginsenosides. (e) Confocal laser scanning of the distribution of lipid rafts labeled with cholera toxin subunit B (CT-B) in U251-WT and U251-R cells treated with 5 µg/ml cholesterol and 100 µM ginsenoside or DMSO. Alexa Fluor 594-conjugated CT-B emits red fluorescence, and the blue fluorescence shows 4', 6-diamidino-2-phenylindole (DAPI)-labeled nucleus. The arrows point to the area where lipid rafts accumulated on the cell membrane (magnification, × 600; scale bar, 10 µm). The dots represent the value of each sample, the midlines or histograms display the mean, and the error bars indicate SD. $P^{****} < 0.0001$.

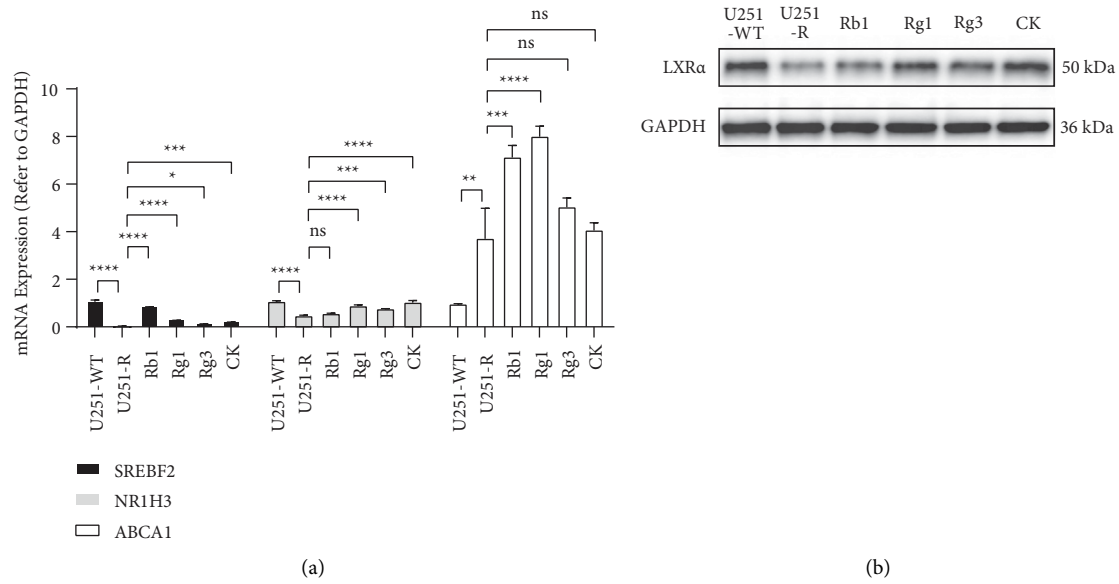


FIGURE 4: Ginsenosides modulated the transcription and translation of cholesterol metabolism factors in temozolomide (TMZ)-resistant U251 (U251-R) cells. (a) The expression of *SREBF2*, *NR1H3*, and *ABCA1* mRNAs in wild-type U251 (U251-WT) and U251-R cells. All cells were pretreated with 5 μ g/ml cholesterol. (b, c) The protein expression of LXR α and ABCA1 (integrated density referred to GAPDH) in U251-WT and U251-R cells. U251-WT cells were treated with DMSO, and U251-R cells were treated with 100 μ M Rb1, Rg1, Rg3, compound K (CK), or DMSO. The top of the histograms or the center lines of boxes display the mean, and the error bars indicate SD. $P^* < 0.05$, $P^* < 0.05$, $P^{**} < 0.01$, $P^{***} < 0.001$, $P^{****} < 0.0001$; ns, no significant.

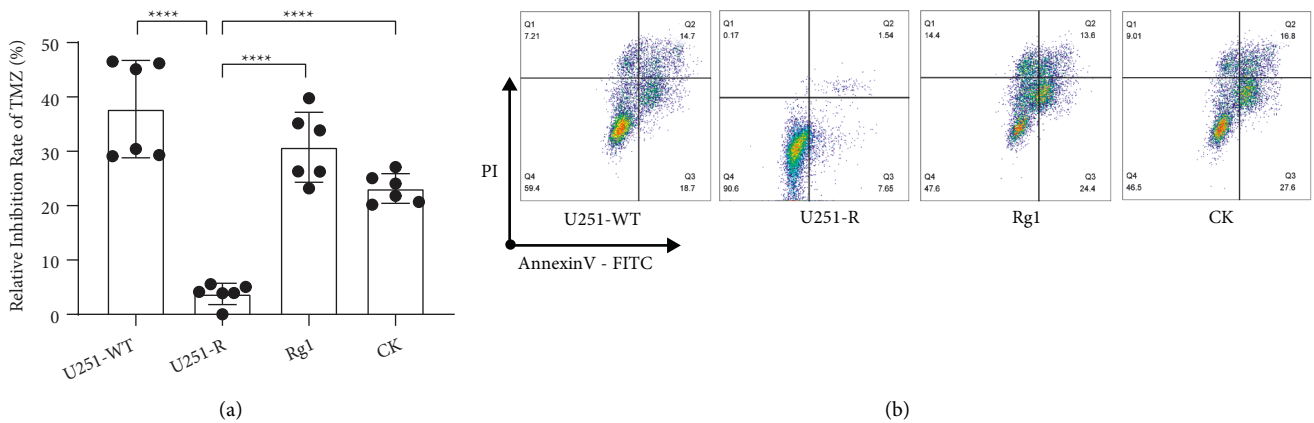


FIGURE 5: Continued.

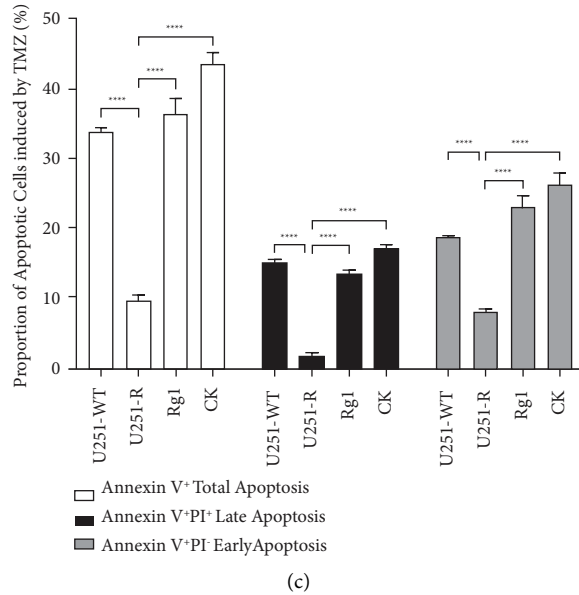


FIGURE 5: Ginsenosides Rg1 and compound K (CK) raised the sensitivity of resistant U251 cells (U251-R) to temozolomide (TMZ) in the presence of cholesterol. (a) Inhibition rate on U251 wild-type (U251-WT) and U251-R cells evaluated by CCK-8. (b, c) Proportion of apoptosis in U251-WT and U251-R cells at each stage. After incubation with 5 μg/ml cholesterol, U251-WT cells were treated with DMSO, and U251-R cells were treated with DMSO, Rg1, or CK. $P^{****} < 0.0001$.

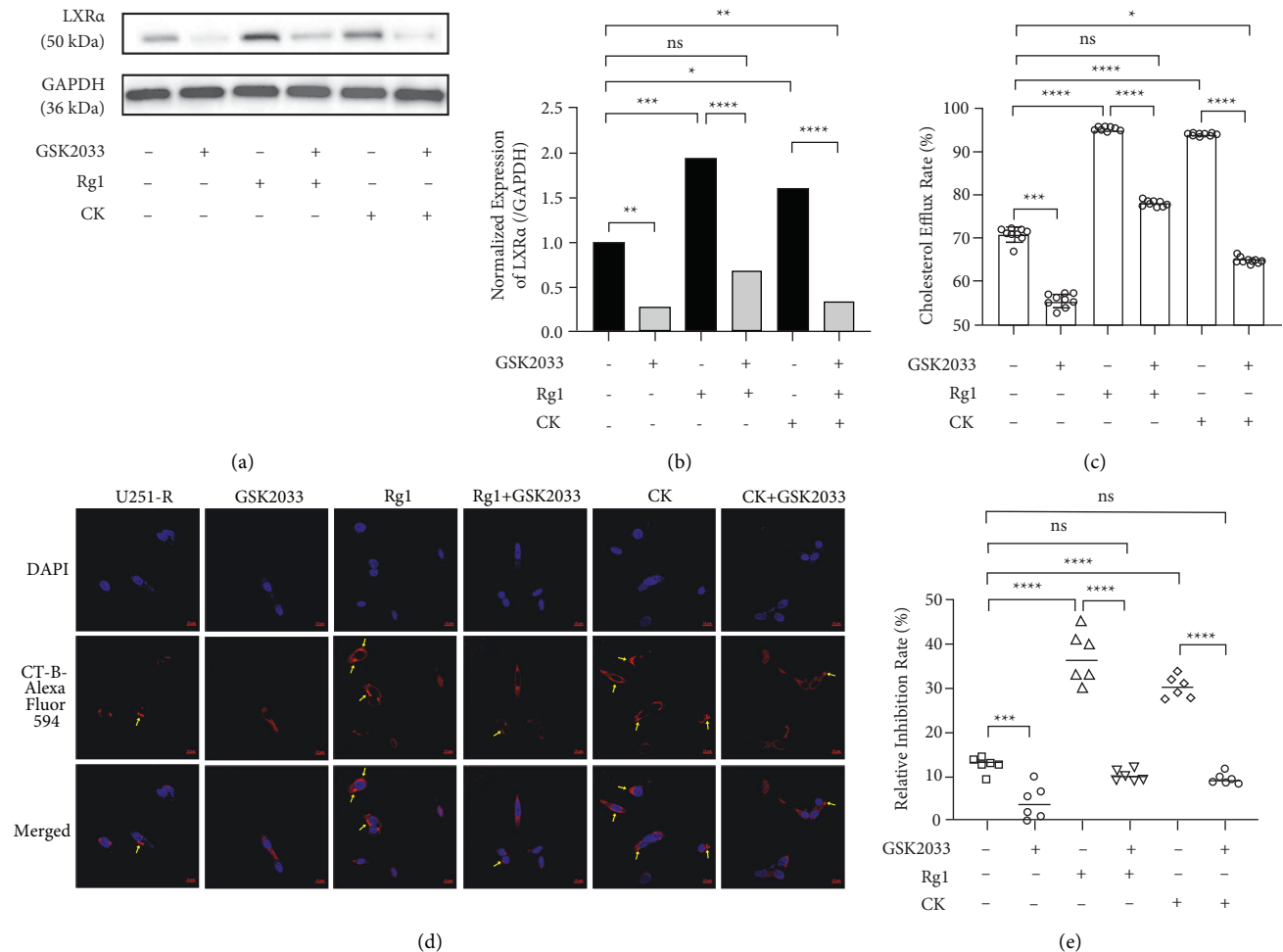


FIGURE 6: Continued.

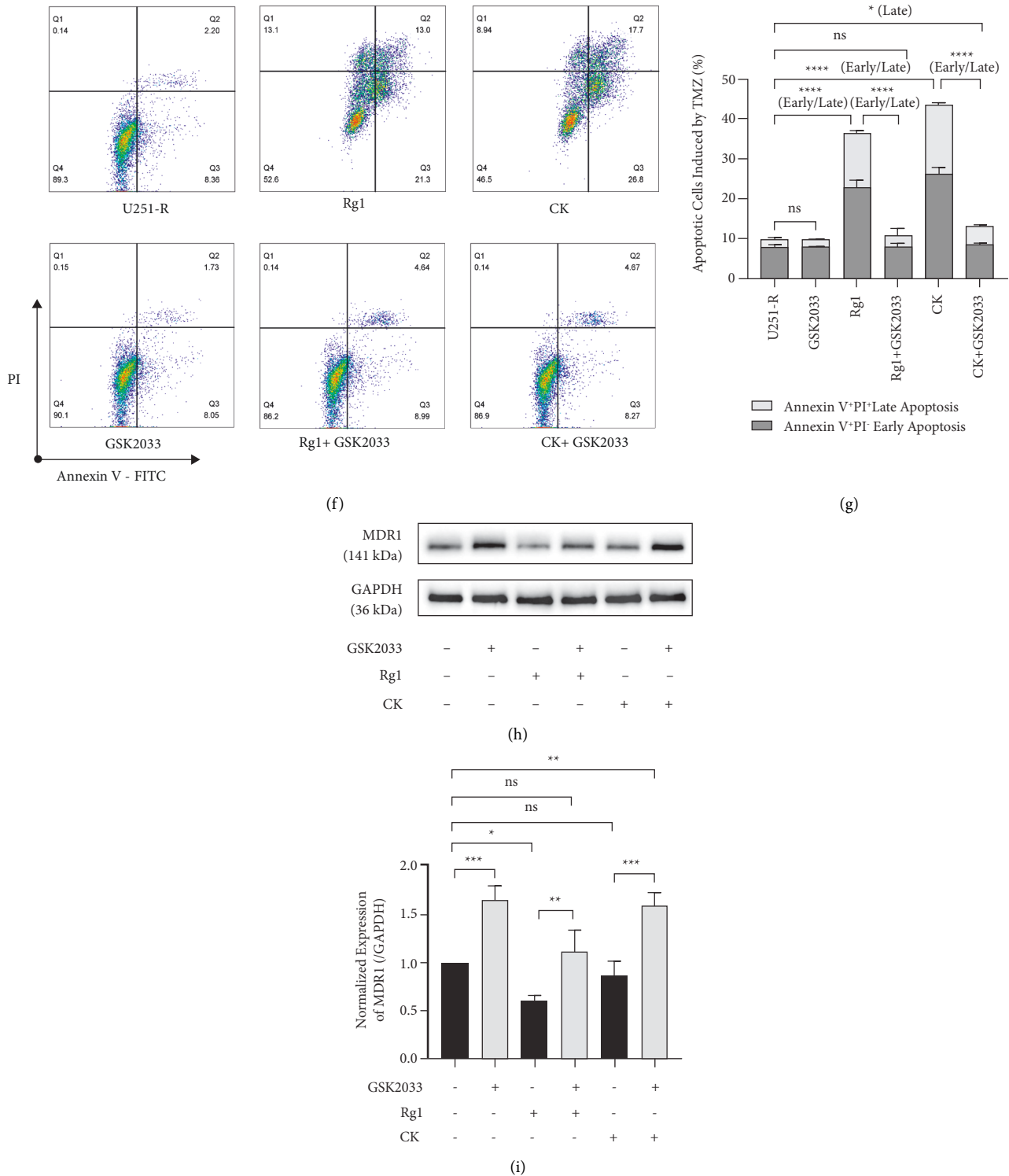


FIGURE 6: Ginsenosides Rg1 and compound K (CK) regulated cholesterol metabolism and lipid raft distribution and inhibited the temozolamide (TMZ) resistance of U251 cells by upregulating LXR α . (a, b) The protein expression of LXR α (integrated density referred to GAPDH) in TMZ-resistant U251 (U251-R) cells. (c) NaTC-induced cholesterol efflux rate in U251-R cells incubated with 10 μ g/mL 25-NBD cholesterol. (d) Confocal laser scanning of the distribution of lipid rafts labeled with cholera toxin subunit B (CT-B) in U251-R cells. Alexa Fluor 594-conjugated CT-B emits red fluorescence, and the blue fluorescence shows 4', 6-diamidino-2-phenylindole (DAPI)-labeled nucleus. The arrows point to the area where lipid rafts accumulated on the cell membrane (magnification, $\times 600$; scale bar, 10 μ m). (e) Inhibition rate on U251-R cells assessed by CCK-8. (f, g) The proportion of apoptotic U251-R cells at each stage. (h, i) The protein expression of MDR1 (integrated density referred to GAPDH) in U251-R cells. Cells in all groups were pretreated with 5 μ g/ml cholesterol and dosed with 200 μ M TMZ, and cells were additionally supplemented with 100 μ M Rg1 or CK in the presence or absence of 100 nM GSK2033. The histogram and dots represent the mean, and the error bars indicate SD. $P^* < 0.05$, $P^{**} < 0.01$, $P^{***} < 0.001$, $P^{****} < 0.0001$; ns, no significant.

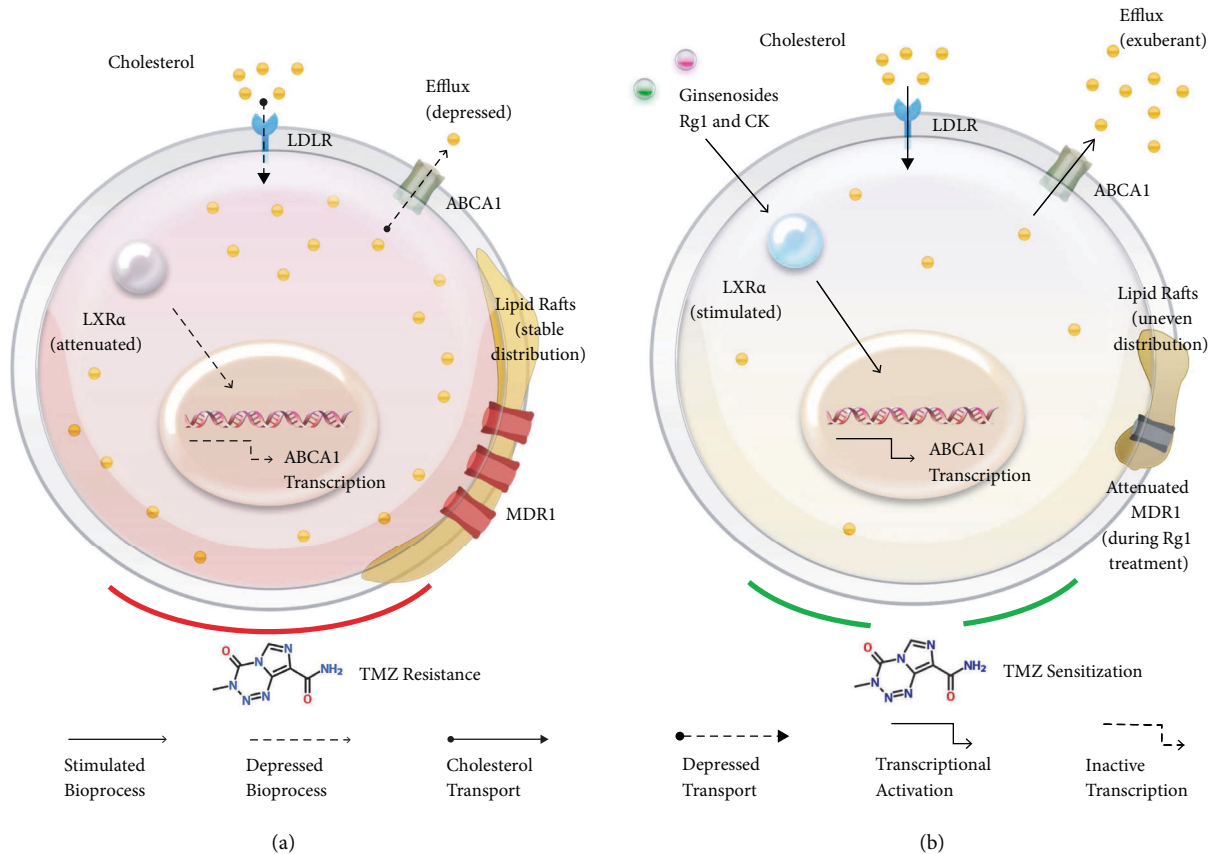


FIGURE 7: Ginsenosides Rg1 and compound K (CK) increased the sensitivity of resistant glioblastoma cells to temozolomide (TMZ) by governing cholesterol metabolism and lipid raft distribution. (a) Cholesterol in the brain tumor microenvironment is taken up in the form of cholesterol esters by low-density lipoprotein receptor (LDLR). Restricted expression of LXR α in TMZ-resistant glioblastoma cells leads to attenuated ABCA1-mediated cholesterol efflux, which retains a higher concentration of intracellular cholesterol to maintain a stable distribution of lipid rafts and increases the resistance to TMZ. The amplified TMZ resistance is potentially associated with the upregulation of MDR1 in lipid rafts. (b) Ginsenosides Rg1 and CK facilitated cholesterol efflux by stimulating the expression of LXR α . The decreased intracellular cholesterol redistributed lipid rafts in an uneven and aggregated state and reserved the cytotoxicity of TMZ on glioblastoma cells. Following the regulation of cholesterol metabolism, Rg1 treatment also diminished MDR1 expression.

especially at the Annexin V⁺ PI⁺ late stage (Figures 5(b) and 5(c)). The additional treatment of Rg1 and CK restored the sensitivity of resistant cells to TMZ and promoted TMZ-induced cell apoptosis at all stages. To explore how ginsenosides Rg1 and CK attenuated TMZ resistance in GBM cells in cholesterol-containing matrices, we focused on LXR α .

In consideration of the correlation of LXR α with the survival and transcription level of MDR1 in TMZ-treated HGG patients (Supplementary Figure S4), we evaluated the role of LXR inhibitor GSK2033 on the effects of ginsenosides Rg1 and CK in regulating cholesterol metabolism and TMZ resistance. GSK2033 greatly inhibited LXR α expression in TMZ-resistant U251 cells and blocked the induction of LXR α translation by Rg1 and CK (Figures 6(a) and 6(b)). Following changes in LXR α levels, GSK2033 inhibited cholesterol efflux to NaTC in resistant cells and blocked the facilitation of cholesterol efflux by Rg1 and CK (Figure 6(c)). GSK2033 also more homogeneously distributed lipid rafts in resistant U251 cells and reversed the aggregated remodeling of lipid rafts by Rg1 and CK (Figure 6(d)). These changes in cholesterol metabolism were ultimately reflected in the cytotoxicity of TMZ to resistant GBM cells. In the presence

of cholesterol, GSK2033-mediated LXR α inhibition resisted the sensitization of Rg1 and CK to TMZ (Figures 6(e), 6(f), and 6(g)). It is worth mentioning that even in the presence of GSK2033, CK still increased the level of Annexin V⁺ PI⁺ late apoptosis in resistant U251 cells. Besides, GSK2033 increased MDR1 expression in resistant U251 cells exposed to cholesterol while regulating lipid raft distribution (Figures 6(h) and 6(i)). Although Rg1 downregulated MDR1 expression in resistant cells, this effect was inhibited by GSK2033. No effect of CK on MDR1 expression was identified, although CK increased the cytotoxicity of TMZ to resistant cells. Our work not only identified ginsenosides Rg1 and CK with activity to attenuate TMZ resistance but also confirmed that the cytotoxic sensitization of these ginsenosides was through stimulating LXR α -mediated cholesterol efflux and lipid raft redistribution.

4. Discussion

Tumor cells are adaptable to the environment. In addition to microenvironmental oxygen, glucose, and glutamine, cholesterol has also become an essential material basis for

tumor cells to attain energy and synthesize organelles after metabolic reprogramming [40]. Although astrocytes are the main source of cholesterol in brain tissues [41], cholesterol from peripheral blood can also be taken up through the BBB expressing abundant LDLR [42]. Hence, the brain tumor microenvironment possesses high levels of cholesterol that can be deployed by GBM cells. We identified that TMZ resistance of GBM cells was dependent on cholesterol in the microenvironment. The addition of cholesterol led to attenuated apoptosis and reduced expression of the lipid raft-related drug resistance protein MDR1 in resistant cells, which tended to retain more cholesterol intracellularly with inhibited efflux and maintained lipid raft distribution. MGMT, which mediates the alkylation repair of the 6th oxygen of guanine on DNA, is another TMZ resistance vector of GBM cells. Both hypermethylation status of MGMT promoter and MGMT overexpression are independent risk factors for desensitization to TMZ therapy [8, 43]. Although the increased expression of MGMT was observed in the resistant cells, the addition of cholesterol failed to further modify its level. Different from MGMT, the expression and activity of MDR1 are determined by lipid rafts and are associated with cholesterol-maintained lipid raft homeostasis [24, 25]. Consequently, faded cholesterol efflux and stable lipid raft distribution may be involved in sustaining the expression of MDR1 in resistant GBM cells. The development of drugs to target cholesterol metabolism is a favorable strategy to control TMZ resistance in GBM.

Ginsenosides are the active components of the *Panax* genus, *Araliaceae*, which have a steroid structure similar to cholesterol and have the potential to govern cholesterol metabolism. Rb1, Rg1, Rg3, and CK are subtypes of ginsenosides that have been reported to have CNS effects and brain penetration [12–14, 39]. Rb1, Rg3, and CK belong to protopanaxadiol, while Rg1 belongs to protopanaxatriol. We found that Rb1, Rg1, Rg3, and CK induced cholesterol efflux in TMZ-resistant GBM cells, reduced intracellular cholesterol concentrations, and redistributed lipid rafts at different levels. It has been reported that CK promoted cholesterol efflux by stimulating LXR α [29, 30], and we recognized the increased expression of LXR α in resistant GBM cells after treated with Rb1, Rg1, and Rg3, in addition to CK. We further observed that Rg1 and CK raised the sensitivity of resistant GBM cells to TMZ, and this effect was via upregulation of LXR α . According to the structure of Rg1 and CK (Figure 1), hydroxyl at R1 position and O- β -D-glucopyranosyl at R3 position on the core of saponin may be effector groups stimulating LXR α and controlling drug resistance in GBM cells.

The increase in intracellular cholesterol level mediated by downregulation of LXR α plays an important role in promoting TMZ resistance in GBM cells. Based on our analysis of the CGGA database, in tumor tissues of GBM patients treated with TMZ, the level of LXR α mRNA (*NR1H3*) was associated with prolonged survival, while the level of the raft resistance gene MDR1 was negatively correlated with *NR1H3* and positively correlated with cholesterol uptake gene *LDLR* and synthetic gene

SREBF2. It was recently reported that cholesterol accumulation mediated by the downregulation of LXR α promoted GBM cell growth, whereas the activation of LXR α -mediated cholesterol efflux exhibited the opposite effects [19, 44]. Although a study identified an increase in TMZ-induced apoptosis in resistant GBM cells treated with cholesterol [45], the dose of cholesterol was up to 20 μ g/ml [46]. We applied a small dose of cholesterol (5 μ g/ml) and found that cholesterol strengthened the TMZ resistance of GBM cells, and the expression of LXR α was depressed in resistant cells. In cholesterol-maintained TMZ-resistant cells, ginsenosides Rg1, Rg3, and CK upregulated LXR α and stimulated LXR α -mediated cholesterol efflux, which were initially depressed to retain intracellular cholesterol and improve lipid raft distribution. We demonstrated that subtypes Rg1 and CK increased the sensitivity of resistant cells to TMZ through their stimulatory effects on LXR α by a LXR inhibitor, further supporting the positive effect of this protein and cholesterol efflux in controlling resistance. The upregulation of LXR α and promotion of cholesterol efflux by CK were weaker than that of Rg1, which is consistent with the redistribution of lipid rafts. This may be the reason for the mild inhibitory effect of CK on the raft resistance protein MDR1. Nonetheless, from the results, CK and Rg1 displayed similar chemosensitization effects on resistant cells, implying that they are both potential agents for the treatment of TMZ resistance.

The drug resistance of GBM cells requires cholesterol, and GBM cells adjust their cholesterol homeostasis according to the concentration of environmental cholesterol. Studies have discovered that in the absence of external cholesterol, the intracellular cholesterol content of resistant U251 cells was higher than wild type [45], reflecting the activated cholesterol de novo synthesis. However, we found that the expression of the cholesterol synthesis gene *SREBF2* in TMZ-resistant GBM cells declined, and the cholesterol efflux was diminished after obtaining external cholesterol. The transcription level of *SREBF2* raised along with LXR α after treated with ginsenoside, indicating that GBM cells may ensure the intracellular supply of cholesterol by modifying the ability of cholesterol synthesis. Even so, the feedback upregulation of *SREBF2* is still less obvious than the upregulation of ginsenosides on LXR α , which ultimately performed as the inhibition of TMZ resistance. In view of the self-regulation of cholesterol metabolism in GBM cells, the development of cholesterol efflux stimulators such as ginsenosides Rg1 and CK, combined with the strategy of cholesterol synthesis inhibition, could block the TMZ resistance of GBM cells far more effectively than simply blocking cholesterol intake.

Although we demonstrated that ginsenosides Rg1 and CK controlled the resistance to TMZ in GBM cells by stimulating LXR α -mediated cholesterol efflux, some limitations remain in this study. The mechanism of resistance inhibition was initially confirmed by LXR inhibitors, which require further validation in LXR α knockout and overexpressing cells. What is more, to increase the feasibility of these ginsenosides in clinical studies, animal studies are required for data on *in vivo* efficacy against TMZ resistance and the concentration of each subtype in the

cerebrospinal fluid after peripheral administration. These will be augmented in subsequent work.

5. Conclusions

Ginsenosides Rg1 and CK can induce cholesterol efflux by upregulating LXR α , decreasing intracellular cholesterol content, and redistributing lipid rafts in TMZ-resistant GBM cells. These modulations of cholesterol metabolism controlled the resistance of GBM cells to TMZ (Figure 7). Our findings uncovered a potential adjuvant drug for standard TMZ treatment, promising a novel approach for improving prognosis in GBM patients resistant to chemotherapy.

Abbreviations

BBB:	Blood-brain barrier
CGGA:	Chinese Glioma Genome Atlas
CK:	Compound K
GBM:	Glioblastoma
HGG:	High-grade glioma
LDLR:	Low-density lipoprotein receptor
MDR:	Multidrug resistance protein
MGMT:	O6-methylguanine-DNA methyltransferase
NaTC:	Sodium taurocholate
PI:	Propidium iodide
STR:	Short tandem repeat
TMZ:	Temozolomide.

Data Availability

RNA sequencing datasets generated and analyzed during this study are available in the Chinese Glioma Genome Atlas (CGGA) repository, <https://www.cgga.org.cn/>. Other data that support this study are available from the corresponding author on reasonable request.

Disclosure

An earlier version of this study is available as a preprint [47], URL: [file:///C:/Users/e504635/Downloads/Supplementary%20Information%20\(1\).pdf](file:///C:/Users/e504635/Downloads/Supplementary%20Information%20(1).pdf).

Conflicts of Interest

The authors declare that they have no conflicts of interest.

Authors' Contributions

Runze Qiu and Jingjing Zhang contributed equally to this work.

Acknowledgments

The authors appreciate Jiangsu KeyGEN BioTECH for confocal microscopy and STR identification. This work was supported by the Science and Technology Development Fund of Nanjing Medical University (Grant nos. NMUB2019153 and NMUB2019178).

Supplementary Materials

The methods and results of STR identification of TMZ-resistant U251 cells, the amplification efficiency of primers, the analysis results of the transcriptome sequencing database, the validation of drug resistance, and the raw images of the immunoblot bands are presented in the supplementary materials. Figure S1. Genotyping map of short tandem repeat (STR) and Amelogenin locus in temozolomide-resistant U251 (U251TMZ) cells. About 1×10^6 constructed temozolomide-resistant U251 cells were collected, and genomic DNA was extracted by PureLink Genomic DNA Mini Kit (Life Technologies, #K182001). DNA was amplified by PowerPlex 18D System (Promega, #DC1802), and the alleles were detected on STR and Amelogenin locus by an ABI 3500 Genetic Analyzer (Life Technologies, USA). The genetic test results of resistant cells were compared with cell line data in several databases to identify the genetic stability. The strain matching the resistant cells was named U251 MG (No. CVCL 0021 Best) in the EXPASY database (<https://www.expasy.org/>). No multiple alleles were detected in resistant cells. Figure S2. Integral images of the immunoblot bands used for analysis in the main text. 3 biological replicates were executed in each group. (a) The protein expression of MGMT, MDR1, and GAPDH during treatment of temozolomide (TMZ) and cholesterol (Chol). Immunoblot bands for MDR1 and GAPDH were cut from the same PVDF membrane, while MGMT was cut from the other. (b) The protein expression of LXR α , ABCA1, and GAPDH during treatment of ginsenosides in the presence of cholesterol. The immunoblot bands were cut from the same PVDF membrane. (c) The protein expression of LXR α , MDR1, and GAPDH during treatment of Rg1 and CK in the presence or absence of GSK2033 in cholesterol-containing medium. The immunoblot bands were cut from the same PVDF membrane. U251-WT, wild-type U251 cells, U251-R, and TMZ-resistant U251 cells. Figure S3. Amplification efficiency of primers for qRT-PCR, including *SREBF2*, *NRIH3*, *ABCA1*, and *GAPDH*. The X-axis represents the gene copies of the cDNA standards for 5 concentration gradients, and the Y-axis exhibits the amplification cycles (CT value) for each concentration. Figure S4. Correlation between temozolomide resistance and cholesterol metabolism genes including *LDLR*, *SREBF*, *HMGCR*, *NRIH3*, *ABCA1*, and *ABCG1* in adult patients with high-grade glioma through Chinese Glioma Genome Atlas (CGGA) database. (a) The difference in the expression of cholesterol metabolism mRNAs in tumor tissues between patients who received temozolomide treatment with OS < 0.5 years and OS \geq 5 years. (b) The influence of the methylation status of MGMT on the expression of cholesterol metabolism mRNAs in tumor tissues. (c) The Pearson correlation test of the expression of resistance gene *MDR1* and cholesterol metabolism genes in tumor tissues. The mean lines are presented in the graph, and the error bars on both sides of the mean line indicate SD. $P^{****} < 0.0001$; ns, no significant. Figure S5. Dose-viability curves of wild-type U251 (U251-WT) and temozolomide (TMZ)-resistant U251 (U251-R) cells

treated with TMZ. The dots indicate the mean value of cell viability at each dose, and the error bars indicate SD. (*Supplementary Materials*)








References

- [1] K. D. Miller, Q. T. Ostrom, and C. Kruchko, "Brain and other central nervous system tumor statistics," *CA: A Cancer Journal for Clinicians*, vol. 71, no. 5, pp. 381–406, 2021.
- [2] B. M. Alexander and T. F. Cloughesy, "Adult glioblastoma," *Journal of Clinical Oncology: Official Journal of the American Society of Clinical Oncology*, vol. 35, no. 21, pp. 2402–2409, 2017.
- [3] A. Thomas, M. Tanaka, J. Trepel, W. C. Reinhold, V. N. Rajapakse, and Y. Pommier, "Temozolomide in the era of precision medicine," *Cancer Research*, vol. 77, no. 4, pp. 823–826, 2017.
- [4] A. Karachi, F. Dastmalchi, D. A. Mitchell, and M. Rahman, "Temozolomide for immunomodulation in the treatment of glioblastoma," *Neuro-Oncology*, vol. 20, no. 12, pp. 1566–1572, 2018.
- [5] A. C. Tan, D. M. Ashley, G. Y. López, M. Malinzak, H. S. Friedman, and M. Khasraw, "Management of glioblastoma: state of the art and future directions," *CA: A Cancer Journal for Clinicians*, vol. 70, no. 4, pp. 299–312, 2020.
- [6] M. Schaich, L. Kestel, M. Pfirrmann et al., "A MDR1 (ABCB1) gene single nucleotide polymorphism predicts outcome of temozolomide treatment in glioblastoma patients," *Annals of Oncology*, vol. 20, no. 1, pp. 175–181, 2009.
- [7] F. Lin, M. C. de Gooijer, E. M. Roig et al., "ABCB1, ABCG2, and PTEN determine the response of glioblastoma to temozolomide and ABT-888 therapy," *Clinical Cancer Research*, vol. 20, no. 10, pp. 2703–2713, 2014.
- [8] B. Oldrini, N. Vaquero-Siguero, Q. Mu et al., "MGMT genomic rearrangements contribute to chemotherapy resistance in gliomas," *Nature Communications*, vol. 11, no. 1, p. 3883, 2020.
- [9] K.-S. Baek, Y.-S. Yi, Y.-J. Son et al., "Comparison of anticancer activities of Korean Red Ginseng-derived fractions," *Journal of Ginseng Research*, vol. 41, no. 3, pp. 386–391, 2017.
- [10] J. Wang, F. Qi, Z. Wang et al., "A review of traditional Chinese medicine for treatment of glioblastoma," *Bioscience Trends*, vol. 13, no. 6, pp. 476–487, 2019.
- [11] L. Liu, F.-R. Xu, and Y.-Z. Wang, "Traditional uses, chemical diversity and biological activities of *Panax L.* (Araliaceae): a review," *Journal of Ethnopharmacology*, vol. 263, Article ID 112792, 2020.
- [12] Y.-N. Zhao, X. Shao, L.-F. Ouyang, L. Chen, and L. Gu, "Qualitative detection of ginsenosides in brain tissues after oral administration of high-purity ginseng total saponins by using polyclonal antibody against ginsenosides," *Chinese Journal of Natural Medicines*, vol. 16, no. 3, pp. 175–183, 2018.
- [13] J. Oh and J.-S. Kim, "Compound K derived from ginseng: neuroprotection and cognitive improvement," *Food and Function*, vol. 7, no. 11, pp. 4506–4515, 2016.
- [14] Y.-Z. Wang, Q. Xu, W. Wu et al., "Brain transport profiles of ginsenoside Rb1 by glucose transporter 1: *in vitro* and *in vivo*," *Frontiers in Pharmacology*, vol. 9, p. 398, 2018.
- [15] Z. Chen, X. Wei, L. Shen, H. Zhu, and X. Zheng, "20 (S)-ginsenoside-Rg3 reverses temozolomide resistance and restrains epithelial-mesenchymal transition progression in glioblastoma," *Cancer Science*, vol. 110, no. 1, pp. 389–400, 2019.
- [16] J. M. Dietschy, "Central nervous system: cholesterol turnover, brain development and neurodegeneration," *Bchm*, vol. 390, no. 4, pp. 287–293, 2009.
- [17] R. Qiu, Y. Zhong, Q. Li, Y. Li, and H. Fan, "Metabolic remodeling in glioma immune microenvironment: intercellular interactions distinct from peripheral tumors," *Frontiers in Cell and Developmental Biology*, vol. 9, Article ID 693215, 2021.
- [18] G. R. Villa, J. J. Hulce, C. Zanca et al., "An LXR-cholesterol axis creates a metabolic co-dependency for brain cancers," *Cancer Cell*, vol. 30, no. 5, pp. 683–693, 2016.
- [19] R. Fang, X. Chen, S. Zhang et al., "EGFR/SRC/ERK-stabilized YTHDF2 promotes cholesterol dysregulation and invasive growth of glioblastoma," *Nature Communications*, vol. 12, no. 1, p. 177, 2021.
- [20] D. Guo, F. Reinitz, M. Youssef et al., "An LXR agonist promotes glioblastoma cell death through inhibition of an EGFR/AKT/SREBP-1/LDLR-dependent pathway," *Cancer Discovery*, vol. 1, no. 5, pp. 442–456, 2011.
- [21] A. Yan, Z. Jia, C. Qiao, M. Wang, and X. Ding, "Cholesterol metabolism in drug-resistant cancer (Review)," *International Journal of Oncology*, vol. 57, no. 5, pp. 1103–1115, 2020.
- [22] A. K. Altwaairgi, W. A. Alghareeb, F. H. AlNajjar et al., "Atorvastatin in combination with radiotherapy and temozolomide for glioblastoma: a prospective phase II study," *Investigational New Drugs*, vol. 39, no. 1, pp. 226–231, 2021.
- [23] S. Kim, M. Lee, D. N. Dhanasekaran, and Y. S. Song, "Activation of LXR α/β by cholesterol in malignant ascites promotes chemoresistance in ovarian cancer," *BMC Cancer*, vol. 18, no. 1, p. 1232, 2018.
- [24] D. Lingwood and K. Simons, "Lipid rafts as a membrane-organizing principle," *Science (New York, N.Y.)*, vol. 327, no. 5961, pp. 46–50, 2010.
- [25] U.-J. Yun, J.-H. Lee, K. H. Koo et al., "Lipid raft modulation by Rp1 reverses multidrug resistance via inactivating MDR-1 and Src inhibition," *Biochemical Pharmacology*, vol. 85, no. 10, pp. 1441–1453, 2013.
- [26] D. M. Ye, S. C. Ye, S. Q. Yu et al., "Drug-resistance reversal in colorectal cancer cells by destruction of flotillins, the key lipid raft proteins," *Neoplasma*, vol. 66, no. 04, pp. 576–583, 2019.
- [27] J.-S. Han, J. H. Sung, and S. K. Lee, "Inhibition of cholesterol synthesis in HepG2 cells by GINST-decreasing HMG-CoA reductase expression via AMP-activated protein kinase," *Journal of Food Science*, vol. 82, no. 11, pp. 2700–2705, 2017.
- [28] S. Lee, M.-S. Lee, C.-T. Kim, I.-H. Kim, and Y. Kim, "Ginsenoside Rg3 reduces lipid accumulation with AMP-activated protein kinase (AMPK) activation in HepG2 cells," *International Journal of Molecular Sciences*, vol. 13, no. 5, pp. 5729–5739, 2012.
- [29] Y. Huang, H. Liu, Y. Zhang et al., "Synthesis and biological evaluation of ginsenoside Compound K derivatives as a novel class of LXR α activator," *Molecules*, vol. 22, no. 7, p. 1232, 2017.
- [30] L. Zhou, Y. Zheng, Z. Li et al., "Compound K attenuates the development of atherosclerosis in ApoE (–/–) mice via LXR α activation," *International Journal of Molecular Sciences*, vol. 17, no. 7, p. 1054, 2016.
- [31] J.-S. Yi, H.-J. Choo, B.-R. Cho et al., "Ginsenoside Rh2 induces ligand-independent Fas activation via lipid raft disruption," *Biochemical and Biophysical Research Communications*, vol. 385, no. 2, pp. 154–159, 2009.
- [32] E. K. Park, E. J. Lee, S. H. Lee et al., "Induction of apoptosis by the ginsenoside Rh2 by internalization of lipid rafts and

- caveolae and inactivation of Akt,” *British Journal of Pharmacology*, vol. 160, no. 5, pp. 1212–1223, 2010.
- [33] Z. Zhao, K.-N. Zhang, Q. Wang et al., “Chinese glioma genome atlas (CGGA): a comprehensive resource with functional genomic data from Chinese glioma patients,” *Genomics, Proteomics and Bioinformatics*, vol. 19, no. 1, 12 pages, 2021.
- [34] J. Si, W. Li, X. Li, L. Cao, Z. Chen, and Z. Jiang, “Heparanase confers temozolomide resistance by regulation of exosome secretion and circular RNA composition in glioma,” *Cancer Science*, vol. 112, no. 9, pp. 3491–3506, 2021.
- [35] K. Nagao, Y. Zhao, K. Takahashi, Y. Kimura, and K. Ueda, “Sodium taurocholate-dependent lipid efflux by ABCA1: effects of W590S mutation on lipid translocation and apolipoprotein A-I dissociation,” *Journal of Lipid Research*, vol. 50, no. 6, pp. 1165–1172, 2009.
- [36] S. Wang and J. D. Smith, “ABCA1 and nascent HDL biogenesis,” *BioFactors*, vol. 40, no. 6, pp. 547–554, 2014.
- [37] F. Bonacina, D. Coe, G. Wang et al., “Myeloid apolipoprotein E controls dendritic cell antigen presentation and T cell activation,” *Nature Communications*, vol. 9, no. 1, p. 3083, 2018.
- [38] P. W. Janes, S. C. Ley, and A. I. Magee, “Aggregation of lipid rafts accompanies signaling via the T cell antigen receptor,” *Journal of Cell Biology*, vol. 147, no. 2, pp. 447–461, 1999.
- [39] A. Kang, T. Xie, D. Zhu, J. Shan, L. Di, and X. Zheng, “Suppressive effect of ginsenoside Rg3 against lipopolysaccharide-induced depression-like behavior and neuroinflammation in mice,” *Journal of Agricultural and Food Chemistry*, vol. 65, no. 32, pp. 6861–6869, 2017.
- [40] R. Riscal, N. Skuli, and M. C. Simon, “Even cancer cells watch their cholesterol,” *Molecular Cell*, vol. 76, no. 2, pp. 220–231, 2019.
- [41] F. W. Pfrieger and N. Ungerer, “Cholesterol metabolism in neurons and astrocytes,” *Progress in Lipid Research*, vol. 50, no. 4, pp. 357–371, 2011.
- [42] L. Han and C. Jiang, “Evolution of blood-brain barrier in brain diseases and related systemic nanoscale brain-targeting drug delivery strategies,” *Acta Pharmaceutica Sinica B*, vol. 11, no. 8, pp. 2306–2325, 2021.
- [43] A. Mansouri, L. D. Hachem, S. Mansouri et al., “MGMT promoter methylation status testing to guide therapy for glioblastoma: refining the approach based on emerging evidence and current challenges,” *Neuro-Oncology*, vol. 21, no. 2, pp. 167–178, 2019.
- [44] C.-J. Zhang, N. Zhu, J. Long et al., “Celastrol induces lipophagy via the LXR α /ABCA1 pathway in clear cell renal cell carcinoma,” *Acta Pharmacologica Sinica*, vol. 42, no. 9, pp. 1472–1485, 2021.
- [45] Y. Yamamoto, A. Tomiyama, N. Sasaki et al., “Intracellular cholesterol level regulates sensitivity of glioblastoma cells against temozolomide-induced cell death by modulation of caspase-8 activation via death receptor 5-accumulation and activation in the plasma membrane lipid raft,” *Biochemical and Biophysical Research Communications*, vol. 495, no. 1, pp. 1292–1299, 2018.
- [46] K. Gotoh, R. Kariya, M. M. Alam et al., “The antitumor effects of methyl- β -cyclodextrin against primary effusion lymphoma via the depletion of cholesterol from lipid rafts,” *Biochemical and Biophysical Research Communications*, vol. 455, no. 3–4, pp. 285–289, 2014.
- [47] R. Qiu, J. Zhang, G. Chun et al., “Cholesterol analogs ginsenosides Rg1 and Compound K control temozolomide resistance in glioblastoma cells by regulating cholesterol efflux and lipid raft distribution,” 2022, <https://europepmc.org/article/ppr/ppr480646>.

Research Article

The Preventive Effects of Naringin and Naringenin against Paclitaxel-Induced Nephrotoxicity and Cardiotoxicity in Male Wistar Rats

Shimaa S. Khaled ¹, Hanan A. Soliman,¹ Mohammed Abdel-Gabbar ¹,
Noha A. Ahmed ², Kandil Abdel Hai Ali Attia ³, Hesham A. Mahran ^{4,5},
El-Shaymaa El-Nahass ⁶ and Osama M. Ahmed ²

¹Biochemistry Department, Faculty of Science, Beni-Suef University, P.O. Box 62521, Beni-Suef, Egypt

²Physiology Division, Zoology Department, Faculty of Science, Beni-Suef University, P.O. Box 62521, Beni-Suef, Egypt

³Clinical Nutrition Department, College of Applied Medical Sciences, Jazan University, P.O. Box 114, Jazan 45142, Saudi Arabia

⁴Health Informatics Department, College of Public Health & Tropical Medicine, Jazan University, P.O. Box 114, Jazan 45142, Saudi Arabia

⁵Hygiene, Zoonosis and Epidemiology Department, Faculty of Veterinary Medicine, Beni-Suef University, Beni-Suef, Egypt

⁶Department of Pathology, Faculty of Veterinary Medicine, Beni-Suef University, P.O. Box 62521, Beni-Suef, Egypt

Correspondence should be addressed to Noha A. Ahmed; drnohascience@science.bsu.edu.eg

Received 29 June 2022; Revised 14 August 2022; Accepted 28 August 2022; Published 30 September 2022

Academic Editor: Mohammed El-Magd

Copyright © 2022 Shimaa S. Khaled et al. This is an open access article distributed under the Creative Commons Attribution License, which permits unrestricted use, distribution, and reproduction in any medium, provided the original work is properly cited.

This study assessed the preventive properties of naringin and naringenin on paclitaxel-induced nephrotoxicity and cardiotoxicity in adult male Wistar rats. Intraperitoneal injection of paclitaxel 2 mg/kg body weight, two days/week on the 2nd and 5th days of each week, with or without oral administration of naringin and/or naringenin 10 mg/kg body weight every other day, was continued for six weeks. Treatment of rats with naringin and/or naringenin significantly reversed elevated serum creatinine, urea, and uric acid levels caused by paclitaxel, reflecting improved kidney function. Similarly, heart dysfunction induced by paclitaxel was alleviated after treatment with naringin and/or naringenin, as evidenced by significant decreases in elevated CK-MB and LDH activities. After drug administration, histopathological findings and lesion scores in the kidneys and heart were markedly decreased by naringin and/or naringenin. Moreover, the treatments reversed renal and cardiac lipid peroxidation and the negative impacts on antioxidant defenses via raising GSH, SOD, and GPx. The preventive effects of naringin and naringenin were associated with suppressing oxidative stress and reestablishing antioxidant defenses. A combination of naringin and naringenin was the most efficacious in rescuing organ function and structure.

1. Introduction

Paclitaxel is a natural tricyclic diterpenoid isolated from the bark of *Taxus brevifolia* (Pacific yew). The chemical is a taxane, an intermediary metabolite that displays potent anticancer activity [1–3]. Taxanes are used for treating different forms of cancer and are initial therapy for earlier stages of these diseases [4–7]. Moreover, paclitaxel is recognized worldwide as the number one chemotherapeutic agent [8]. Paclitaxel is used in the treatment of aggressive

and metastatic breast cancer, ovarian cancer, lung cancer, pancreatic cancer, and many other malignancies [9]. Unfortunately, paclitaxel is poorly soluble in water and other solvents for the formulation of injectables and causes serious side effects, such as hypersensitivity, neutropenia, myelosuppression, neutropenia, and neurotoxicity [10].

A paclitaxel formulation using Cremophor EL (CrEL) as a solvent (Taxol) induced cumulative sensory-dominant peripheral nephrotoxicity in humans, clinically characterized by numbness and paresthesia of the extremities. This

toxicity was a result of CrEL exposure. Serum creatinine levels increased in association with increased damage [11–15]. Additionally, paclitaxel caused cardiac complications, especially conduction blocks, sinus bradycardia, bradycardia, ventricular tachycardia, and ischemic manifestations [16, 17].

Paclitaxel produces cytotoxicity by enhancing the formation of reactive oxygen species (ROS), thus inducing oxidative stress [18, 19]. Hence, a search for natural chemicals that augment the antitumor activity of paclitaxel or moderate its toxicity, such as flavonoids and polyphenols, are attractive alternatives [20–23].

Natural therapeutics have been investigated to prevent the side effects of anticancer drugs [24–28], highlighting the relevance of medicinal herbs and their bioactive constituents [29–32]. Moreover, phytochemicals may prove clinically useful for improving treatment efficacy for cancer patients and reducing the incidence of adverse reactions [33]. Flavonoids are phytochemicals that inhibit the growth of tumor cells *in vitro* and *in vivo* [34]. Flavonoids exhibit several biological properties, including antioxidant, antimutagen, anticancer, antibacterial, and anti-inflammatory [35]. Naringin and naringenin are citrus flavonoids with pharmacological properties, especially antioxidant, antifree radical, anti-inflammatory, and blood lipid reduction [36]. Additionally, naringin and naringenin are potent anticancer agents and play a role in the management of various tumors [37].

Concerning previous studies, using plant constituents with antioxidant and anti-inflammatory properties will be our strategy to counteract and treat the side effects of anticancer drugs. As a result, this investigation was carried out to assess the renal and cardiac toxicity prevention by naringin and naringenin coincident with paclitaxel-treated Wistar rats. We assessed toxicity by examining kidney and heart function, oxidative stress, and antioxidant defense systems, as well as histopathology.

2. Materials and Methods

2.1. Experimental Animals. Fifty adult male Wistar rats with weights of ~130–150 g were collected from the VACSERA Vaccination Centers' Animal House in Dokki, Giza, Egypt. In order to rule out any concurrent infections, animals were watched for 15 days before the experiment began. Rats were housed in polypropylene cages with ventilated stainless steel lids at a standard air temperature of (25 ± 5°C) and with a 12-hour light cycle. Animals had free access to water and received a sufficiently balanced standard diet on a daily basis *ad libitum*. All animal-related procedures were performed, complying with the recommendations and instructions of the Experimental Animal Ethics Committee, Faculty of Science, Beni-Suef University, Egypt (Ethical Approval Number: BSU/FS/2017/7.) We did everything we could to lessen animals' pain and suffering.

2.2. Chemicals. Paclitaxel (Taxol®) was obtained from the Bristol-Myers Squibb global biopharmaceutical company (batch code: 7E05628). Naringin (batch code: BCBM4171 V)

and naringenin (batch code: BCBJ2179 V) were obtained from Sigma (MO, USA). The creatinine reagent kit (catalog numbers: M11502c-18) and the urea reagent kit (catalog numbers: M11536c-16) were purchased from Biosystem S.A. (Spain). Uric acid, CK-MB, and LDH reagent kits were purchased from Spin React (Spain), with catalog numbers MD41001, MD41254, and MX41214, respectively. Chemicals of oxidative stress including trichloroacetic acid were obtained from PanReac AppliChem ITW Companies (Spain) (batch code: 5O011689), thiobarbituric acid was obtained from Sd Fine Chem Limited(SDFCL) Company (India) (batch code: L 16 A/1916/1212/13), 1,1,3,3 tetra-methoxy propane was obtained from Sigma-Aldrich (MO, USA) (catalog no: T9889), metaphosphoric acid was obtained from ALPHA CHEMIKA Company (India) (batch code: M 21519), 5,5- dithiobis nitrobenzoic acid was obtained from Sigma-Aldrich (MO, USA) (batch code: 40K3652), GSH was obtained from PanReac AppliChem ITW Companies (Spain) (batch code: 3W010085), and pyrogallol was obtained from Research Lab Company (India) (batch code: 1280B251114).

2.3. Experimental Design. In this study, adult male Wistar rats were divided into five groups, each with ten rats.

- (1) Normal group: rats were administered 5 mL 1% carboxymethyl cellulose (CMC) kg body weight (b.wt) orally every other day and 2 mL saline twice per week intraperitoneally for six weeks.
- (2) Paclitaxel-administered control group: rats were administered paclitaxel intraperitoneally at a dose level of 2 mg/kg b.wt [38] twice weekly on the 2nd and 5th days of each week. This group was also given the corresponding amount of 1% CMC (5 mL/kg b.wt) orally every other day for six weeks.
- (3) Paclitaxel-administered group treated with naringin: rats were administered paclitaxel intraperitoneally as in group 2 and received oral naringin 10 mg/kg b.wt treatment [39] every other day for six weeks (dismantled in 5 mL 1% CMC).
- (4) Paclitaxel-administered group treated with naringenin: rats were treated as above but were administered naringenin at a dose level 10 mg/kg b.wt [40] (dismantled in 5 mL 1% CMC) instead of naringin every other day for six weeks.
- (5) Paclitaxel-administered group treated with a combination of naringin and naringenin: rats were treated as above but received both naringin and naringenin at dose levels of 10 mg/kg (dismantled in 5 mL 1% CMC) b.wt every other day for six weeks.

2.4. Collection of Blood and Tissue Samples. Using diethyl ether inhalation anesthesia before decapitation and dissection and at the end of the experiment, blood samples were taken from each animal's jugular vein into gel and clot activator tubes, allowed to coagulate at room temperature, and then centrifuged at 3,000 rpm for 15 min. Clearly, nonhemolyzed sera were aspirated quickly, divided into four

aliquots, and kept at 30°C until they were needed for biochemical testing. Each animal's kidney and heart tissues were rapidly removed and weighed after decapitation and dissection. A portion of tissue of each organ was preserved in phosphate-buffered formalin (10%) for 24 h before being transferred to 70% alcohol for histological analysis. About 0.5 g of each tissue was homogenized in 5 mL saline (0.9% NaCl) with a Teflon homogenizer (Glas-Col, Terre Haute, USA). After the homogenates had been centrifuged for 15 minutes at 3,000 rpm, the supernatants were aspirated from the homogenates and kept in a deep freezer at -20°C for determination of oxidative/antioxidant status.

2.5. Examination of Serum Biomarkers for Kidney Function. Creatinine and urea levels in serum were measured as previously described by Fabiny and Ertingshausen [41] and Tabacco et al. [42]. Uric acid was assessed using the method of Fossati et al. [43].

2.6. Examination of Serum Biomarkers for Heart Function. CK-MB and LDH activities in serum were assayed as described by Young [44] and Young [45].

2.7. Assessment of Kidney and Heart Oxidative Stress and Antioxidant Levels. Kidney and heart lipid peroxidation (LPO) was estimated as previously described by Preuss et al. [46]. Briefly, protein was precipitated by adding 75 μ L of 76% trichloroacetic acid (TCA) to 0.5 mL of the kidney or heart homogenate. Then, 175 μ L of 1.07% thiobarbituric acid (TBA) was added. After 30 minutes in a water bath at 80°C, the formed faint pink color was detected at 532 nm. The standard was MDA (malondialdehyde or 1,1,3,3-tetramethoxypropane).

Kidney and heart GSH content was estimated by following the findings reported by Beutler et al. [47] with modifications by the addition of 0.5 mL 5,5'-dithiobis (2-nitrobenzoic acid) or Ellman's reagent for color development and phosphate buffer solution (pH 7) to homogenate supernatants after protein precipitation. The generated yellow color in samples and GSH standards were quantified at 412 nm against blank.

Kidney and heart glutathione peroxidase (GPx) activity was measured as previously described by Matkovic et al. [48]. This method is based on detecting GSH that has been transformed into oxidized glutathione (GSSG) through the detection of residual GSH and deducting it from the total. Briefly, 50 μ L of the homogeneous supernatant was placed in a Wasserman tube containing 350 μ L Tris buffer (pH 7.6), 50 μ L GSH solution (2 mM), and 50 μ L H₂O₂ (3.38 mM). The residual GSH content was determined after a 10-minute incubation period, as indicated previously. A standard was made by substituting 50 μ L distilled water for 50 μ L of the sample, and a blank was made by substituting 100 μ L distilled water for 50 μ L of the sample and 50 μ L GSH solution. The amount of GSH transformed to GSSG was then determined using the residual GSH content, and the enzyme activity was calculated.

The activity of superoxide dismutase (SOD) in the kidney and the heart was measured as previously described by Marklund and Marklund [49]. The procedure is focused on the suppression of auto-oxidation of pyrogallol by SOD. The presence of superoxide ions is required for the process to work. One unit of enzyme activity is the amount of an enzyme that reduces extinction by 50% in one minute relative to the control.

2.8. Histopathological Examination. Parts of the kidneys and hearts of rats were collected and fixed in 10% neutral buffered formalin for 24 h. Tissues were then washed with water and dehydrated in a series of ethyl alcohol dilutions (50%, 70%, 90%, 95%, 100%). Specimens were cleaned with xylene before being embedded in paraffin wax for 24 hours at 56°C in a furnace. Four μ m sections were cut from paraffin wax tissue blocks with a sliding microtome. For regular examination under an electric light microscope, the tissue sections were fixed on glass slides, dewaxed, and hematoxylin and eosin stained (H&E) [50]. Histopathological lesion scores were identified as previously described by El-Far et al. [51]. Score scale: 0 = normal; + \leq 25%; ++ = 26–50%; +++ = 51–75%; ++++ = 76–100%. The lesions were graded in a blinded manner.

2.9. Statistical Analysis. All data were presented as the mean \pm standard error of the mean (SEM). For statistical analysis, Statistical Package for the Social Sciences (SPSS) programme (version 22) (IBM software, USA) was utilized. Tukey's post hoc test was used to compare mean values pairwise. Differences were deemed significant at $p < 0.05$.

3. Results

3.1. Effect of Treatments on Kidney Function Parameters in Serum. Administration of paclitaxel to rats for 6 weeks produced a significant increase ($p < 0.05$) in serum urea, creatinine, and uric acid levels. Percentage changes were +52.43, +106.98, and +352.46%, respectively, compared to normal controls.

The increased urea, creatinine, and uric acid levels in paclitaxel-administered rats were significantly reduced after treatment with naringin and the combination. However, treatment with naringenin produced significant decreases only in elevated creatinine and urea levels; uric acid levels decreased but not significantly ($p > 0.05$). The naringin and naringenin combination seemed to be the most efficacious for normalizing elevated serum levels. Percentage decreases in urea, creatinine, and uric acid were -28.75, -47.19, and -40.22%, respectively, compared with paclitaxel alone (Table 1).

$$\% \text{change} = \left(\frac{\text{Final value} - \text{Initial value}}{\text{Initial value}} \right) \times 100 [52]. \quad (1)$$

3.2. Effect of Treatments on Heart Function Biomarkers in Serum. Administration of paclitaxel to rats for 6 weeks stimulated a significant rise in serum CK-MB and LDH

TABLE 1: Effect of naringin and/or naringenin on serum parameters related to kidney function.

Parameters and groups	Creatinine (mg/dl)	% change	Urea (mg/dl)	% change	Uric acid mg/dl	% change
Normal	0.43 ± 0.04	—	26.70 ± 1.17	—	0.61 ± 0.09	—
Paclitaxel	0.89 ± 0.04 ^a	106.98	40.70 ± 1.98 ^a	52.43	2.67 ± 0.29 ^a	352.46
Paclitaxel + naringin	0.65 ± 0.05 ^{ab}	-26.97	29.20 ± 1.66 ^b	-28.26	1.72 ± 0.13 ^{ab}	-37.68
Paclitaxel + naringenin	0.53 ± 0.04 ^b	-40.45	30.80 ± 1.08 ^b	-24.32	2.22 ± 0.79 ^a	-19.57
Paclitaxel + naringin + naringenin	0.47 ± 0.02 ^b	-47.19	29.00 ± 1.37 ^b	-28.75	1.65 ± 0.08 ^{ab}	-40.22

Data are expressed as mean ± SEM ($n=6$). ^a $p < 0.05$: significant compared with the normal group. ^b $p < 0.05$: significant compared with the paclitaxel-administered group. Percentage changes were calculated by comparing the paclitaxel-administered group with the normal and the paclitaxel-administered groups treated with naringin and/or naringenin with the paclitaxel-administered group.

activities with percentage changes of +359.26 and +293.55%, respectively, in comparison to the normal control group. The treatment of paclitaxel-administered rats with naringin and naringenin and their combination produced significant decreases in the elevated CK-MB activity with percentage changes of -46.13, -55.52, and -47.76%, respectively. Similarly, LDH activity also significantly decreased after treatment with naringin and naringenin and their combination recording percentage decreases of -46.41, -48.86, and -50.81%, respectively (Table 2).

$$\% \text{change} = \frac{\text{Final value} - \text{Initial value}}{\text{Initial value}} \times 100 [52]. \quad (2)$$

3.3. Effect of Treatments on the Parameters of Antioxidant Defence and Oxidative Stress in the Kidneys and the Heart. As outlined in Table 3, administration of paclitaxel to rats significantly raised kidney LPO (+54.93%) and significantly decreased GSH levels (-53.09%) and SOD (-8.19%) and GPx (-23.23%) activities in comparison to the normal control group. The oral dose of naringin and naringenin and their combination improved kidney LPO significantly. Additionally, treatment with naringin and naringenin or their combination resulted in a significant increase in kidney GSH content. Also, these treatments reversed the decline in activities of kidney SOD and GPx.

$$\% \text{change} = \frac{\text{Final value} - \text{Initial value}}{\text{Initial value}} \times 100 [52]. \quad (3)$$

In a similar way as in the kidney, paclitaxel administration resulted in a significant increase in LPO in heart tissue, whereas heart GSH content, SOD activity, and GPx activity decreased significantly. Naringin and naringenin and their combination significantly increased cardiac LPO. Additionally, heart GSH content was significantly increased as a result of the treatment with naringin and the combination. However, the treatment with naringenin resulted in a nonsignificant rise in heart GSH content. Moreover, all three treatments significantly enhanced heart SOD and GPx activities (Table 4).

$$\% \text{change} = \frac{\text{Final value} - \text{Initial value}}{\text{Initial value}} \times 100 [52]. \quad (4)$$

3.4. Kidney Histopathology. Renal lesions are illustrated in Table 5 and Figure 1. Histological examination of kidney sections of normal control rats exhibited normal histological construction (Figure 1(a)). Conversely, paclitaxel administration resulted in deleterious histological changes and a variety of lesions, including severe lesions, mostly in the form of severe mononuclear leukocyte inflammatory cell infiltration, degenerative changes combined with nuclear pyknosis of the renal lining epithelium, and apoptosis (Figures 1(b) and 1(c)). The apoptotic morphological changes include cell shrinkage, nuclear shrinkage, hyper-eosinophilic cytoplasm due to cytoplasmic condensation, nuclear condensation, nuclear fragmentation (karyorrhexis), nuclear pyknosis, apoptotic blebs, and rounded hyperchromatic apoptotic bodies. Severe glomerulonephritis was also observed. Additionally, there was focal interstitial nephritis that was escorted by glomerular tuft and interstitial blood capillary congestion (Figure 1(b)). When rats receiving paclitaxel were given naringin, some histological changes and a number of lesions were observed, such as the degeneration and necrosis of the renal lining epithelium and focal mononuclear leukocyte inflammatory cells in interstitial tissues, which were accompanied by mild glomerulonephritis and mild apoptosis (Figure 1(d)). Paclitaxel/naringenin-treated rats exhibited milder lesions than paclitaxel/naringin-treated rats (Figure 1(e)). The administration of paclitaxel/naringin/naringenin showed a quite improvement in renal lesions compared to other treated rats (Figure 1(f)).

3.5. Heart Histopathology. Cardiac pathological lesions are described in Table 6 and Figure 2. Intact histological structures in cardiac muscles were observed in tissues from normal controls (Figure 2(a)). The paclitaxel administration produced many heart histological deleterious changes, including severe degenerative changes and necrosis of cardiac muscles, as well as mild apoptotic changes (AP) represented by apoptotic cells characterized by condensed eosinophilic cytoplasm and condensed pyknotic nuclei (Figure 2(b)). Also, minimal apoptotic changes are shown in Figure 2(c). Treatment with naringin (Figure 2(d)), naringenin (Figure 2(e)), and their combination (Figure 2(f)) produced notable reversal of paclitaxel-induced histological changes.

TABLE 2: Effect of naringin and/or naringenin on serum parameters related to heart function.

Parameters and groups	CK-MB(U/L)	% change	LDH (U/L)	% change
Normal	8.42 ± 0.71	—	586.75 ± 36.85	—
Paclitaxel	38.67 ± 4.41 ^a	359.26	2309.17 ± 105.09 ^a	293.55
Paclitaxel + naringin	20.83 ± 1.72 ^{ab}	-46.13	1237.50 ± 152.19 ^{ab}	-46.41
Paclitaxel + naringenin	17.20 ± 1.05 ^b	-55.52	1180.83 ± 105.25 ^{ab}	-48.86
Paclitaxel + naringin + naringenin	20.20 ± 1.54 ^{ab}	-47.76	1135.83 ± 48.25 ^{ab}	-50.81

Data are expressed as mean ± SEM (n = 6). a $p < 0.05$: significant compared with normal group. b $p < 0.05$: significant compared with paclitaxel-administered group. Percentage changes were calculated by comparing paclitaxel-administered group with normal, and paclitaxel-administered groups treated with naringin and/or naringenin with paclitaxel-administered group.

TABLE 3: Effect of naringin and/or naringenin on kidney LPO, GSH content, and SOD and GPx activities.

Parameters and groups	LPO (nmol MDA/100 mg tissue/hour)	% change	GSH (nmol/100 mg tissue)	% change	SOD (U/g)	% change	GPx (mU/100 mg tissue)	% change
Normal	14.20 ± 0.83	—	108.12 ± 3.32	—	18.93 ± 0.19	—	104.16 ± 1.12	—
Paclitaxel	22.00 ± 0.93 ^a	54.93	50.7 ± 3.95 ^a	-53.09	17.38 ± 0.20 ^a	-8.19	79.962.18 ^a	-23.23
Paclitaxel + naringin	14.80 ± 0.81 ^b	-32.73	96.22 ± 3.77 ^b	89.74	18.48 ± 0.11 ^b	6.33	91.96 ± 1.43 ^{ab}	15.01
Paclitaxel + naringenin	17.40 ± 0.51 ^b	-20.91	89.95 ± 4.20 ^{ab}	77.38	18.59 ± 0.14 ^b	6.96	88.45 ± 0.93 ^{ab}	10.62
Paclitaxel + naringin + naringenin	16.20 ± 1.3 ^b	-26.36	92.42 ± 3.37 ^{ab}	82.25	18.62 ± 0.23 ^b	7.13	86.72 ± 2.69 ^a	8.45

Data are expressed as mean ± SEM (n = 6). a $p < 0.05$: significant compared with normal group. b $p < 0.05$: significant compared with paclitaxel-administered group. Percentage changes were calculated by comparing paclitaxel-administered group with normal, and paclitaxel-administered groups treated with naringin and/or naringenin with paclitaxel-administered group.

TABLE 4: Effect of naringin and/or naringenin on heart LPO, GSH content, and SOD and GPx activities.

Parameters and groups	LPO (nmol MDA/100 mg tissue/hour)	% change	GSH (nmol/100 mg tissue)	% change	SOD (U/g)	% change	GPx (mU/100 mg tissue)	% change
Normal	11.90 ± 0.67	—	89.30 ± 3.30	—	18.82 ± 0.04	—	100.90 ± 1.60	—
Paclitaxel	22.40 ± 0.63 ^a	88.24	53.60 ± 2.90 ^a	-40	17.05 ± 0.19 ^a	-9.40	86.40 ± 1.70 ^a	-14.37
Paclitaxel + naringin	12.50 ± 0.98 ^b	-44.20	71.40 ± 1.40 ^{ab}	33.21	18.47 ± 0.08 ^b	8.32	98.20 ± 0.70 ^b	13.66
Paclitaxel + naringenin	12.90 ± 0.79 ^b	-42.41	63.50 ± 4.20 ^a	18.47	18.38 ± 0.06 ^{ab}	7.80	92.20 ± 0.30 ^{ab}	6.71
Paclitaxel + naringin + naringenin	16.80 ± 0.15 ^{ab}	-25.00	86.20 ± 0.80 ^b	60.82	18.36 ± 0.04 ^{ab}	7.68	95.50 ± 1.40 ^{ab}	10.53

Data are expressed as mean ± SEM (n = 6). a $p < 0.05$: significant compared with normal group. b $p < 0.05$: significant compared with paclitaxel-administered group. Percentage changes were calculated by comparing paclitaxel-administered group with normal, and paclitaxel-administered groups treated with naringin and/or naringenin with paclitaxel-administered group.

4. Discussion

Paclitaxel is largely effective for ancillary treatment of tumors in ovarian [53] and breast cancer [54, 55]. Unfortunately, paclitaxel therapy can increase acquired resistance, resulting in chemotherapy failure [56]. Further, paclitaxel has limited clinical application due to its low water solubility and low compatibility with excipients in formulations [5]. Paclitaxel raised levels of oxidative and nitrosative stress markers in mice [57] and may have caused kidney damage due to ROS generation, which induces oxidative stress [58]. Moreover, paclitaxel induces oxidative stress and cardiotoxicity in adult male Wistar rats [59].

The current study showed the impact of serial intraperitoneal injections of paclitaxel over a period of six weeks at the dose level of 2 mg/kg b.wt 2 days/week. These injections induced nephrotoxicity evidenced biochemically by a significant elevation of serum urea, creatinine, and uric acid levels. Thus, the drug impairs renal function and may

compromise urinary excretion of toxic metabolites. Our data are consistent with those reported by Adikwu et al. [58]. Ahmed et al. [60] also found that paclitaxel affected renal function, reflected in significant elevation of serum urea and creatinine levels in adult male albino rats. In the current investigation, histopathological analysis of renal sections of paclitaxel-administered rats supported the previous biochemical results. The kidney exhibited several adverse histological changes and lesions, including severe degenerative changes in renal epithelium associated with focal lymphocytic infiltration and severe glomerulonephritis. Moreover, focal interstitial nephritis and moderate apoptotic lesions were observed, accompanied by congestion in interstitial blood capillaries and the glomerular tuft. Previous studies indicated that paclitaxel treatment causes congested glomerular capillaries, cellular infiltration, extravasation, and vacuolated tubular cells [60]. Similarly, Choudhury et al. [61] observed atrophic changes in glomeruli and kidney tubules in experimental animals treated with paclitaxel, which may

TABLE 5: Pathological renal lesion scores in different groups.

Parameters and groups	Degenerative of renal tubules	Necrosis of renal tubules	Congestion	Leukocyte infiltration	Glomerulonephritis	Apoptosis
Normal	-	-	-	-	-	-
Paclitaxel	+++	++	+++	+++	+++	++++
Paclitaxel + naringin	++	++	++	++	++	++
Paclitaxel + naringenin	++	+	++	-	+	+
Paclitaxel + naringin + naringenin	+	-	+	-	-	+

Lesion types are (-) absence, (+) minimal, (++) mild, (+++) moderate, and (++++) severe.

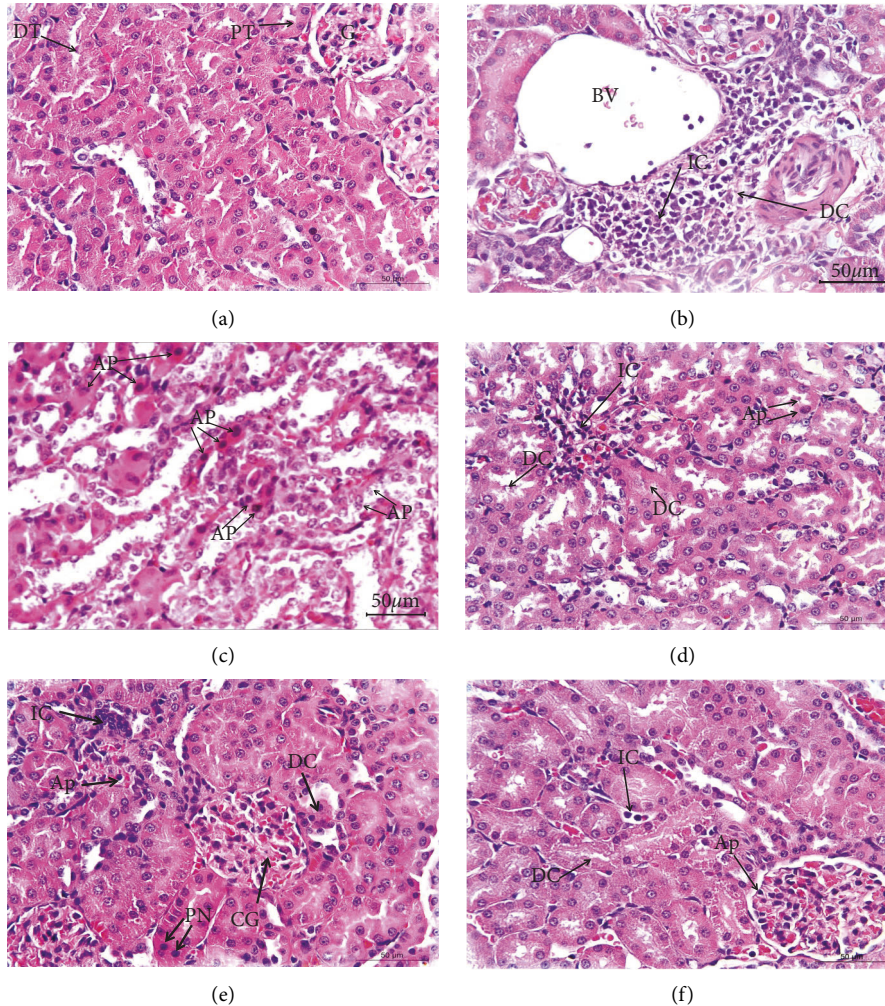


FIGURE 1: Photomicrographs of kidney sections of different experimental groups. (a) A photomicrograph of a kidney segment of healthy rats revealed glomeruli (G), proximal tubules (PTs), and distal tubules (DTs) and all had typical histologic structures. (b) A photomicrograph of the kidney section of paclitaxel-administered rats passing through the blood vessel (BV) underwent significant degenerative changes (DCs) that were linked with localized mononuclear leukocyte infiltration (IC). (c) Another kidney section of paclitaxel-administered rats revealed the presence of severe apoptotic changes (AP). (d) A photomicrograph of the kidney section of rats given paclitaxel and treated with naringin revealed mild apoptotic changes (AP) and mild degenerative changes (DCs) linked with lymphocytic infiltration (IC). (e) A photomicrograph of the kidney section of rats given paclitaxel and treated with naringenin showing congested glomerulus (CG), mild degenerative changes (DCs), minor apoptotic changes (AP), focal pyknotic nuclei (PN), and significant inflammatory cell infiltration were all visible (IC). (f) A kidney section of rats given paclitaxel and treated with a combination of naringin and naringenin showing infiltration of inflammatory cells (ICs), minor apoptotic changes (AP), and minor degenerative changes (DCs) (H&E; 400X).

TABLE 6: Pathological cardiac lesion scores in different groups.

Parameters and groups	Coagulative necrosis (hyalinosis)	Leukocyte infiltration	Apoptosis
Normal	–	–	–
Paclitaxel	++	+++	++
Paclitaxel + naringin	+	–	+
Paclitaxel + naringenin	++	+	–
Paclitaxel + naringin + naringenin	+	+	–

Lesion types are (–) absence, (+) minimal, (++) mild, (+++) moderate, and (+++++) severe.

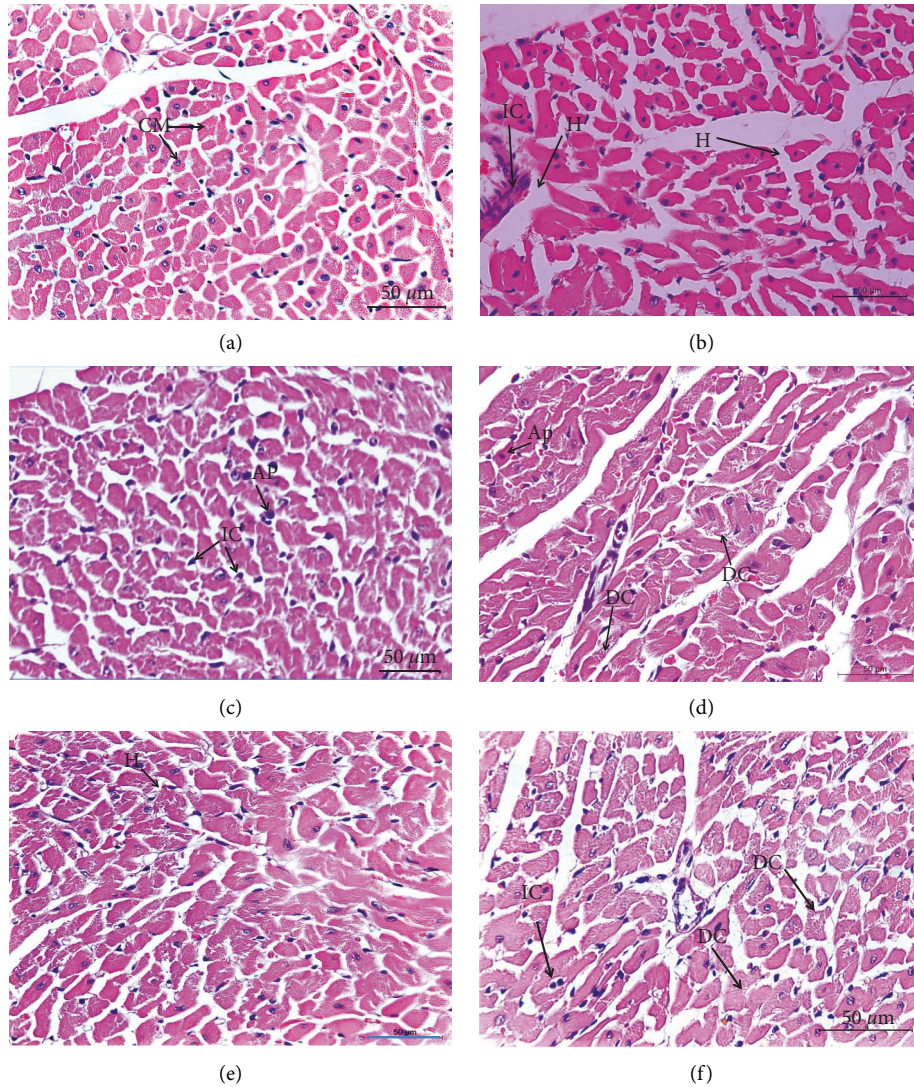


FIGURE 2: Photomicrographs of heart sections of different experimental groups. (a) A section of the rat's normal heart was photographed, revealing the typical histologic anatomy of its cardiac muscles (CM). (b, c) The heart of a paclitaxel-treated rat is shown in a photomicrograph, with marked degenerative changes (DCs), inflammatory cell infiltration (IC), hyalinosis (H), and apoptotic changes (AP). (d) The cardiac tissue of rats given paclitaxel and naringin revealed moderate degenerative changes (DCs) and minor apoptotic changes (AP). (e) Mild hyalinosis (H) was visible in the cardiac section of paclitaxel-administered rats treated with naringenin. (f) A section of the heart of paclitaxel-administered rats treated with a combination of naringin and naringenin revealed moderate degenerative changes (DCs) linked with minimal inflammatory cell infiltration (IC) (H&E; 400X).

be due to high CrEL content. Paclitaxel also adversely affected renal morphology by inducing hypercellular glomeruli and tubular necrosis combined with apoptotic changes [58,62]. Apoptosis is mediated by caspases, a family of cysteine proteases whose stimulation is triggered by specific apoptotic stimuli and whose substrates include numerous proteins [63], and the restricted cleavage of which results in apoptosis-like morphological features [62].

Citrus flavonoids naringin and naringenin have anti-inflammatory and antioxidant effects both *in vivo* and *in vitro* [64]. In comparison to many previous studies, natural products offer the best hope for improving tumor-targeting drugs [65–69]. In our study, treatment of paclitaxel-administered rats with naringin and naringenin or their combination reduced elevated urea, creatinine, and uric acid levels and substantially restored histological integrity in agreement with previous studies by Ahmed et al. [70] who reported that naringin and naringenin enhanced kidney function and structural integrity in male rats. Also, naringin countered nephrotoxicity induced by methotrexate in male rats [71], and naringenin was nephroprotective against carbon tetrachloride-induced nephrotoxicity in mice [72]. Quercetin, a similar flavonoid, has been shown to alleviate renal and pancreatic tissue alterations caused by D-galactose in rats [51].

In the present study, paclitaxel administration also induced cardiotoxicity, evidenced biochemically by a significant increase in serum activity of CK-MB and LDH. Histopathological findings supported these changes in serum enzyme activities. The hearts of the paclitaxel-administered group exhibited several adverse histological changes and lesions, including severe degenerative changes and necrosis of cardiac muscles accompanied by the presence of inflammatory and apoptotic cells. These findings concur with those of Saad et al. [73] who indicated that paclitaxel treatment resulted in a marked increase in serum activities of (LDH and CK-MB) and also produced cytoplasmic vacuolation of heart myocytes. Additionally, Malakinejad et al. [59] found that paclitaxel increased CK-BM activity and produced pathological lesions, such as diffuse edema, hemorrhage, hyaline exudates, congestion, and necrosis. Moreover, increased LDH activities in patients treated with paclitaxel are associated with oxidative pre-hemolytic injury, as observed previously *in vitro* [74]. Besides, paclitaxel treatment affects adult cardiomyocytes, mainly noticeable in changes in myofibrillar structure and function [75]. Paclitaxel was also reported to induce apoptosis in cardiac tissue [76].

In the current study, treatment of paclitaxel-administered rats with naringin and/or naringenin resulted in improvement in cardiac biomarkers and histological integrity. These outcomes are in line with those of Rajadurai and Prince [77] who showed that naringin improved cardiac biochemical and histopathological alterations induced by isoproterenol in Wistar rats. The agent also protects against cardiac toxicity induced by doxorubicin *in vivo* and *in vitro* [78–80]. Moreover, Zhao et al. [81]

reported that naringenin protects the cardiovascular system from palmitate-induced apoptosis in endothelial cells of human umbilical veins.

Renal and cardiac toxicity in paclitaxel-administered rats was correlated with a noticeable rise in kidney and heart LPO and a reduction in nonenzymatic antioxidant GSH content and enzymatic antioxidant (SOD and GPx) activities. These findings corroborate the findings of several other researchers [82–84] who reported that paclitaxel treatment weakens antioxidant defense systems. Paclitaxel administration caused renal damage *via* ROS generation, resulting in oxidative stress [58, 85]. Also, strong evidence exists that oxidative stress is closely associated with cardiotoxicity induced by antitumor drugs [86]. Moreover, administration of paclitaxel caused a notable increase in LPO as well as an increase in NO levels in the heart [59].

The current study's findings showed that administering naringin and/or naringenin decreases LPO, increases GSH content, and augments SOD and GPx activities in kidney and heart tissue after six weeks of treatment. This improvement may be attributed to scavenging ROS and free radicals induced by paclitaxel intoxication. These findings are consistent with those of the research by Fukui et al. [87] who proved that flavonoids inhibit paclitaxel-induced ROS generation. Moreover, Cavia-Saiz et al. [88] showed that naringin and naringenin are potent free radical scavengers and can prevent LPO. Harisa [89] proposed that naringin reversed paclitaxel-induced erythrocyte aging by reducing oxidative stress. Also, Sahu et al. [90] suggested that naringenin restored antioxidant enzymes by scavenging free radicals *via* its OH group and that this scavenging was responsible for reduced hepatic and renal damage.

5. Conclusion

Naringin and naringenin and their combination prevent many adverse impacts on renal and cardiac function and histological integrity induced by paclitaxel in Wistar rats. This action is due to suppressing oxidative stress and enhancing antioxidant defense systems in both organs. The combination of naringin and naringenin was the most efficacious for protecting kidney and heart function and structural integrity. An important limitation of the study is the shortage of kidney and heart samples to perform Western blot analysis for determination of various mediators of apoptosis and inflammations due to their exhaustion in detection of oxidative stress/antioxidants biomarkers and histological investigations. Furthermore, clinical studies are required to assess the safety and efficacy of naringin and naringenin and their combination against paclitaxel-deteriorated effects on the heart and kidneys in human beings.

Data Availability

All data are available from the corresponding author upon reasonable request.

Conflicts of Interest

The authors declare that they have no conflicts of interest.

References

- [1] A. M. Seca and D. C. Pinto, "Plant secondary metabolites as anticancer agents: successes in clinical trials and therapeutic application," *International Journal of Molecular Sciences*, vol. 19, no. 1, p. 263, 2018.
- [2] J. Arnst, "When Taxol met tubulin," *Journal of Biological Chemistry*, vol. 295, no. 41, pp. 13994-13995, 2020.
- [3] L. Zhu and L. Chen, "Progress in research on paclitaxel and tumor immunotherapy," *Cellular and Molecular Biology Letters*, vol. 24, no. 1, pp. 40-11, 2019.
- [4] B. Gorain, H. Choudhury, M. Pandey, and P. Kesharwani, "Paclitaxel loaded vitamin E-TPGS nanoparticles for cancer therapy," *Materials Science And Engineering: C*, vol. 91, pp. 868-880, 2018.
- [5] S. Ezrahi, A. Aserin, and N. Garti, "Basic principles of drug delivery systems—the case of paclitaxel," *Advances in Colloid and Interface Science*, vol. 263, pp. 95-130, 2019.
- [6] N. P. Staff, J. C. Fehrenbacher, M. Caillaud, M. I. Damaj, R. A. Segal, and S. Rieger, "Pathogenesis of paclitaxel-induced peripheral neuropathy: a current review of *in vitro* and *in vivo* findings using rodent and human model systems," *Experimental Neurology*, vol. 324, Article ID 113121, 2020.
- [7] T. M. Abu Samaan, M. Samec, A. Liskova, P. Kubatka, and D. Büsselberg, "Paclitaxel's mechanistic and clinical effects on breast cancer," *Biomolecules*, vol. 9, no. 12, p. 789, 2019.
- [8] A. M. Sofias, M. Dunne, G. Storm, and C. Allen, "The battle of "nano" paclitaxel," *Advanced Drug Delivery Reviews*, vol. 122, pp. 20-30, 2017.
- [9] I. Klein and H. C. Lehmann, "Pathomechanisms of paclitaxel-induced peripheral neuropathy," *Toxics*, vol. 9, no. 10, p. 229, 2021.
- [10] X. Du, A. R. Khan, M. Fu, J. Ji, A. Yu, and G. Zhai, "Current development in the formulations of non-injection administration of paclitaxel," *International Journal of Pharmaceutics*, vol. 542, no. 1, pp. 242-252, 2018.
- [11] P. Evenepoel, "Acute toxic renal failure," *Best Practice & Research Clinical Anaesthesiology*, vol. 18, no. 1, pp. 37-52, 2004.
- [12] N. Lameire, W. Van Biesen, and R. Vanholder, "Acute renal failure," *The Lancet*, vol. 365, no. 9457, pp. 417-430, 2005.
- [13] Y. Shimeda, Y. Hirotani, Y. Akimoto et al., "Protective effects of capsaicin against cisplatin-induced nephrotoxicity in rats," *Biological and Pharmaceutical Bulletin*, vol. 28, no. 9, pp. 1635-1638, 2005.
- [14] M. Haghghi, M. Nematbakhsh, A. Talebi et al., "The role of angiotensin II receptor 1 (AT1) blockade in cisplatin-induced nephrotoxicity in rats: gender-related differences," *Renal Failure*, vol. 34, no. 8, pp. 1046-1051, 2012.
- [15] M. Nematbakhsh, F. Ashrafi, T. Safari et al., "Administration of vitamin E and losartan as prophylaxes in cisplatin-induced nephrotoxicity model in rats," *Journal of Nephrology*, vol. 25, no. 3, pp. 410-417, 2012.
- [16] G. Alloatti, C. Penna, M. P. Gallo et al., "Differential effects of paclitaxel and derivatives on Guinea pig isolated heart and papillary muscle," *Journal of Pharmacology and Experimental Therapeutics*, vol. 284, no. 2, pp. 561-567, 1998.
- [17] H. M. Babiker, A. McBride, M. Newton et al., "Cardiotoxic effects of chemotherapy: a review of both cytotoxic and molecular targeted oncology therapies and their effect on the cardiovascular system," *Critical Reviews in Oncology*, vol. 126, pp. 186-200, 2018.
- [18] A. Meshkini and R. Yazdanparast, "Involvement of oxidative stress in taxol-induced apoptosis in chronic myelogenous leukemia K562 cells," *Experimental & Toxicologic Pathology*, vol. 64, no. 4, pp. 357-365, 2012.
- [19] A. N. Ilinskaya, J. D. Clogston, S. E. McNeil, and M. A. Dobrovolskaia, "Induction of oxidative stress by Taxol® vehicle Cremophor-EL triggers production of interleukin-8 by peripheral blood mononuclear cells through the mechanism not requiring de novo synthesis of mRNA," *Nanomedicine: Nanotechnology, Biology and Medicine*, vol. 11, no. 8, pp. 1925-1938, 2015.
- [20] J. Meng, F. Guo, H. Xu, W. Liang, C. Wang, and X. D. Yang, "Combination therapy using co-encapsulated resveratrol and paclitaxel in liposomes for drug resistance reversal in breast cancer cells *in vivo*," *Scientific Reports*, vol. 6, no. 1, pp. 22390-22411, 2016.
- [21] P. Chowdhury, P. K. Nagesh, E. Hatami et al., "Tannic acid-inspired paclitaxel nanoparticles for enhanced anticancer effects in breast cancer cells," *Journal of Colloid and Interface Science*, vol. 535, pp. 133-148, 2019.
- [22] Y. Ding, T. Wang, T. Chen, C. Xie, and Q. Zhang, "Sesquiterpenoids isolated from the flower of *Inula Japonica* as potential antitumor leads for intervention of Paclitaxel-resistant non-small-cell lung cancer," *Bioorganic Chemistry*, vol. 101, Article ID 103973, 2020.
- [23] Y. Wang, H. Yu, S. Wang et al., "Targeted delivery of quercetin by nanoparticles based on chitosan sensitizing paclitaxel-resistant lung cancer cells to paclitaxel," *Materials Science and Engineering: C*, vol. 119, Article ID 111442, 2021.
- [24] A. Rašković, N. Stilić, J. Kolarović, V. Vasović, S. Vukmirović, and M. Mikov, "The protective effects of silymarin against doxorubicin-induced cardiotoxicity and hepatotoxicity in rats," *Molecules*, vol. 16, no. 10, pp. 8601-8613, 2011.
- [25] J. S. Choi, Y. J. Piao, and K. W. Kang, "Effects of quercetin on the bioavailability of doxorubicin in rats: role of CYP3A4 and P-gp inhibition by quercetin," *Archives of Pharmacological Research*, vol. 34, no. 4, pp. 607-613, 2011.
- [26] A. H. M. Viswanatha Swamy, U. M. Patel, B. C. Koti, P. C. Gadad, N. L. Patel, and A. H. M. Thippeswamy, "Cardioprotective effect of *Saraca indica* against cyclophosphamide induced cardiotoxicity in rats: a biochemical, electrocardiographic and histopathological study," *Indian Journal of Pharmacology*, vol. 45, no. 1, pp. 44-48, 2013.
- [27] A. I. Matouk, A. Taye, G. H. Heeba, and M. A. El-Moselhy, "Quercetin augments the protective effect of losartan against chronic doxorubicin cardiotoxicity in rats," *Environmental Toxicology and Pharmacology*, vol. 36, no. 2, pp. 443-450, 2013.
- [28] E. Şengül, V. Gelen, S. Gedikli et al., "The protective effect of quercetin on cyclophosphamide-Induced lung toxicity in rats," *Biomedicine & Pharmacotherapy*, vol. 92, pp. 303-307, 2017.
- [29] A. K. Verma and S. Singh, "Phytochemical analysis and *in vitro* cytostatic potential of ethnopharmacological important medicinal plants," *Toxicology Reports*, vol. 7, pp. 443-452, 2020.
- [30] A. Hajdari, B. Mustafa, L. Hyseni et al., "Phytochemical study of eight medicinal plants of the lamiaceae family traditionally used as tea in the Sharri Mountains region of the Balkans," *The Scientific World Journal*, vol. 2020, pp. 1-9, 2020.

- [31] A. V. Anand, B. Balamuralikrishnan, M. Kaviya et al., "Medicinal plants, phytochemicals, and herbs to combat viral pathogens including SARS-CoV-2," *Molecules*, vol. 26, no. 6, p. 1775, 2021.
- [32] A. A. Alzandi, E. A. Taher, N. A. Al-Sagheer, A. W. Al-Khulaidi, M. Azizi, and D. M. Naguib, "Phytochemical components, antioxidant and anticancer activity of 18 major medicinal plants in Albaha region, Saudi Arabia," *Biocatalysis and Agricultural Biotechnology*, vol. 34, Article ID 102020, 2021.
- [33] A. S. Choudhari, P. C. Mandave, M. Deshpande, P. Ranjekar, and O. Prakash, "Phytochemicals in cancer treatment: from preclinical studies to clinical practice," *Frontiers in Pharmacology*, vol. 10, p. 1614, 2019.
- [34] F. Turati, M. Rossi, C. Pelucchi, F. Levi, and C. La Vecchia, "Fruit and vegetables and cancer risk: a review of southern European studies," *British Journal of Nutrition*, vol. 113, no. S2, pp. S110–S102, 2015.
- [35] F. N. Ekinçi Akdemir, İ. Gülçin, B. Karagöz, R. Soslu, and S. H. Alwasel, "A comparative study on the antioxidant effects of hesperidin and ellagic acid against skeletal muscle ischemia/reperfusion injury," *Journal of Enzyme Inhibition and Medicinal Chemistry*, vol. 31, no. sup4, pp. 114–118, 2016.
- [36] E. Gerçek, H. Zengin, F. E. Erişir, and Ö. Yılmaz, "Biochemical changes and antioxidant capacity of naringin and naringenin against malathion toxicity in *Saccharomyces cerevisiae*. Comparative Biochemistry and Physiology Part C," *Toxicology & Pharmacology*, vol. 241, Article ID 108969, 2021.
- [37] A. Rauf, M. A. Shariati, and M. Imran, "Comprehensive Review on Naringenin and Naringin Polyphenols as a Potent Anticancer Agent," *Environmental Science and Pollution Research*, vol. 29, pp. 1–17, 2022.
- [38] W. Gao, Y. Zan, Z. J. Wang, X. Y. Hu, and F. Huang, "Quercetin ameliorates paclitaxel-induced neuropathic pain by stabilizing mast cells, and subsequently blocking PKC ϵ -dependent activation of TRPV1," *Acta Pharmacologica Sinica*, vol. 37, no. 9, pp. 1166–1177, 2016.
- [39] T. K. Reddy, I. Nagaraju, K. H. Kumar, V. Lokanatha, C. D. Reddy, and G. C. Jagetia, "Cardioprotective effect of naringin in mice treated with doxorubicin," *Planta Medica*, vol. 74, no. 03, 2008.
- [40] M. Roghani, F. Fallahi, and S. Moghadami, "Citrus flavonoid naringenin improves aortic reactivity in streptozotocin-diabetic rats," *Indian Journal Of Pharmacology*, vol. 44, no. 3, pp. 382–386, 2012.
- [41] D. L. Fabiny and G. Ertingshausen, "Automated reaction-rate method for determination of serum creatinine with the CentrifChem," *Clinical Chemistry (Washington, DC, United States)*, vol. 17, no. 8, pp. 696–700, 1971.
- [42] A. Tabacco, F. Meiattini, E. Moda, and P. Tarli, "Simplified enzymic/colorimetric serum urea nitrogen determination," *Clinical Chemistry*, vol. 25, no. 2, pp. 336–337, 1979.
- [43] P. Fossati, L. Prencipe, and G. Berti, "Use of 3, 5-dichloro-2-hydroxybenzenesulfonic acid/4-aminophenazone chromogenic system in direct enzymic assay of uric acid in serum and urine," *Clinical Chemistry*, vol. 26, no. 2, pp. 227–231, 1980.
- [44] D. S. Young, *Effects of Drugs on Clinical Laboratory Tests*, AACC press, 1995.
- [45] D. S. Young, *Effects of Drugs on Clinical Laboratory Tests*, AACC press, 2000.
- [46] H. G. Preuss, S. T. Jarrell, R. Scheckenbach, S. Lieberman, and R. A. Anderson, "Comparative effects of chromium, vanadium and *Gymnema sylvestre* on sugar-induced blood pressure elevations in SHR," *Journal of the American College of Nutrition*, vol. 17, no. 2, pp. 116–123, 1998.
- [47] E. Beutler, O. Duren, and B. M. Kelly, "Improved method for the determination of blood glutathione," *The Journal of Laboratory and Clinical Medicine*, vol. 61, pp. 882–888, 1963.
- [48] B. Matkoviics, M. Kotorman, I. S. Varga, D. Q. Hai, and C. Varga, "Oxidative stress in experimental diabetes induced by streptozotocin," *Acta Physiologica Hungarica*, vol. 85, no. 1, pp. 29–38, 1998.
- [49] S. Marklund and G. Marklund, "Involvement of the superoxide anion radical in the autoxidation of pyrogallol and a convenient assay for superoxide dismutase," *European Journal of Biochemistry*, vol. 47, no. 3, pp. 469–474, 1974.
- [50] J. D. Bancroft, A. Stevens, and D. R. Turner, *Theory and Practice of Histological Techniques*, Churchill living stone New York, London, San Francisco, Tokyo, 1996.
- [51] A. H. El-Far, M. A. Lebda, A. E. Noreldin et al., "Quercetin attenuates pancreatic and renal D-galactose-induced aging-related oxidative alterations in rats," *International Journal of Molecular Sciences*, vol. 21, no. 12, pp. 4348–48, 2020.
- [52] A. M. Zaazaa, "Studying the anticancer properties of bone MarrowDerived mesenchymal stem cells against hepatocellular carcinoma induced by N-nitrosodiethylamine in male rats," *Biointerface Research in Applied Chemistry*, vol. 13, no. 1, pp. 1–13, 2022.
- [53] F. Gu, H. Zhang, L. Yao et al., "Leptin contributes to the taxol chemoresistance in epithelial ovarian cancer," *Oncology Letters*, vol. 18, no. 1, pp. 561–570, 2019.
- [54] X. Hou, Z. Niu, L. Liu et al., "miR-1207-5p regulates the sensitivity of triple-negative breast cancer cells to Taxol treatment via the suppression of LZTS1 expression," *Oncology Letters*, vol. 17, no. 1, pp. 990–998, 2019.
- [55] A. Tomko, L. O'Leary, H. Trask et al., "Antitumor activity of abnormal cannabidiol and its analog O-1602 in taxol-resistant preclinical models of breast cancer," *Frontiers in Pharmacology*, vol. 10, p. 1124, 2019.
- [56] Y. Wang, Y. Zhou, Z. Zheng, J. Li, Y. Yan, and W. Wu, "Sulforaphane metabolites reduce resistance to paclitaxel via microtubule disruption," *Cell Death & Disease*, vol. 9, no. 11, pp. 1134–1215, 2018.
- [57] N. Ishii, H. Tsubouchi, A. Miura et al., "Ghrelin alleviates paclitaxel-induced peripheral neuropathy by reducing oxidative stress and enhancing mitochondrial anti-oxidant functions in mice," *European Journal of Pharmacology*, vol. 819, pp. 35–42, 2018.
- [58] E. Adikwu, N. Ebinyo, and D. O. Orakpor, "Coenzyme Q10 and resveratrol protect against paclitaxel-induced nephrotoxicity in rats," *Trends in Pharmaceutical Sciences*, vol. 7, pp. 49–58, 2021.
- [59] H. Malekinejad, S. Ahsan, F. Delkhosh-Kasmaie, H. Cheraghi, A. Rezaei-Golmisheh, and H. Janbaz-Acyabar, "Cardioprotective effect of royal jelly on paclitaxel-induced cardiotoxicity in rats," *Iranian journal of basic medical sciences*, vol. 19, no. 2, pp. 221–227, 2016.
- [60] S. M. Ahmed, M. Z. Mohammed, and A. A. Mahmoud, "The role of gold nanoparticles on taxol-induced renal cortex damage in adult male albino rats," *Egyptian Journal of Histology*, vol. 41, no. 3, pp. 1–13, 2018.
- [61] H. Choudhury, B. Gorain, R. K. Tekade, M. Pandey, S. Karmakar, and T. K. Pal, "Safety against nephrotoxicity in paclitaxel treatment: oral nanocarrier as an effective tool in preclinical evaluation with marked *in vivo* antitumor activity," *Regulatory Toxicology and Pharmacology*, vol. 91, pp. 179–189, 2017.

- [62] S. O. Rabah, "Acute Taxol nephrotoxicity: histological and ultrastructural studies of mice kidney parenchyma," *Saudi Journal of Biological Sciences*, vol. 17, no. 2, pp. 105–114, 2010.
- [63] G. S. Salvesen, "Caspases and apoptosis," *Essays in Biochemistry*, vol. 38, pp. 9–19, 2002.
- [64] E. Tripoli, M. L. Guardia, S. Giammanco, D. D. Majo, and M. Giammanco, "Citrus flavonoids: molecular structure, biological activity and nutritional properties: a review," *Food Chemistry*, vol. 104, no. 2, pp. 466–479, 2007.
- [65] A. H. El-Far, K. Godugu, A. E. Noreldin et al., "Thymoquinone and costunolide induce apoptosis of both proliferative and doxorubicin-induced-senescent colon and breast cancer cells," *Integrative Cancer Therapies*, vol. 20, pp. 153473542110354–20, 2021.
- [66] O. R. Metawea, M. A. Abdelmoneem, N. S. Haiba et al., "A novel 'smart'PNIPAM-based copolymer for breast cancer targeted therapy: synthesis, and characterization of dual pH/temperature-responsive lactoferrin-targeted PNIPAM-co-AA," *Colloids and Surfaces B: Biointerfaces*, vol. 202, Article ID 111694, 2021.
- [67] A. F. Khafaga, R. N. Shamma, A. Abdeen et al., "Celecoxib repurposing in cancer therapy: molecular mechanisms and nanomedicine-based delivery technologies," *Nanomedicine*, vol. 16, no. 19, pp. 1691–1712, 2021.
- [68] A. F. Khafaga, A. E. M. Barakat, A. E. Noreldin, and D. Johar, *Beneficial Outcomes of Cancer Therapeutic Modalities Based on Targeting Apoptosis*, Current Drug Targets, 2022.
- [69] M. A. Atallah, M. A. Sallam, M. A. Abdelmoneem et al., "Green self-assembled lactoferrin carboxymethyl cellulose nanogels for synergistic chemo/herbal breast cancer therapy," *Colloids and Surfaces B: Biointerfaces*, vol. 217, Article ID 112657, 2022.
- [70] O. M. Ahmed, H. I. Fahim, H. Y. Ahmed, B. Mahmoud, S. A. S. Aljohani, and W. H. Abdelazeem, "The nephroprotective and antioxidant effects of navel orange peel hydroethanolic extract, naringin and naringenin in n-acetyl-p-aminophenol-administered Wistar rats," *Advances in Animal and Veterinary Sciences*, vol. 7, no. 2, pp. 96–105, 2019.
- [71] H. Elsayy, A. M. Alzahrani, M. Alfwuaires, A. M. Abdelmoneim, and M. Khalil, "Nephroprotective effect of naringin in methotrexate induced renal toxicity in male rats," *Bio-medicine & Pharmacotherapy*, vol. 143, Article ID 112180, 2021.
- [72] A. Hermenean, A. Ardelean, M. Stan et al., "Protective effects of naringenin on carbon tetrachloride-induced acute nephrotoxicity in mouse kidney," *Chemico-Biological Interactions*, vol. 205, no. 2, pp. 138–147, 2013.
- [73] S. Y. Saad, T. A. O. Najjar, and M. Alashari, "Cardiotoxicity of doxorubicin/paclitaxel combination in rats: effect of sequence and timing of administration," *Journal of Biochemical and Molecular Toxicology*, vol. 18, no. 2, pp. 78–86, 2004.
- [74] A. N. Colado Simão, A. A. Suzukawa, M. F. Casado, R. D. Oliveira, F. A. Guarnier, and R. Cecchini, "Genistein abrogates pre-hemolytic and oxidative stress damage induced by 2, 2'-Azobis (Amidinopropane)," *Life Sciences*, vol. 78, no. 11, pp. 1202–1210, 2006.
- [75] L. Pentassuglia, F. Timolati, F. Seifriz, K. Abudukadier, T. M. Suter, and C. Zuppinger, "Inhibition of ErbB2/neuregulin signaling augments paclitaxel-induced cardiotoxicity in adult ventricular myocytes," *Experimental Cell Research*, vol. 313, no. 8, pp. 1588–1601, 2007.
- [76] J. Li, T. Yin, L. Wang, L. Yin, J. Zhou, and M. Huo, "Biological evaluation of redox-sensitive micelles based on hyaluronic acid-deoxycholic acid conjugates for tumor-specific delivery of paclitaxel," *International Journal of Pharmaceutics*, vol. 483, no. 1-2, pp. 38–48, 2015.
- [77] M. Rajadurai and P. Stanely Mainzen Prince, "Preventive effect of naringin on lipid peroxides and antioxidants in isoproterenol-induced cardiotoxicity in Wistar rats: biochemical and histopathological evidences," *Toxicology*, vol. 228, no. 2-3, pp. 259–268, 2006.
- [78] H. M. Arafa, M. F. Abd-Ellah, and H. F. Hafez, "Abatement by naringenin of doxorubicin-induced cardiac toxicity in rats," *Journal of the Egyptian National Cancer Institute*, vol. 17, no. 4, pp. 291–300, 2005.
- [79] E. J. Anderson, L. A. Katunga, and M. S. Willis, "Mitochondria as a source and target of lipid peroxidation products in healthy and diseased heart," *Clinical and Experimental Pharmacology and Physiology*, vol. 39, no. 2, pp. 179–193, 2012.
- [80] M. Kwatra, V. Kumar, A. Jangra et al., "Ameliorative effect of naringin against doxorubicin-induced acute cardiac toxicity in rats," *Pharmaceutical Biology*, vol. 54, no. 4, pp. 637–647, 2015.
- [81] Q. Zhao, H. Yang, F. Liu et al., "Naringenin exerts cardiovascular protective effect in a palmitate-induced human umbilical vein endothelial cell injury model via autophagy flux improvement," *Molecular Nutrition & Food Research*, vol. 63, no. 24, Article ID 1900601, 2019.
- [82] J. Alexandre, Y. Hu, W. Lu, H. Pelicano, and P. Huang, "Novel action of paclitaxel against cancer cells: bystander effect mediated by reactive oxygen species," *Cancer Research*, vol. 67, no. 8, pp. 3512–3517, 2007.
- [83] T. Hadzic, N. Aykin-Burns, Y. Zhu et al., "Paclitaxel combined with inhibitors of glucose and hydroperoxide metabolism enhances breast cancer cell killing via H₂O₂-mediated oxidative stress," *Free Radical Biology and Medicine*, vol. 48, no. 8, pp. 1024–1033, 2010.
- [84] C. Panis, A. C. S. A. Herrera, V. J. Victorino et al., "Oxidative stress and hematological profiles of advanced breast cancer patients subjected to paclitaxel or doxorubicin chemotherapy," *Breast Cancer Research and Treatment*, vol. 133, no. 1, pp. 89–97, 2012.
- [85] I. Arany, J. S. Clark, D. Reed, I. Szabo, I. Ember, and L. A. Juncos, "The role of p66shc in taxol-and dichloroacetic acid-dependent renal toxicity," *Anticancer Research*, vol. 33, no. 8, pp. 3119–3122, 2013.
- [86] G. Varricchi, P. Ameri, C. Cadeddu et al., "Antineoplastic drug-induced cardiotoxicity: a redox perspective," *Frontiers in Physiology*, vol. 9, p. 167, 2018.
- [87] M. Fukui, N. Yamabe, and B. T. Zhu, "Resveratrol attenuates the anticancer efficacy of paclitaxel in human breast cancer cells *in vitro* and *in vivo*," *European Journal of Cancer*, vol. 46, no. 10, pp. 1882–1891, 2010.
- [88] M. Cavia-Saiz, M. D. Busto, M. C. Pilar-Izquierdo, N. Ortega, M. Perez-Mateos, and P. Muñoz, "Antioxidant properties, radical scavenging activity and biomolecule protection capacity of flavonoid naringenin and its glycoside naringin: a comparative study," *Journal of the Science of Food and Agriculture*, vol. 90, no. 7, pp. 1238–1244, 2010.
- [89] G. I. Harisa, "Naringin mitigates erythrocytes aging induced by paclitaxel: an *in vitro* study," *Journal of Biochemical and Molecular Toxicology*, vol. 28, no. 3, pp. 129–136, 2013.
- [90] N. Sahu, G. Mishra, H. K. Chandra, S. K. Nirala, and M. Bhadauria, "Naringenin mitigates antituberculosis drugs induced hepatic and renal injury in rats," *Journal of Traditional and Complementary Medicine*, vol. 10, no. 1, pp. 26–35, 2020.

Research Article

Antitumor Potential of Sericite Treatment Mediated by Cell Cycle Arrest in Triple-Negative MDA-MB231 Breast Cancer Cells

Seonhee Kim,¹ Harsha Nagar,¹ Ikjun Lee,¹ Su-Jeong Choi,¹ Shuyu Piao,¹ Byeong Hwa Jeon,¹ Shin Kwang Kang ,² Hee-Jung Song ,³ and Cuk-Seong Kim ¹

¹Department of Physiology and Medical Science, School of Medicine, Chungnam National University, Daejeon, Republic of Korea

²Department of Thoracic and Cardiovascular Surgery, Chungnam National University Hospital, Chungnam National University School of Medicine, Daejeon, Republic of Korea

³Department of Neurology, Chungnam National University College of Medicine and Sejong Hospital, Sejong, Republic of Korea

Correspondence should be addressed to Shin Kwang Kang; cskkwang@gmail.com, Hee-Jung Song; nrsono@cnuh.co.kr, and Cuk-Seong Kim; cskim@cnu.ac.kr

Received 23 May 2022; Revised 19 July 2022; Accepted 4 August 2022; Published 25 September 2022

Academic Editor: Mohammed El-Magd

Copyright © 2022 Seonhee Kim et al. This is an open access article distributed under the Creative Commons Attribution License, which permits unrestricted use, distribution, and reproduction in any medium, provided the original work is properly cited.

Breast cancer is the most common cancer and the leading cause of cancer-related mortality among females worldwide. Triple-negative breast cancer (TNBC) accounts for about 10–15% of all breast cancers and is usually more aggressive and has a poorer prognosis. Sericite has been known to have antitumor and immune-stimulatory effects. Although the chemopreventive potential of sericite has been demonstrated in other cancers, its molecular pathways in TNBC still require investigation. Thus, in the present study, the antitumor mechanism of sericite against MDA-MB231 breast cancer cells was examined *in vitro* and in an *in vivo* xenograft mouse model. Sericite treatment reduced cell proliferation and cell proliferation marker proliferating cell nuclear antigen (PCNA) in MDA-MB231 cells. It also decreased the total cell number and arrested cells in the G0/G1 phase of the cell cycle with an increase in the phosphorylation of P53 and upregulation of cell cycle regulatory proteins P21 and P16. In addition, sericite treatment also induced apoptosis signaling, which was evident by the upregulation of apoptotic protein markers cleaved caspases 3 and 9. A reduction in reactive oxygen species (ROS), NADPH oxidase 4 (NOX4), p22phox, and heat shock proteins (HSPs) was also observed. Similar results were obtained *in vivo* with significantly reduced tumor volume in sericite-administered mice. Collectively, these findings suggest that sericite has antitumor potential based on its property to induce cell cycle arrest and apoptotic cell death and therefore could serve as a potential therapeutic agent and crucial candidate in anticancer drug development for TNBC.

1. Introduction

Cancer is a severe life-threatening disease that ranks as a leading cause of death worldwide. Breast cancer is the most common type of cancer and also the leading cause of cancer-related mortality in women [1, 2]. Breast cancer incidence and mortality rates greatly depend on the socioeconomic backgrounds of countries, with incidence rates estimated at 54.4% and 31.3% in developed and developing countries, respectively. Breast cancer is categorized into four primary molecular subtypes: luminal A and B, human epidermal growth factor receptor 2 (HER2)

overexpressed, and basal-like subtypes [3]. Triple-negative breast cancer (TNBC) is similar to the basal-like subtype of breast cancer, as there is a lack of expression of hormone receptors (estrogen receptor (ER) and progesterone receptor (PR)) and HER-2 gene amplification in TNBC.

For the management and treatment of breast cancer, radiation, surgical resection, and systemic therapy, including hormonal or endocrine therapy, targeted therapy, chemotherapy, or a combination of these therapies, have been used in breast cancer patients [4]. Unfortunately, for TNBC, conventional targeted treatment options and endocrine therapies are limited, and outcomes are substantially worse

[5]. Therefore, chemotherapy remains the only systemic modality available for TNBC because these cells do not express ER or PR and lack HER-2 overexpression. However, there are several side effects associated with chemotherapy, which include weakness, nausea, reduced resistance to infections, vomiting, and hair loss. Therefore, developing a suitable strategy for TNBC treatment to increase patient survival and reduce side effects is essential.

Inorganic nanomaterials show great potential for clinical applications as they possess many unique characteristics. The intrinsic physicochemical characteristics of inorganic nanoparticles make them outstanding therapeutic agents for cancer treatment. Sericite is the name given to very fine, ragged grains and aggregates of white or colorless micas, typically made of muscovite. Sericite is highly refractive and is found in hydrothermally altered rocks [6]. Traditionally, sericite has been used to alleviate pain in the reproductive organs and to treat bleeding, dysentery, gastric diseases, and inflammation [7]. It has been shown previously that mica demonstrates chemopreventive potential against colorectal cancers by blocking the cell cycle and proliferation [8]. In addition, mica has the ability to stimulate immune responses against viral infection. Therefore, mica has been used as feed supplements for enhancing immune responses [9]. Heat shock proteins (HSPs) are present or induced in all living cells to protect them from high-temperature stress and have been extensively associated with various cancers and their behaviors [10]. They have various tumorigenic properties, including inhibition of apoptosis and senescence and promotion of angiogenesis, invasion, and metastasis [11]. Due to its vital role in tumorigenesis, inhibition of HSP activity has been accepted as a significant biological strategy for designing chemotherapeutics against cancer.

The need for more efficacious and innovative therapies for the treatment of TNBC prompted us to investigate the antitumor effect of sericite in MDA-MB231 cells, a triple-negative human breast carcinoma cell line, and in a xenograft mouse model. Thus, this study aimed to investigate if sericite may be utilized as an adjuvant to mainline cancer treatment and if it can be developed as a therapeutic anticancer agent in TNBC therapy.

2. Materials and Methods

2.1. Cell Culture and Cell Growth. Human breast epithelial cells (MCF10A, CRL-10317), triple positive breast cancer cells (BT474, HTB-20), ER+/PR+/HER2-breast cancer cells (MCF7, HTB-22), ER-/PR-/HER2+ breast cancer cells (SKBR3, HTB-30), and triple-negative breast cancer cells (BT549, HTB-122 and MDA-MB231, and HTB-26) were obtained from American Type Culture Collection (ATCC, VA, USA). These cells were cultured at 37°C with 5% CO₂ according to the manufacturer's instructions. Sericite (Gumcheon Corp., Okcheon-gun, Chungcheongbuk-do, South Korea) was dissolved in complete media first at concentrations of 10 mg/ml and 3 mg/ml. These were serially diluted further to 1 mg/ml and 0.3 mg/ml, respectively; and all the concentrations were then directly treated in the cells

for 24 h. Cell counting was performed using ADAM-MC Automatic Cell Counter (Digital Bio. Seoul, South Korea) that functions using the Propidium Iodide (PI) staining method of dead cell staining. After treatment with sericite, cell counting was performed according to the manufacturer's instructions. The initial doses of sericite for the first screening were selected based on previous publications [8, 9] and the final dose range was chosen after preliminary experiments were performed to decide the best suitable dose for all further experiments.

2.2. Mouse Xenograft Models. All animal studies were performed in the animal facility following the guidelines of the Institutional Animal Use and Care Committee at Chungnam National University (CNUH-018-A0024-1). The animal experiments complied with the ARRIVE (Animal Research: Reporting of In Vivo Experiments) guidelines for the use of experimental animals with the approval of the Chungnam National University. Female Balb/c nude mice (4 weeks) were purchased from OrientBio Inc (Gyeonggi-do, KOREA). Mice were maintained in a controlled environment (ambient temperature 22–24°C; humidity 50–60%; 12-h light/dark cycle). In order to generate subcutaneous tumors, mice were anesthetized using Avertin (250 mg/kg), and MDA-MB231 cells (1×10^7 cells/mouse) mixed with Matrigel (Corning, 356230) were injected subcutaneously into the flanks of the mice. For cancer assessment, cancer length and width were measured daily with digital calipers, and the volumes were calculated using the following formula: $(\text{length} \times \text{width}^2/2)$. Sericite was dissolved in saline in the same manner as for the in vitro studies, and based on pilot studies, the same doses as the in vitro experiments were administered. Following the establishment of subcutaneous MDA-MB231 xenograft in mice 24 days after tumor cell injection, mice with the same cancer volume (mm^3) were divided into three groups (saline, 1 mg/kg sericite, or 3 mg/kg sericite) and fed 100 μl of sericite solution (1 mg/kg or 3 mg/kg) or 100 μl of saline daily for 12 days by oral gavage, after which the mice were sacrificed by an overdose of Avertin and the tumors were dissected for further experiments.

2.3. Immunoblotting. The following antibodies were used: anti-p16 (sc-377412), anti-p21 (sc-6246), anti-p53 (sc-393031), and anti-GAPDH (sc-47724) (Santa Cruz Biotechnology, Santa Cruz, CA, USA); anti-P-p53 (S15) (9284S), anti-cleaved Cas9 (9509S), and anti-cleaved Cas3 (9664S) (Cell Signaling Technology, Danvers, MA, USA); anti-Shc (610878, BD Biosciences, Franklin Lakes, NJ, USA); anti-P-p66Shc (S36) (ALX-804-358) (Enzo Life Sciences, Inc., NY, USA), anti-MMP9 (MA5-15886, ThermoFisher), and anti-PCNA (PC 10, Sigma-Aldrich, USA). Immunoblotting of 30 μg of whole-cell lysate or tissue homogenate was performed as described previously [12]. Briefly, MDA-MB231 cells and cancer tissues were harvested and lysed in RIPA buffer containing protease and phosphatase inhibitors for 30 min on ice. After centrifugation at 13,000 rpm for 10 min, the protein concentration

of cell and tissue lysates were measured using a bicinchoninic acid (BCA) protein assay kit (iNtRON, cat. 21071). Equal amounts of protein per well were resolved in 10–15% sodium dodecyl sulfate-polyacrylamide gel electrophoresis (SDS-PAGE) and transferred onto a nitrocellulose membrane. The membranes were then washed with Tris-buffered saline (10 mM Tris, 150 mM NaCl) containing 0.1% Tween 20 (TBST) and blocked in TBST containing 5% bovine serum albumin Fraction V (Roche, Basel, Switzerland) followed by incubation in appropriate primary and secondary antibodies. The chemiluminescent signal was developed using Super Signal West Pico or Femto Substrate (Pierce Biotechnology, Rockford, IL, USA). Band densities were quantified on a Gel Doc 2000 Chemi Doc system using Quantity One software (Bio-Rad, Hercules, CA, USA). Values were normalized to β -actin (loading control).

2.4. Real-Time PCR. Total RNA was isolated from cells using TRIzol reagent (Thermo Fisher Scientific). Complementary DNA (cDNA) was generated from total RNA using the MAXIME RT Premix Kit (iNtRON Biotechnology, Gyeonggi, South Korea). Relative RNA expression levels were determined by PCR using a SYBR qPCR premix (Enzynomics, Daejeon, Republic of Korea). The primer sequences are provided in Table S1. A preincubation for 10 min at 95°C was followed by 40 amplification cycles: 10 sec at 95°C, 20 sec at 60°C, and 30 sec at 72°C. The melting curve for PCR product analysis was determined by rapid cooling down from 95°C to 65°C and incubation at 65°C for 15 sec before heating to 95°C. To normalize for equal mRNA/cDNA amounts, PCR reactions with target-specific and with GAPDH-specific primer sets were always run in parallel for each sample, and relative expression levels were determined by the $2^{-\Delta\Delta C_t}$ method.

2.5. Histological Analysis. After washing with phosphate-buffered saline, tumor tissues were fixed with 4% (w/v) paraformaldehyde and then embedded in paraffin. Paraffin sections were deparaffinized and rehydrated according to standard protocols and stained with hematoxylin-eosin (H&E). For immunohistochemistry staining, tumor tissues were stained with primary antibodies anti-MMP9 (diluted in 1:100; Cat.MA5-15886, ThermoFisher), anti-CD31 (diluted in 1:100; Cat.550274, BD science), and anti-PCNA (diluted in 1:100; PC 10; Sigma-Aldrich) overnight at 4°C. HRP-conjugated anti-rabbit and anti-mouse IgG was treated for 60 min at room temperature. The color was developed for 30 secs by incubation with 3,3'-diaminobenzidine (DAB). Sections were counterstained with hematoxylin and examined using a microscope (Motic, Richmond, BC, Canada) at 100x magnification.

2.6. CCK-8 Cell Proliferation Assay. Cells were treated with sericite for 24 h. Cell proliferation was measured using a CCK-8 kit (Dojindo, Japan) according to the manufacturer's instructions. Briefly, cells were washed with PBS and

suspended in a growth medium, including CCK-8 reagent added at 1/50 the media volume. Cells were then incubated at 37°C for 1 h in the dark. Cell proliferation was measured at a wavelength of 450 nm.

2.7. TUNEL Assay. TUNEL assay was used to detect DNA fragmentation, such as apoptosis. Cells were treated with sericite for 24 h. After 24 h incubation, cells were washed twice with PBS, detached from the plate using trypsin, and collected in a 15 ml tube. These cells were fixed in 100% ethanol overnight at 4°C. TUNEL assay was performed according to the manufacturer's instructions (FITC Abcam, cat. ab66108). Stained cells were analyzed by flow cytometry for FITC using a NovoCyte flow cytometer as per the manufacturer's instructions (ACEA Biosciences, San Diego, CA, USA). Flow cytometry data were analyzed using NovoExpress software. Fluorescence images were captured using a fluorescence microscope (Zeiss Axio imager M1).

2.8. Flow Cytometry. Cells were treated with sericite for 24 h. The next day, cells were analyzed by flow cytometry for cell cycle using a NovoCyte flow cytometer as per the manufacturer's instructions. Cells were washed twice with PBS and fixed in 70% ethanol overnight at 4°C followed by staining with PI (5 μ g/ml) (Thermo Fisher, 00-6990-50) and RNase A (1 mg/ml) (Sigma-Aldrich, R875-100 mg) in 500 μ l PBS for 30 min at 37°C. Flow cytometry data were analyzed using NovoExpress software.

2.9. ROS Detection. Amplex Red (A22188, Invitrogen, USA) was used to detect intracellular ROS production. MDA-MB231 cells, MCF10A cells, and tumor tissues were treated with saline or sericite. The reaction mixture contained 50 μ M Amplex Red and 0.1 U/ml HRP in Krebs–Ringer phosphate (KRPG) buffer (145 mM NaCl, 5.7 mM sodium phosphate, 4.86 mM KCl, 0.54 mM CaCl₂, 1.22 mM MgSO₄, 5.5 mM glucose, pH 7.35). Each reaction had a volume of 100 μ l. Moreover, 20 μ l of 1.5×10^4 cells suspended in KRPG buffer was added to the 100 μ l reaction mixture. Absorbance was measured at an excitation of 500–530 nm and emission at 590 nm. In the case of cancer tissue, it was finely chopped in the reaction mixture, centrifuged, and then progressed in the same way as cells.

2.10. Mice Blood Analysis. Blood parameters (aspartate aminotransferase (AST), alanine aminotransferase (ALT), gamma-glutamyl transferase (GGT), and creatinine (CREA)) were analyzed using a Samsung LABGEOPT Biochemistry Test 9 Kit (PR-PT05) with a Samsung LABGEO PT10 Analyzer according to the manufacturer's instructions.

2.11. Statistical Analysis. All statistical analyses were performed using GraphPad Prism 8 software (GraphPad Software, La Jolla, CA, USA), and differences between groups were evaluated using *t*-tests. For multiple

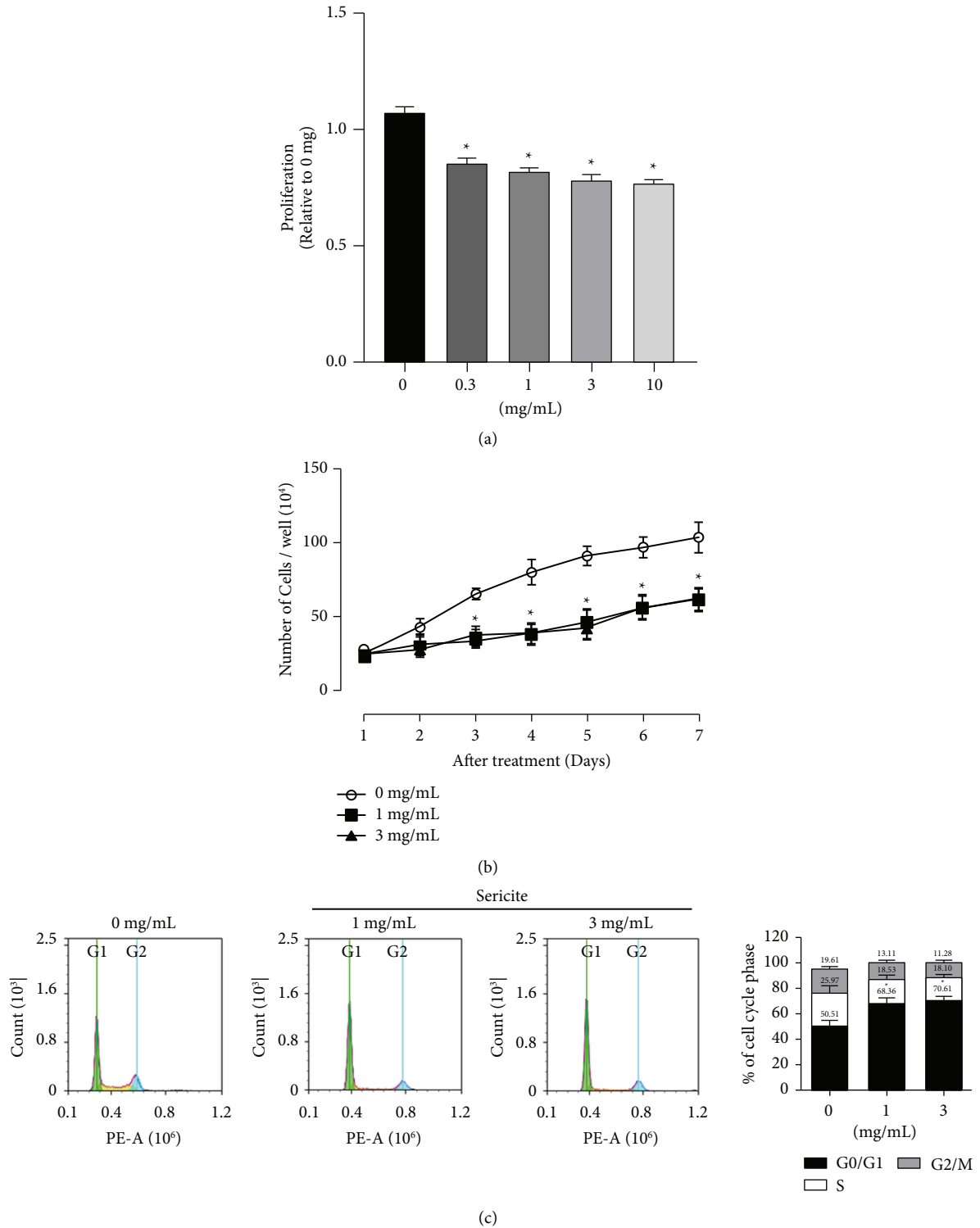


FIGURE 1: Continued.

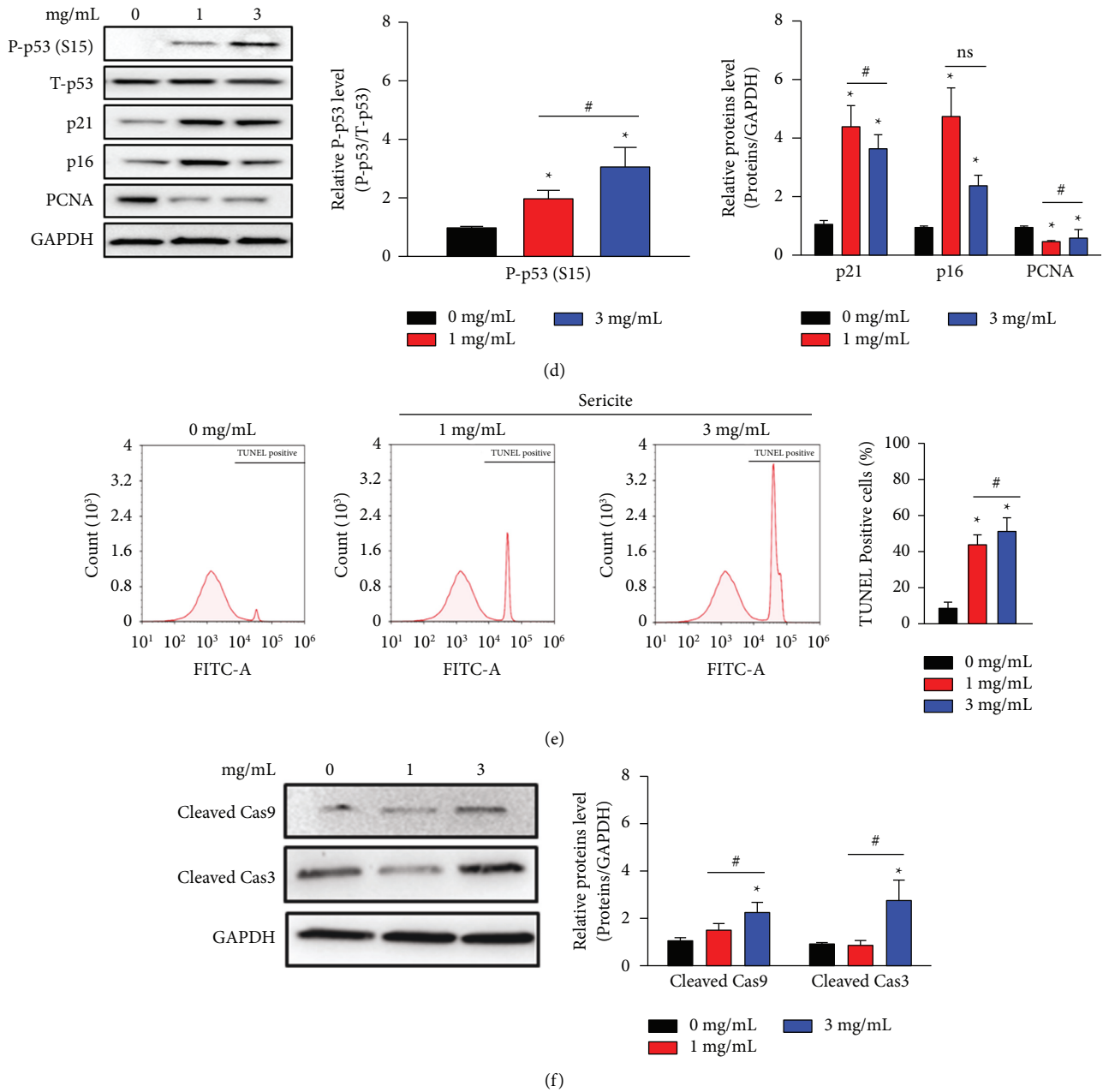


FIGURE 1: Sericite inhibits cell proliferation by inducing cell cycle arrest and apoptosis in MDA-MB231 cells. MDA-MB231 cells were treated with different concentrations of sericite for 24 h. (a) Cell proliferation assay was performed using a CCK-8 kit. (b) Cell number was measured using an ADAM-MC cell counting machine during 7 days of sericite treatment. (c) Cell number was detected using fluorescence-activated cell sorting (FACS) analysis. (d) Cell cycle arrest-related proteins were detected by immunoblotting. (e) The apoptotic rare in MDA-MB231 cells was measured by TUNEL staining after sericite treatment. (f) Apoptotic proteins were detected by immunoblotting. GAPDH was used as an internal control. The protein levels were qualified by densitometric analysis (right panel). All data are representative of three independent experiments. Data are presented as mean \pm SEM of three independent experiments. * $P < 0.05$ vs. 0 mg/mL sericite-treated MDA-MB231 cells. # $P < 0.05$ vs. 1 mg/mL sericite-treated MDA-MB231 cells.

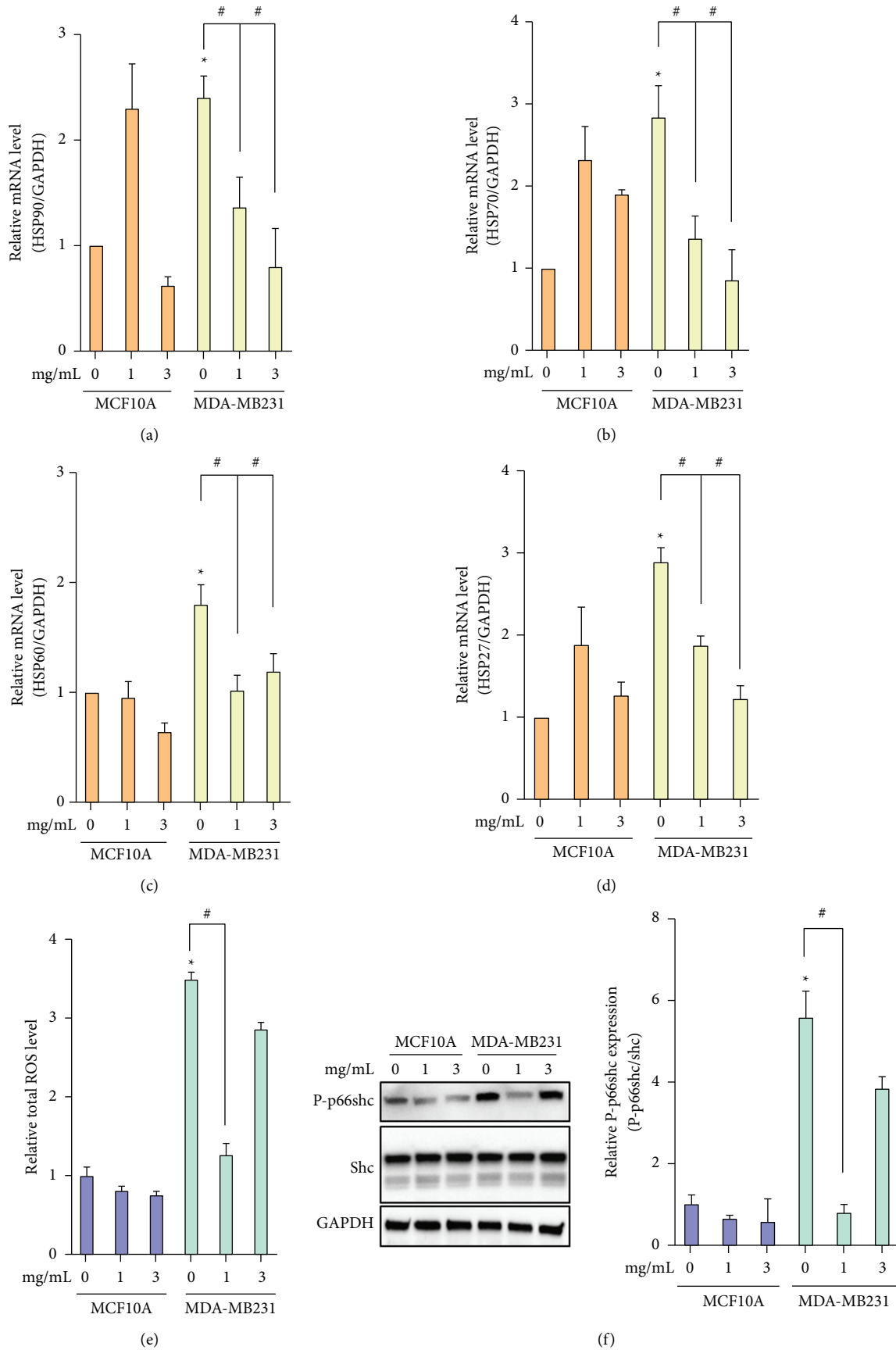


FIGURE 2: Continued.

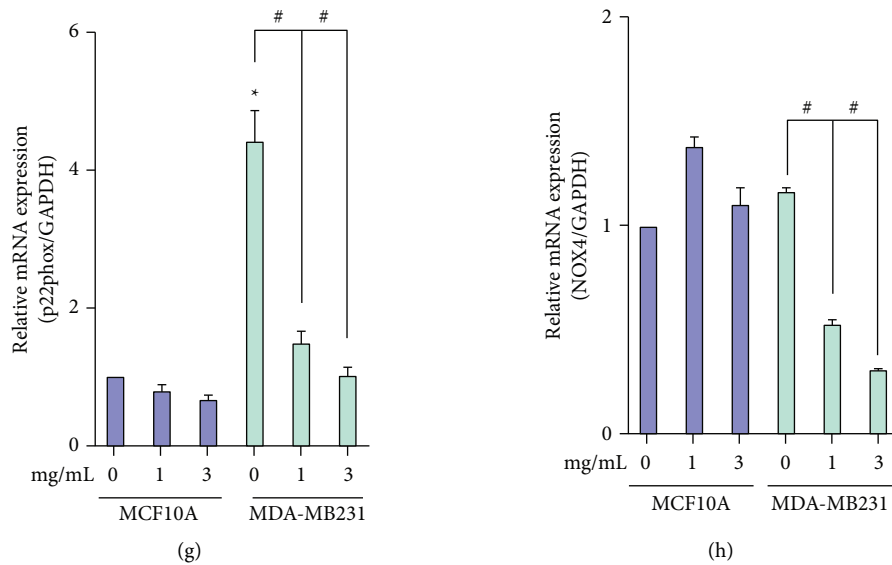


FIGURE 2: Sericite regulated HSPs and ROS in MDA-MB231 cells. MDA-MB231 cells were treated with different concentrations of sericite for 24h. (a–d) mRNA expressions were detected using an Amplex Red assay. (f) Phosphorylation of p66shc was measured by immunoblotting. (g, h) mRNA expressions of p22phox and NOX4 were detected by qPCR. GAPDH was used as an internal control for both immunoblotting and qPCR. All data are representative of three independent experiments. Data are presented as mean \pm SEM of three independent experiments. * $P < 0.05$ vs. 0 mg/mL sericite-treated MDA-MB231 cells. # $P < 0.05$ vs. 1 mg/mL sericite-treated MDA-MB231 cells.

comparisons, a one-way analysis of variance was performed, and Tukey's tests were carried out for post hoc analyses. Data are presented as the mean \pm standard error of the mean. $P \leq 0.05$ was considered statistically significant. All data are representative of at least three independent experiments.

3. Results

3.1. Sericite Inhibits Cell Proliferation by Inducing Cell Cycle Arrest and Apoptosis in MDA-MB231 Cells. We first investigated whether sericite could suppress the proliferation of human breast cancer cell lines BT474 (triple positive), MCF7 (ER and PR positive and HER2 negative), SKBR3 (ER and PR negative and HER2 positive), BT549 and MDA-MB231 (triple-negative), and MCF10A (normal breast epithelial cells). After treatment with sericite at different concentrations for 24 h, a CCK-8 cell proliferation assay was performed. The sericite-induced decrease in cell proliferation was more effective in MDA-MB231 cells than other breast cancer cells (Figure 1(a) and Supplementary Figure 1). We chose MDA-MB231 cells and sericite concentrations of 1 mg/mL and 3 mg/mL for further investigation of anti-cancer mechanisms. Figure 1(b) and Supplementary Figure 2A show that sericite treatment decreased cell growth; therefore, the number of cells after sericite treatment was significantly lower than those untreated cells and the cells treated with sericite slowly started showing features of apoptosis. Sericite arrested cells in the G0/G1 phase of the cell cycle (Figure 1(c)), increased the levels of the cell cycle regulatory proteins: p21, p16, and phosphorylation of p53 at its serine 15 site (S15), which is the primary target of DNA

damage response on the p53 protein, while decreasing the level of PCNA (Figure 1(d)). Furthermore, to determine the mechanism by which sericite treatment induces apoptosis in MDA-MB231 cells, we examined DNA damage using a terminal deoxynucleotidyl transferase (TdT) dUTP Nick end labeling (TUNEL) assay and fluorescence microscopy (Figure 1(e) and Supplementary Figure 2B). Data shows that sericite treatment induced DNA fragmentation in MDA-MB231 cells, a hallmark of apoptosis. We also looked for changes in apoptotic protein markers and found a significant induction of cleaved caspase-9 and increased activation of caspase-3 cleavage, which activated apoptosis in sericite-treated cells (Figure 1(f)).

3.2. Sericite Downregulates HSPs and ROS in MDA-MB231 Cells. HSPs act as stress proteins, rapidly created after exposure to unfavorable extrinsic factors such as high temperature, hypoxia, or cytokine release. Increased levels of HSP are required by the oncoproteins of cancer for their folding, aggregation, stabilization, function, activation, and proteolytic degradation. The expressions and activities of Hsp27, Hsp70, and Hsp90 chaperones are markedly higher in cancer [13]. We quantified the levels of HSP mRNA in MDA-MB231 cells and a normal breast epithelial cell line, MCF10A. HSP90, HSP70, HSP60, and HSP27 were overexpressed in MDA-MB231 compared to MCF10A cells; however, this overexpression was reduced by sericite treatment (Figures 2(a)–2(d)). These data demonstrate that overexpression of HSPs strengthens cancer cell proliferation and that sericite attenuates this proliferation via a reduction in HSP expression.

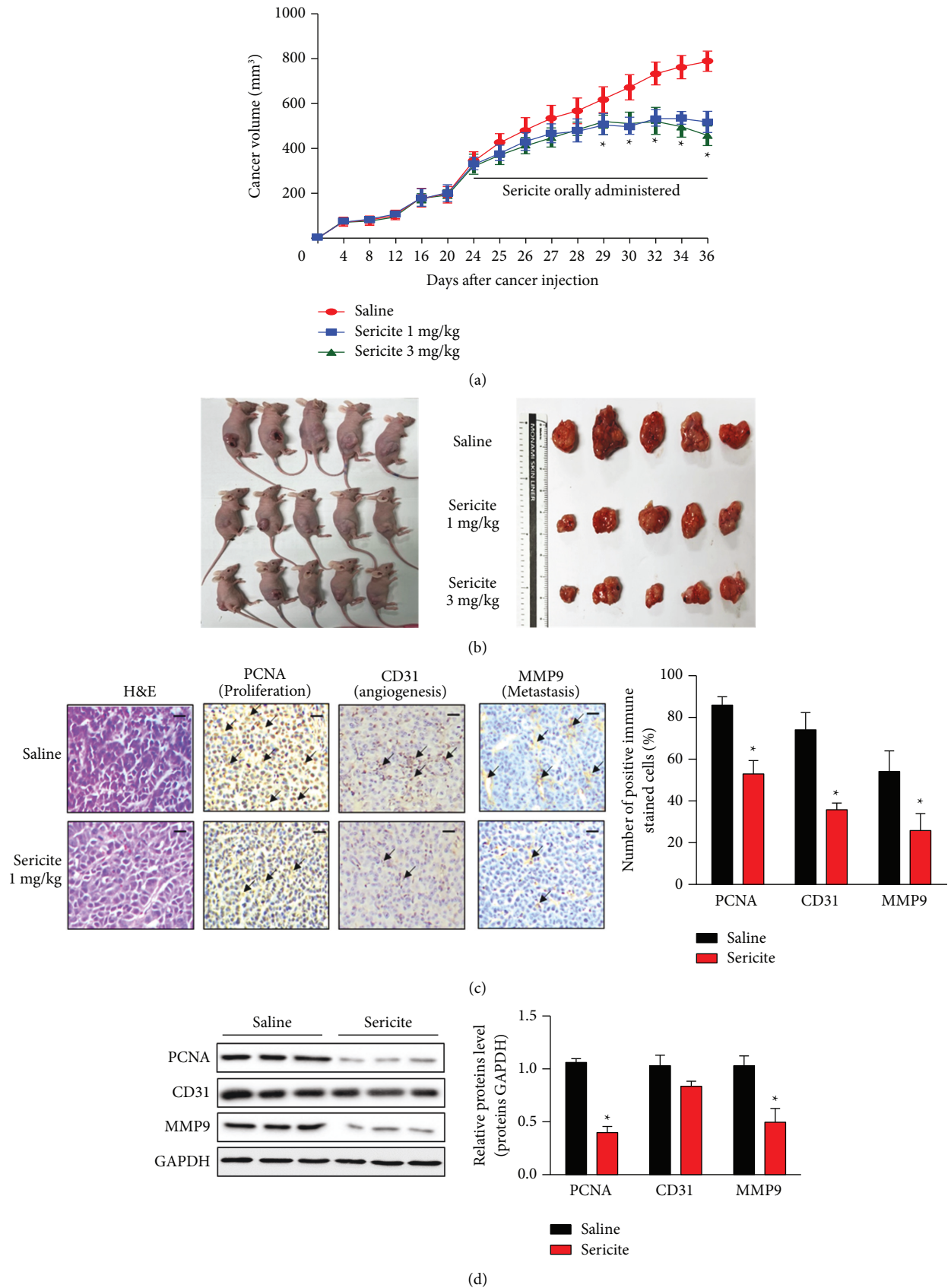


FIGURE 3: Sericite suppresses cell proliferation in an MDA-MB231 xenograft mouse model. MDA-MB231 cells were xenotransplanted into mice followed by a 24-day stabilization period, after which sericite was orally administered daily in two different doses (1 mg/kg or 3 mg/kg) for 12 days. Tumor size was measured daily. (a) The 12-day tumor volume measurements. (b) Photographs of mice bearing tumors and tumors after extraction from the mice. (c) Isolated tumors were stained with H and E for PCNA, CD31, and MMP9. Scale bar, 50 μ m. Arrows indicate positive DAB staining. (d) PCNA, CD31, and MMP9 protein expression were detected by immunoblotting. All data are representative of three independent experiments. Data are presented as mean \pm SEM of three independent experiments. * $P < 0.05$ vs. sericite-fed mice.

Generally, the expression of ROS in cancer cells is higher than in normal cells. ROS can promote protumorigenic signaling and facilitate cancer cell proliferation, survival, and adaptation to hypoxia [14]. Therefore, reducing the ROS levels to impede their role in the cellular transformation of cancer cells could be a possible ROS-related anticancer therapeutic strategy. We first confirmed that ROS were significantly upregulated in MDA-MB231 cells compared to MCF10A and found that sericite treatment suppressed the total ROS level in MDA-MB231 cells as measured by the Amplex Red assay (Figure 2(e)). Phosphorylation of p66shc is known as a key regulator of ROS metabolism involved in aging and several diseases [15]. We found that sericite treatment reduced p66shc phosphorylation in both MDA-MB231 and MCF10A cells (Figure 2(f)). As an oxygen sensor, the NADPH oxidase 4 (NOX4)/p22phox enzymatic complex plays a diverse role in cell proliferation, migration, and cell death. Increased expression of the NOX4/p22phox complex in cancer has been previously reported, which activates angiogenesis and metastasis [16]. Sericite treatment effectively attenuated p22phox and NOX4 mRNA expression in MDA-MB231 cells (Figures 2(g) and 2(h)).

3.3. Sericite Suppresses Cancer Growth in an MDA-MB231 Xenograft Mouse Model. Over a period of 36 days, the cancer volume ($\text{length} \times \text{width}^2/2$) of the control group grew from 400 mm^3 to 900 mm^3 . However, the sericite-treated groups demonstrated reduced cancer growth, with mean cancer volumes only reaching 600 mm^3 in the same period (Figures 3(a) and 3(b)). Furthermore, there was no significant change in the weight of the mice until the end of the experiment (Supplementary Figure 3A). To investigate any side effects of sericite treatment in the mice, we performed blood analysis of control and sericite-treated mice to analyze the kidney and liver functions based on the measurement of aspartate aminotransferase (AST), alanine aminotransferase (ALT), and gamma-glutamyl transpeptidase (GGT) for the liver function, and creatinine (CREA) for the kidney function. No significant difference was found between the two groups, and the values were in the normal range (Supplementary Figure 3B). We chose a 1 mg/kg sericite concentration to investigate possible anticancer mechanisms *in vivo*. Tumor paraffin sections from saline-fed mice and 1 mg/kg sericite-fed mice were subjected to hematoxylin and eosin (H&E) staining, which revealed compact and loose epithelial cells in the saline and sericite-fed groups, respectively (Figure 3(c)). Proliferating cell nuclear antigen (PCNA) is a marker of cell proliferation in various cancers. We stained tumor sections using anti-PCNA antibodies and found that the sericite group showed lower proliferation (brown) compared to tumor sections from the saline group (Figure 3(c)). Neovascularization is the formation of new blood vessels originating from the endothelium of existing vasculature. Tumor sections from sericite-fed mice exhibited less neovascularization (CD31, brown) and a lower metastatic index (MMP-9, brown) than those from the saline group (Figure 3(c)). We also examined the protein expressions of PCNA, CD31, and MMP9 and found similar

results (Figure 3(d)). Taken together, our results suggest that sericite treatment inhibits MDA-MB231 cell proliferation, neovascularization, and metastasis.

3.4. Sericite Downregulates HSP and ROS Levels in an MDA-MB231 Xenograft Mouse Model. Since we found that sericite treatment suppressed the proliferation of MDA-MB231 cells, we investigated the effects of sericite on cell protection *in vivo*. After sericite treatment, the mRNA levels of HSP90, HSP70, and HSP27 were attenuated in the MDA-MB231 xenograft model (Figures 4(a)–4(d)). We also observed that intracellular ROS was significantly decreased in sericite-treated mouse neoplasms (Figure 4(e)), along with reduced phosphorylation of p66shc (Figure 4(f)) and reduced mRNA expression of p22phox (Figure 4(g)) and NOX4 (Figure 4(h)), which are upstream regulators of p66shc. These findings suggest that sericite reduces the growth of MDA-MB231 cells *in vivo* by suppressing HSPs and ROS.

4. Discussion

TNBC demonstrates higher malignancy, lower survival rates, frequent relapses, and higher mortality rates among all breast cancer subtypes. Moreover, TNBC incidence is more frequent and prevalent in younger patients than in elderly patients [17, 18]. Therefore, young women are in need of novel TNBC treatments, and a better understanding of the molecular mechanisms responsible for cancer metastasis may provide a vision to improve TNBC patient survival. In the present study, we investigated antitumor effects of sericite against MDA-MB231 breast cancer cells. Sericite administration effectively suppressed tumor growth of MDA-MB231 cells in a xenograft mouse model. Previous studies have provided evidence that minerals have an antitumor effect in breast cancer cells [19, 20]. Most of these studies found that treating cancer cells with minerals like mica inhibits cell growth or induces apoptosis by the regulation of crucial receptors or signaling pathways. Our results are consistent with these studies and support the notion that sericite inhibits cell growth and proliferation and induces apoptosis in MDA-MB231 cells.

Evidence suggests that minerals have antitumor activity in several types of cancer. For instance, selenium, arsenic trioxide, zinc, and cadmium have been reported to have antitumor effects in various cancers, including breast cancer [8]. Similarly, mica particles have been studied to discern their function and to find the most effective formulation for oral supplements. The immune-enhancing effects of mica in animals have been evaluated as a dietary aluminosilicate supplement (DAS) in mice. A DAS showed clearance effects on pig circovirus type 2 in experimentally infected pigs, and mild side effects in mice and pigs were observed during the daily administration of the DAS [21].

In the present study, we first investigated the *in vitro* effects of sericite in MDA-MB231 cells. Sericite treatment decreased cell proliferation and cell number in a concentration-dependent manner. A reduction in cell proliferation has been proven to be an effective tumor-suppressing

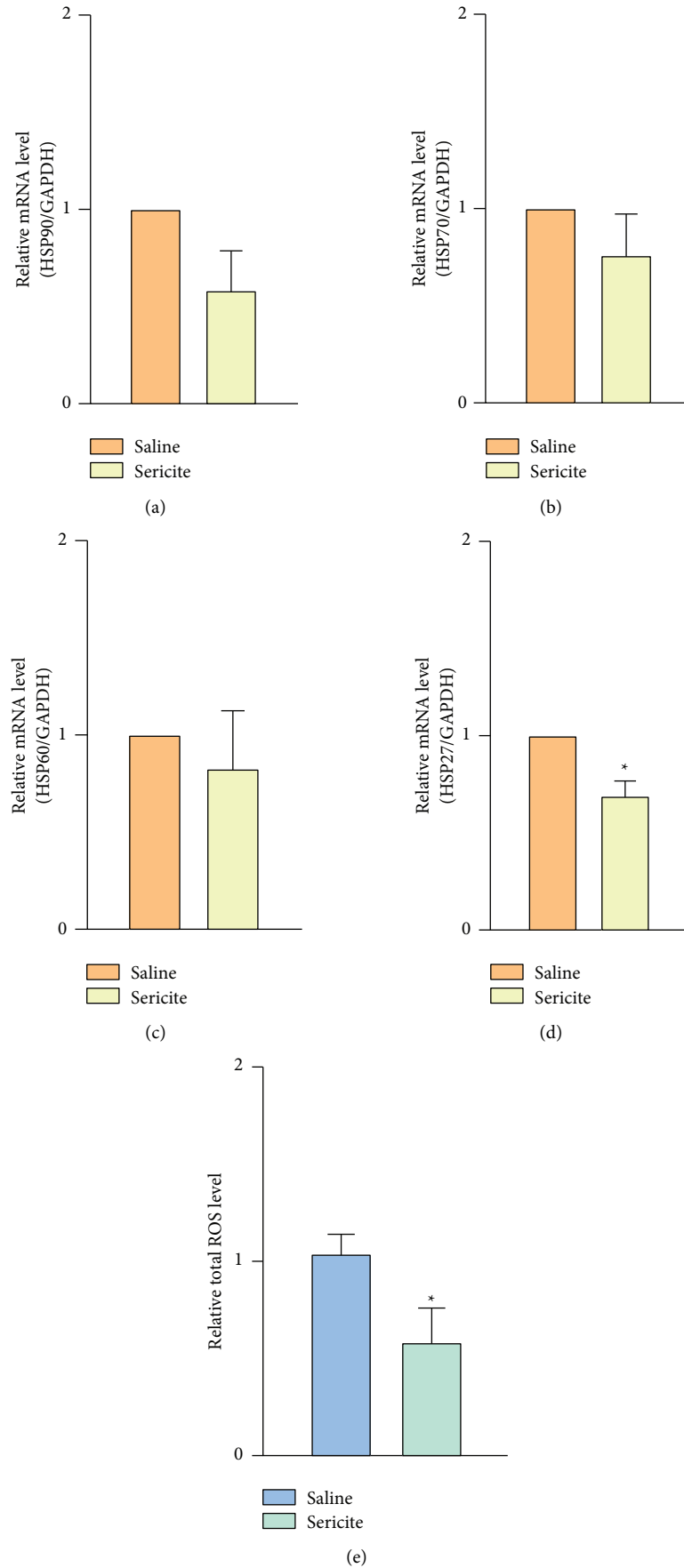
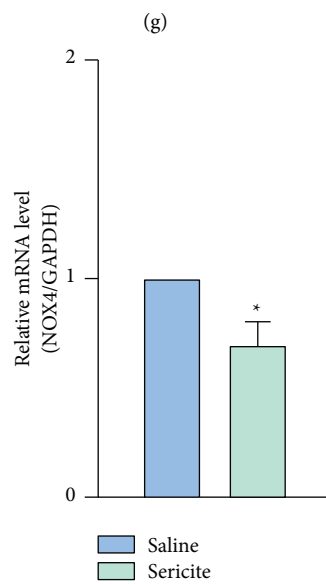
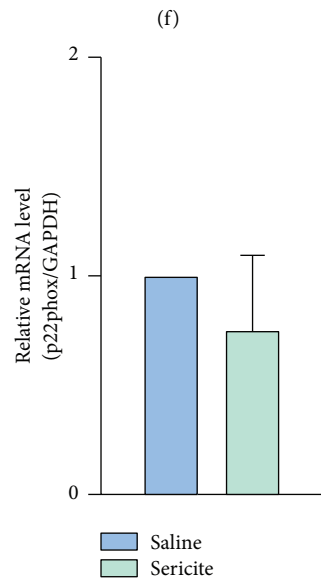
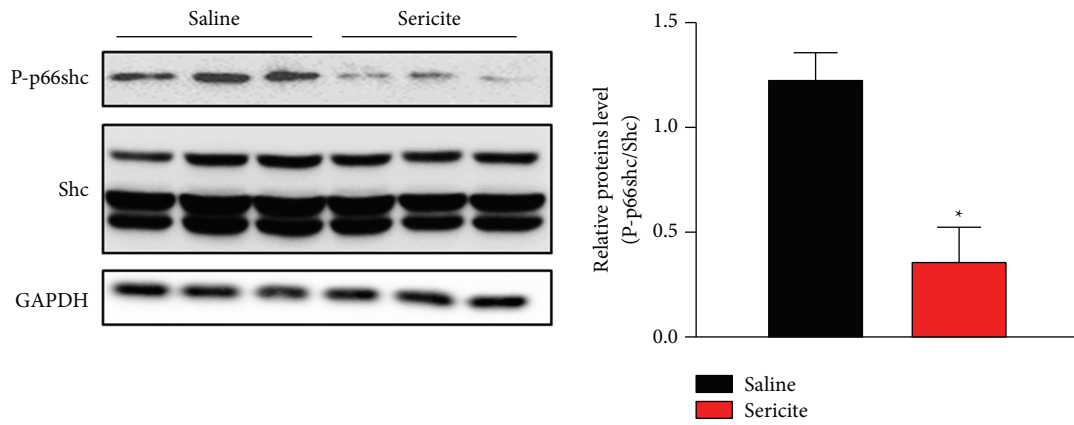


FIGURE 4: Continued.



(h)

FIGURE 4: Sericite attenuates HSP- and ROS-related pathways in an MDA-MB231 xenograft mouse model. (a–d) mRNA expressions of HSPs in saline-fed mice and 1 mg/kg sericite-fed mice. (e) Intracellular ROS was detected using an Amplex Red assay. (f) Phosphorylation of p66shc was measured by immunoblotting. (g and h) mRNA expressions of p22phox and NOX4 were detected by qPCR. All data are representative of three independent experiments. Data are presented as mean \pm SEM of three independent experiments. * $P < 0.05$ vs. sericite-fed mice.

mechanism. Previous studies have shown that celecoxib (CBX), which is a nonsteroidal anti-inflammatory drug (NSAIDs), and a potent COX-2 selective inhibitor suppresses cell proliferation *in vitro* and *in vivo* by mechanisms that include inhibition of cell cycle [22]. Similarly, sericite may inhibit proliferation by inducing a growth arrest in tumor cells. We demonstrated that sericite treatment increased the G0/G1 cell population in a concentration-dependent manner and enhanced the expression of the cell cycle arrest markers P53, P21, and P16. Some bioactive ingredients such as thymoquinone (TQ) and costunolide (COS) have been reported to promote apoptosis in human colon and breast cancer cell lines via a p53 dependence. Similarly, doxorubicin (DOX), a chemotherapy drug, induces upregulation of phosphorylation of p53 at S15, consequently upregulating p21 and inducing cell cycle arrest [23]. Furthermore, the present study investigated the mechanism responsible for sericite-mediated cytotoxicity. Promoting tumor cell apoptosis is one of the most important methods of tumor treatment. Induction of apoptosis in cancer cells by treatment with CBX has been documented earlier in gastric cancer cell lines [22]. The results of our TUNEL assay revealed that sericite-treated cancer cells underwent apoptosis. This fact was supported by a western blot analysis of the apoptosis markers caspase-9 and caspase-3, which were found to be upregulated in sericite-treated cells confirming the apoptotic effect.

HSPs are ubiquitously found in all living organisms and their expression is induced/regulated by stress. Previously, it was thought that HSPs are induced by heat alone; however, it is now known that various types of physiological or pathological stresses may regulate their expression [24]. The HSPs expression is increased during oncogenesis, resulting in malignant transformation and promoting rapid somatic evolution. Recently, HSPs are evolving as molecular targets in cancer therapy by the interference of their diverse functions in cancer cells following different approaches. There are clinical trials for various cancers, including breast cancer, using HSP-inhibitor compounds, and other HSP-based strategies [25, 26].

Similarly, high levels of ROS have been detected in cancer cells due to various changes like increased receptor signaling, increased metabolic and peroxisomal activities, mitochondrial dysfunction, and oncogenic activity [27]. Previous studies have revealed that various prospective compounds, namely quercetin, metformin, vitamin C, and curcumin, have been found to downregulate ROS in the cellular apoptotic process. Furthermore, some have been shown to promote apoptosis in cancer cells [28]. *Shc* gene regulates the level of ROS, apoptosis induction, and lifespan in mammals. *Shc* is a *Src* homology 2 domain-containing protein and is a member of an adaptor family of proteins. *Shc* has 3 isoforms based on the molecular weight of 46, 52, and 66 kDa (p46shc, p52shc, and p66shc) [29]. p66shc is the longest isoform with an additional CH2 domain containing a S36 residue which is phosphorylated in response to oxidative stress along with a role in apoptosis [30]. p46shc and p52shc are universally expressed; however, p66shc is expressed at different levels in different tissues [31]. p66shc is

part of a signal transduction pathway activated in response to increased ROS. It is phosphorylated on ser36 after exposure to oxidative stress from H₂O₂ or ultraviolet light, and this phosphorylation is critical for the cell death response evoked by oxidative damage [32]. In this study, sericite treatment reduced the levels of HSPs, ROS, and p66shc both *in vitro* and *in vivo*. Furthermore, sericite treatment attenuated the expression of the survival gene PCNA, reduced the typical angiogenesis marker CD31, and reduced the expression of the metastasis marker MMP9 in tumor tissues, indicating the antiproliferative, antiangiogenic, and antimetastatic activity of sericite in a xenograft model along with a reduction in tumor volume. One of the limitations of this study is the poor solubility of sericite powder in the cell culture media and in saline for the *in vitro* and *in vivo* experiments, respectively. Consequently, the concentration range used in this study was limited, and future work will be required to solve this problem by finding new dilution methods or ways to improve sericite solubility.

5. Conclusion

In conclusion, these findings suggest that sericite has chemopreventive potential in TNBC, which could be a basis for developing alternative therapies to treat tumor cells using natural compounds.

Data Availability

The data used to support the findings of this study are available from the corresponding author upon request.

Conflicts of Interest

The authors declare that there are no conflicts of interest regarding the publication of this article.

Authors' Contributions

Seonhee Kim and Harsha Nagar contributed equally to this work.

Acknowledgments

This work was supported by the Basic Science Research Program through the National Research Foundation of Korea (NRF), funded by the Ministry of Education (Grant nos. NRF-2014R1A6A1029617 and NRF-2019R1I1A3A0105949712) and by the research fund of Chungnam National University and Jowin Corp.

Supplementary Materials

Supplementary Fig.1. Effect of sericite treatment on cell proliferation of different breast cancer cell lines. (A) MCF10A, (B) BT474, (C) MCF7, (D) SKBR3, and (E) BT549 cells were treated with different concentrations of sericite for 24 h, followed by detection of cell proliferation using CCK-8 assay. Data are presented as the mean \pm SEM of

three independent experiments. * $P < 0.05$ vs. 0 mg/mL sericite-treated cells. *Supplementary Fig.2*. Effect of sericite treatment on cell morphology and apoptosis in MDA-MB231 cells. (A) Effect of sericite treatment on cell morphology up to 7 days of incubation. (B) Images show merged staining with Propidium Iodide/RNase A (red) and FITC-dUTP (green) (TUNEL) after sericite treatment in MDA-MB231 cells. Scale bar = 20 μm . Data are presented as the mean \pm SEM of three independent experiments. *Supplementary Fig.3*. Effect of sericite treatment on the health of mice. (A) Changes in animal body weight. (B) Blood analysis of mice was performed to analyze the kidney and liver function. Aspartate aminotransferase (AST), alanine aminotransferase (ALT), and gamma-glutamyl transpeptidase (GGT) are a measure of liver function. Creatinine (CREA) is the measure of kidney function. The values of all the components were in the normal range (AST: 0–40 U/L, ALT: 0–45 U/L, GGT: 0–66 U/L, and CREA: 0.5–1.3 mg/dl). Data are presented as the mean \pm SEM of five independent experiments. *Table S1*. Information on qPCR primers. *Supplementary Fig.5–Supplementary Fig.9*. Full-length western blot gel images. (*Supplementary Materials*)

References

- [1] A. G. Waks and E. P. Winer, "Breast cancer treatment: a review," *JAMA*, vol. 321, no. 3, pp. 288–300, 2019.
- [2] F. Bray, J. Ferlay, J. Soerjomataram, R. L. Siegel, L. A. Torre, and A. Jemal, "Global cancer statistics 2018: GLOBOCAN estimates of incidence and mortality worldwide for 36 cancers in 185 countries," *CA: A Cancer Journal for Clinicians*, vol. 68, no. 6, pp. 394–424, 2018.
- [3] A. Prat, M. J. Ellis, and C. M. Perou, "Practical implications of gene-expression-based assays for breast oncologists," *Nature Reviews Clinical Oncology*, vol. 9, no. 1, pp. 48–57, 2011.
- [4] N. Harbeck, F. Penault-Llorca, J. Cortes et al., "Breast cancer," *Nature Reviews Disease Primers*, vol. 5, no. 1, p. 66, 2019.
- [5] C. Denkert, C. Liedtke, A. Tutt, and G. von Minckwitz, "Molecular alterations in triple-negative breast cancer—the road to new treatment strategies," *The Lancet*, vol. 389, no. 10087, pp. 2430–2442, 2017.
- [6] C. H. Lee, J. W. Roh, C. Y. Lim, J. H. Hong, J. K. Lee, and E. G. Min, "A multicenter, randomized, double-blind, placebo-controlled trial evaluating the efficacy and safety of a far infrared-emitting sericite belt in patients with primary dysmenorrhea," *Complementary Therapies in Medicine*, vol. 19, no. 4, pp. 187–193, 2011.
- [7] S. Nasrin, S. C. Bachar, and M. S. K. Choudhuri, "Toxicological studies of "Chondrokola Rosh," an Ayurvedic preparation on liver function tests of rats," *African Journal of Traditional, Complementary and Alternative Medicines: AJTCAM*, vol. 8, no. 5, pp. 170–174, 2011.
- [8] S. Y. Cho, H. J. Lee, S. M. Cho, B. Kim, Y. K. Jung, and S. H. Kim, "Particled Mica, STB-HO has chemopreventive potential via G1 arrest, and inhibition of proliferation and vascular endothelial growth factor receptor 2 in HCT colorectal cancer cells," *BMC Complementary and Alternative Medicine*, vol. 13, no. 1, p. 189, 2013.
- [9] T. W. Kang, H. S. Kim, B. C. Lee et al., "Mica nanoparticle, STB-HO eliminates the human breast carcinoma cells by regulating the interaction of tumor with its immune micro-environment," *Scientific Reports*, vol. 5, no. 1, p. 17515, 2015.
- [10] F. C. M. Zoppino, M. E. Guerrero-Gimenez, G. N. Castro, and D. R. Ciocca, "Comprehensive transcriptomic analysis of heat shock proteins in the molecular subtypes of human breast cancer," *BMC Cancer*, vol. 18, no. 1, p. 700, 2018.
- [11] R. Sundararajan, P. Giri, S. Madhivanan et al., "Cisplatin-based electrochemotherapy significantly downregulates key heat shock proteins in MDA-MB-231-human triple-negative breast cancer cells," *Applied Biochemistry and Biotechnology*, vol. 194, no. 1, pp. 517–528, 2022.
- [12] S. Kim, S. Piao, I. Lee et al., "CR6 interacting factor 1 deficiency induces premature senescence via SIRT3 inhibition in endothelial cells," *Free Radical Biology and Medicine*, vol. 150, pp. 161–171, 2020.
- [13] A. Aboelnour, A. E. Noreldin, and I. M. Saadeldin, "Hsp90 is a pivotal player in retinal disease and cancer," in *Heat Shock Protein 90 in Human Diseases and Disorders*, pp. 183–200, Springer, Berlin, Germany, 2019.
- [14] B. Perillo, M. Di Donato, A. Pezone et al., "ROS in cancer therapy: the bright side of the moon," *Experimental and Molecular Medicine*, vol. 52, no. 2, pp. 192–203, 2020.
- [15] J. Oshikawa, S. J. Kim, E. Furuta et al., "Novel role of p66Shc in ROS-dependent VEGF signaling and angiogenesis in endothelial cells," *American Journal of Physiology-Heart and Circulatory Physiology*, vol. 302, no. 3, pp. H724–H732, 2012.
- [16] S. Guo and X. Chen, "The human Nox4: gene, structure, physiological function and pathological significance," *Journal of Drug Targeting*, vol. 23, no. 10, pp. 888–896, 2015.
- [17] G. J. Morris, S. Naidu, A. K. Topham et al., "Differences in breast carcinoma characteristics in newly diagnosed African-American and caucasian patients: a single-institution compilation compared with the national cancer institute's surveillance, epidemiology, and end results database," *Cancer*, vol. 110, no. 4, pp. 876–884, 2007.
- [18] L. Yin, J. J. Duan, X. W. Bian, and Sc Yu, "Triple-negative breast cancer molecular subtyping and treatment progress," *Breast Cancer Research*, vol. 22, no. 1, p. 61, 2020.
- [19] J. Xia, Y. Li, Q. Yang et al., "Arsenic trioxide inhibits cell growth and induces apoptosis through inactivation of notch signaling pathway in breast cancer," *International Journal of Molecular Sciences*, vol. 13, no. 8, pp. 9627–9641, 2012.
- [20] M. Brama, L. Gnessi, S. Basciani et al., "Cadmium induces mitogenic signaling in breast cancer cell by an ER α -dependent mechanism," *Molecular and Cellular Endocrinology*, vol. 264, no. 1–2, pp. 102–108, 2007.
- [21] B. G. Jung, N. T. Toan, S. J. Cho, Jh Ko, Y. K. Jung, and B. J. Lee, "Dietary aluminosilicate supplement enhances immune activity in mice and reinforces clearance of porcine circovirus type 2 in experimentally infected pigs," *Veterinary Microbiology*, vol. 143, no. 2–4, pp. 117–125, 2010.
- [22] A. F. Khafaga, R. N. Shamma, A. Abdeen et al., "Celecoxib repurposing in cancer therapy: molecular mechanisms and nanomedicine-based delivery technologies," *Nanomedicine*, vol. 16, no. 19, pp. 1691–1712, 2021.
- [23] A. H. El-Far, K. Godugu, A. E. Noreldin et al., "Thymoquinone and costunolide induce apoptosis of both proliferative and doxorubicin-induced-senescent colon and breast cancer cells," *Integrative Cancer Therapies*, vol. 20, 2021.
- [24] D. R. Ciocca and S. K. Calderwood, "Heat shock proteins in cancer: diagnostic, prognostic, predictive, and treatment implications," *Cell Stress & Chaperones*, vol. 10, no. 2, pp. 86–103, 2005.
- [25] D. R. Ciocca, N. Cayado-Gutierrez, M. Maccioni, and F. Cuello-Carrion, "Heat shock proteins (HSPs) based anti-

- cancer vaccines,” *Current Molecular Medicine*, vol. 12, no. 9, pp. 1183–1197, 2012.
- [26] F. Rappa, F. Farina, G. Zummo et al., “HSP-molecular chaperones in cancer biogenesis and tumor therapy: an overview,” *Anticancer Research*, vol. 32, no. 12, pp. 5139–5150, 2012.
- [27] M. A. Khan, R. Singh, S. Siddiqui et al., “Anticancer potential of *Phoenix dactylifera* L. seed extract in human cancer cells and pro-apoptotic effects mediated through caspase-3 dependent pathway in human breast cancer MDA-MB-231 cells: an in vitro and in silico investigation,” *BMC Complementary Medicine and Therapies*, vol. 22, no. 1, p. 68, 2022.
- [28] C. H. Jeong and S. H. Joo, “Downregulation of reactive oxygen species in apoptosis,” *European Journal of Cancer Prevention*, vol. 21, no. 1, pp. 13–20, 2016.
- [29] H. Nagar, S. Jung, S. K. Kwon et al., “CRIF1 deficiency induces p66shc-mediated oxidative stress and endothelial activation,” *PLoS One*, vol. 9, no. 6, Article ID e98670, 2014.
- [30] L. Luzi, S. Confalonieri, P. P. Di Fiore, and P. G. Pelicci, “Evolution of Shc functions from nematode to human,” *Current Opinion in Genetics & Development*, vol. 10, no. 6, pp. 668–674, 2000.
- [31] S. S. Bhat, D. Anand, and F. A. Khanday, “p66Shc as a switch in bringing about contrasting responses in cell growth: implications on cell proliferation and apoptosis,” *Molecular Cancer*, vol. 14, no. 1, p. 76, 2015.
- [32] V. P. Skulachev, “The p66shc protein: a mediator of the programmed death of an organism?” *IUBMB Life*, vol. 49, no. 3, pp. 177–180, 2000.

Research Article

Yifei sanjie Pills Alleviate Chemotherapy-Related Fatigue by Reducing Skeletal Muscle Injury and Inhibiting Tumor Growth in Lung Cancer Mice

Yingchao Wu ¹, **Dajin Pi**,¹ **Yiliu Chen**,¹ **Qian Zuo**,² **Lizhu Lin** ³, and **Mingzi Ouyang** ¹

¹School of Traditional Chinese Medicine, Jinan University, Guangzhou 510632, Guangdong, China

²MOE Key Laboratory of Tumor Molecular Biology and Key Laboratory of Functional Protein Research of Guangdong Higher Education Institutes, Institute of Life and Health Engineering, College of Life Science and Technology, Jinan University, Guangzhou 510632, Guangdong, China

³Oncology Center, The First Affiliated Hospital of Guangzhou University of Chinese Medicine, Guangzhou 510405, Guangdong, China

Correspondence should be addressed to Lizhu Lin; lizhulin26@yahoo.com and Mingzi Ouyang; mingziouy@jnu.edu.cn

Received 9 June 2022; Accepted 2 August 2022; Published 22 August 2022

Academic Editor: Mohammed El-Magd

Copyright © 2022 Yingchao Wu et al. This is an open access article distributed under the Creative Commons Attribution License, which permits unrestricted use, distribution, and reproduction in any medium, provided the original work is properly cited.

Chemotherapy-related fatigue (CRF), one of the most severe adverse effects observed in cancer patients, has been theoretically related to oxidative stress, and antioxidant treatment might be one of the most valuable therapeutic approaches. However, there are still few effective pharmacological therapies. *Yifei Sanjie pills* (YFSJ), a classical formula used to treat lung cancer as complementary and alternative medicine, have been proved to alleviate CRF of lung cancer patients in clinical practices. However, the underlying mechanisms have not been clarified. In this study, our data showed that YFSJ alleviated CRF presented as reversing the decline of swimming time and locomotor activity induced by cisplatin (DDP). Moreover, YFSJ significantly reduces the occurrence of mitophagy and mitochondrial damage and reduces apoptosis in skeletal muscle tissues caused by DDP. It probably works by decreasing the oxidative stress, inhibiting the activation of the AMPK/mTOR pathway, decreasing protein expression levels of Beclin1 and other autophagy-related proteins, and attenuating the activation of Cytochrome c (cyto. C), Cleaved Caspase-9 (c-Casp 9), and other apoptosis-related proteins. Furthermore, YFSJ enhanced DDP sensitivity by specifically promoting oxidative stress and activating apoptosis and autophagy in the tumor tissues of mice. It was also found that YFSJ reduced the loss of body weight caused by DDP, reversed the ascent of serum concentrations of alanine aminotransferase (ALT), aminotransferase (AST), and creatinine (CREA), increased the spleen index, and prolonged the survival time of mice. Taken together, these results revealed that YFSJ could alleviate CRF by reducing mitophagy and apoptosis induced by oxidative stress in skeletal muscle; these results also displayed the effects of YFSJ on enhancing chemotherapy sensitivity, improving quality of life, and prolonging survival time in lung cancer mice received DDP chemotherapy.

1. Introduction

Although advances have been made in targeted therapy and immunotherapy, platinum-based chemotherapy is still the standard treatment for advanced lung cancer, with a large proportion [1–3]. Chemotherapy-related fatigue (CRF), one of the most severe adverse effects caused by chemotherapeutic treatments, has been observed in 27–82% of patients with advanced lung cancer [4], presenting as a persistent

distressing, subjective sense of tiredness or exhaustion [5], which affects the long-term quality of life or even result in the deaths of patients [6].

Despite the prevalence of this condition, the etiology of CRF has not been fully elucidated. Some studies found that the possible mechanisms were associated with energy unbalance, inflammation, changes in circadian rhythm, depression, and immune system disorders [7]. However, increasing evidence indicates that the occurrence of CRF is related to the

dysfunction of skeletal muscle, which has an essential proportion in maintaining the energy homeostasis of the human body [8]. A study on chemotherapy-treated patients reported that chemotherapy always indistinguishably targets the mitochondria of both cancerous and noncancerous cells, inducing fatigue due to high oxidative stress [9–12]. Its potential mechanism is that the damage pathways of noncancerous cells, especially in highly metabolic organs such as skeletal muscle, will be stimulated by adaptive responses to oxidative stress and induce reactive oxygen species (ROS) over-generation [13–18]. Accumulation of ROS-caused mitochondrial damage can be removed by an autophagic process called “mitophagy” to maintain cell homeostasis [19]. However, when more devastating damage is beyond the capability of mitophagy, the dysfunctional mitochondria will induce apoptotic cell death, which can lead to the onset of CRF [20, 21]. While CRF has been theoretically related to oxidative stress, and antioxidant treatment might be one of the most valuable therapeutic approaches for CRF, there are still few effective pharmacological therapies that can successfully eliminate CRF [22]. At the same time, tumor size is also closely related to CRF [23]. Therefore, further research is urgently needed to raise new interventions to prevent, postpone or eliminate fatigue in cancer patients.

The use of Traditional Chinese Medicine (TCM) might be one such possible strategy, which is widely used in CRF treatment to reduce fatigue or improve the quality of life in cancer patients [24]. *Yifei Sanjie pills* (YFSJ), also known as “*Yiqi Chutan Tang*,” is a TCM formula used to treat lung cancer as complementary and alternative medicine, which consists of *Panax quinquefolius Radix* (Xi yang shen), *Ranunculi Ternati Radix* (Mao zhao cao), *Sarcandrae Herba* (Zhong jie feng), *Pinelliae Rhizoma Praeparatum* (Fa ban xia), *Ganoderma* (Ling zhi), *Bombyx batryticatus* (Chao jiang can), *Cremastrae Pseudobulbus Pleiones Pseudobulbus* (Shan ci gu), and *Fritillariae Thunbergii Bulbus* (Zhe bei mu). Previous studies reported that the major herbs of YFSJ, such as *Panax quinquefolius Radix* and *Ganoderma*, have been approved for anti-CRF effects in the clinic and preclinical studies due to the inhibition of oxidative stress and the improvement of mitochondrial function in skeletal muscles [25–32]. Phytochemicals absorbed from *Thunbergii Bulbus*, *Bombyx batryticatus*, and *Pinelliae Rhizoma Praeparatum* could also reduce oxidative stress by decreasing free radical formation and scavenging free radicals [33–35], which were commonly associated with fatigue. Furthermore, our previous clinical practices have shown the effects of YFSJ to prolong the median survival time [36, 37] and alleviate CRF in non-small-cell lung cancer (NSCLC) patients [38, 39]. However, the underlying mechanisms have not been clarified. In this study, in addition to its usual antitumor effects, we have focused on the oxidative stress, mitochondria autophagy, and apoptosis in skeletal muscle of CRF mice model to demonstrate the underlying mechanisms of YFSJ against CRF.

2. Materials and Methods

2.1. YFSJ Preparation. YFSJ was composed of eight herbs formed by pill preparation and was purchased from the First

Affiliated Hospital of Guangzhou University of Chinese Medicine (Guangdong, China). YFSJ (8 g/packet) was dissolved in 24 mL normal saline, and the solution was promoted by eddy vibration to the final concentration of 0.33 g/mL before use. Details of the herbal materials are listed in Supplementary Figure 1 and Supplementary Table 1. Chemical constituents of YFSJ were identified based on the Q-Orbitrap high-resolution liquid/mass spectrometry (Q-Orbitrap-LC/MS). The data collected by high-resolution liquid mass were processed by CD2.1 (Thermo Fisher) and then searched and compared in the database (MZCloud, MZVault, ChemSpider). The peak intensity chromatograms of chemical constituents in YFSJ were displayed in Supplementary Figure 2. The obtained compounds were cross-linked with the known traditional Chinese medicine components in YFSJ to screen out the possible compounds listed in Supplementary Table 2.

2.2. Chemicals and Reagents. Cisplatin (DDP, Cat.#H20010743) injection was purchased from Jiangsu Hausen Pharmaceutical Co., Ltd (Jiangsu, China). Dulbecco's modified Eagle's medium (DMEM, Cat.#11965092), fetal bovine serum (FBS, Cat.#10270106), penicillin/streptomycin (Cat.#10378016), and phosphate-buffered saline (PBS, Cat.#10010023) were supplied by Gibco (NY, USA). Primary antibodies against Beclin1 (Cat.#11306-1-AP), p62 (Cat.#66184-1-Ig), Cytochrome *c* (cyto. C, Cat.#66264-1-Ig), and DAPK1 (Cat.#25136-1-AP) were purchased from Proteintech (Wuhan, China). Primary antibodies against Phospho-AMPK α (p-AMPK α , Cat.#50081S), Phospho-mTOR (p-mTOR, Cat.#5536T), Atg7 (Cat.#8558T), LC3A/B (Cat.#12741S), Cleaved Caspase-9 (c-Casp 9, Cat.#20750S), Cleaved Caspase-3 (c-Casp 3, Cat.#9661T), Cleaved PARP (c-PARP, Cat.#5625T), Phospho-SAPK/JNK (p-JNK, Cat.#9255S), Phospho-p53 (p-p53, Cat.#9284T), Bax (Cat.#2772T), and GAPDH (Cat.#5174T) and rabbit (Cat.#7074P2) or mouse (Cat.#7076P2) secondary antibodies were purchased from Cell Signaling Technology (Danvers, MA, USA).

2.3. Cell Culture. Lewis lung cancer (LLC) cells were acquired from the Guangzhou University of Chinese Medicine (Guangzhou, China). The cells were cultured in the DMEM medium containing 10% FBS, 1% streptomycin, and 1% penicillin and maintained in a 5% CO₂ incubator at 37°C. Cells were subcultured when the density reached 90% to proliferate enough and were used for subsequent experiments.

2.4. Lung Cancer Xenogeneic Mouse Model. A total of 100 five-week-old C57/BL mice (15 ± 1 g) were purchased from Beijing HFK Bioscience Co., Ltd., [Approval No. SCXK (Jing) 2019–0008, Beijing, China]. All experiments were conducted according to the relevant laws and institutional guidelines and with the approval of the Animal Ethics Committee of Jinan University (Approval No. IACUC-20200923-06). After acclimatizing for 10 days, 20 mice were randomly selected as the NC group (normal control). The

remaining mice were given subcutaneous injections with 1×10^6 LLC cells in the right flank to establish the lung cancer xenogeneic mice model. When the tumor size reached 80–100 mm³, the xenografts mice were randomly divided into four groups ($n = 20$): (1) TC group (mice with tumor but without any treatment); (2) DDP group (mice with tumor and treated with DDP, intraperitoneal, 5 mg/kg, 0.1 ml, once weekly); (3) DDP + YFSJ group (mice with tumor and cotreated with DDP and YFSJ; DDP, intraperitoneal, 5 mg/kg, 0.1 ml, once weekly; YFSJ, intragastrical, 3 g/kg, 0.2 ml, once daily); (4) YFSJ group (mice with tumor and treated with YFSJ, intragastrical, 3 g/kg, 0.2 ml, once daily). The NC and TC groups have received administration of normal saline (with the same route and volume of DDP and YFSJ). Each group of mice was randomly divided into two subgroups, one for survival analysis and the other for other experiments.

2.5. Behavioral Tests

2.5.1. Weight-Loaded Swimming Test (WST). Mice were subjected to WST before administration and on the 7th, 14th, and 21st days after administration, respectively, as the previous study described [29]. The mouse was placed separately in the swimming pool with 20 cm in diameter, 35 cm high, and at stationary temperature ($25^\circ\text{C} \pm 1^\circ\text{C}$), where the mouse could just touch the bottom with its feet to support itself. A 7% of the body weight tin wire was fixed on the root of the tail to weight load the mouse. When it failed to rise to the water surface to breathe within a 10 sec period, the mouse would be determined to be exhausted and salvaged from the water, dried with a towel, and placed back in the original cage. The time spent by the mouse floating in the water with necessary movements until exhausting its strength was recorded, which was considered a negative correlation with fatigue.

2.5.2. Open-Field Test (OFT). Twenty-four hours after the WST, the OFT was conducted in an arena made of plexiglass ($100 \times 100 \times 50 \text{ cm}^3$). The arena was divided into the center area with a $50 \times 50 \text{ cm}^2$ square and the peripheral area with twelve $25 \times 25 \text{ cm}^2$ squares. The mouse was placed separately in the arena for 5 minutes. Locomotor activity was monitored using an infrared camera. The total movement distance, distance, and time spent in each mouse's central and peripheral areas in the specified observation time were calculated and analyzed using the EthoVision XT 14 software (Noldus Information Technology Co., Ltd, Beijing, China). Each mouse was returned to its home cage after the behavioral test. The OFT apparatus was thoroughly cleaned with 70% ethyl alcohol to eliminate any olfactory cues between tests.

2.6. Determination of the Survival Time of Mice, Body Weight, and Tumor Volume of YFSJ. Ten mice from each group were randomly selected for survival analysis, and the survival time was recorded up to 90 days after the beginning of treatment. At the end of the survival analysis, the still-alive mice were

terminated individually by deeply anesthetized with pentobarbital sodium by intraperitoneal injection (150 mg/kg). Another ten mice from each group were selected for other experiments, and the body weight and tumor volume of the mice were measured every three days. The computational formula of tumor volume = long diameter (L) \times short diameter (W)² $\times 0.5$.

2.7. Mouse Sacrifice, Sample Collection, and Detection of Serum Biochemical Indices. After all behavioral tests, the other 10 mice of each group were anesthetized with isoflurane inhalation (RWD Life Science Pharmaceutical Co., Ltd., Shenzhen, China). The tumors and bilateral gastrocnemius muscles of mice were immediately removed on ice for the following examination when the mice were unconscious. The spleen was removed and weighed to measure the spleen index (weight of spleen/body weight $\times 10 \times 100\%$). The whole blood samples were collected, placed at room temperature for 2 hours, and centrifuged at 3000 r/min at 4°C for 15 min, and the supernatants were taken for biochemical measurement. The levels of serous alanine aminotransferase (ALT), aminotransferase (AST), and creatinine (CREA) were detected according to the procedures provided in the kits (Rayto Life Sciences Inc., Shenzhen, China) and analyzed by the automatic biochemical analyzer Chemray 800 (Redu Life Technology Inc., Shengzhen, Chian).

2.8. Determination of the Concentrations of Oxidative Stress Markers. The tissue ROS assay kit (Cat.#BB-470532, Best-Bio, Shanghai, China) was used to measure gastrocnemius muscle and xenograft tumor tissues ROS concentrations. The Cu/Zn-SOD and Mn-SOD assay kit with WST-8 (Cat.#S0103, Beyotime, Shanghai, China) was used to measure gastrocnemius muscle and xenograft tumor tissues SOD concentrations. The Lipid Peroxidation MDA assay kit (Cat.#S0131S, Beyotime, Shanghai, China) was used to measure MDA concentrations in gastrocnemius muscle and xenograft tumor tissues. In short, we completed the determination of ROS, SOD, and MDA concentrations according to the kit's instructions. These experiments were performed in triplicate. ROS data are expressed as the percentage of the fluorescence intensity relative to that of the control group. The data of SOD are expressed in U/mg protein. The data of MDA are expressed in $\mu\text{mol/mg}$ protein.

2.9. Examination of the Gastrocnemius Muscle Tissues

2.9.1. Electron Microscopy (EM). The fresh muscle tissue was dissected further into $2 \times 2 \text{ mm}^3$ samples immediately, fixed with 2.5% glutaraldehyde for 4 h at 4°C , and triple rinsed with PBS. Then, the samples were fixed with 1% osmic acid for 2 h, triple rinsed with PBS again, and dehydrated with alcohol of gradient concentration (50%, 70%, 80%, 90%, and 95%) acetone for 20 min. After that, muscle tissue was immersed in Epon812 overnight and polymerized in a 45°C drying oven for 12 h. At last, samples were cut into 70 nm slices, stained with uranyl acetate and lead citrate, and

captured under an electron microscope (HITACHI HT7700, Japan). The condition of mitochondria and autophagosomes was assessed using Image-pro plus 6.0 system (Media Cybernetics, Inc., Rockville, USA).

2.9.2. Hematoxylin and Eosin (HE) Staining. A portion of the left fresh muscle tissue was fixed with 4% paraformaldehyde, dehydrated, embedded in paraffin, cut into 5 μ m slices, then stained with hematoxylin for 30 min and eosin for 5 min, vitrified with xylene, and sealed with neutral resin. The stained slices were observed and photographed under a light microscope at 200x magnification (NIKON Eclipse ci, Japan). Semiquantitative scoring of tissue lesions was calculated according to El-Far et al. [40]. Briefly, lesions in 3 fields were chosen randomly from each slide for each mouse and averaged. The lesions were scored in a blinded way (score scale: 0 = normal; 1 \leq 25%; 2 = 26–50%; 3 = 51–75%; and 4 = 76–100%).

2.9.3. Terminal-Deoxynucleotidyl Transferase Mediated Nick End Labeling (TUNEL) Staining. The rest paraffin-embedded muscle tissue section detected the apoptosis level using the TUNEL apoptosis detection kit (AtaGenix, Hubei, China). After dewaxing, the section was added 20 μ g/mL protease K for 30 min at 37°C and triple rinsed in PBS. Then, the samples were stained with 4', 6-diamidino-2-phenylindole (DAPI, 0.05 μ g/mL, Servicebio, Wuhan, China) in PBS for 10 min and sealed after rinsing three times with PBS. Fluorescent images were captured at 400x magnification under a fluorescence microscope (NIKON Eclipse ci, Japan). These experiments were performed in triplicate. The integrated densities of TUNEL-positive areas were measured using ImageJ (v1.46r; NIH, Bethesda, MD, USA) [41].

2.10. Western Blotting. An appropriate amount of mouse's tumor and right gastrocnemius muscle were dissected and immediately separated on ice. Tissues were homogenized with the Scientz-48 High-throughput tissue grinder (Xinzhi Biological Co., Ltd, Ningbo, China) and RIPA Lysis Buffer (Cell Signaling Technology, Inc. Massachusetts, USA), centrifuged at 4°C, 12000g for 10 min. The supernatant was collected for detecting protein concentration and western blot analysis. The protein concentration in the obtained supernatant was determined using an Enhanced BCA Protein Assay Kit (Beyotime Biotechnology, Shanghai, China). The target protein was separated with 8–10% SDS-PAGE (Beyotime, Shanghai), transferred to a polyvinylidene fluoride (PVDF) membrane (Millipore, Marlborough, USA), sealed with 5% skimmed milk powder at room temperature for 60 min, and incubated with the primary antibodies at 4°C overnight: anti-p-AMPK α (1:1000), anti-p-mTOR (1:1000), anti-Beclin1 (1:1000), anti-Atg7 (1:1000), anti-LC3A/B (1:1000), anti-p62 (1:1000), anti-cyto. C (1:1000), anti-c-Casp 9 (1:1000), anti-c-Casp 3 (1:1000), anti-c-PARP (1:1000), anti-p-JNK (1:1000), anti-p-p53 (1:1000), anti-Bax (1:1000), anti-DAPK1 (1:1000), and anti-GAPDH (1:2500). Subsequently, the target protein was washed with

Tris-buffered Saline Tween-20 (TBST) solution three times, incubated with the corresponding secondary anti-rabbit or anti-mouse antibody (1:5000) at room temperature for 60 min, washed with TBST solution three times again, and visualized by hypersensitive ECL kit (Beyotime, Shanghai). These experiments were performed in triplicate. Density values of the bands were captured and documented through a gel image analysis system (ChemiDox™, Bio-Rad, USA) and normalized to GAPDH.

2.11. Statistical Analysis. All data were expressed as the mean \pm standard deviation (SD) and analyzed by SPSS 13.0 (SPSS Inc., IL, USA) or GraphPad Prism 9 software (GraphPad Software, LLC, California, USA). The experimental data of repeated observations were analyzed with repeated measures ANOVA. The survival times of animals were analyzed with Kaplan–Meier analysis. The other data were analyzed by one-way ANOVA and Student's *t*-test. The significance of statistical differences was considered at *P* less than 0.05.

3. Result

3.1. The Effects of YFSJ on CRF in Mice. To evaluate the effect of YFSJ on CRF in mice, we assessed the swimming time of the WST, total movement distance, and the ratio of the central region to the total movement distance of the OFT. As is shown in Figure 1(a), the tumor-bearing group mice with/without treatment showed a significant decrease in swimming time compared to the mice in the tumor-free group (NC group). Meanwhile, the DDP treatment induced a pronounced decrease in the swimming time of tumor-bearing mice. However, the decline in swimming time induced by DDP was significantly reversed after 21 days of treatment with YFSJ. Additionally, the swimming time of tumor-bearing mice in the YFSJ group is longer than in the TC group, indicating the dual role of YFSJ in treating both cancer- and chemotherapy-related fatigues. It is further validated by the results of movement distance and residence time in the central area that YFSJ treatment not only significantly extended the total movement distance of mice but also increased the ratio of the central region to total movement distance in comparison with mice treated with DDP alone (Figure 1(b)). However, there was no significant change in the ratio of the central region to total movement distance among mice in the YFSJ and TC groups (Figure 1(b) iii). These data collectively demonstrated that YFSJ treatment might play a key role in alleviating CRF.

3.2. The Effects of YFSJ on Oxidative Stress-Induced Mitophagy in Mouse Skeletal Muscle. Since CRF is characterized by increased oxidative stress and dysfunctional mitochondria, which are involved in regulating mitochondria autophagy, we proposed that the restrained oxidative stress by YFSJ treatment contributes to the inhibition of autophagy in skeletal muscle cells; thus, the effect of YFSJ on oxidative stress is assessed. We first examined the ROS, SOD, and MDA concentrations in mice to evaluate the effect of YFSJ on oxidative stresses. These data revealed that the aberrant

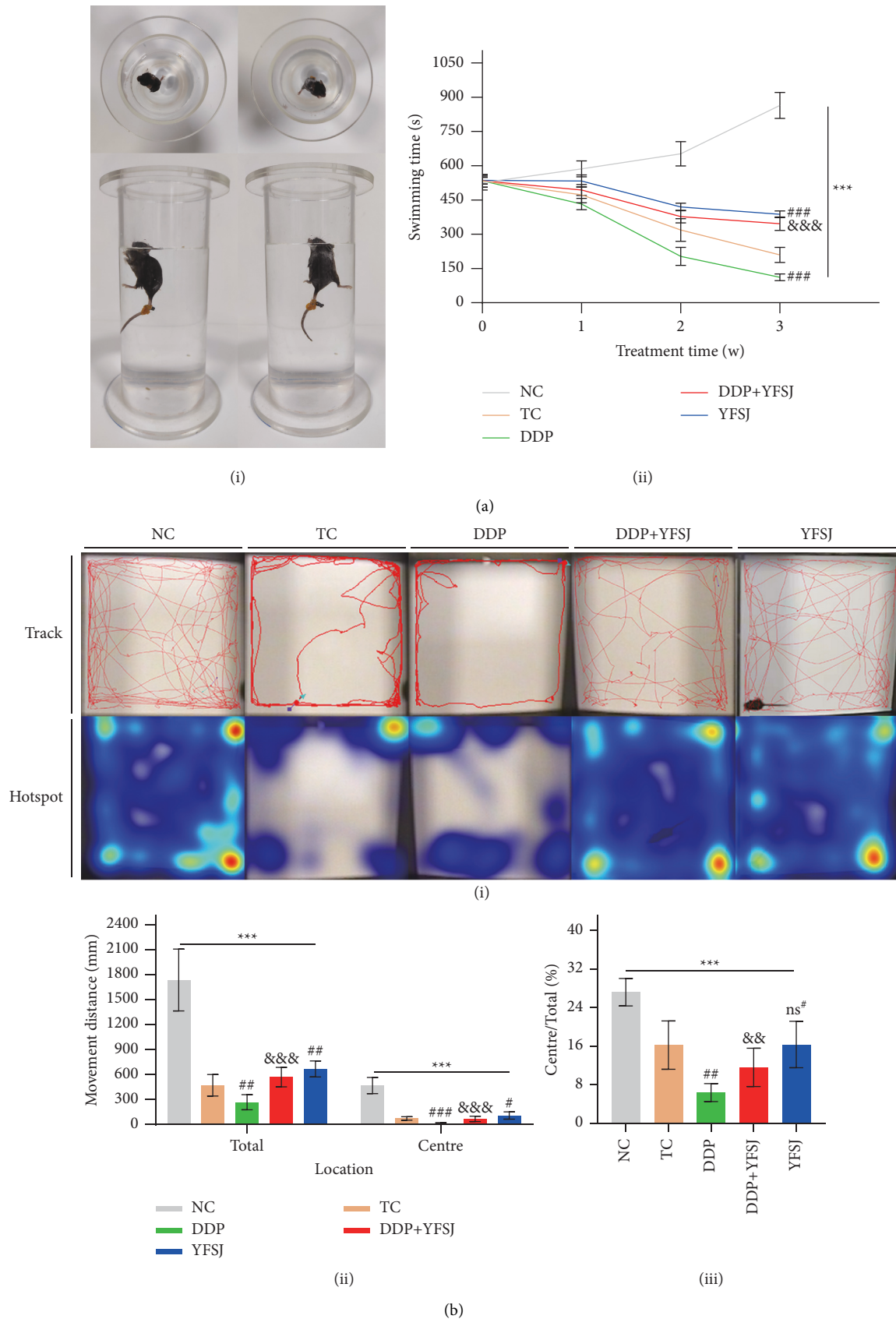


FIGURE 1: The effects of YFSJ on CRF. (a) WST: (i) schematic diagram of WST; (ii) the swimming time of the WST. (b) OFT: (i) pathway map and regional residence time heatmap of mouse movement in OFT; (ii) the movement distance of mice, including total movement distance and central movement distance; (iii) the proportion of the movement distance in the central region to the total movement distance of mice. The data are presented as the means \pm SD of triplicate experiments, $n = 10$. ^{ns*} $p > 0.05$, ^{***} $p < 0.001$ compared with the NC group. [#] $p < 0.05$, ^{##} $p < 0.01$, ^{###} $p < 0.001$ compared with the TC group. ^{&&&} $p < 0.01$, ^{&&&&} $p < 0.001$ compared with the DDP group.

production of ROS and MDA by DDP treatment could be significantly rescued by YFSJ (Figures 2(a)–2(c)). Consistently, the reduced levels of SOD were markedly elevated in DDP + YFSJ and YFSJ groups (Figure 2(b)). As shown in the electron microscopy of skeletal muscle mitochondria (Figure 2(d)), the DDP group manifested increasing swollen, vacuolar damaged mitochondria, which were surrounded by the double membrane phagophore structure forming autophagosomes compared to the TC group. However, YFSJ significantly inhibited the formation of autophagosomes. Moreover, Western blot data showed that YFSJ treatment inhibited the activation of the AMPK/mTOR pathway, counteracting the accumulated turnover of LC3-A to LC3-B by DDP, which was further evidenced by the changed protein expression levels of Beclin1, Atg7, and p62 in skeletal muscle cells of mice from the DDP + YFSJ group (Figures 2(e) and 2(f)). Taken together, these results revealed that oxidative stress-mediated mitophagy is responsible for the inhibitory effect of YFSJ on CRF.

3.3. The Effects of YFSJ on Chemotherapy-Induced Apoptosis in Mouse Skeletal Muscle. HE staining results showed that the tissue structures of skeletal muscles were clear and complete in the DDP + YFSJ group while destroyed in the DDP group with an amount of muscle fiber breakage, such as swelling between muscle cells or broken connections between muscle cells (Figure 3(a)). TUNEL assay was performed to detect apoptosis levels. As shown in Figure 3(b), mice treated with DDP + YFSJ attenuated the elevated skeletal muscle cell apoptosis by DDP. To substantiate the above findings, a series of proapoptotic proteins (e.g., cyto. C, c-Casp 9, c-Casp 3, and c-PARP) were detected. Western blot data revealed that YFSJ treatment attenuated the promoting effect of DDP on skeletal muscle cell apoptosis (Figure 3(c)), which is consistent with the results of the TUNEL assay. Thus, reduced apoptosis in skeletal muscle cells by alleviating oxidative-mediated mitophagy may be the potential mechanism of YFSJ in the treatment of CRF.

3.4. The Effects of YFSJ on Xenograft Tumors in Mice. The antitumor effects of YFSJ were investigated *in vivo*. As is shown in Figure 4(a), xenografts-bearing mice treated with DDP + YFSJ exhibited the lowest growth rate compared to other groups. Tumor size and tumor weight were significantly reduced in DDP + YFSJ-treated mice. Although xenografts treated with DDP or YFSJ alone showed a decrease compared to xenografts in the TC group, the combined treatment of DDP and YFSJ exhibited a more significant antitumor effect. Additionally, we assessed the ROS, SOD, and MDA concentrations in tumor tissues. The results demonstrated that either single or combined treatment could significantly promote ROS and MDA production (Figures 4(b) and 4(d)), while SOD, as an antioxidant index, showed an opposite trend (Figure 4(c)). Subsequently, Western blots were performed to detect apoptosis and autophagy in xenografts. Consistently, xenografts treated with DDP or YFSJ alone both displayed activated cell apoptosis and autophagy, while the combined treatment of DDP + YFSJ showed the most potent effects (Figures 4(e)–

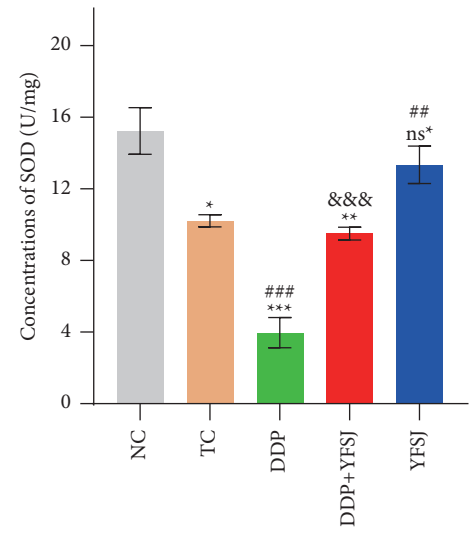
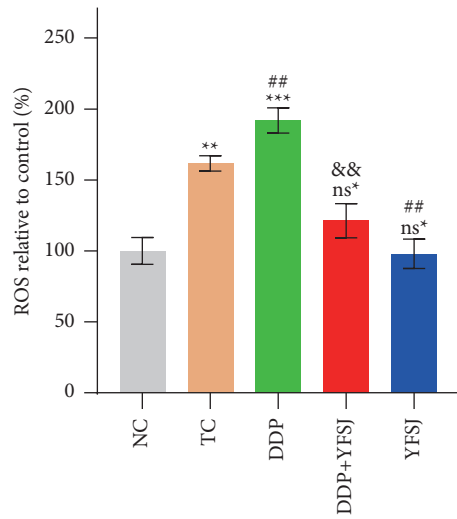
4(h)), as evidenced by activation of the JNK/p53 pathway, increasing Bax, c-Casp 3, c-PARP, Beclin1, Atg7, and LC3B and reducing p62 in protein expression levels. In conclusion, YFSJ has an inhibitory effect on tumor growth and is synergistic with the antitumor effect of DDP.

3.5. The Effects of YFSJ on the Quality of Life and Survival Time in Mice. Accumulating evidence has highlighted the importance of CRF in patients with cancers' quality of life and survival time [42]. To investigate whether reduced fatigue of mice by YFSJ treatment could contribute to a better prognosis and desirable quality of life, we evaluated the survival time, body weight, and serum concentrations of ALT, AST, and CREA of the mice. As is shown in Figure 5(a), the survival time of mice in the NC group is the longest compared to tumor-bearing mice in other groups. Further analysis revealed that DDP treatment did not substantially prolong the survival time. In contrast, the combined therapies of DDP and YFSJ or YFSJ treatment alone could significantly extend the survival time of tumor-bearing mice. Afterward, body weight, ALT, AST, and CREA concentrations were detected. The results demonstrated that compared with the TC group, mice's body weights were slightly reduced after DDP treatments. Nevertheless, YFSJ treatments significantly restore the body weight loss of mice induced by DDP (Figure 5(b)). Analysis of serum markers exhibited ascending concentrations of ALT, AST, and CREA in mice of the DDP group while descending levels in the DDP + YFSJ group (Figure 5(d)). Pathologically, the spleen was compensatively enlarged due to the retention of immunocytes in the spleen [43]. As a result, the spleen index of mice in the TC group was the highest. By contrast, the spleen index of the DDP-treated group was reduced significantly; the DDP + YFSJ group increased the spleen index compared to mice treated with DDP alone, which indicated the immunosuppression resulting from the DDP treatment could be activated by YFSJ (Figure 5(c)). The above results revealed that YFSJ could overcome the toxicity and improve the quality of life of mice by DDP.

4. Discussion

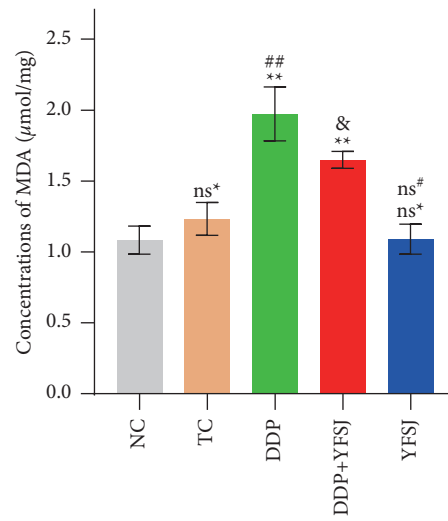
YFSJ is a proprietary medicine developed from traditional Chinese medicine prescriptions, Yiqi Chutan Tang, with lung cancer treatment. Interestingly, in clinical observation, we found that it had a significant effect on the improvement of CRF [38, 39]. In order to clarify the underlying mechanisms, in the current research, the xenogeneic model was established in C57/BL mice using LLC cells and treated with DDP to simulate a CRF situation that occurs in humans; the WST and OFT were used for the evaluation of fatigue related to chemotherapy. Moreover, we used the model to evaluate the effect of YFSJ on the fatigue caused by DDP.

The WST assessed the endurance and fatigue status [44]. The indices of locomotor activities were tested in the OFT [45–47] to evaluate the physical and psychological fatigue, respectively. In this study, the TC and DDP group showed more obvious physical and psychological fatigue than the NC group by significantly decreasing swimming time, less locomotor distance, and residence time in the central area.

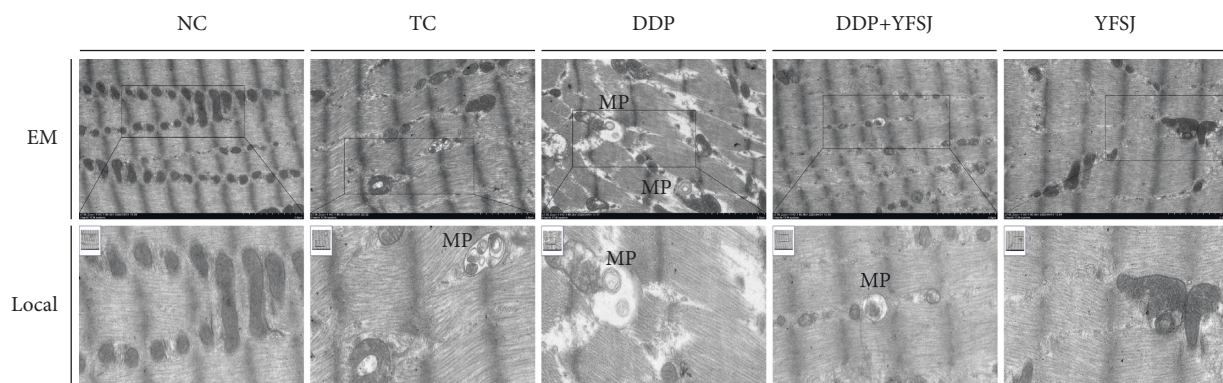


(a)

(b)



(c)



(d)

FIGURE 2: Continued.

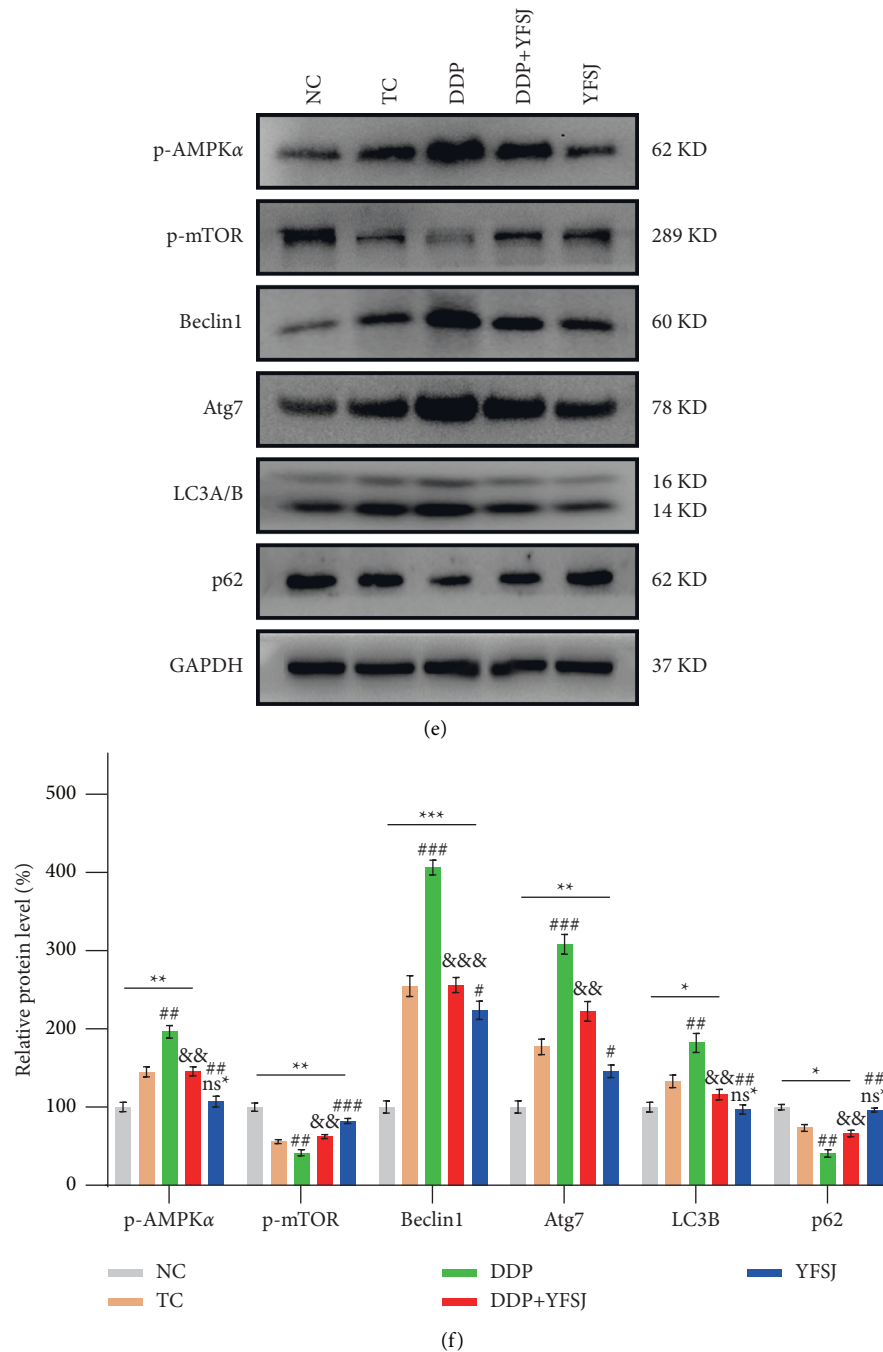


FIGURE 2: The effects of YFSJ on oxidative stress-induced mitophagy in mouse skeletal muscle. Indicators of oxidative stress in skeletal muscle tissues: (a) the relative concentrations of ROS in skeletal muscle tissues; (b) the SOD concentrations in skeletal muscle tissues; (c) the MDA concentrations in skeletal muscle tissues. (d) Electron microscopy of mitophagy in skeletal muscle tissues. Scale bars = 2 μ m; local magnification = 15X; MP = mitophagosomes. Autophagy-related proteins in skeletal muscle tissues: (e) Western blotting bands of autophagy-related proteins; (f) relative expression levels of autophagy-related proteins. The data are presented as the means \pm SD of triplicate experiments, $n = 3$. ns $p > 0.05$, * $p > 0.05$, ** $p < 0.01$, *** $p < 0.001$ compared with the NC group. $^{ns\#}$ $p > 0.05$, $^{\#}$ $p < 0.05$, $^{\#\#}$ $p < 0.01$, $^{\#\#\#}$ $p < 0.001$ compared with the TC group. $^{\&}$ $p < 0.05$, $^{\&\&}$ $p < 0.01$, $^{\&\&\&}$ $p < 0.001$ compared with the DDP group.

Between the two groups, the DDP group presented more severe fatigue than the TC group, reflecting that the fatigue of tumor-bearing mice was aggravated by DDP chemotherapy, which was accordant with previous research that some cancer patients presented severer fatigue after receiving chemotherapy [48, 49]. At the same time, the decline in swimming

time and locomotor activities induced by DDP were significantly reversed after 21 days of treatment with YFSJ, indicating that YFSJ could alleviate the CRF, which was consistent with previous clinical studies [13–15, 38, 39, 50].

Numerous studies proved that increased oxidative stress would aggravate muscle fatigue [51–53]. Oxidative stress can

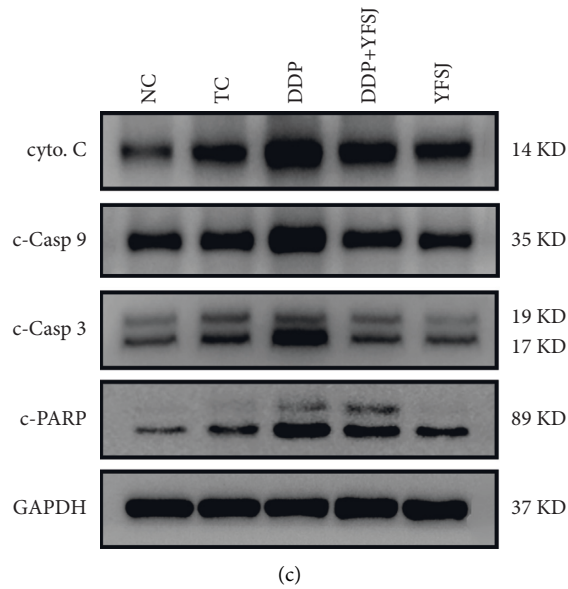
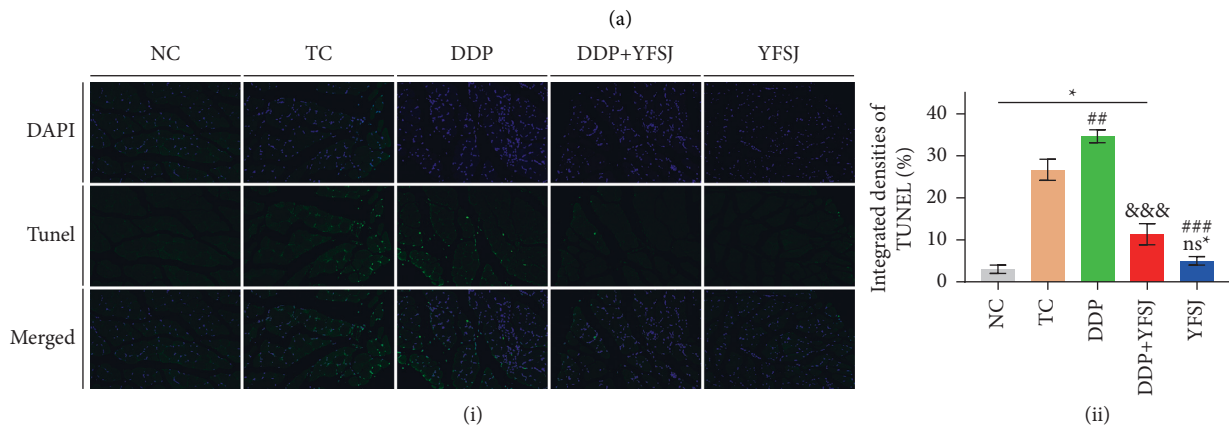
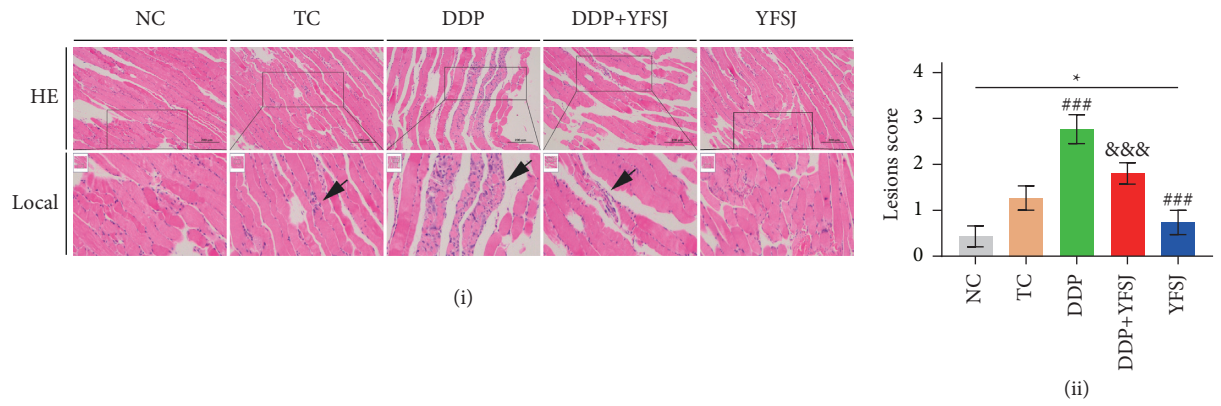


FIGURE 3: Continued.

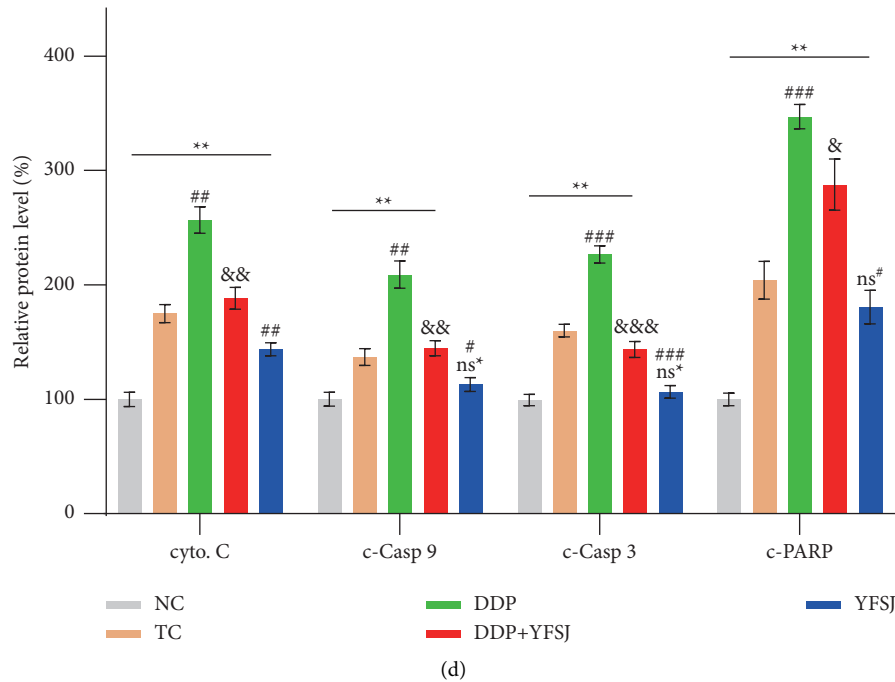


FIGURE 3: The effects of YFSJ on chemotherapy-induced apoptosis in mouse skeletal muscle. (a) (i) HE staining of skeletal muscle tissues. Scale bars = 200 μm ; local magnification = 15x. (ii) HE semiquantitative scoring of lesions ($n = 10$). (b) (i) TUNEL staining of skeletal muscle tissues. Magnification = 100x. (ii) Integrated densities of TUNEL ($n = 3$). Apoptosis-related proteins in skeletal muscle tissues: (c) western blotting bands of apoptosis-related proteins; (d) relative expression levels of apoptosis-related proteins. The data are presented as the means \pm SD of triplicate experiments, $n = 3$. $^{ns*} p > 0.05$, $^* p < 0.05$, $^{**} p < 0.01$ compared with the NC group. $^{ns\#} p > 0.05$, $^{\#} p < 0.05$, $^{##} p < 0.01$, $^{###} p < 0.001$ compared with the TC group. $^{\&} p < 0.05$, $^{\&\&} p < 0.01$, $^{\&\&\&} p < 0.001$ compared with the DDP group.

be produced by tumors themselves [54] and directly or indirectly given rise by numerous chemotherapeutic agents [55, 56]. In the oxidative stress state, overproduced free radicals like ROS will ultimately produce MDA, directly reflecting the degree of lipid peroxidation [57]. An antioxidant such as SOD plays an essential role in removing these productions of oxidative stress [58]. Therefore, ROS, SOD, and MDA were chosen as biomarkers to evaluate the degree of oxidative stress in skeletal muscle. This study showed that the DDP elevated the ROS and MDA concentrations and weakened the SOD activity significantly in the muscle tissue; however, the oxidative stress phenomena were alleviated significantly in the DDP + YFSJ group. That may be related to some components of YFSJ (Supplementary Table 2), such as ginsenoside Rg2 and ginsenoside Rg3 [59], which have been shown to have antioxidant effects on normal tissues. At the same time, oxidative stress-induced damage to mitochondrial DNA, membrane lipids, and proteins can be degraded by mitophagy [60]. That is because oxidative stress leads to phosphorylation of AMPK α in the mitochondria, which activates AMPK [61]. Activation of AMPK inhibited the phosphorylation of mTOR [62] and weakened the inhibition of p-mTOR on the autophagy key factor Beclin1 [63]. Mechanistically, Beclin1 is a crucial protein for autophagy initiation, which, together with PIK3C3 and PIK3R4, forms a protein complex Class III PI3K, and ultimately regulates the formation and maturation of autophagosomes [64–66]. Atg7 and LC3B are markers of autophagosome formation [67, 68]. LC3B is

involved in the recruitment of p62 to autophagosomes [69], which is eventually degraded, and the protein level of p62 decreases [70]. The electron microscopy results of skeletal muscle mitochondria in the present study provide direct evidence of mitophagy in the DDP group manifesting increasing swollen, vacuolar damaged mitochondria, which were surrounded by the double membrane phagophore structure forming the autophagosomes. YFSJ treatment reduced the occurrence of mitophagy and damage caused by DDP. In order to strengthen the evidence, mitophagy-related proteins were detected in this study. The results showed that YFSJ could reverse the expression level of DDP-induced mitochondrial autophagy-related proteins. Proper regulation of mitophagy is essential for normal cellular and physiological function [71]. However, excessive mitophagy can trigger cell death [72]. Skeletal muscle cells were also observed under the microscope. DDP induced severe damage such as twisted, broken, and irregular arrangements of muscle fibers and even apoptosis in the muscle tissue. Because in the process of mitochondrial autophagy, apoptotic factors (such as cyto. C) are released, which further activate Caspase-9 and Caspase-3 [73–77], ultimately transmitting the death signal to the downstream molecules, such as PARP [78], reducing the stability of DNA, to promote apoptosis. At the same time, ROS can also promote the release of cyto. C from mitochondria, leading to the occurrence of apoptosis [79]. In the present study, the results obtained from western blot revealed that the DDP group exhibited increased protein expression levels of cyto. C,

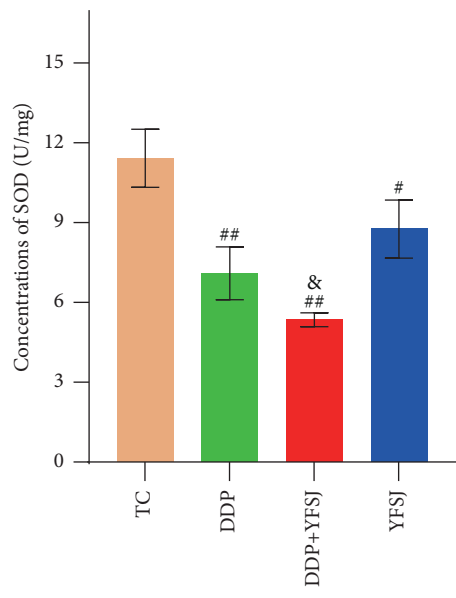
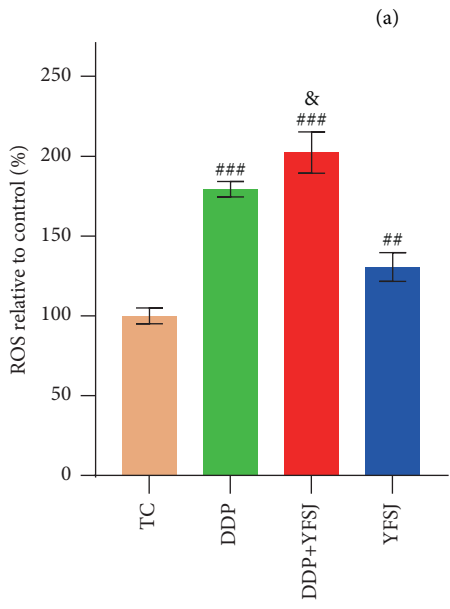
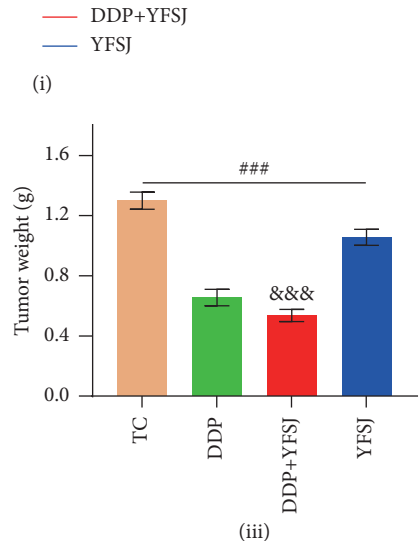
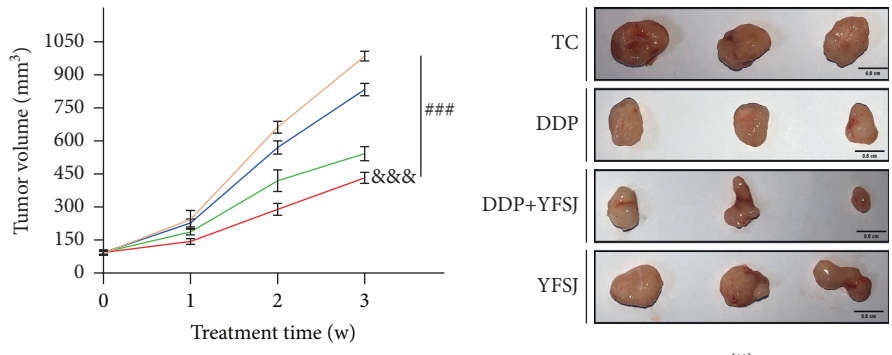
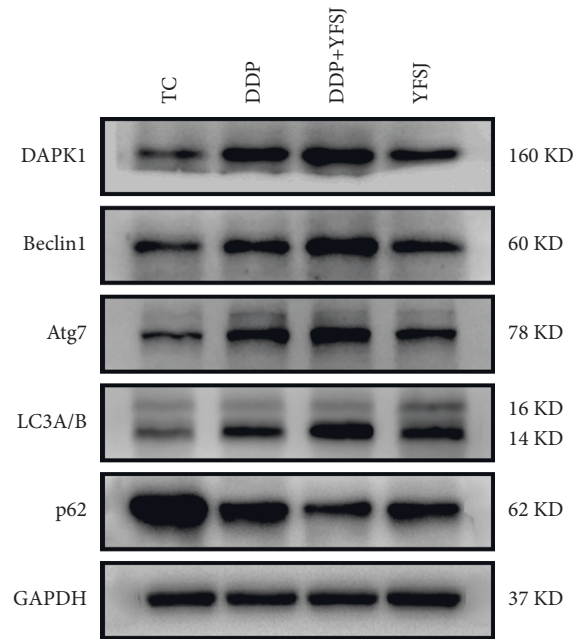
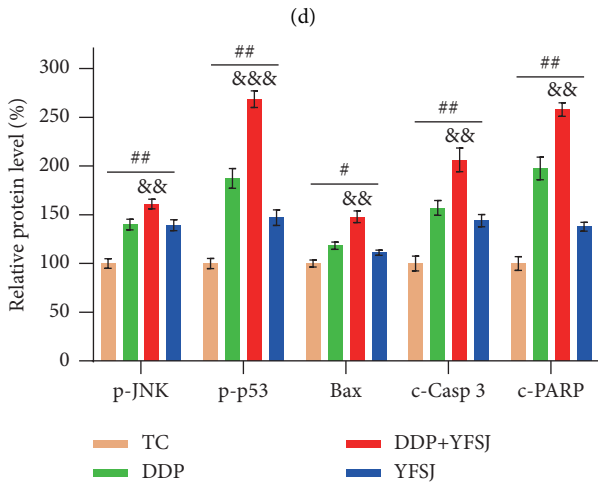
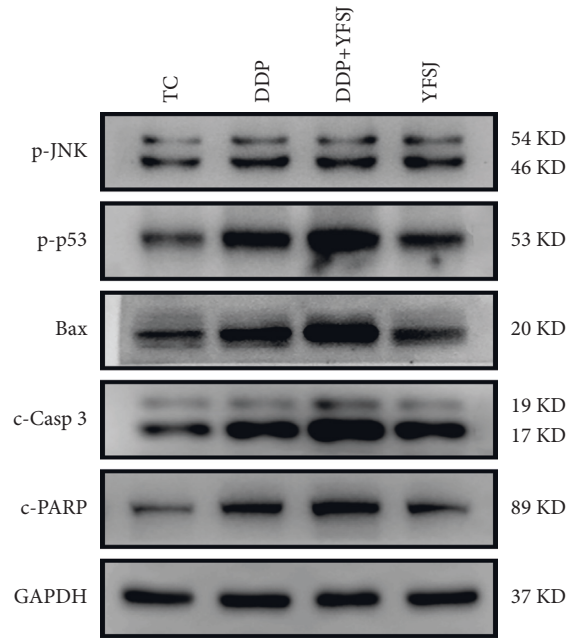
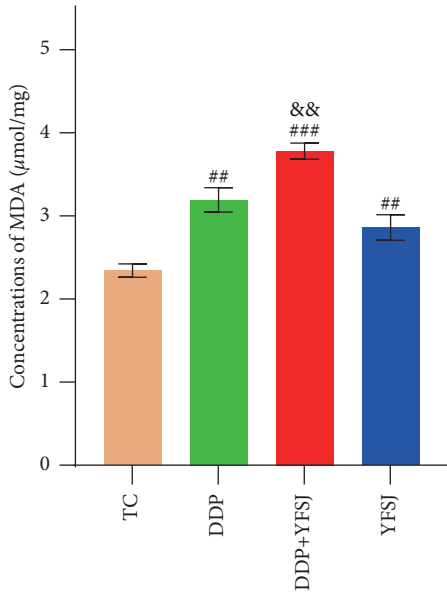


FIGURE 4: Continued.



(d)

(e)

(f)

(g)

FIGURE 4: Continued.

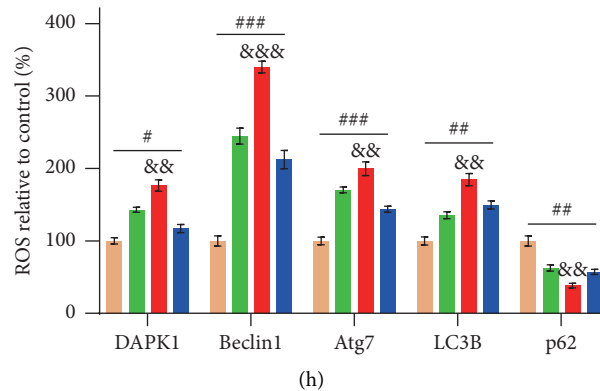


FIGURE 4: The effects of YFSJ on xenografts in mice. (a) The condition of the tumor: (i). The volume of the tumor, $n = 10$; (ii) representative image pictures of the tumor; (iii) weight of tumor in mice, $n = 10$. Indicators of oxidative stress in tumor tissues: (b) the relative concentrations of ROS in tumor tissues; (c) the SOD concentrations in tumor tissues; (d) the MDA concentrations in tumor tissues. Apoptosis-related proteins in tumor tissues: (e) western blotting bands of apoptosis-related proteins; (f) relative expression levels of apoptosis-related proteins. Autophagy-related proteins in tumor tissues: (g) western blotting bands of autophagy-related proteins; (h) relative expression levels of autophagy-related proteins. The data are presented as the means \pm SD of triplicate experiments, $n = 3$, unless otherwise specified. $^{\#}p < 0.05$, $^{##}p < 0.01$, $^{###}p < 0.001$ compared with the TC group. $^{\&\&}p < 0.01$, $^{\&\&\&}p < 0.001$ compared with the DDP group.

c-Casp 9, c-Casp 3, and c-PARP in skeletal muscle tissues of mice, which were consistent with the results of the TUNEL staining assay. However, YFSJ can obviously reverse this phenomenon caused by DDP. To sum up, YFSJ treatment decreased oxidative stress, inhibited the activation of the AMPK/mTOR pathway, decreased protein expression levels of Beclin1 and other autophagy-related proteins, and attenuated the activation of cyto. C, c-Casp 9, and other apoptosis-related proteins in skeletal muscle tissues by DDP. These results revealed that YFSJ might reduce skeletal muscle apoptosis by alleviating oxidative stress-mediated mitophagy for the inhibitory effect on CRF.

Previous studies proved that promoting ROS production is the most critical pathway chemotherapy follows in cancer elimination [80, 81]. By increasing ROS concentrations (which may be associated with some components of YFSJ, such as Quercetin and Oleanolic acid [82, 83]), patients have high overall survival and a good prognosis as ROS overgeneration enhances DDP sensitivity and apoptosis induction [84]. In tumor cells, increased ROS content activates the JNK/p53 pathway, increasing Bax expression. Bax is a proapoptotic protein, and the increase of Bax will activate Casp3, and C-Casp3 will further promote PARP cleavage, which will reduce the stability of double-stranded DNA and eventually lead to apoptosis [85]. Meanwhile, the activation of p53 promotes the expression of DAPK1 [86], which further promotes the expression of Beclin1 [87], a key autophagy factor, and ultimately leads to autophagy in tumor cells. Similar results were observed in our study; YFSJ enhanced DDP sensitivity by promoting ROS and MDA production, decreasing the SOD concentrations, and activating the cell apoptosis and autophagy in the tumor tissues of mice. It was also found that YFSJ reduced the loss of body weight caused by DDP, ascended the serum levels of ALT, AST, and CREA, increased the spleen index, and prolonged the survival time of mice. In conclusion, YFSJ can specifically increase the ROS

content of tumor cells and increase chemotherapy sensitivity. So, YFSJ can alleviate the hepatorenal toxicity and immunosuppression caused by DDP. Our results showed that YFSJ can inhibit tumor growth and improve the quality of life of patients.

In this study, we found an interesting phenomenon: YFSJ administration decreased the ROS concentrations in the muscle tissue but increased them in the tumor tissue. However, they were enhanced in whatever tissues after DDP treatment. In the tumor microenvironment of cancer cells, low to moderate levels of cellular ROS are produced to regulate cell signaling and promote cell proliferation [88], as one of the unique characteristics of cancer [89]. The persistent mild elevated level of ROS can provide metabolic reprogramming to deal with the stress induced by cancer therapies and even enhance tumor resistance [90]. However, unlike tumor tissue, skeletal muscle tissue typically has good blood oxygen content and is prone to produce excessive ROS under the cancer therapy's stress [91]. In addition to some of the components mentioned, as a traditional Chinese medicinal formula based on the concept of holism, YFSJ is often used to adjust the macroscopic state of the human body not only to resolve the masses to reduce the solid tumor but also tonify qi (vital energy) and improve the blood circulation. These effects of YFSJ can improve the nutritional status of the human body under DDP chemotherapy. Studies have confirmed that poor nutritional status can lead to excessive ROS production in mitochondria and activate autophagy [92, 93]. On the other hand, improving nutritional status may improve the body's ability to recognize tumors and break the relatively stable tumor microenvironment. Based on these functions, we assume that YFSJ might break the relatively stable hypoxic microenvironment of tumor tissue and promote ROS overgeneration to enhance DDP sensitivity. At the same time, improved blood circulation could accelerate the elimination of the excessive ROS produced by skeletal

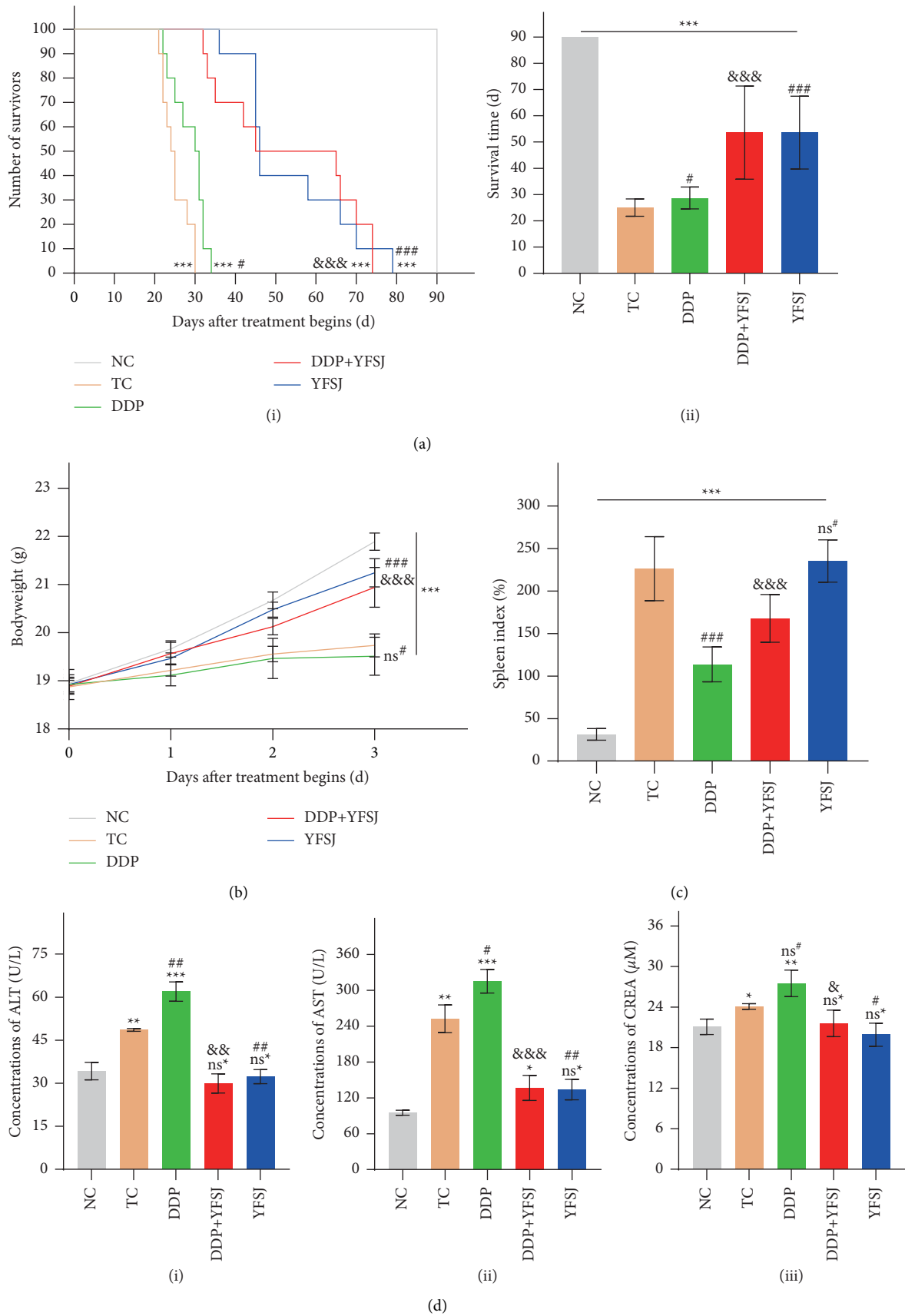


FIGURE 5: The effects of YFSJ on the quality of life and survival time in mice. (a) Survival analysis: (i) survival curve in mice; (ii) Mouse survival time. (b) The body weight of mice. (c) Spleen index in mice. (d) Serum biochemical indices of mice, $n = 3$: (i) the ALT concentrations in mice serum; (ii) the AST concentrations in mice serum; (iii) the CREA concentrations in mice serum. The data are presented as the means \pm SD of triplicate experiments, $n = 10$. $^{ns*} p > 0.05$, $^* p < 0.05$, $^{**} p < 0.01$, $^{***} p < 0.001$ compared with the NC group. $^{ns\#} p > 0.05$, $^{\#} p < 0.05$, $^{\#\#} p < 0.01$, $^{\#\#\#} p < 0.001$ compared with the TC group. $^{\&} p < 0.05$, $^{\&\&} p < 0.01$, $^{\&\&\&} p < 0.001$ compared with the DDP group.

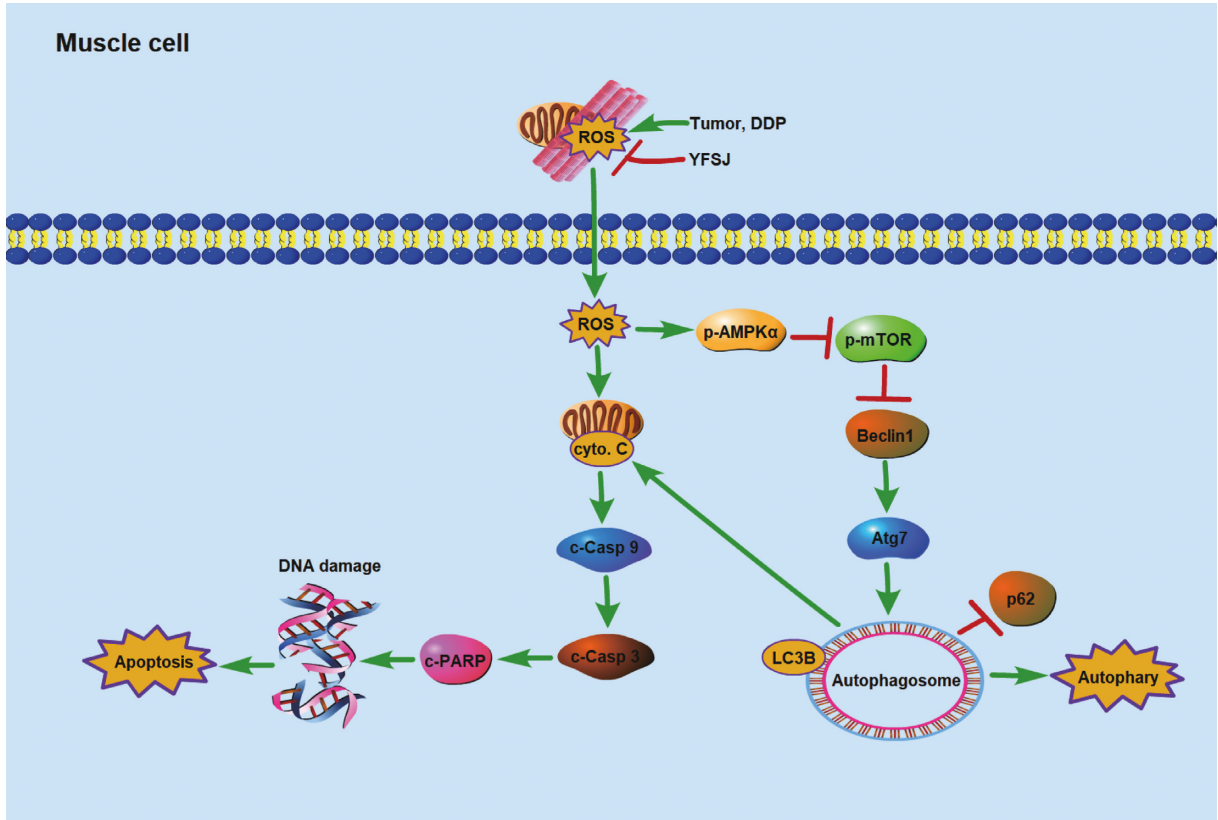


FIGURE 6: Schematic illustration of the potential underlying mechanism responsible for reducing skeletal muscle injury by YFSJ.

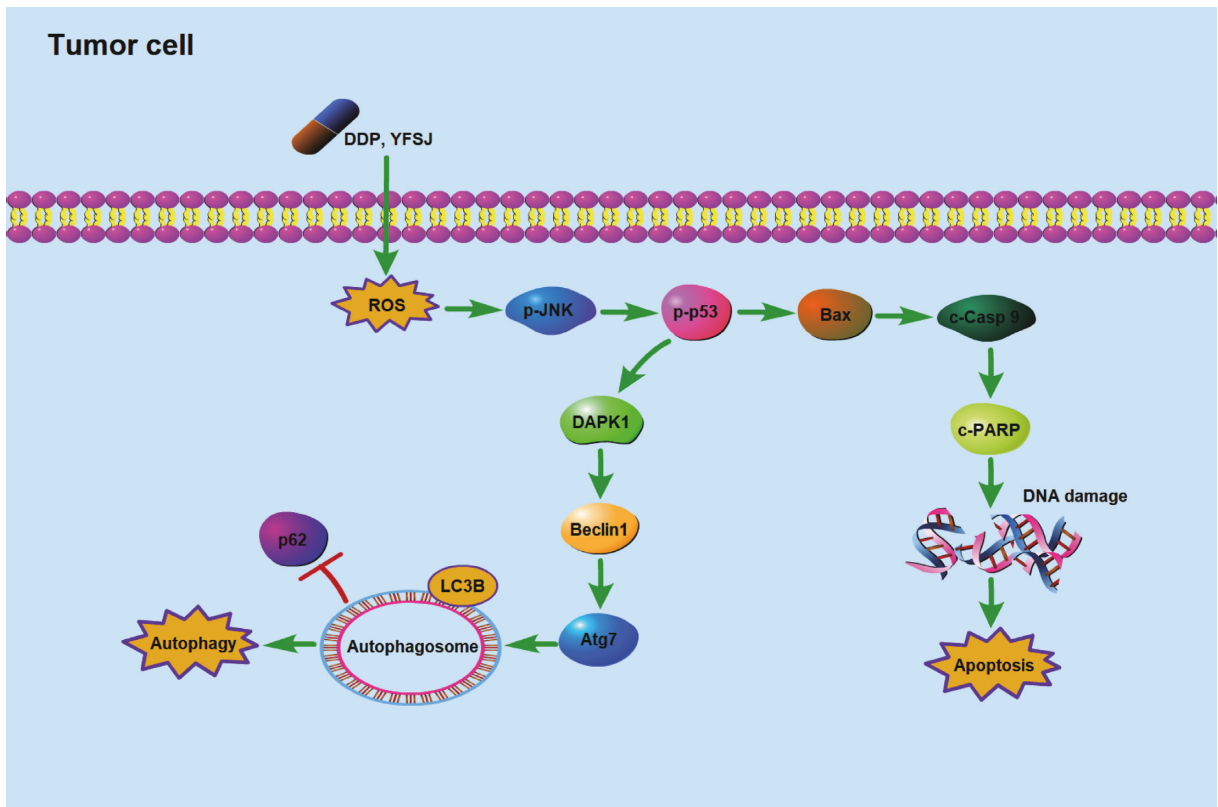


FIGURE 7: Schematic illustration of the potential underlying mechanism responsible for inhibiting tumor growth by YFSJ.

muscle cells due to stress. Further experiments will be carried out on this hypothesis in the future. This study was conducted only in vivo experiments but not in vitro verification. We will carry out in vitro verification experiments based on the results of this experiment in the future.

The hypothetical mechanism by which YFSJ alleviates CRF by reducing oxidative stress levels in skeletal muscle cells is shown in Figure 6. The hypothetical mechanism of YFSJ inhibiting tumor growth by increasing the ROS content of tumor cells to enhance chemotherapy sensitivity is shown in Figure 7. In conclusion, YFSJ specifically regulates ROS concentration in different tissues to reduce skeletal muscle injury and inhibit tumor growth and is directly and closely related to CRF treatment.

5. Conclusions

In this study, all results demonstrated that YFSJ could alleviate CRF by reducing mitophagy and apoptosis due to reducing oxidative stress of skeletal muscle. These results also displayed the effects of YFSJ on enhancing chemotherapy sensitivity, improving quality of life, and prolonging survival time in lung cancer mice who received DDP chemotherapy.

Data Availability

The datasets used and/or analyzed during the current study are available from the corresponding author upon reasonable request.

Disclosure

Yingchao Wu and Dajin Pi are co-first authors.

Conflicts of Interest

The authors declare that there are no conflicts of interest regarding the publication of this paper.

Authors' Contributions

Yingchao Wu and Dajin Pi performed the experiments and wrote the manuscript. Yiliu Chen and Qian Zuo conducted the experiments and analyzed the data. Lizhu Lin provided the YFSJ pills used in the study. Mingzi Ouyang designed the study and provided the initial idea. All authors read and approved the final manuscript. Yingchao Wu and Dajin Pi contributed equally.

Acknowledgments

The medical experiment center of Basic Medicine and Public Health School of Jinan University supported this study. This work was supported by the National Natural Science Foundation of China (Grant nos. 81873155 and 81403340), which supported the design, analysis, and interpretation of data in this study. The Medical Scientific Research Foundation of Guangdong Province of China (Grant no.

A2018006) and Project of Administration of Traditional Chinese Medicine of Guangdong Province of China (Grant no. 20191079) both provided the animals, medicine, and other materials needed in the study.

Supplementary Materials

Supplementary Figure 1: (a) The packaging and appearance of the YFSJ pill. (b) Representative figures of herbs in YFSJ. Supplementary Table 1: List of botanical, herbal, Chinese names of the corresponding herbs in YFSJ. Supplementary Figure 2: (a) Q-Orbitrap-LC/MS analysis base peak intensity chromatograms of YFSJ in positive mode. (b) Q-Orbitrap-LC/MS analysis base peak intensity chromatograms of YFSJ in negative mode. Supplementary Table 2: Identification of components of YFSJ by Q-Orbitrap-LC/MS analysis. (*Supplementary Materials*)

References

- [1] M. D. Hellmann, B. T. Li, J. E. Chaft, and M. G. Kris, "Chemotherapy remains an essential element of personalized care for persons with lung cancers," *Annals of Oncology*, vol. 27, no. 10, pp. 1829–1835, 2016.
- [2] K. E. Rosenzweig and J. E. Gomez, "Concurrent chemotherapy and radiation therapy for inoperable locally advanced non-small-cell lung cancer," *Journal of Clinical Oncology*, vol. 35, no. 1, pp. 6–10, 2017.
- [3] P. Lv, S. Man, L. Xie, L. Ma, and W. Gao, "Pathogenesis and therapeutic strategy in platinum resistance lung cancer," *Biochimica et Biophysica Acta (BBA)—Reviews on Cancer*, vol. 1876, no. 1, Article ID 188577, 2021.
- [4] H. S. Wu and J. K. Harden, "Symptom burden and quality of life in survivorship: a review of the literature," *Cancer Nursing*, vol. 38, no. 1, pp. E29–E54, 2015.
- [5] A. M. Berger, K. Mooney, A. Alvarez-Perez et al., "Cancer-related fatigue, version 2.2015," *Journal of the National Comprehensive Cancer Network*, vol. 13, no. 8, pp. 1012–1039, 2015.
- [6] A. Sobrero, F. Puglisi, A. Guglielmi et al., "Fatigue: a main component of anemia symptomatology," *Seminars in Oncology*, vol. 28, pp. 15–18, 2001.
- [7] J. E. Bower, "Cancer-related fatigue--mechanisms, risk factors, and treatments," *Nature Reviews Clinical Oncology*, vol. 11, no. 10, pp. 597–609, 2014.
- [8] X. S. Wang and J. F. Woodruff, "Cancer-related and treatment-related fatigue," *Gynecologic Oncology*, vol. 136, no. 3, pp. 446–452, 2015.
- [9] Y. Zhou, H. Xu, W. Xu et al., "Exosomes released by human umbilical cord mesenchymal stem cells protect against cisplatin-induced renal oxidative stress and apoptosis in vivo and in vitro," *Stem Cell Research & Therapy*, vol. 4, no. 2, 2013.
- [10] J. M. Argiles, F. J. Lopez-Soriano, and S. Busquets, "Muscle wasting in cancer: the role of mitochondria," *Current Opinion in Clinical Nutrition and Metabolic Care*, vol. 18, no. 3, pp. 221–225, 2015.
- [11] B. G. Eid and N. A. El-Shitany, "Captopril downregulates expression of Bax/cytochrome C/caspase-3 apoptotic pathway, reduces inflammation, and oxidative stress in cisplatin-induced acute hepatic injury," *Biomedicine & Pharmacotherapy*, vol. 139, Article ID 111670, 2021.
- [12] M. A. Ibrahim, I. A. Albahlol, F. A. Wani et al., "Resveratrol protects against cisplatin-induced ovarian and uterine toxicity

- in female rats by attenuating oxidative stress, inflammation and apoptosis," *Chemico-Biological Interactions*, vol. 338, Article ID 109402, 2021.
- [13] D. G. Deavall, E. A. Martin, J. M. Horner, and R. Roberts, "Drug-induced oxidative stress and toxicity," *Journal of Toxicology*, vol. 2012, Article ID 645460, 13 pages, 2012.
- [14] E. C. Neefjes, R. M. van den Hurk, S. Blauwhoff-Buskermolen et al., "Muscle mass as a target to reduce fatigue in patients with advanced cancer," *Journal of Cachexia, Sarcopenia and Muscle*, vol. 8, no. 4, pp. 623–629, 2017.
- [15] J. Doherty and E. H. Baehrecke, "Life, death and autophagy," *Nature Cell Biology*, vol. 20, no. 10, pp. 1110–1117, 2018.
- [16] S. Yang, S. Chu, Y. Gao et al., "A narrative review of cancer-related fatigue (CRF) and its possible pathogenesis," *Cells*, vol. 8, no. 7, p. 738, 2019.
- [17] B. N. Vanderveen, D. K. Fix, B. R. Counts, and J. A. Carson, "The effect of wheel exercise on functional indices of cachexia in tumor-bearing mice," *Medicine & Science in Sports & Exercise*, vol. 52, no. 11, pp. 2320–2330, 2020.
- [18] H. E. Wilson, D. A. Stanton, S. Rellick, W. Geldenhuys, and E. E. Pistilli, "Breast cancer-associated skeletal muscle mitochondrial dysfunction and lipid accumulation is reversed by PPAR γ ," *American Journal of Physiology—Cell Physiology*, vol. 320, no. 4, pp. C577–C590, 2021.
- [19] E. Obrador, R. Salvador-Palmer, R. Lopez-Blanch, A. Jihad-Jebbar, S. L. Valles, and J. M. Estrela, "The link between oxidative stress, redox status, bioenergetics and mitochondria in the pathophysiology of ALS," *International Journal of Molecular Sciences*, vol. 22, no. 12, 2021.
- [20] L. Galluzzi, O. Kepp, and G. Kroemer, "Mitochondria: master regulators of danger signalling," *Nature Reviews Molecular Cell Biology*, vol. 13, no. 12, pp. 780–788, 2012.
- [21] E. Marzetti, R. Calvani, M. Cesari et al., "Mitochondrial dysfunction and sarcopenia of aging: from signaling pathways to clinical trials," *The International Journal of Biochemistry & Cell Biology*, vol. 45, no. 10, pp. 2288–2301, 2013.
- [22] C. Klasson, M. Helde Frankling, C. Lundh Hagelin, and L. Bjorkhem-Bergman, "Fatigue in cancer patients in palliative care—A review on pharmacological interventions," *Cancers*, vol. 13, no. 5, 2021.
- [23] D. Goldstein, B. K. Bennett, K. Webber et al., "Cancer-related fatigue in women with breast cancer: outcomes of a 5-year prospective cohort study," *Journal of Clinical Oncology*, vol. 30, no. 15, pp. 1805–1812, 2012.
- [24] C. L. Rush, T. Lobo, A. Serrano, M. Blasini, C. Campos, and K. D. Graves, "Complementary and alternative medicine use and latina breast cancer survivors' symptoms and functioning," *Healthcare*, vol. 4, no. 4, p. 80, 2016.
- [25] N. M. Wheeldon, "Chronic atrial fibrillation: optimizing anticoagulation," *QJM*, vol. 90, no. 10, pp. 609–611, 1997.
- [26] Y. Fu and L. L. Ji, "Chronic ginseng consumption attenuates age-associated oxidative stress in rats," *Journal of Nutrition*, vol. 133, no. 11, pp. 3603–3609, 2003.
- [27] H. Zhao, Q. Zhang, L. Zhao, X. Huang, J. Wang, and X. Kang, "Spore powder of *Ganoderma lucidum* improves cancer-related fatigue in breast cancer patients undergoing endocrine therapy: a pilot clinical trial," *Evidence-based Complementary and Alternative Medicine*, vol. 2012, Article ID 809614, 8 pages, 2012.
- [28] D. L. Barton, H. Liu, S. R. Dakhil et al., "Wisconsin Ginseng (*Panax quinquefolius*) to improve cancer-related fatigue: a randomized, double-blind trial, N07C2," *JNCI Journal of the National Cancer Institute*, vol. 105, no. 16, pp. 1230–1238, 2013.
- [29] M. Z. Ouyang, L. Z. Lin, W. J. Lv et al., "Effects of the polysaccharides extracted from *Ganoderma lucidum* on chemotherapy-related fatigue in mice," *International Journal of Biological Macromolecules*, vol. 91, pp. 905–910, 2016.
- [30] D. Li, J. W. Ren, T. Zhang et al., "Anti-fatigue effects of small-molecule oligopeptides isolated from *Panax quinquefolium* L. in mice," *Food & Function*, vol. 9, no. 8, pp. 4266–4273, 2018.
- [31] J. N. Hu, J. Y. Yang, S. Jiang et al., "Panax quinquefolium saponins protect against cisplatin evoked intestinal injury via ROS-mediated multiple mechanisms," *Phytomedicine*, vol. 82, Article ID 153446, 2021.
- [32] A. Abulizi, L. Hu, A. Ma et al., "Ganoderic acid alleviates chemotherapy-induced fatigue in mice bearing colon tumor," *Acta Pharmacologica Sinica*, vol. 42, no. 10, pp. 1703–1713, 2021.
- [33] Y. Ye, J. Li, X. Cao, Y. Chen, C. Ye, and K. Chen, "Protective effect of n-butyl alcohol extracts from *Rhizoma Pinelliae* Pedatisectae against cerebral ischemia-reperfusion injury in rats," *Journal of Ethnopharmacology*, vol. 188, pp. 259–265, 2016.
- [34] M. Hu, Y. Liu, L. He, X. Yuan, W. Peng, and C. Wu, "Anti-epileptic effects of protein-rich extract from *Bombyx batryticatus* on mice and its protective effects against H₂O₂-induced oxidative damage in PC12 cells via regulating PI3K/akt signaling pathways," *Oxidative Medicine and Cellular Longevity*, vol. 2019, Article ID 7897584, 13 pages, 2019.
- [35] Y. Chen, X. Zhu, K. Wang, W. Zou, and F. Zhou, "Tubemioside II inhibits TGF- β 1-induced metastatic progression of human retinoblastoma cells through suppressing redox-oxosome-dependent EGFR activation," *Chemico-Biological Interactions*, vol. 335, Article ID 109367, 2021.
- [36] Y. L. Wei, S. M. Wang, Q. O. Liu, and Y. Luo, "Study on the mechanism of Yiqi chutan recipe in the treatment of lung cancer with splenasthenic syndrome," *Zhong Yao Cai*, vol. 39, no. 9, pp. 2097–2101, 2016.
- [37] Z. Daihan, L. Lizhu, T. Huaqin et al., "Effect on the survival of elderly patients with non—small cell lung cancer treated by the traditional Chinese medicine treatment based on Yiqi Huatan method: a multicenter, clinically prospective cohort study," *World Chinese Medicine*, vol. 9, pp. 833–838, 2014.
- [38] L. Wenjiao, O. Mingzi, L. Lizhu, and Z. Jingxu, "Effects of Yiqi chutan decoction on chemotherapy-related fatigue of patients with non-small cell lung cancer," *Guiding Journal of Traditional Chinese Medicine and Pharmacy*, vol. 21, no. 10, pp. 31–34, 2015.
- [39] G. Jieshan, O. Mingzi, X. Zhiwei, L. Lizhu, and Z. Kexue, "Effects of Yiqi chutan decoction on chemotherapy-related fatigue," *Liaoning Journal of Traditional Chinese Medicine*, vol. 496, no. 6, pp. 1211–1213, 2016.
- [40] A. H. El-Far, M. A. Lebda, A. E. Noreldin et al., "Quercetin attenuates pancreatic and renal D-galactose-induced aging-related oxidative alterations in rats," *International Journal of Molecular Sciences*, vol. 21, no. 12, 2020.
- [41] A. E. Noreldin, M. S. Gewaily, I. M. Saadeldin, M. M. Abomughaid, A. F. Khafaga, and Y. H. Elewa, "Osteoblast-activating peptide exhibits a specific distribution pattern in mouse ovary and may regulate ovarian steroids and local calcium levels," *American Journal of Tourism Research*, vol. 13, no. 6, pp. 5796–5814, 2021.
- [42] L. M. Buffart, I. C. De Backer, G. Schep, A. Vreugdenhil, J. Brug, and M. J. Chinapaw, "Fatigue mediates the relationship between physical fitness and quality of life in cancer

- survivors," *Journal of Science and Medicine in Sport*, vol. 16, no. 2, pp. 99–104, 2013.
- [43] S. Wang, X. Yang, W. Wang et al., "Interpretation of the absorbed constituents and pharmacological effect of Spica Schizonepetae extract on non-small cell lung cancer," *PLoS One*, vol. 16, no. 3, Article ID e0248700, 2021.
- [44] W. C. Huang, Y. J. Hsu, L. Wei, Y. J. Chen, and C. C. Huang, "Association of physical performance and biochemical profile of mice with intrinsic endurance swimming," *International Journal of Medical Sciences*, vol. 13, no. 12, pp. 892–901, 2016.
- [45] M. M. van Gaalen and T. Steckler, "Behavioural analysis of four mouse strains in an anxiety test battery," *Behavioural Brain Research*, vol. 115, no. 1, pp. 95–106, 2000.
- [46] J. Podhorna and R. E. Brown, "Strain differences in activity and emotionality do not account for differences in learning and memory performance between C57BL/6 and DBA/2 mice," *Genes, Brain and Behavior*, vol. 1, no. 2, pp. 96–110, 2002.
- [47] V. Kazlauckas, J. Schuh, O. P. Dall'Igna, G. S. Pereira, C. D. Bonan, and D. R. Lara, "Behavioral and cognitive profile of mice with high and low exploratory phenotypes," *Behavioural Brain Research*, vol. 162, no. 2, pp. 272–278, 2005.
- [48] S. Spazzapan, A. Bearz, and U. Tirelli, "Fatigue in cancer patients receiving chemotherapy: an analysis of published studies," *Annals of Oncology*, vol. 15, no. 10, p. 1576, 2004.
- [49] P. Nieboer, C. Buijs, S. Rodenhuis et al., "Fatigue and relating factors in high-risk breast cancer patients treated with adjuvant standard or high-dose chemotherapy: a longitudinal study," *Journal of Clinical Oncology*, vol. 23, no. 33, pp. 8296–8304, 2005.
- [50] Z. Daihan, L. Lizhu, Z. Yiqiang et al., "The role of TCM method for invigorating qi and removing the phlegm in prolonging median survival time in the patient with non-small cell lung cancer," *Journal of Traditional Chinese Medicine*, vol. 46, no. 8, pp. 8296–8304, 2005.
- [51] S. K. Powers and M. J. Jackson, "Exercise-induced oxidative stress: cellular mechanisms and impact on muscle force production," *Physiological Reviews*, vol. 88, no. 4, pp. 1243–1276, 2008.
- [52] G. S. Supinski and L. A. Callahan, "Free radical-mediated skeletal muscle dysfunction in inflammatory conditions," *Journal of Applied Physiology*, vol. 102, no. 5, pp. 2056–2063, 1985.
- [53] Y. Chen, P. Jungsuwadee, M. Vore, D. A. Butterfield, and D. K. St Clair, "Collateral damage in cancer chemotherapy: oxidative stress in nontargeted tissues," *Molecular Interventions*, vol. 7, no. 3, pp. 147–156, 2007.
- [54] L. Muinelto-Romay, L. Alonso-Alconada, M. Alonso-Nocelo, J. Barbazan, and M. Abal, "Tumor invasion and oxidative stress: biomarkers and therapeutic strategies," *Current Molecular Medicine*, vol. 12, no. 6, pp. 746–762, 2012.
- [55] S. H. Akbas, M. Timur, and T. Ozben, "The effect of Quercetin on topotecan cytotoxicity in MCF-7 and MDA-MB 231 human breast cancer Cells1," *Journal of Surgical Research*, vol. 125, no. 1, pp. 49–55, 2005.
- [56] H. E. Mohamed, M. E. Asker, S. I. Ali, and T. M. Abd El Fattah, "Protection against doxorubicin cardiomyopathy in rats: role of phosphodiesterase inhibitors type 4," *Journal of Pharmacy and Pharmacology*, vol. 56, no. 6, pp. 757–768, 2010.
- [57] P. Srivastava, M. Sahu, S. Khanna, and H. D. Khanna, "Evaluation of oxidative stress status following polyherbal formulation therapy in patients of cholelithiasis with cholecholelithiasis," *Ancient Science of Life*, vol. 24, no. 3, pp. 143–151, 2005.
- [58] Y. Cigremis, H. Turel, K. Adiguzel et al., "The effects of acute acetaminophen toxicity on hepatic mRNA expression of SOD, CAT, GSH-Px, and levels of peroxynitrite, nitric oxide, reduced glutathione, and malondialdehyde in rabbit," *Molecular and Cellular Biochemistry*, vol. 323, pp. 31–38, 2009.
- [59] M. J. Bak, W. S. Jeong, and K. B. Kim, "Detoxifying effect of fermented black ginseng on H₂O₂-induced oxidative stress in HepG2 cells," *International Journal of Molecular Medicine*, vol. 34, no. 6, pp. 1516–1522, 2014.
- [60] L. Poillet-Perez, G. Despouy, R. Delage-Mourroux, and M. Boyer-Guittaut, "Interplay between ROS and autophagy in cancer cells, from tumor initiation to cancer therapy," *Redox Biology*, vol. 4, pp. 184–192, 2015.
- [61] Y. J. Jiang, S. J. Sun, W. X. Cao et al., "Excessive ROS production and enhanced autophagy contribute to myocardial injury induced by branched-chain amino acids: roles for the AMPK-ULK1 signaling pathway and alpha 7nAChR," *Biochimica et Biophysica Acta, Molecular Basis of Disease*, vol. 1867, no. 1, Article ID 165980, 2021.
- [62] J. An, L. Zhou, H. Pang, X. Luo, P. Sun, and J. Song, "Role of AMP-activated protein kinase signal path in cell autophagy activation at early brain injury in rats after subarachnoid hemorrhage," *Chinese Journal of Neuromedicine*, vol. 14, no. 11, pp. 1095–1099, 2015.
- [63] G. Liu, S. Mao, M. He, T. Ma, and L. Tang, "Experiment research of curcumin induced autophagy in human medulloblastoma Daoy cell," *Journal of Chongqing Medical University*, vol. 39, no. 3, pp. 332–336, 2014.
- [64] C. Reidick, F. El Magraoui, H. E. Meyer, H. Stenmark, and H. W. Platta, "Regulation of the tumor-suppressor function of the Class III phosphatidylinositol 3-kinase complex by ubiquitin and SUMO," *Cancers*, vol. 7, no. 1, pp. 1–29, 2014.
- [65] X. Yu, Y. C. Long, and H. M. Shen, "Differential regulatory functions of three classes of phosphatidylinositol and phosphoinositide 3-kinases in autophagy," *Autophagy*, vol. 11, no. 10, pp. 1711–1728, 2015.
- [66] F. Boutouja, R. Brinkmeier, T. Mastalski, F. El Magraoui, and H. W. Platta, "Regulation of the tumor-suppressor BECLIN 1 by distinct ubiquitination cascades," *International Journal of Molecular Sciences*, vol. 18, no. 12, p. 2541, 2017.
- [67] H. Cawthon, R. Chakraborty, J. R. Roberts, and S. K. Backues, "Control of autophagosomal size and number by Atg7," *Biochemical and Biophysical Research Communications*, vol. 503, no. 2, pp. 651–656, 2018.
- [68] Y. Zhou, Z. Wang, Y. Huang et al., "Membrane dynamics of ATG4B and LC3 in autophagosome formation," *Journal of Molecular Cell Biology*, vol. 13, no. 12, pp. 853–863, 2022.
- [69] E. Shvets, A. Abada, H. Weidberg, and Z. Elazar, "Dissecting the involvement of LC3B and GATE-16 in p62 recruitment into autophagosomes," *Autophagy*, vol. 7, no. 7, pp. 683–688, 2011.
- [70] Y. Wei, J. Ren, Z. Luan, and Y. Wang, "Effects of various autophagy modulators on the expression of autophagic markers LC3II and p62," *Journal of China Pharmaceutical University*, vol. 49, no. 3, pp. 341–347, 2018.
- [71] C. De Palma, F. Morisi, S. Cheli et al., "Autophagy as a new therapeutic target in Duchenne muscular dystrophy," *Cell Death & Disease*, vol. 3, no. 11, 2012.
- [72] A. J. Kowaltowski and A. E. Vercesi, "Mitochondrial damage induced by conditions of oxidative stress," *Free Radical Biology and Medicine*, vol. 26, pp. 463–471, 1999.
- [73] S. B. Bratton and G. S. Salvesen, "Regulation of the apaf-1-caspase-9 apoptosome," *Journal of Cell Science*, vol. 123, no. 19, pp. 3209–3214, 2010.

- [74] Y. Maejima, M. Isobe, and J. Sadoshima, "Regulation of autophagy by Beclin 1 in the heart," *Journal of Molecular and Cellular Cardiology*, vol. 95, pp. 19–25, 2016.
- [75] W. Yu, J. Liao, F. Yang et al., "Chronic tribasic copper chloride exposure induces rat liver damage by disrupting the mitophagy and apoptosis pathways," *Ecotoxicology and Environmental Safety*, vol. 212, Article ID 111968, 2021.
- [76] O. R. Metawea, M. A. Abdelmoneem, N. S. Haiba et al., "A novel "smart" PNIPAM-based copolymer for breast cancer targeted therapy: synthesis, and characterization of dual pH/temperature-responsive lactoferrin-targeted PNIPAM-co-AA," *Colloids and Surfaces B: Biointerfaces*, vol. 202, Article ID 111694, 2021.
- [77] A. H. El-Far, K. Godugu, A. E. Noreldin et al., "Thymoquinone and costunolide induce apoptosis of both proliferative and doxorubicin-induced-senescent colon and breast cancer cells," *Integrative Cancer Therapies*, vol. 20, Article ID 153473542110354, 2021.
- [78] J. Estaquier, F. Vallette, J. L. Vayssiere, and B. Mignotte, "The mitochondrial pathways of apoptosis," *Advances in Experimental Medicine and Biology*, vol. 942, pp. 157–183, 2012.
- [79] X. Chen and M. Fang, "Oxidative stress mediated mitochondrial damage plays roles in pathogenesis of diabetic nephropathy rat," *European Review for Medical and Pharmacological Sciences*, vol. 22, no. 16, pp. 5248–5254, 2018.
- [80] W. Wang, X. Dong, Y. Liu et al., "Itraconazole exerts anti-liver cancer potential through the Wnt, PI3K/AKT/mTOR, and ROS pathways," *Biomedicine & Pharmacotherapy*, vol. 131, Article ID 110661, 2020.
- [81] Y. Wu, D. Pi, Y. Chen, Q. Zuo, S. Zhou, and M. Ouyang, "Ginsenoside Rh4 inhibits colorectal cancer cell proliferation by inducing ferroptosis via autophagy activation," *Evidence-based Complementary and Alternative Medicine*, vol. 2022, Article ID 6177553, 19 pages, 2022.
- [82] L. Gibellini, M. Pinti, M. Nasi et al., "Interfering with ROS metabolism in cancer cells: the potential role of Quercetin," *Cancers*, vol. 2, no. 2, pp. 1288–1311, 2010.
- [83] Y. Yang, L. Liu, and Y. Shang, "The role of ROS on the apoptosis of HL-60 cells induced by oleanolic acid," *Chinese Journal of Gerontology*, vol. 31, no. 11, pp. 1997–1999, 2011.
- [84] C. Sun, E. Guo, B. Zhou et al., "A reactive oxygen species scoring system predicts cisplatin sensitivity and prognosis in ovarian cancer patients," *BMC Cancer*, vol. 19, no. 1, p. 1061, 2019.
- [85] Q. Wu, J. Deng, D. Fan et al., "Ginsenoside Rh4 induces apoptosis and autophagic cell death through activation of the ROS/JNK/p53 pathway in colorectal cancer cells," *Biochemical Pharmacology*, vol. 148, pp. 64–74, 2018.
- [86] A. Martoriati, G. Doumont, M. Alcalay, E. Bellefroid, P. G. Pelicci, and J. C. Marine, "dapk1, encoding an activator of a p19ARF-p53-mediated apoptotic checkpoint, is a transcription target of p53," *Oncogene*, vol. 24, no. 8, pp. 1461–1466, 2005.
- [87] Z. Wang, X. Wang, F. Cheng et al., "Rapamycin inhibits glioma cells growth and promotes autophagy by miR-26a-5p/DAPK1 Axis," *Cancer Management and Research*, vol. 13, pp. 2691–2700, 2021.
- [88] B. Kalyanaraman, G. Cheng, M. Hardy, O. Ouari, B. Bennett, and J. Zielonka, "Teaching the basics of reactive oxygen species and their relevance to cancer biology: mitochondrial reactive oxygen species detection, redox signaling, and targeted therapies," *Redox Biology*, vol. 15, pp. 347–362, 2018.
- [89] V. Aggarwal, H. S. Tuli, A. Varol et al., "Role of reactive oxygen species in cancer progression: molecular mechanisms and recent advancements," *Biomolecules*, vol. 9, no. 11, 2019.
- [90] S. Mirzaei, K. Hushmandi, A. Zabolian et al., "Elucidating role of reactive oxygen species (ROS) in cisplatin chemotherapy: a focus on molecular pathways and possible therapeutic strategies," *Molecules*, vol. 26, no. 8, p. 2382, 2021.
- [91] L. A. Gilliam, K. H. Fisher-Wellman, C. T. Lin, J. M. Maples, B. L. Cathey, and P. D. Neuffer, "The anticancer agent doxorubicin disrupts mitochondrial energy metabolism and redox balance in skeletal muscle," *Free Radical Biology and Medicine*, vol. 65, pp. 988–996, 2013.
- [92] D. H. Kang, "Oxidative stress, DNA damage, and breast cancer," *AACN Clinical Issues: Advanced Practice in Acute and Critical Care*, vol. 13, no. 4, pp. 540–549, 2002.
- [93] C. S. Opuwari and R. R. Henkel, "An update on oxidative damage to spermatozoa and oocytes," *BioMed Research International*, vol. 2016, Article ID 9540142, 11 pages, 2016.

Research Article

Grain-Sized Moxibustion Heightens the AntiTumor Effect of Cyclophosphamide in Hepa1-6 Bearing Mice

Tao Zhu ¹, Yanzhu Ma ¹, Jianyun Wang ¹, Xiaolin Chen ², Jianhao Li ²,
Liqiang Meng ¹, Yuduo Hou ¹ and Yanting Cheng ¹

¹Shanxi University of Chinese Medicine, Jinzhong 030600, China

²Department of Infectious Diseases, First Affiliated Hospital of Zhengzhou University, Zhengzhou 450052, China

Correspondence should be addressed to Yanting Cheng; chengyanting@sxtcm.edu.cn

Received 23 May 2022; Revised 25 June 2022; Accepted 4 July 2022; Published 8 August 2022

Academic Editor: Mohammed El-Magd

Copyright © 2022 Tao Zhu et al. This is an open access article distributed under the Creative Commons Attribution License, which permits unrestricted use, distribution, and reproduction in any medium, provided the original work is properly cited.

Objective. The side effects of chemotherapy as a treatment of liver cancer cannot be ignored. Grain-sized moxibustion, a characteristic external therapy, has been shown to reduce the toxic and side effects of chemotherapy and regulate the immune function. The purpose of this study was to explore the synergistic antitumor activity of grain-sized moxibustion combined with cyclophosphamide (CTX). **Methods.** A hepatoma 1-6 (Hepa1-6)-bearing mouse model was established by injecting mice with Hepa1-6 cancer cells. CTX and grain-sized moxibustion on Dazhui (DU14), Zusanli (ST36), and Sanyinjiao (SP6) were used for treatment, and mouse survival status, body weight, and tumor growth, weight, and volume were measured. White blood cells (WBCs) and bone marrow nucleated cells (BMNCs) were quantified. The spleens and livers of Hepa1-6-bearing mice were pathologically examined and scored. Serum aspartate aminotransferase (AST) and alanine aminotransferase (ALT) levels were measured with enzyme-linked immunosorbent assay (ELISA) kits, and protein and mRNA expression levels of Ki67 and proliferating cell nuclear antigen (PCNA) in tumor tissues were measured with immunohistochemistry and real-time quantitative polymerase chain reaction (RT-qPCR) techniques. **Results.** Both grain-sized moxibustion and CTX could restrain the growth of Hepa1-6 tumors, reducing both tumor volume and weight; the combined treatment had a greater effect. Grain-sized moxibustion down-regulated the expression of proliferation genes Ki67 and PCNA, weakened the proliferation ability of Hepa1-6 tumor cells, inhibited tumor growth, and enhanced the antitumor effect of CTX. In addition, grain-sized moxibustion significantly improved the signs of CTX-induced toxicity (including weight loss, leukopenia, bone marrow suppression, and hepatotoxicity), down-regulated serum AST and ALT levels, reduced spleen and liver inflammation, and improved liver and spleen indices. **Conclusion.** Grain-sized moxibustion can synergize with CTX to enhance the antitumor effect of CTX and alleviate its toxic and side effects. It may be a promising adjuvant therapy to chemotherapy.

1. Introduction

Hepatocellular carcinoma is one of the most common malignant tumors worldwide, with rapid progression and high mortality [1, 2]. In the clinic, chemotherapy is still an important treatment for inoperable liver cancer or post-operative recurrence of liver cancer [3, 4]. Cyclophosphamide (CTX), as an alkylating agent that selectively targets tumor cells, is significant in the treatment of malignant tumors through releasing nitrogen from phosphoramidase to inhibit liver cancer [5].

Although CTX inhibits tumor cells, it also causes certain damage to normal cells. One example of this damage is the inhibition of myeloid cell differentiation, resulting in decreased blood cells, damage to immune cells, and a decrease in body immune resistance [6–8]. Therefore, chemotherapy is of vital importance to treat malignant tumors, but its side effects are still a medical problem. It is necessary to find new chemotherapy adjuvant therapies or drugs that reduce toxicity and enhance antitumor activity to achieve better efficacy.

Grain-sized moxibustion, a characteristic external therapy, can directly stimulate specific acupoints to treat

diseases through the photothermal stimulation of specific acupoints in a short period of time. It plays the roles of dredging the meridians, regulating qi and blood, strengthening the body, and eliminating the pathogens [9, 10]. In terms of adjuvant chemotherapy in the treatment of malignant tumors, reports on moxibustion can be traced back to the 1970s. For example, many clinical studies have shown that moxibustion can treat leukopenia [11]. Subsequently, we carried out the screening of moxibustion and acupoint prescriptions and conducted relevant basic experimental research [12]. Based on the above, this study aimed to determine whether grain-sized moxibustion can reduce the toxic and side effects of CTX and explored whether it can synergistically inhibit the liver cancer.

Thus, this study investigated the effect of grain-sized moxibustion alone or in combination with CTX on the hepatoma 1-6 (Hepa1-6)-bearing mouse model to evaluate the antitumor activity of grain-sized moxibustion *in vivo* in an effort to identify potential clinical treatment options.

2. Materials and Methods

2.1. Animals. Forty healthy and clean C57BL/6J male mice (4–6 weeks old, body weight 16–18 g, $n = 40$) were purchased from Beijing Vital River Laboratory Animal Technology Co., Ltd. (Beijing, China) (Animal laboratory license number: SCXK Beijing 2016–0006).

All the mice were raised in the Key Laboratory of the First Affiliated Hospital of Zhengzhou University, with a light-dark cycle of 12/12 hours, an ambient temperature of 22–25°C, a humidity of $45 \pm 10\%$, and free feeding and drinking. In addition, all operations on mice were authorized according to ethical regulations and the Animal Care Ethics Committee of Shanxi University of Chinese Medicine (License number: 2019DW233).

2.2. Cell Culture. Hepa1-6 cells were obtained from the Cell Bank of the Chinese Academy of Sciences (Shanghai, China) and cultured in Dulbecco's modified Eagle medium (DMEM; Gibco, USA) containing 10% fetal bovine serum (FBS; Gibco, USA) and 1% penicillin/streptomycin (Gibco, USA) at 37 °C in a 5% CO₂ humid environment.

After the frozen Hepa1-6 cells were removed from liquid nitrogen, they were continuously shaken in a 37°C water bath to promote their thawing. They were next moved into a 15 mL centrifuge tube and 10 mL preheated complete DMEM medium was added. The cells were gently blown into a suspension and centrifuged at 2000 rpm for 2 minutes and the supernatant was discarded. Ten milliliters DMEM were added to wash the pellet and the supernatant was discarded. Ten milliliters complete DMEM were added to the cells, which were gently blown into a suspension and cultured in a 5% CO₂ cell incubator. When the cell density of Hepa1-6 cells reached 80–90%, the medium was removed and the cells were washed twice with 10 mL phosphate-buffered saline (PBS). Three milliliters trypsin containing 0.25% ethylenediaminetetraacetic acid (EDTA) was added to the cell culture flask for 3 minutes. One milliliter complete

DMEM was added to stop trypsin digestion and the cells were transferred to a 15 mL centrifuge tube. Ten milliliters complete DMEM were added to a clean cell culture plate. The cells transferred to the 15 mL centrifuge tube were centrifuged at 2000 rpm for 2 minutes and the supernatant was discarded. Ten milliliters PBS were added to create the cell suspension and 10 μ l of the suspension was removed for counting cells using the cell counting plate. The cells were plated according to 3×10^6 cells/mL inoculation.

2.3. Model Establishment and Treatment. After a week of adaptation, all mice were randomly divided into four groups ($n = 10$ each), which included the control group (C), grain-sized moxibustion group (G), CTX group (T), and grain-sized moxibustion plus CTX group (GT). The density of the Hepa1-6 tumor cells was adjusted to 3×10^6 cells/mL [13], and 0.2 mL was extracted and inoculated subcutaneously into right armpit of C57BL/6 mice to establish the Hepa1-6-bearing mouse model [14]. As seen in Figure 1(a), five days after injection tumors were palpable (approximately 50 mm³ in size). Hepa1-6-bearing mice in the T and the GT groups were administered CTX (Baxter Oncology GmbH, Germany, Approval number: 9L353 A) at 30 mg/kg by intraperitoneal injection on the 6th, 7th, and 8th day [15], whereas mice in the C group were administered an equivalent volume (0.2 mL) 0.9% sodium chloride by intraperitoneal injection [16]. From day 6 to day 15, mice in the G and GT groups were treated with grain-sized moxibustion upon three chosen acupoints (Figure 1(a)): Dazhui (DU14, unilateral), Zusanli (ST36, bilateral), and Sanyinjiao (SP6, bilateral). Five moxa cones were placed at each acupoint once a day (the G and the GT groups were treated with grain-sized moxibustion at the same time every day). The size and operation methods of the grain-sized moxibustion were as follows [17–19]: after the mice were immobilized, the moxibustion acupoints were depilated. The moxa velvet (Nanyang Kangaiduo Wormwood Products Co., Ltd. Nanyang, Henan, China) was made into a moxa cone the size of a grain of wheat (about 0.5 g/grain), which was placed to burn on the acupoint where the petroleum jelly (Vaseline, Unilever, London, United Kingdom) was applied. When the moxa cone burned to 3/4, the remaining moxa cone was quickly removed with tweezers. The next one was then lit.

On day 16, mice in each group were weighed and anesthetized with ether, and blood samples were drawn from the medial canthus of each mouse. After mice were sacrificed with cervical dislocation, the tumor, spleen, and liver tissues were collected under sterile conditions. The residual blood was then removed with filter paper and accurately weighed. The visceral index, tumor volume, and tumor inhibition rate were calculated. The formulas were as follows: visceral index = organ weight/body weight, tumor volume (mm³) = (length \times width²)/2 [20], and tumor inhibition rate (%) = (average tumor mass in the control group – average tumor mass in the treatment group)/average tumor mass of the control group \times 100% [21].

The body weights of mice in each group were measured at 9:00 a.m. on days 3, 6, 9, 12, and 15 of the experiment. The

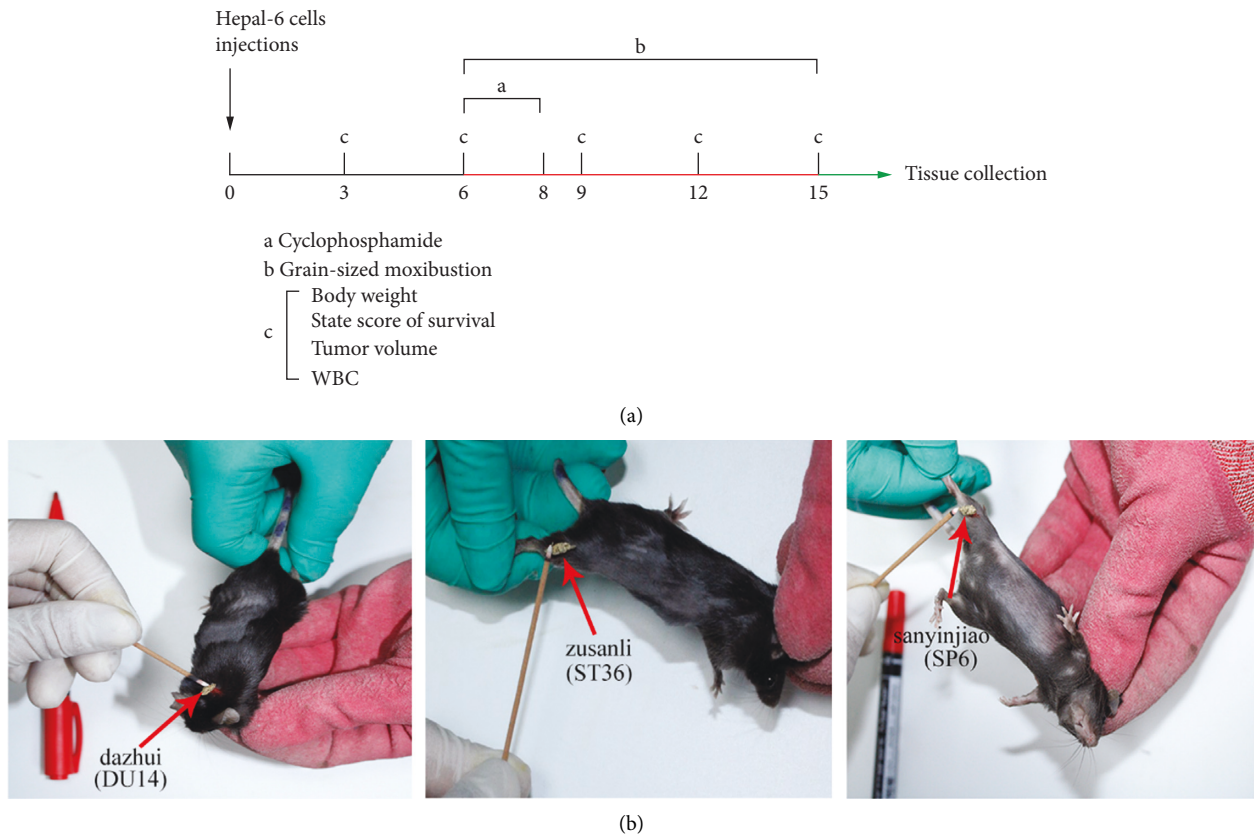


FIGURE 1: Schematic diagram of the experimental procedure and mouse acupoints. (a) Flowchart of experimental interventions. a. Cyclophosphamide (CTX), (b) Grain-sized moxibustion, c. Body weight, state score of survival, tumor volume, white blood cell (WBC). The Hepal-6-bearing mice in the T and GT groups were treated with CTX on days 6, 7, and 8. The tumor-bearing mice in the G and the GT groups were treated with moxibustion on days 6–15 (once a day). The tumor volume, state of survival, and WBCs were measured on days 3, 6, 9, 12, and 15, and mice were sacrificed on day 16 for tissue collection. b. The location of acupoints (Dazhui DU14, Zusanli ST36, and Sanyinjiao SP6, red arrow) in Hepal-6-bearing mice. c. Control group; g. grain-sized moxibustion group; T: CTX group, GT: grain-sized moxibustion plus CTX group.

survival status of each mouse was observed and scored. Survival status scores are shown in Table S1 [22].

2.4. Biochemical and Hematological Analysis. On the 3rd, 6th, 9th, 12th, and 15th days of the experiment, the tail vein blood of each tumor-bearing mouse was drawn to observe the changes in the number of white blood cells (WBCs). After treatment, blood was collected from the intraocular canthus of the Hepal-6-bearing mice and put into an EDTA anticoagulation tube. Serum alanine aminotransferase (ALT) and aspartate aminotransferase (AST) levels of Hepal-6-bearing mice in each group were determined by enzyme-linked immunosorbent assay (ELISA) kits (AST 13320-1-AP, ALT 16757-1-AP; Proteintech, USA). In addition, the right femurs of Hepal-6-bearing mice in each group were taken, and the bone marrow cavity of each femur was repeatedly washed with PBS buffer until it turned white. The bone marrow cell suspension was resuspended, and the number of bone marrow nucleated cells (BMNCs) was counted using a light microscope (CX33; Olympus, Tokyo, Japan) after lysis of the red blood cells.

2.5. Histological Analysis. Formalin-fixed spleen and liver tissues were dehydrated in graded ethanol solutions, transparent in xylene, immersed in paraffin, and then embedded in conventional paraffin to make wax blocks. The tissue wax blocks were cut into tissue slices 3–5 μm thick and then adhered to the tissue sections. They were dewaxed in xylene, rehydrated in gradient alcohol, immersed in hematoxylin (H) for 3 minutes, differentiated, returned to blue, and washed with pure water. Eosin (E) was added dropwise for 20 s; the tissue was washed with pure water, dehydrated with graded ethanol solutions, cleared in xylene for 10 minutes, and sealed with neutral gum. Pathological changes were observed using a light microscope (CX33; Olympus, Tokyo, Japan). The pathology scores are as shown in Tables S2 and S3 [23, 24].

2.6. Immunohistochemistry to Detect Ki67 and PCNA Protein Expression. The tumor tissues were fixed with 4% paraformaldehyde and then made into paraffin blocks. Subsequently, the tissue wax block was cut into tissue sections with a thickness of about 5 μm , dewaxed, and rehydrated with pure water for washing. Sodium citrate (pH 6.0) was used for

microwave antigen retrieval at 98°C. The sections were then cooled down to room temperature, incubated in 3% hydrogen peroxide solution for 10 minutes, and blocked with 3% bovine serum albumin (BSA) for 50 minutes. The tumor tissue sections were individually incubated with 50 μ L primary antibodies (1:500 anti-Ki67 antibodies, 1:1,000 anti-PCNA antibodies; Wuhan Servicebio Biotechnology Co., Ltd. Wuhan, China) overnight at 4°C. The next day the tumor tissue sections were incubated with 50 μ L HRP-labeled secondary antibody (goat anti-rabbit IgG, 1:200; Wuhan Servicebio Biotechnology Co., Ltd. Wuhan, China) for 50 minutes at room temperature, washed with PBS three times for 10 min each, and subsequently incubated with diaminobenzidine for color development. After the nuclei were stained with hematoxylin, the sections were dehydrated, cleared, and mounted with neutral gum. Immunohistochemistry of the tumor tissues was observed using a light microscope (CX33; Olympus, Tokyo, Japan). Images were captured using a microscope, and PCNA and Ki67 expression were evaluated by counting the number of positive cells from three randomly selected fields in the residual viable tumor tissue among the necrotic areas using a light microscope at magnifications of 200 \times and 400 \times . Digital images were then analyzed with Image J to evaluate the percentage of positive area for all antibodies used in the immunohistochemistry analyses [25, 26].

2.7. Real-Time Quantitative Polymerase Chain Reaction (RT-qPCR) to Detect Ki67 and PCNA mRNA Expression. After the tumor tissues were fully crushed, the total RNA of tumor tissue was extracted with a Trizol kit (Wuhan Servicebio Biotechnology Co., Ltd. Wuhan, China), and its concentration and purity were detected with a UV-Vis spectrophotometer (ES-2, Malcom, Tokyo, Japan). The reverse transcription kit synthesized cDNA from the RNA. Primer design and synthesis were completed by Shanghai Bioengineering Co., Ltd. Total mRNA was used as a template for reverse transcription into cDNA for real-time fluorescence quantitative PCR amplification in a 20 μ L system. The reaction system was as follows: 1 μ L qPCR primer, 1 μ L cDNA product, and 10 μ L SYBR Green qPCR Master Mix (2 \times). Amplification conditions: pre-denaturation 95°C for 10 min followed by 40 cycles of 95°C for 15 s and 60°C for 60 s. The melting curve is completed at 60°C for 95°C, and the temperature was increased by 0.3°C every 15 s. Glyceraldehyde-3-phosphate dehydrogenase was used as an endogenous reference, and the $2^{-\Delta\Delta Ct}$ method was used to analyze and calculate the relative expression of the target gene. The primer sequences are shown in Table S4.

2.8. Statistical Analysis. All data were entered into SPSS 25.0 software (IBM SPSS Inc., Chicago, IL, USA) for analytical processing and testing for homogeneity of variance and normality. All data were expressed as mean \pm SD. $P < 0.05$ was considered statistically significant. One-way analysis of variance was used for eligible groups of three or more. If the variances were unequal, Dunnett's T3 method was used. If

the data did not conform to a non-normal distribution, the nonparametric Kruskal–Wallis test was used.

3. Results

3.1. The Effect of Grain-Sized Moxibustion Combined with CTX on Tumor Growth in Hepa1-6-Bearing Mice. To observe whether grain-sized moxibustion can heighten the antitumor effect of CTX, we evaluated changes in body weight, survival status, and tumor growth curves in Hepa1-6 bearing mice treated with grain-sized moxibustion, CTX, and grain-sized moxibustion combined with CTX. As shown in Figure 2(a) and 2(b), the survival status of Hepa1-6-bearing mice in each group was higher before the intervention; the difference was not statistically significant. However, survival status of the Hepa1-6-bearing mice in the T and GT groups deteriorated significantly on the 9th day compared with that of the C group ($P < 0.01$ and $P < 0.05$, respectively). The body weight of the Hepa1-6-bearing mice in the T group was also greatly reduced ($P < 0.01$), which may be due to the toxicity of CTX. On day 12, the Hepa1-6-bearing mice in group C had a slow weight gain and poor survival status, which may be due to cachexia. Compared with the C group, the body weight of Hepa1-6-bearing mice in the G group was significantly higher ($P < 0.01$) and the survival status was improved, whereas the weight of Hepa1-6-bearing mice in the T and GT groups was significantly lower ($P < 0.001$ and $P < 0.01$, respectively). Compared with the T group, survival status of the Hepa1-6-bearing mice in the GT group was significantly higher ($P < 0.05$). On the 15th day, the weight of Hepa1-6-bearing mice in the G group was significantly higher compared with the C group ($P < 0.001$). The survival status was significantly improved ($P < 0.05$), whereas the weight of Hepa1-6-bearing mice in the T and GT groups was significantly lower ($P < 0.001$ and $P < 0.05$, respectively), especially in the T group. The survival status of the Hepa1-6-bearing mice was significantly lower compared to C group ($P < 0.001$). Compared with the T group, the weight of the Hepa1-6-bearing mice in the GT group was significantly higher ($P < 0.01$) and the survival status also significantly improved ($P < 0.001$). In addition, the difference in tumor volume of the Hepa1-6-bearing mice in each group (5 days after tumor cell transplantation) was not statistically significant. As shown in Figure 2(c), on day 12 (1 week after intervention, 2 weeks after tumor cell transplantation), compared with group C, the tumor volume of Hepa1-6 tumor-bearing mice in group T and GT decreased significantly ($P < 0.01$ and $P < 0.001$, respectively). On the 15th day, the tumor volume of the Hepa1-6-bearing mice in the G group was lower than that in the C group, but the difference was not statistically significant. The tumor volume of the Hepa1-6-bearing mice in the T group and the GT group was significantly lower than that in the C group (both $P < 0.001$). It is worth noting that Hepa1-6-bearing mice in the GT group experienced a stronger inhibitory effect on the tumor growth than did the T group, and the tumor volume was significantly lower than that in the C group ($P < 0.05$). Similar results were observed in images of tumors and tumor weights of mice on day 16 (Figures 2(d) and 2(e)). In

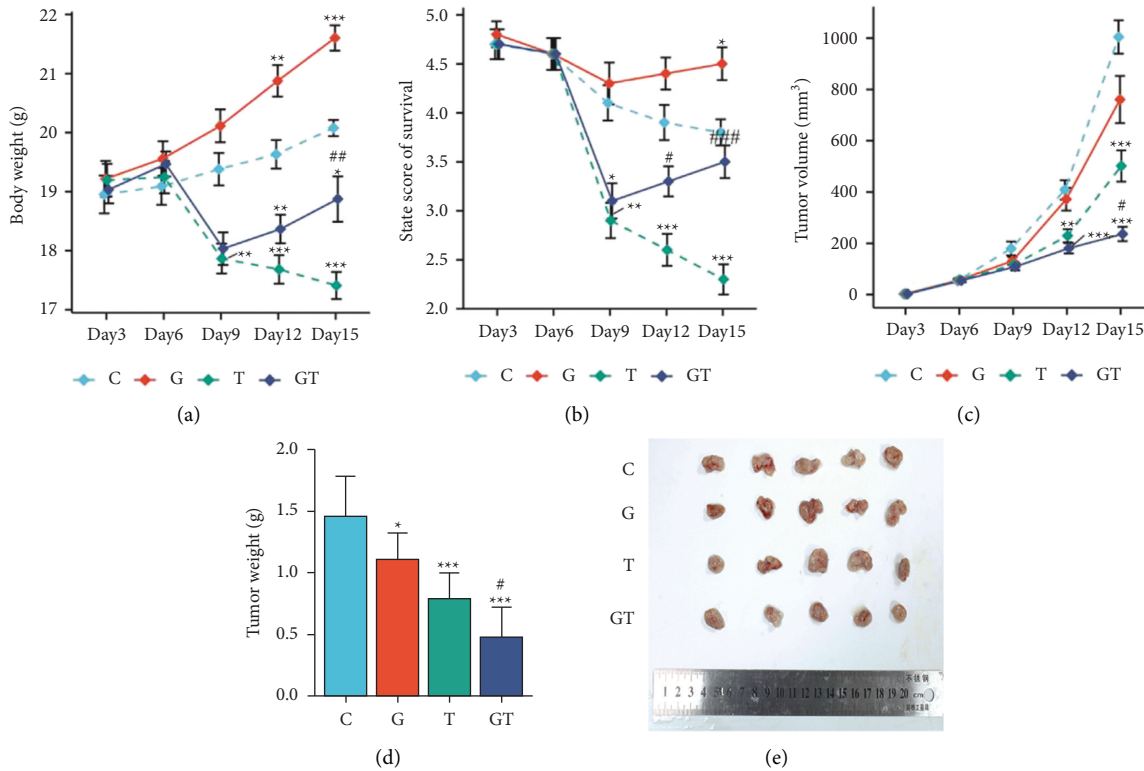


FIGURE 2: The effect of grain-sized moxibustion combined with CTX on tumor growth in Hepa1-6-bearing mice. (a) Body weight (days 6, 9, 12, and 15). (b) State score of survival (days 6, 9, 12, and 15). (c) Tumor volume (days 6, 9, 12, and 15). (d) Tumor weight. (e) Tumor photograph. All values are presented as means \pm SD ($n = 10$). Notes: * $P < 0.05$, ** $P < 0.01$, *** $P < 0.001$ vs. C group; # $P < 0.05$, ## $P < 0.01$ vs. T group. C: control group; G: grain-sized moxibustion group; T: CTX group; GT: grain-sized moxibustion plus CTX group.

addition, the tumor inhibition rate in group G was 23.9%, in group T was 45.9%, and in group GT was 67.1%, indicating that grain-sized moxibustion could heighten the antitumor effect of CTX.

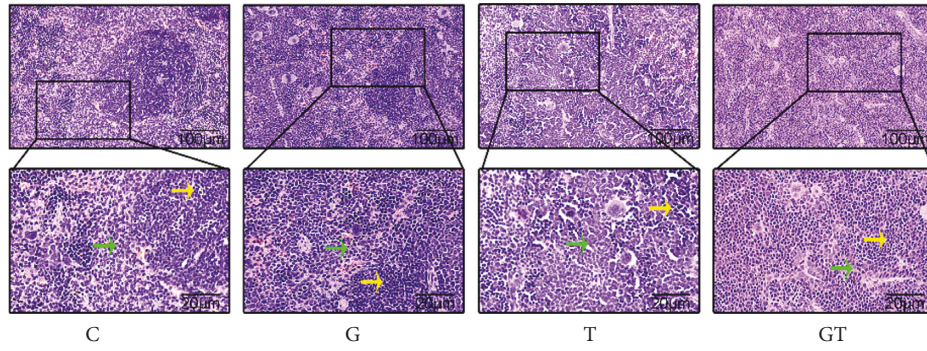
3.2. The Effect of Grain-Sized Moxibustion in Combination with CTX on Spleen and Liver Tissue of Hepa1-6-Bearing Mice.

To determine whether grain-sized moxibustion combined with CTX affects the spleen and liver weights in Hepa1-6-bearing mice, spleen and liver indices were calculated. As shown in Figure 3(c), the spleen index of the mice in the G group was higher than that of the C group, but there was no statistical significance. The spleen index of the mice in the T group and the GT group was significantly lower than that of the C group ($P < 0.001$ and $P < 0.01$, respectively). Compared with the T group, the spleen index of the GT group was significantly higher ($P < 0.05$). It is worth noting that the differences in the liver indices among the four groups were not significant, suggesting that the grain-sized moxibustion combined with CTX may have little influence on liver weight.

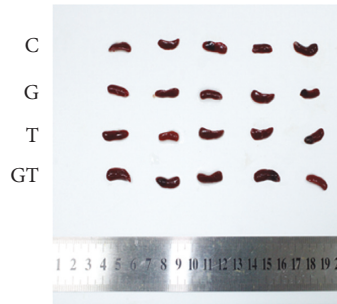
Next, to further explore whether the grain-sized moxibustion can improve the organ damage caused by CTX in Hepa1-6-bearing mice, H&E staining was performed on the spleens and livers of Hepa1-6-bearing mice in each group. Pathomorphological changes were observed (100 \times , 400 \times), and inflammation scores were recorded.

See Figure 3(a) shows a histological micrograph of the spleen. In group C, a clear boundary between the red and white pulp was observed and the cells were neat and dense. A clear boundary between the red and white pulp was also observed in the G group. The density of periarteriolar lymphoid sheath (PALS) and lymphoid nodule (LN) cells was not significantly different than that of group C. In the T group, the boundary between red and white pulp was unclear and the density of PALS and LN cells increased ($P < 0.01$ and $P < 0.05$, respectively). However, cells in the GT group were denser than those in the T group and the boundary of the red pulp and the white pulp was clearer. This indicated that grain-sized moxibustion could reduce the density of cells in the PALS and the proliferation of LN cells, suggesting that grain-sized moxibustion could reduce CTX-induced spleen damage in Hepa1-6-bearing mice.

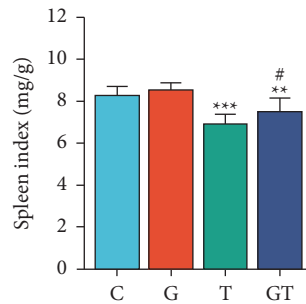
See Figure 3(f) shows microscopic pictures of liver histology. In the C group, the structures of hepatocyte nuclei were clear and the cell infiltration was low. The nuclei of hepatocytes in the G group were clearly displayed. There was no obvious abnormal change in the cell structure. In comparison to group C, hepatocytes in group T were severely degenerated and swollen, cell boundaries were blurred or even absent, inflammatory cells infiltrated around the central vein, and the cellular inflammation was distinct ($P < 0.05$). Compared with the T group, the hepatocyte structures of the GT group were different and the degree of cell necrosis and inflammation was milder, but the difference



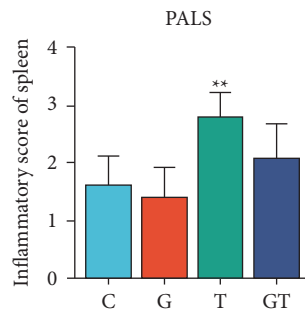
(a)



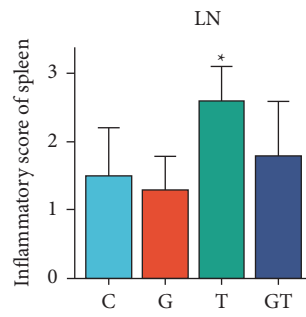
(b)



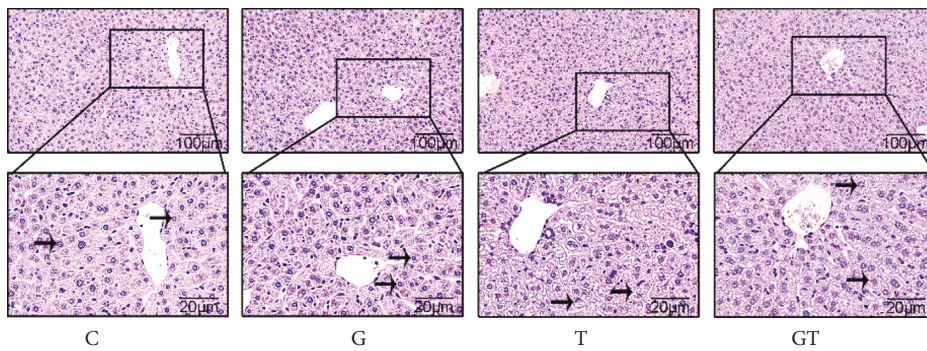
(c)



(d)



(e)



(f)

FIGURE 3: Continued.

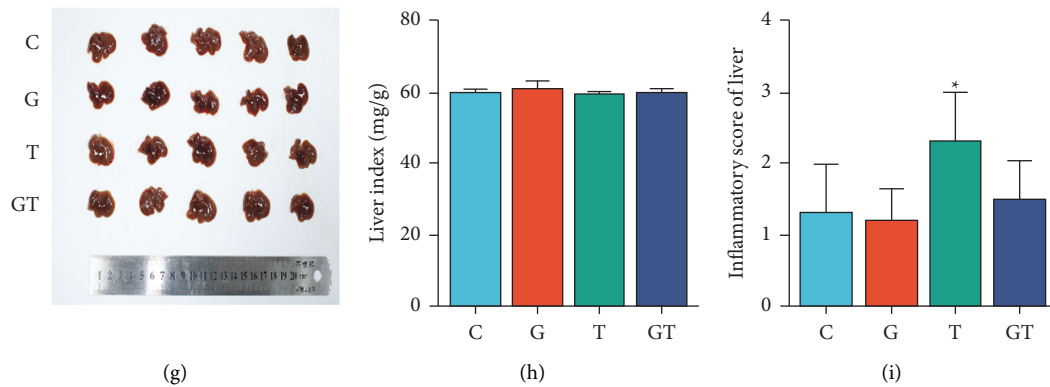


FIGURE 3: The effect of grain-sized moxibustion combined with CTX on spleen and liver tissue of Hepa1-6-bearing mice. (a) H and E staining of the spleen ($\times 100$, $\times 400$). (b) Spleen photograph. (c) Spleen index. (d) Inflammatory score of periarteriolar lymphoid sheath (PALS). (e) Inflammatory score of lymphoid nodule (LN). (f) H&E staining of the liver ($\times 100$, $\times 400$). (g) Liver photograph. (h) Liver index. (i) Inflammatory score of liver. All values are presented as means \pm SD ($n = 10$). PALS as yellow arrow), LN as green arrow, and Hepatocyte as black arrow. Notes: * $P < 0.05$, ** $P < 0.01$, *** $P < 0.001$ vs. C group; # $P < 0.05$, ## $P < 0.01$ vs. T group. C: control group; G: grain-sized moxibustion group; T: CTX group; GT: grain-sized moxibustion plus CTX group.

was not statistically significant. The results suggest that grain-sized moxibustion could alleviate the pathological changes of liver tissues caused by CTX. Changes in liver structures may be caused by the toxicity of CTX rather than moxibustion. Notably, the infiltration of inflammatory cells in the C group may be induced by Hepa1-6 cancer cells.

3.3. The Effect of Grain-Sized Moxibustion in Combination with CTX on Blood and Biochemical/Hematological (or Cellular) Indexes in Hepa1-6-Bearing Mice. Biochemical indicators are important biological indicators to characterize the experimental animals [27]. In comparison to those in group C, serum ALT and AST levels in group G were significantly lower ($P < 0.05$ and $P < 0.01$, respectively) (Figures 4(a) and 4(b)). Serum ALT and AST levels in the T group were significantly higher than those of group C (both $P < 0.001$). In the GT group, serum ALT levels were significantly higher than those of group C ($P < 0.01$), whereas serum AST levels were higher but not statistically significant. Compared with those in the T group, serum AST levels in the GT group were significantly lower ($P < 0.01$). Serum ALT levels were lower but not statistically significant. These results indicate that grain-sized moxibustion could significantly improve the liver injury caused by CTX, which was consistent with the results of liver inflammation scoring.

As shown in Figure 4(d), the numbers of WBCs in groups T and GT were significantly lower than those in group C on the 9th day (both $P < 0.001$). Compared with those in the T group, the numbers of WBCs in the GT group were significantly higher ($P < 0.01$). On the 12th day, the numbers of WBCs in groups T and GT were significantly lower than those in group C (both $P < 0.001$). In comparison to those in group T, the numbers of WBCs in group GT were significantly higher ($P < 0.05$). On day 15, the numbers of WBCs in group T were significantly lower in comparison to group C ($P < 0.001$). Compared with those in the T group, the numbers of WBCs in the GT group were significantly higher ($P < 0.05$). Notably, the number of WBCs in the T

group increased slowly after day 9, indicating that the inhibitory effect of CTX on WBCs may be short-lived. In addition, we measured the number of BMNCs in Hepa1-6-bearing mice. The results showed that the number of BMNCs in the G group was higher than that of the C group, but not statistically significant, whereas the numbers of BMNCs in the T and GT groups were significantly lower ($P < 0.01$ and $P < 0.001$, respectively). Compared with those of the T group, the number of BMNCs in GT group was significantly higher ($P < 0.05$). These findings indicate that grain-sized moxibustion could improve bone marrow suppression induced by CTX.

3.4. The Effect of Grain-Sized Moxibustion in Combination with CTX on Tumor Cell Proliferation in Hepa1-6-Bearing Mice. To assess the proliferative activity of tumor cells and observe whether the inhibitory effect of grain-sized moxibustion combined with CTX on tumor growth in mice is related to the proliferation genes Ki67 and PCNA, we performed immunohistochemical analysis of tumor proliferation activity. Compared with those in the C group, the numbers of Ki67- and PCNA-positive cells in tumor tissues of the G, T, and GT groups were lower (Figures 5(a) and 5(b)) and the Ki67 and PCNA protein expression levels were significantly lower (all $P < 0.001$). Compared with those in group T, the number of Ki67- and PCNA-positive cells in tumor tissues of group GT was lower and the Ki67 and PCNA protein expression levels were significantly lower (both $P < 0.001$).

Based on the above results, we carried out RT-qPCR analysis to further clarify the mechanism of grain-sized moxibustion combined with CTX in vivo. As shown in Figures 5(c) and 5(d), the relative mRNA expression levels of Ki67 and PCNA in group G were significantly lower after treatment with grain-sized moxibustion in comparison to those in group C ($P < 0.01$ and $P < 0.05$, respectively). The relative mRNA expression levels of Ki67 and PCNA in the T and GT groups were significantly lower than those of group

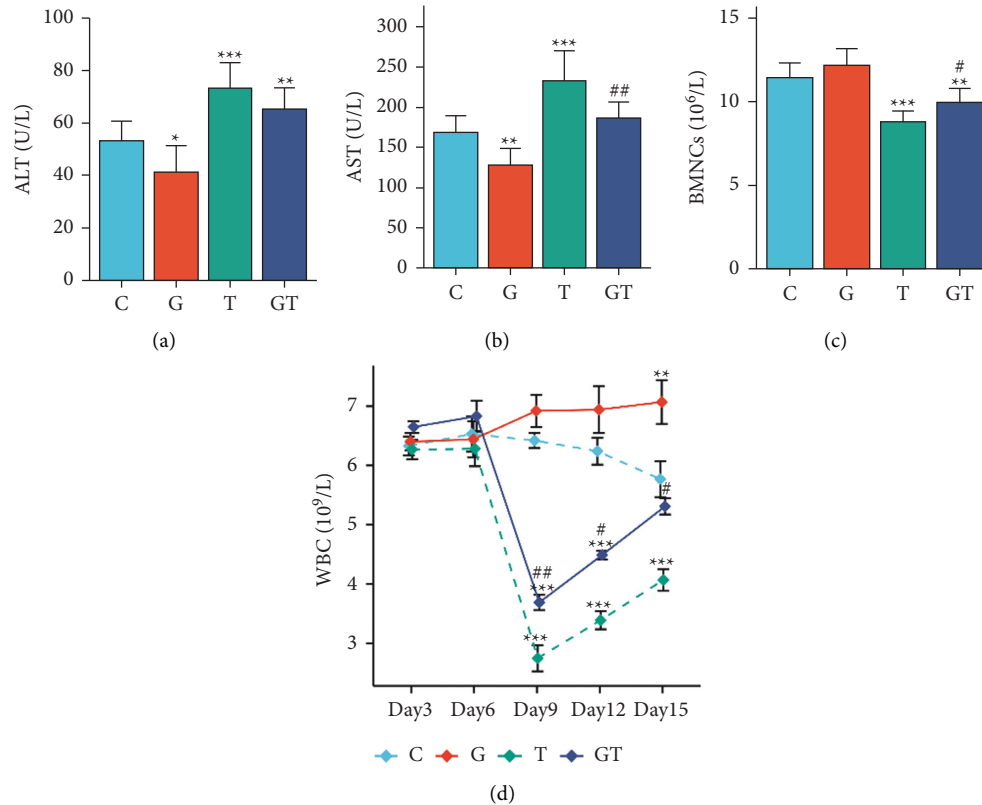


FIGURE 4: The effect of grain-sized moxibustion combined with CTX on hematological and biochemical indexes of Hepa1-6-bearing mice. (a) ALT: alanine aminotransferase. (b) AST: aspartate transaminase. (c) BMNCs: bone marrow nucleated cells. (d) WBCs: white blood cells (days 6, 9, 12, and 15). All values are presented as means \pm SD ($n = 10$). Notes: * $P < 0.05$, ** $P < 0.01$, *** $P < 0.001$ vs. C group; # $P < 0.05$, ## $P < 0.01$ vs. T group. C: control group; G: grain-sized moxibustion group; T: CTX group, GT: grain-sized moxibustion plus CTX group.

C (all $P < 0.001$). However, the relative mRNA expression levels of Ki67 in the GT group were significantly lower compared with those of the T group ($P < 0.01$); the relative mRNA expression levels of PCNA were lower, but it had no statistical significance. These results suggest that grain-sized moxibustion inhibited tumor growth by down-regulating the expression of proliferation genes Ki67 and PCNA, consistent with the results of immunohistochemical analysis. Likewise, the combined application of grain-sized moxibustion and CTX could enhance the antitumor effects, inhibit the proliferation of tumor cells, and exert a synergistic effect.

4. Discussion

This study evaluated the effect of grain-sized moxibustion and CTX on tumor growth, weight, volume, and inhibition rate. The body weight and survival status of Hepa1-6-bearing mice were significantly decreased after CTX treatment. However, after treatment with grain-sized moxibustion, the weight and survival status of Hepa1-6-bearing mice in the GT group were significantly higher than those in the T group. Furthermore, the results showed that both grain-sized moxibustion and CTX could effectively inhibit tumor growth.

The combined use of grain-sized moxibustion and CTX had a synergistic effect, which could significantly increase

the tumor inhibition rate. CTX is one of the most effective and widely used drugs in the synthesis of many chemotherapeutic drugs. It works mainly through the replacement of nitrogen mustard methyl groups with CTX rings to form intra- and inter-strand DNA cross-links, thereby interfering with DNA replication and inhibiting tumor growth [28, 29]. Compared with other therapies, grain moxibustion has unique advantages in treating cancer [30, 31]. In recent years, relevant basic research and clinical trials have shown that moxibustion can increase the number of lymphocytes and their subsets, activate natural killer cells, and stimulate the activity of cytokines (e. g., interleukin (IL)-1 and IL-2) to improve the body's immune response [32] and the survival status of patients with cancer [33]. These findings are consistent with our experimental results. At present, there is no research on whether grain-sized moxibustion combined with CTX has a synergistic effect on the treatment of tumors. This study observed synergistic effects of grain-sized moxibustion on Hepa1-6-bearing mice and the effect of reducing toxicity of chemotherapy drugs (e. g., CTX).

It is well known that the most common clinical adverse reactions caused by CTX are leukopenia [34], bone marrow suppression [35], and hepatotoxicity [36]. It also has a certain impact on the hematopoietic system [37]. The hematopoietic system is one of the most sensitive targets of toxic compounds and is often regarded as an important parameter of physiological and pathological states in

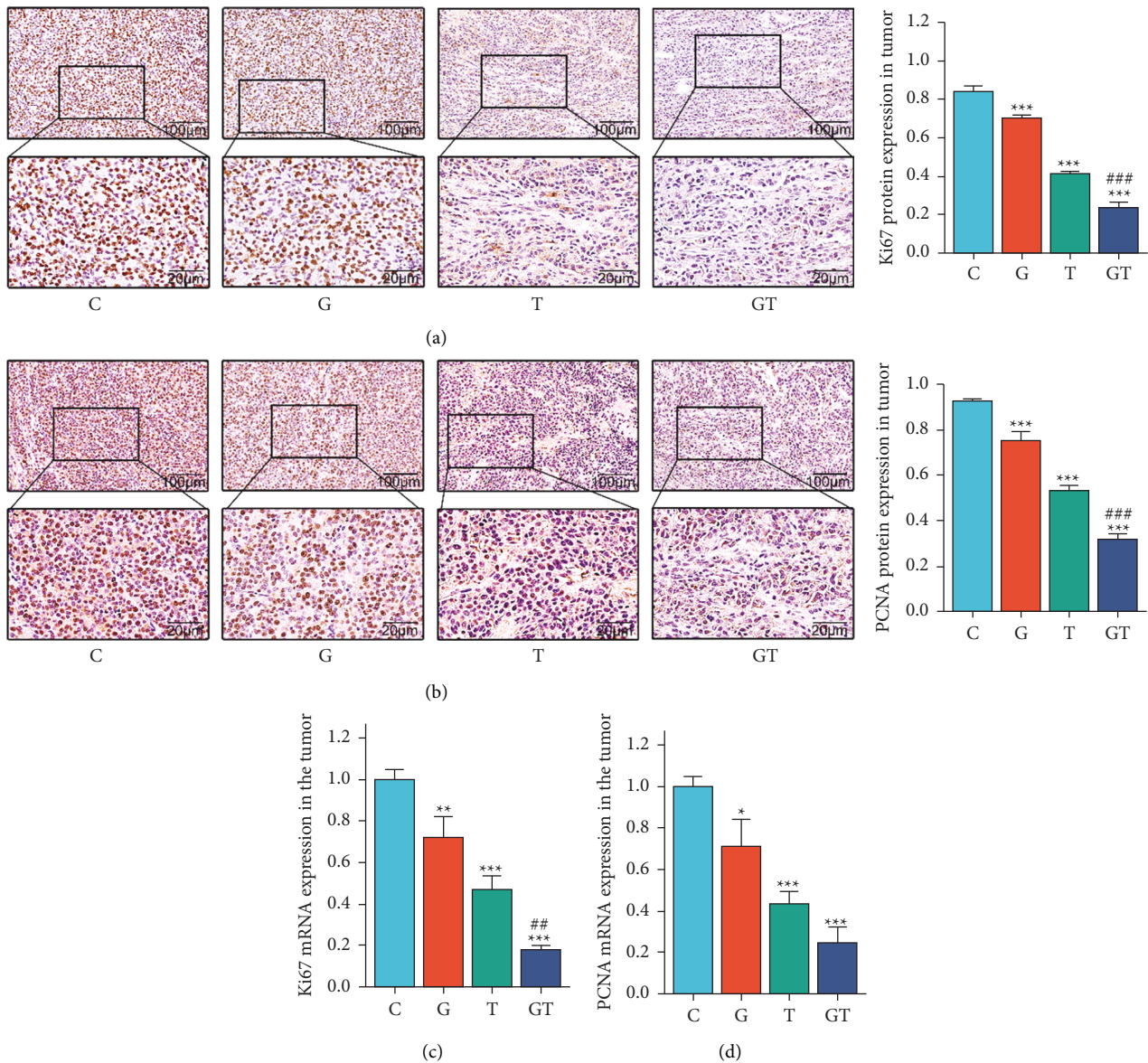


FIGURE 5: The effect of grain-sized moxibustion combined with CTX on the proliferation of tumor cells in Hepa1-6-bearing mice. (a) Expression of Ki67 protein in tumor tissue. (b) Expression of PCNA protein in tumor tissue. (c) The relative expression of Ki67 mRNA in tumor tissue. (d) The relative expression of PCNA mRNA in tumor tissue. All values are presented as means \pm SD ($n = 3$). Notes. * $P < 0.05$, ** $P < 0.01$, *** $P < 0.001$ vs. C group; # $P < 0.05$, ## $P < 0.01$ vs. T group. C: control group; G: grain-sized moxibustion group; T: CTX group, GT: grain-sized moxibustion plus CTX group.

humans and animals [38]. To study the relevant mechanism, we observed the effect of grain-sized moxibustion and CTX on WBCs and BMNCs and conducted related research. The results showed that grain-sized moxibustion combined with CTX could significantly increase the numbers of WBCs and BMNCs compared with those of CTX alone and had a certain protective effect on the hematopoietic system. Serum ALT and AST are sensitive markers to detect whether liver function is reduced, which can reflect different degrees of liver damage [39]. Grain-sized moxibustion can significantly reduce serum ALT and AST levels and alleviate CTX-induced hepatotoxicity. Organ weight is one of the most sensitive indicators of drug toxicity, and changes in organ

weights often precede morphological changes [10]. This study found that grain-sized moxibustion could significantly reduce the damage to the liver and spleen caused by CTX and increase the liver and spleen indices. It has been reported that the cancer usually occurs at sites of chronic inflammation [40]. Moreover, inflammatory cells are also involved in the formation of tumors and impair immunity. Remarkably, the density of PALS cells in the spleen was lower, the proliferation of LN was inhibited, and the degeneration and swelling of hepatocytes were lower in the GT group than in the C group. Grain-sized moxibustion could significantly improve CTX-induced splenic lymphocyte reduction and reduce liver inflammation, thereby improving

the pathological changes of spleen and liver and exerting an immunoregulatory effect. Overall, grain-sized moxibustion combined with CTX could significantly improve the survival status of Hepa1-6-bearing mice, increase body weight, improve symptoms such as leukopenia, myelosuppression, and hepatotoxicity, reduce the organ inflammatory response, and improve liver and spleen indices. These findings are consistent with the research of some domestic scholars, specifically that moxibustion could reduce the adverse reactions and damage to the body induced by chemotherapy [41].

Ki67 is a nuclear protein associated with cellular proliferation [42], and the quantity of nuclear staining cells is associated with tumor stage and disease development [43]. PCNA is a protein involved in the replication and repair of DNA and the adjustment of the cell cycle [44] and plays an important role in DNA replication and maintaining gene stability [45]. Ki67 and PCNA were shown to be strongly expressed in stained cells in previous investigations, implying that tumor cells were active and proliferated rapidly [46]. Consequently, Ki67 and PCNA could reflect the proliferative activity of tumor cells, suggesting their potential status as prognostic indicators. In this study, Ki67 and PCNA were greatly overexpressed in group C as shown by many brown-yellow particles in the nucleus, indicating that the tumor cells were in an active stage and a bad prognosis. The expression levels of Ki67 and PCNA in the G and T groups were significantly lower than those in the C group, whereas the expression levels of Ki67 and PCNA in the GT group were lower than those in the T group. The results of immunohistochemistry and RT-qPCR confirmed those of the other, indicating that the combination therapy could enhance the antitumor activity accompanied by an improved prognosis. Furthermore, our results showed that grain-sized moxibustion could assist CTX in the inhibition of tumor cell proliferation. The inhibitory effect is more obvious with time and its survival time is predicted to be prolonged, which may be the significance of grain-sized moxibustion as adjuvant chemotherapy.

This study preliminarily investigated the effect of grain-sized moxibustion on the antitumor effects of CTX in Hepa1-6-bearing mice and provided new insights into the antitumor effects of grain-sized moxibustion and the reduction of the toxic and side effects of CTX. Nonetheless, this study has limitations such as a short observation time and small sample size. To further study the therapeutic mechanism of grain-sized moxibustion, the effect of grain-sized moxibustion on tumor cell apoptosis can be further observed and studied by extending the course of treatment and increasing the sample size. Hence, we anticipate that relevant basic research and clinical follow-up studies will improve our experimental conclusions.

5. Conclusion

The antitumor effect of grain-sized moxibustion combined with CTX on Hepa1-6-bearing mice is greater than that of CTX alone. The mechanism by which grain-sized moxibustion enhances the antitumor activity of CTX may

include restraining tumor cell proliferation and reducing the toxicity of CTX. Thus, grain-sized moxibustion may be a promising external therapy for adjuvant chemotherapy.

Abbreviations

Hepa1-6:	Hepatoma 1–6
CTX:	Cyclophosphamide
FBS:	Fetal bovine serum
BSA:	Bovine serum albumin
AST:	Aspartate aminotransferase
ALT:	Alanine aminotransferase
BMNCs:	Bone marrow nucleated cells
WBC:	White blood cell
PALS:	Periarteriolar lymphoid sheath
LN:	Lymphoid nodule
RT-qPCR:	Real-time quantitative polymerase chain reaction.

Data Availability

The data used to support the findings of this study are included within the article.

Disclosure

The funding body had no role in the design of the study, in the collection, analysis, and interpretation of the data, or in the manuscript writing.

Conflicts of Interest

The authors declare that they have no conflicts of interest.

Authors' Contributions

These authors contributed equally to this work. All authors read and approved the manuscript.

Acknowledgments

This study was supported by funds from the Natural Science Foundation of Shanxi (201901D111336).

Supplementary Materials

Table S1: Survival status scores of tumor-bearing mice in this study. (*Supplementary Materials*)

References












- [1] J. Lokau, V. Schoeder, J. Haybaeck, and G. Garbers, "Jak-stat signaling induced by interleukin-6 family cytokines in hepatocellular carcinoma," *Cancers*, vol. 11, no. 11, p. 1704, 2019.
- [2] J. Wang, H. Zhao, J. Yu et al., "MiR-320b/RAD21 axis affects hepatocellular carcinoma radiosensitivity to ionizing radiation treatment through DNA damage repair signaling," *Cancer Science*, vol. 112, no. 2, pp. 575–588, 2021.
- [3] Q. Liu, X. Yu, M. Yang et al., "A study of the mechanism of lncRNA-CR594175 in regulating proliferation and invasion of hepatocellular carcinoma cells in vivo and in vitro," *Infectious Agents and Cancer*, vol. 15, no. 1, p. 55, 2020.

- [4] Y. Zhang, C. Xie, A. Li et al., "PKI-587 enhances chemosensitivity of oxaliplatin in hepatocellular carcinoma through suppressing DNA damage repair pathway (NHEJ and HR) and PI3K/AKT/mTOR pathway," *American Journal of Translational Research*, vol. 11, no. 8, pp. 5134–5149, 2019.
- [5] A. D. Podgurskaya, M. M. Slotvitsky, V. A. Tsvelaya et al., "Cyclophosphamide arrhythmogenicity testing using human-induced pluripotent stem cell-derived cardiomyocytes," *Scientific Reports*, vol. 11, no. 1, p. 2336, 2021.
- [6] M. Shi, J. Zhang, X. Li et al., "Mitochondria-targeted delivery of doxorubicin to enhance antitumor activity with HER-2 peptide-mediated multifunctional pH-sensitive DQAsomes," *International Journal of Nanomedicine*, vol. 13, no. 13, pp. 4209–4226, 2018.
- [7] Y. Huang, Y. He, S. Ye, Q. Zhong, and Z. Chen, "Combined use of cyclophosphamide and Chalone 19-peptide in experimental breast cancer," *Oncology Targets and Therapy*, vol. 6, pp. 861–867, 2013.
- [8] F. Amiri, M. Hamzeh, S. Hosseinimehr, A. Khalatbary, H. Mohammadi, and A. Dashti, "Atorvastatin mitigates cyclophosphamide-induced hepatotoxicity via suppression of oxidative stress and apoptosis in rat model," *Research in Pharmaceutical Sciences*, vol. 13, no. 5, pp. 440–449, 2018.
- [9] Y. Zhang, J. Li, D. Wei et al., "Genome-wide regulation of electroacupuncture and treadmill exercise on diet-induced obese rats," *Evidence-Based Complementary and Alternative Medicine*, vol. 2020, Article ID 8764507, 9 pages, 2020.
- [10] J. Wen, Z. Zhuang, M. Zhao et al., "Treatment of poststroke constipation with moxibustion: a case report," *Medicine (Baltimore)*, vol. 97, no. 24, Article ID e11134, 2018.
- [11] M. Ma, "TCM treatment and research progress of leukopenia," *Sichuan TCM*, vol. 12, pp. 7–9, 1994.
- [12] Y. T. Cheng and Y. D. Hou, "Literature quality evaluation of randomized controlled trials on acupuncture and moxibustion for secondary leukopenia in China," *Journal of Shanxi University of Traditional Chinese Medicine*, vol. 17, no. 1, pp. 6–7, 2016.
- [13] Z. Liu, Z. Lu, R. Jing et al., "Alarmin augments the antitumor immunity of lentiviral vaccine in ectopic, orthotopic and autochthonous hepatocellular carcinoma mice," *Theranostics*, vol. 9, no. 14, pp. 4006–4018, 2019.
- [14] P. Liu, L. Zhao, J. Pol et al., "Crizotinib-induced immunogenic cell death in non-small cell lung cancer," *Nature Communications*, vol. 10, no. 1, p. 1486, 2019.
- [15] M. M. Farouk, A. El-Molla, F. A. Salib, Y. A. Soliman, and M. Shaalan, "The role of silver nanoparticles in a treatment approach for multidrug-resistant *Salmonella* species isolates," *International Journal of Nanomedicine*, vol. 15, pp. 6993–7011, 2020.
- [16] Z. Wang, X. Y. Xu, and Q. Li, "Anti-tumor effect of ginsenoside Rg1 pyrolysis products (HPPRg1) on H22 tumor-bearing mice," *Chinese Journal of Pharmacy*, vol. 52, no. 15, pp. 1319–1324, 2017.
- [17] X. Zhang, Q. Wan, and T. S. Xu, "Effect of grain-moxibustion on IL-6 and STAT 3 in inflammatory microenvironment of lewis lung cancer mice," *Acupuncture Research*, vol. 42, no. 3, pp. 235–239, 2017.
- [18] W. J. Wang, X. X. Wan, and T. S. Xu, "Effect of moxa-grain-moxibustion on serum Th1/Th2 type cytokines in lewis tumor-bearing mice," *Acupuncture Research*, vol. 39, no. 6, pp. 477–481, 2014.
- [19] D. Hu, W. Shen, C. Gong et al., "Grain-sized moxibustion promotes NK cell antitumor immunity by inhibiting adrenergic signalling in non-small cell lung cancer," *Journal of Cellular and Molecular Medicine*, vol. 25, no. 6, pp. 2900–2908, 2021.
- [20] S. Naito, A. C. von Eschenbach, R. Giavazzi, and I. J. Fidler, "Growth and metastasis of tumor cells isolated from a human renal cell carcinoma implanted into different organs of nude mice," *Cancer Research*, vol. 46, no. 8, pp. 4109–4115, 1986.
- [21] L. Wang and R. Wang, "Effect of rapamycin (RAPA) on the growth of lung cancer and its mechanism in mice with A549," *International Journal of Clinical and Experimental Pathology*, vol. 8, no. 8, pp. 9208–9213, 2015.
- [22] J. Tan, R. D. Yang, H. Zhao, P. Zhuojun, O. Lizhi, and L. Yaping, "Inhibitory effect of moxibustion on tumor growth in rats with gastric tumor," *World Science and Technology-Modernization of Traditional Chinese Medicine*, vol. 21, no. 09, pp. 1994–2000, 2019.
- [23] M. Gao, M. Zhang, M. Si, J.-Y. Chen, and W. Wei, "The expression of CXCL12/CXCR4 in spleen of adjuvant arthritis rats and the effect of paeoniflorin-6'-O-benzene sulfonate," *China Pharmacology Circular*, vol. 34, no. 05, pp. 639–644, 2018.
- [24] Y. L. She, D. Q. Yan, and Y. Q. Liu, "Effect of danggui beimu kushen pill on pathological morphology of tumor and liver, kidney and thymus of H22 tumor-bearing mice treated with cisplatin," *Chinese Journal of TCM Information*, vol. 21, no. 5, pp. 56–60, 2014.
- [25] O. R. M. Metawea, M. A. Abdelmoneem, N. S. Haiba et al., "A novel "smart" PNIPAM-based copolymer for breast cancer targeted therapy: synthesis, and characterization of dual pH/temperature-responsive lactoferrin-targeted PNIPAM-co-AA," *Colloids and Surfaces B: Biointerfaces*, vol. 202, Article ID 111694, 2021.
- [26] Y. Wang, X. Deng, C. Yu et al., "Synergistic inhibitory effects of capsaicin combined with cisplatin on human osteosarcoma in culture and in xenografts," *Journal of Experimental & Clinical Cancer Research*, vol. 37, no. 1, p. 251, 2018.
- [27] X. Chen, H. Yang, and Z. Wang, "The effect of different dietary levels of defatted rice bran on growth performance, slaughter performance, serum biochemical parameters, and relative weights of the viscera in geese," *Animals*, vol. 9, no. 12, 2019.
- [28] A. Emadi, R. J. Jones, and R. A. Brodsky, "Cyclophosphamide and cancer: golden anniversary," *Nature Reviews Clinical Oncology*, vol. 6, no. 11, pp. 638–647, 2009.
- [29] W. van Dorp, R. L. Mulder, L. C. Kremer et al., "Recommendations for premature ovarian insufficiency surveillance for female survivors of childhood, adolescent, and young adult cancer: a report from the international late effects of childhood cancer guideline harmonization group in collaboration with the PanCareSurFup consortium," *Journal of Clinical Oncology*, vol. 34, no. 28, pp. 3440–3450, 2016.
- [30] A. H. El-Far, K. Godugu, A. E. Noreldin et al., "Thymoquinone and costunolide induce apoptosis of both proliferative and doxorubicin-induced-senescent colon and breast cancer cells," *Integrative Cancer Therapies*, vol. 20, Article ID 153473542110354, 2021.
- [31] A. F. Khafaga, R. N. Shamma, A. Abdeen et al., "Celecoxib repurposing in cancer therapy: molecular mechanisms and nanomedicine-based delivery technologies," *Nanomedicine*, vol. 16, no. 19, pp. 1691–1712, 2021.
- [32] J. Pei, H. Wei, Z. D. Liu, Y. M. Yu, C. R. Ni, and H. G. Wu, "Effects of moxibustion on the expression of IL-1beta, IL-2, IL-6 mRNA and protein in the cerebral cortex in tumor-bearing mice," *Acupuncture Research*, vol. 35, no. 4, pp. 243–249, 2010.

- [33] P. Wang, J. Zhu, X. L. Xie et al., "Effects on the tumor specific growth factor and tumor necrosis factor α in rats' precancerous lesion of primary hepatocellular carcinoma by direct moxibustion at Ganshu (BL 18) acupoint," *Chinese Journal of Integrative Medicine*, vol. 22, no. 7, pp. 532–536, 2016.
- [34] L. Ma, Y. Wang, J. Bo et al., "Autologous cytokine-induced killer (CIK) cell immunotherapy combined with cyclophosphamide in five patients with POEMS syndrome," *Clinical and Experimental Immunology*, vol. 184, no. 1, pp. 83–89, 2016.
- [35] K. Evans, J. Duan, T. Pritchard et al., "OBI-3424, a novel AKR1C3-activated prodrug, exhibits potent efficacy against preclinical models of T-ALL," *Clinical Cancer Research*, vol. 25, no. 14, pp. 4493–4503, 2019.
- [36] M. Zhao, H. Zhao, J. Deng, L. Guo, and B. Wu, "Role of the CLOCK protein in liver detoxification," *British Journal of Pharmacology*, vol. 176, no. 24, pp. 4639–4652, 2019.
- [37] Z. C. Ding, X. Lu, M. Yu et al., "Immunosuppressive myeloid cells induced by chemotherapy attenuate antitumor CD4+ T-cell responses through the PD-1-PD-L1 axis," *Cancer Research*, vol. 74, no. 13, pp. 3441–3453, 2014.
- [38] S. Belemkar and P. N. Shendge, "Toxicity profiling of the ethanolic extract of *Citrullus lanatus* seed in rats: behavioral, biochemical and histopathological aspects," *Bioscience Reports*, vol. 41, no. 1, 2021.
- [39] Z. Chen, F. Zhang, L. Jiang, Z. Chen, and H. Sun, "Toxic effects of mycotoxin fumonisin B1 at six different doses on female BALB/c mice," *Toxins*, vol. 14, no. 1, p. 21, 2021.
- [40] Y. Liu, L. Zhang, X. Zhu, Y. Wang, W. Liu, and W. Gong, "Polysaccharide *Agaricus blazei* Murill stimulates myeloid derived suppressor cell differentiation from M2 to M1 type, which mediates inhibition of tumour immune-evasion via the Toll-like receptor 2 pathway," *Immunology*, vol. 146, no. 3, pp. 379–391, 2015.
- [41] H. W. Zhang, Z. X. Lin, F. Cheung, W. C. Cho, and J. L. Tang, "Moxibustion for alleviating side effects of chemotherapy or radiotherapy in people with cancer," *Cochrane Database of Systematic Reviews*, vol. 11, no. 11, 2018.
- [42] E. M. Othman, A. A. Bekhit, M. A. Anany, T. Dandekar, H. M. Ragab, and A. Wahid, "Design, synthesis, and anticancer screening for repurposed pyrazolo[3, 4-d] pyrimidine derivatives on four mammalian cancer cell lines," *Molecules*, vol. 26, no. 10, p. 2961, 2021.
- [43] B. Chandrasekaran, D. Pal, V. Kolluru et al., "The chemopreventive effect of withaferin A on spontaneous and inflammation-associated colon carcinogenesis models," *Carcinogenesis*, vol. 39, no. 12, pp. 1537–1547, 2018.
- [44] H. Okamoto, I. Muraki, H. Okada et al., "Recombinant antithrombin attenuates acute respiratory distress syndrome in experimental endotoxemia," *American Journal of Pathology*, vol. 191, no. 9, pp. 1526–1536, 2021.
- [45] Y. Kamikawa, K. Yokota, K. Oikawa, F. Sato, and Y. Muragaki, "Suppression of MKL1 promotes adipocytic differentiation and reduces the proliferation of myxoid liposarcoma cells," *Oncology Letters*, vol. 20, no. 6, p. 1, 2020.
- [46] Q. S. Wang, L. N. Gao, X. N. Zhu et al., "Co-delivery of glycyrrhizin and doxorubicin by alginate nanogel particles attenuates the activation of macrophage and enhances the therapeutic efficacy for hepatocellular carcinoma," *Theranostics*, vol. 9, no. 21, pp. 6239–6255, 2019.

Research Article

Chemical Composition and the Anticancer, Antimicrobial, and Antioxidant Properties of *Acacia* Honey from the Hail Region: The *in vitro* and *in silico* Investigation

Walid Sabri Hamadou ¹, Nouha Bouali ¹, Riadh Badraoui ^{1,2,3},
Ramzi Hadj Lajimi ^{4,5}, Assia Hamdi ⁶, Mousa Alreshidi ^{1,7}, Mitesh Patel ⁸,
Mohd Adnan ¹, Arif Jamal Siddiqui ¹, Emira Noumi ^{1,9},
Visweswara Rao Pasupuleti ^{10,11} and Mejdi Snoussi^{1,12}

¹Department of Biology, College of Science, University of Hail, P.O. Box 2440, Ha'il, Saudi Arabia

²Section of Histology Cytology, Medicine Faculty of Tunis, University of Tunis El Manar, La Rabta 1007, Road Djebel Lakhdhar, Tunis 1007, Tunisia

³Department of Histo-Embryology and Cytogenetics, Medicine Faculty of Sfax, University of Sfax, Road of Majida Boulia, Sfax 3029, Tunisia

⁴Department of Chemistry, College of Science, University of Ha'il, P.O. Box 2440, Ha'il 81441, Saudi Arabia

⁵Laboratory of Water, Membranes and Environmental Biotechnologies, Center of Researches and Water Technologies, P.O. Box 273, Soliman 8020, Tunisia

⁶Laboratoire de Développement Chimique Galénique et Pharmacologique des Médicaments, Faculté de Pharmacie, Monastir 5000, Tunisia

⁷Molecular Diagnostic and Personalized Therapeutics Unit, University of Ha'il, Ha'il 2440, Saudi Arabia

⁸Department of Biotechnology, Parul Institute of Applied Sciences and Centre of Research for Development, Parul University, Vadodara 391760, Gujarat, India

⁹Laboratory of Bioresources: Integrative Biology and Recovery, High Institute of Biotechnology University of Monastir, Monastir 5000, Tunisia

¹⁰Department of Biomedical Sciences and Therapeutics, Faculty of Medicine & Health Sciences, Universiti Malaysia Sabah, Kota Kinabalu, Sabah 44800, Malaysia

¹¹Centre for International Collaboration and Research, Reva University, Rukmini Knowledge Park, Kattigenahalli, Yelahanka, Bangalore, Karnataka 560064, India

¹²Laboratory of Genetics, Biodiversity and Valorisation of Bioresources, High Institute of Biotechnology University of Monastir, Monastir 5000, Tunisia

Correspondence should be addressed to Visweswara Rao Pasupuleti; pvrao@ums.edu.my

Received 3 April 2022; Revised 27 May 2022; Accepted 28 June 2022; Published 4 August 2022

Academic Editor: Mohammed El-Magd

Copyright © 2022 Walid Sabri Hamadou et al. This is an open access article distributed under the Creative Commons Attribution License, which permits unrestricted use, distribution, and reproduction in any medium, provided the original work is properly cited.

In consideration of the emergence of novel drug-resistant microbial strains and the increase in the incidences of various cancers throughout the world, honey could be utilized as a great alternative source of potent bioactive compounds. In this context, this study pioneers in reporting the phytochemical profiling and the antimicrobial, antioxidant, and anticancer properties of *Acacia* honey (AH) from the Hail region of Saudi Arabia, assessed using *in vitro* and molecular docking approaches. The phytochemical profiling based on high-resolution liquid chromatography-mass spectrometry (HR-LCMS) revealed eight compounds and three small peptide-like proteins as the constituents. The honey samples exhibited promising antioxidant activities (DPPH-IC₅₀ = 0.670 mg/mL; ABTS-IC₅₀ = 1.056 mg/mL; β -carotene-IC₅₀ > 5 mg/mL). In the well-diffusion assay, a high mean growth inhibition zone (mGIZ) was observed against *Staphylococcus aureus* (48.33 ± 1.53 mm), *Escherichia coli* ATCC 10536 (38.33 ± 1.53 mm), and *Staphylococcus epidermidis* ATCC 12228 (39.33 ± 1.15 mm). The microdilution assay revealed that low concentrations of AH could inhibit the growth of almost all the evaluated

bacterial and fungal strains, with the minimal bactericidal concentration values (MBCs) ranging from 75 mg/mL to 300 mg/mL. On the contrary, high AH concentrations were required to kill the tested microorganisms, with the minimal bactericidal concentration values (MBCs) ranging from approximately 300 mg/mL to over 600 mg/mL and the minimal fungicidal concentration values (MFCs) of approximately 600 mg/mL. The AH exhibited effective anticancer activity in a dose-dependent manner against breast (MCF-7), colon (HCT-116), and lung (A549) cancer cell lines, with the corresponding IC_{50} values of 5.053 μ g/mL, 5.382 μ g/mL, and 6.728 μ g/mL, respectively. The *in silico* investigation revealed that the observed antimicrobial, antioxidant, and anticancer activities of the constituent compounds of AH are thermodynamically feasible, particularly those of the tripeptides (Asp-Trp-His and Trp-Arg-Ala) and aminocyclitol glycoside. The overall results highlighted the potential of AH as a source of bioactive compounds with significant antimicrobial, antioxidant, and anticancer activities, which could imply further pharmacological applications of AH.

1. Introduction

The emergence of novel drug-resistant microbial strains and the high prevalence of various cancers have heavily burdened the existing healthcare system. The main challenge is to discover novel therapeutic strategies. Complementary medicine using natural products or their derivative phytochemicals could serve as a great alternative for overcoming these healthcare-related concerns, and honey could be an interesting choice in this regard [1]. Honey and its products have been valorized for their high nutritional value and medicinal properties for a long time. Owing to its therapeutic value, honey is used as an essential ingredient in several formulations of folk medicine. The diversity of the specific phytochemical compositions of honey could provide valuable bioactive molecules to be used in the treatment of various cancers and infections with drug-resistant bacterial strains. Certain highly antioxidant and bioactive constituent molecules in honey have been reported to exhibit prominent therapeutic results against several forms of cancers. So far, over 200 constituent compounds have been reported in honey. This complexity of honey could explain its antimicrobial and anticancer activities and its capacity to modulate oxidative stress. The most common bioactive compounds reported in honey, which are considered responsible for its anticancer activity, are flavonoids and phenolic acids [2]. These compounds exhibit several mechanisms for anticancer activity, including apoptosis, inhibition of the tumor necrosis factor, and antiproliferative, immunomodulatory, and anti-inflammatory effects [2]. Honey samples derived from several regions have been investigated for their antioxidant, antimicrobial, and anticancer activities, with different results reported for different subtypes and various floral and geographical origins of honey [3]. The various kinds of honey derived from Saudi Arabia have been particularly highlighted for their interesting displays of biological activity [4–7]. In the Kingdom of Saudi Arabia, beekeeping constitutes an important economic activity, with several varieties of honey produced as this region has abundant natural flora most suitable for beekeeping. Talh or *Acacia* is the dominant bee plant in this region. This plant belongs to the subfamily Mimosoideae under the family Fabaceae, which comprises several species, including *Acacia albida*, *Acacia asak*, *Acacia ehrenbergiana*, *Acacia etbaica*, *Acacia johnwoodii*, *Acacia oerfota*, and *Acacia tortilis* [8].

Acacia honey (AH) is quite popular in Saudi Arabia owing to its nutritional value and medicinal properties. The composition and properties of AH mainly depend on the geographical and floral origin of the honey and also on the

environmental factors, including seasons. Several studies have highlighted that the chemical composition of honey may even vary with climatic conditions and soil composition [9]. Recent studies revealed that honey samples obtained from different altitudes in the same region exhibited different phytochemical compositions, particularly the levels of total phenols and flavonoids, which could lead to different biological activities. The antioxidant, antimicrobial, and anticancer potentials of AH have been revealed in several studies. The reported results varied according to the bioactive phytochemical composition of AH, which mainly depends on the geographical origin of the honey sample [7]. Therefore, this study aimed at investigating, for the first time, the phytochemical composition of AH from the Hail region using the HR-LCMS technique to evaluate the antioxidant potential of the selected honey and estimate its anticancer activity against human lung, breast, and colon cancer cell lines. In addition, the antimicrobial potential of the selected AH against several bacterial strains, yeast, and molds was investigated using the well-diffusion and microdilution assays. The targeted biological activities were also assessed by studying the molecular interactions with the selected receptors using the molecular docking approach.

2. Materials and Methods

2.1. Honey Sampling. Talh (*Acacia* sp.) honey samples were collected directly from the beekeeper in the melliferous areas of the Hail region. The collected honey samples were stored at 4°C in glass jars in the dark until to be used for subsequent analyses.

2.2. Phytochemical Profiling of *Acacia* Honey

2.2.1. Identification of Bioactive Compounds Using the HR-LCMS Technique. In order to determine the phytochemistry of AH, chromatographic analysis was performed using the UHPLC-PDA-detector mass spectrophotometer (HR-LCMS 1290 INFINITY UHPLC System, Agilent Technologies, Santa Clara (CA, USA), as described previously by Adnan et al. [10]. A 10- μ L aliquot from the honey sample was injected into the SBC18 column (2.1 mm \times 50 mm; particle size 1.8 μ m). The elution was performed using 1% formic acid in deionized water (solvent A) and acetonitrile (solvent B) at a flow rate of 0.350 mL/min. The MS detection was performed using MS Q-TOF in positive and negative atmospheric pressure chemical ionization modes. PubChem was employed as the main tool for the identification of the phytochemical constituents in the honey samples.

2.2.2. Determination of Total Phenols, Flavonoids, and Tannins. Total phenols, flavonoids, and tannins were quantified using the standard protocols described in previous reports [11, 12].

2.3. Antioxidant Activities. The antioxidant activities were evaluated using three tests DPPH, ABTS, and β -carotene bleaching tests. The test protocols used were obtained from previous reports [13, 14].

2.3.1. DPPH Radical-Scavenging Activity. The DPPH (2,2-diphenyl-1-picryl-hydrazyl-hydrate) (Sigma-Aldrich Milano, Italy) free radical-scavenging activities of the honey samples were determined using an antioxidant assay based on electron-transfer reaction. In this assay, DPPH is reduced in the presence of an antioxidant molecule. Several dilutions of the honey were incubated with DPPH for 30 min at room temperature. Ascorbic acid was used as the standard control. The variation in the color of DPPH was assessed based on spectrophotometric analysis at 515 nm. The antioxidant activity was expressed as IC₅₀ (mg/mL) and calculated using the following formula:

$$\text{DPPH - scavenging activity (\%)} = \frac{(A_0 - A_1)}{A_0} \times 100, \quad (1)$$

where A_0 denotes the absorbance of the control and A_1 denotes the absorbance of the sample.

2.3.2. ABTS Radical-Scavenging Activity. The ABTS (2,2-azino-bis (3-ethylbenzothiazoline-6-sulfonic acid); Sigma-Aldrich Milano, Italy) radical-scavenging activity of the honey samples was assessed. In order to generate ABTS⁺, 7 mM ABTS was allowed to react with 2.45 mM K₂S₂O₈ for 12 h in the dark at room temperature. Several concentrations of the honey were mixed with 900 μ L of the solution-containing ABTS⁺, and the mixture was incubated for 30 min. The antioxidant activity was expressed as IC₅₀ (mg/mL), representing the AH concentration scavenging 50% of ABTS⁺. The ABTS-scavenging activity was calculated using the following formula:

$$\text{ABTS - scavenging activity (\%)} = \frac{(A_0 - A_1)}{A_0} \times 100, \quad (2)$$

where A_0 denotes the absorbance of the control and A_1 denotes the absorbance of the sample.

2.3.3. β -Carotene/Linoleic Acid Method. The β -carotene method was performed as described by Ikram et al. [15], and the inhibition of the volatile organic compounds and the conjugated diene hydroperoxides arising from linoleic acid oxidation was measured. In the reaction, the free radical linoleic acid attacked the highly unsaturated β -carotene in the presence of antioxidants (*Acacia* honey in this case). The prepared emulsion mixture was incubated at 50°C in the dark, followed by measuring the absorbance at 470 nm immediately ($t = 0$ min) and after 2 h of incubation ($t = 120$ min). Ascorbic

acid was used as the standard for comparison. The antioxidant activity of honey was estimated using the following equation:

$$\text{PI (\%)} = \left(\frac{A - \beta - \text{carotene } T_{120}}{A - \beta - \text{carotene } t_0} \right) \times 100. \quad (3)$$

2.4. Antimicrobial Activity of the Obtained Crude Extract

2.4.1. Well-Diffusion Assay. One mL of the honey sample to be evaluated (1 mL = 1.0653 g) was diluted in 5% dimethyl sulfoxide (DMSO) to prepare solutions with the final concentration ranging from 532.65 mg/mL to 26 mg/mL. Subsequently, the well-diffusion assay was performed to determine the diameter of the growth inhibition zone on agar medium (Mueller–Hinton for bacteria, Sabouraud Chloramphenicol agar for yeasts, and potato dextrose agar for molds) using the protocols described by Noumi et al. [12, 16]. The evaluated strains were obtained from a huge microbial collection available in the microbiology laboratory of our college and included the following twelve bacteria: *Pseudomonas aeruginosa* (clinical strain, SP-40), *Staphylococcus aureus* ATCC 29213, *S. epidermidis* ATCC 12228, *Escherichia coli* ATCC 10536, *Klebsiella pneumoniae* (clinical strain, 140), *E. coli* (clinical strain, 217), *S. aureus* (clinical strain), *S. sciuri* (environmental strain), *Serratia marcescens*, *Acinetobacter baumannii* (clinical strain, 146), methicillin-resistant *S. aureus* (MRSA clinical strain, 136), and *Enterobacter cloacae* (clinical strain 155). The antifungal activity of the AH to be evaluated was investigated against the following five yeasts and two molds: *Candida albicans* ATCC 20402, *Saccharomyces cerevisiae* (instant yeast), *C. vaginalis* (clinical strain, 136), *C. guilliermondii* ATCC 6260, *C. tropicalis* ATCC 1362, *Aspergillus fumigatus* ATCC 204305, and *A. Niger*. The antibacterial activity was evaluated using the agar well-diffusion assay. Using a sterile borer (diameter 7 mm), four wells were created in the agar plate and filled with 100 μ L of AH at different concentrations (100%, 75%, 50%, and 25%). The pure colonies of microorganisms that appeared on the appropriate agar media were selected to prepare homogenous (bacterial/fungal) suspensions. A cotton swab was used for inoculating fresh Petri dishes.

The treated Petri dishes were maintained at 4°C for 1 h and then incubated at 37°C for the next 24 h. The antimicrobial activity was evaluated by measuring the diameter of the growth inhibition zone around the wells. All tests were performed in triplicate, and the mean diameter of the inhibition zone was used as the final diameter value. The results obtained were interpreted using the scheme proposed by Parveen et al., which was as follows: no activity growth inhibition zone 0 (GIZ 0), low activity (GIZ: 1–6 mm), moderate activity (GIZ: 7–10 mm), high activity (GIZ: 11–15 mm), and extremely high activity (GIZ: 16–20 mm). Ampicillin (10 mg/mL; 10 μ L/disc) and amphotericin B (10 mg/mL; 10 μ L/disc) treatments were performed in the control experiments.

2.4.2. Microdilution Assay. The microdilution method was adopted to determine the MICs and MBCs (minimum bactericidal concentrations)/MFC values of the honey samples, as described previously [17]. First, a stock solution was prepared in 5% DMSO. Next, twofold serial dilutions of the honey samples were prepared in the wells of 96-well plates, beginning from 532.65 mg/mL to 26 mg/mL, using Mueller–Hinton broth for bacteria and Sabouraud Chloramphenicol broth for yeasts and molds. The microbial inoculum (5 μ L) was then added to each well of the microtiter plate containing 0.1 mL of the serially diluted honey. This was followed by incubation at 37°C for 24 h. The minimum inhibitory concentration (MIC) was defined as the lowest concentration of the compound that could inhibit microbial growth. In order to determine the MBC/MFC values, 3 μ L of the medium was removed from the wells with no visible growth and inoculated on Mueller–Hinton/Sabouraud Chloramphenicol agar plates. After 24 h of incubation at 37°C, microbial growth was observed. The concentration at which the microorganisms were killed (no growth) was recorded as the minimum bactericidal/fungicidal concentration. The MBC/MIC and MFC/MIC ratios were used to determine the activity of the honey samples as described in previous reports [18, 19].

2.5. Anticancer Assay Using MTT Assay. The anticancer potential of AH was evaluated against three human cancer cell lines using the MTT (3-(4,5-dimethylthiazolyl-2)-2,5-diphenyl tetrazolium bromide) assay. The three cell lines used in this study, namely, the lung cancer (A549), breast cancer (MCF-7), and colon cancer (HCT-116) cell lines, were provided by the National Centre for Cell Science (NCCS), Pune, India. Doxorubicin (Sigma, India) was used as the reference drug in the MTT assay. The cells were maintained at 37°C, 5% CO₂, and 80% humidity in 25-cm² flasks containing Dulbecco's modified Eagle medium (DMEM) supplemented with 10% fetal bovine serum (FBS), 10,000 U/mL penicillin, and 5 mg/mL streptomycin (Hi-Media, India). When 80% confluence was reached, the cells were seeded in the wells of a 96-well plate at a density of 1×10^5 cells per well, followed by incubation at the conditions stated above. The cells were stained with approximately 0.4% trypan blue stain (Hi-Media, India) to estimate the number of viable cells using a hemocytometer. All treatments were performed in triplicate, each for 24 h and with different concentrations of AH (2%, 4%, 6%, 8%, and 10%) prepared by diluting AH in complete media and sterilized using filtration (0.22 μ m filter). After incubation, the plate was removed from the incubator, and the medium containing AH was aspirated and then washed with phosphate-buffered saline (PBS). Afterward, the cells were incubated with 100 μ L of the MTT (Hi-Media, India) solution (5 mg/mL) for 4 h. Subsequently, 100 μ L of DMSO was added for crystal solubilization, and the absorbance was recorded at the wavelengths of 570 nm and 630 nm using an ELISA reader. The percentage growth inhibition was calculated after subtracting the background and the blank, and the concentration of the

evaluated drug required to inhibit cell growth by 50% (IC₅₀) was calculated from the dose-response curve for the respective cell line as described in a previous report [20].

2.6. The In Silico Analysis. The targeted biological activities were confirmed using the *in silico* molecular docking and interaction approach. The macromolecules identified in the composition of honey samples were obtained from RCSB. The macromolecules with the PDB IDs 1JJJ, 2XCT, 2QZW, and 1HD2 were subjected to the assessment of antibacterial, antifungal, and antioxidant activities. Similarly, 4UYA, 1JNX, and 4BBG were evaluated for their potential anticancer effect on colon, breast, and lung cancers, respectively. The chemical structures of all macromolecules were drawn using ChemDraw and saved in the .sdf format. The docking approach was based on the CHARMM force field after processing the receptors by adding polar hydrogens and Kollman charges and removing the crystal water molecules [21, 22] in AutoDock Vina and DS visualizer. The binding affinity and hydrogen bond assessment calculations were performed as described previously [21–24].

2.7. Statistical Analysis. All experiments and measurements were conducted in triplicate, and the results were presented as mean values \pm SD (standard deviations). ANOVA, Duncan's, and Bonferroni tests were performed using SPSS 16.0 and GraphPad Prism 5.0. The means of the result values obtained in the tests were also evaluated with the least significant differences test at $p < 0.05$.

3. Results

3.1. Phytochemical Profiling of Acacia Honey. High-resolution liquid chromatography-mass spectrometry (HRLCMS) was performed to determine the chemical composition of AH. This technique enabled the separation and identification of the phytoconstituents based on their retention time, database difference (library), experimental *m/z*, MS/MS fragments, metabolite class, and the proposed compounds. The MS data were generated in both negative and positive ionization modes. The complete list is provided in Table 1. The technique identified small peptide-like proteins in AH (one dipeptide and two tripeptides), with the respective molecular weights ranging from 271.1674 g/mol to 456.1732 g/mol.

The negative and positive runs identified 9 compounds belonging to different chemical classes, including 6-(α -D-glucosaminy)-1D-myo-inositol, L-gulonate, anabasamine, bakankoside, palmitic amide, stearamide, acetylenic acids, 10,16-heptadecadien-8-ynoic acid, 7-hydroxy, (E), and 14-fluoro-myristic acid. The chemical structures of the identified molecules are depicted in Figure 1.

3.2. Antimicrobial Activities of Acacia Honey. The mean diameters of the growth inhibition zones observed for the evaluated AH samples against 12 bacteria, 5 yeasts, and 2 molds are listed in Table 2. The highest mGIZ value for all the

TABLE 1: Phytochemical compounds identified by the HR-LCMS technique in AH from Hail region.

No	Compound name	Chemical class	RT	MW	Chemical formula	[m/z]-	[m/z]+
1	6-(alpha-D-Glucosaminyl)-1D-myo-inositol	Aminocyclitol glycosides	0.929	341.1312	C ₁₂ H ₂₃ N O ₁₀	—	342.1385
2	L-Gulonate	Sugar acid	1.062	196.0579	C ₆ H ₁₂ O ₇	195.0507	—
3	Pro-Arg	Dipeptide	1.223	271.1647	C ₁₁ H ₂₁ N ₅ O ₃	—	294.1539
4	Anabasamine	Alkaloid	1.666	253.1543	C ₁₆ H ₁₉ N ₃	—	276.1435
5	Bakankoside	Glycoside	3.038	357.144	C ₁₆ H ₂₃ N O ₈	—	380.133
6	Asp-Trp-His	Tripeptide	3.922	456.1732	C ₂₁ H ₂₄ N ₆ O ₆	—	457.1808
7	Trp-Arg-Ala	Tripeptide	12.066	431.230	C ₂₀ H ₂₉ N ₇ O ₄	—	432.237
8	Palmitic amide	Fatty acid amide	17.145	255.2559	C ₁₆ H ₃₃ N O	—	256.263
9	Stearamide	Fatty acid amide	18.765	283.287	C ₁₈ H ₃₇ N O	—	284.2942
10	10,16-Heptadecadien-8-ynoic acid, 7-hydroxy, (E)	Fatty acid	20.188	278.1935	C ₁₇ H ₂₆ O ₃	277.1865	—
11	14-Fluoro-myristic acid	Fatty acid	27.191	246.2011	C ₁₄ H ₂₇ F O ₂	291.1997	—

Note. RT: retention time (mn); MW: molecular weight (g/mol); [m/z]-: mass-to-charge ratio in negative ionization mode; [m/z]+: mass-to-charge ratio in positive ionization mode.

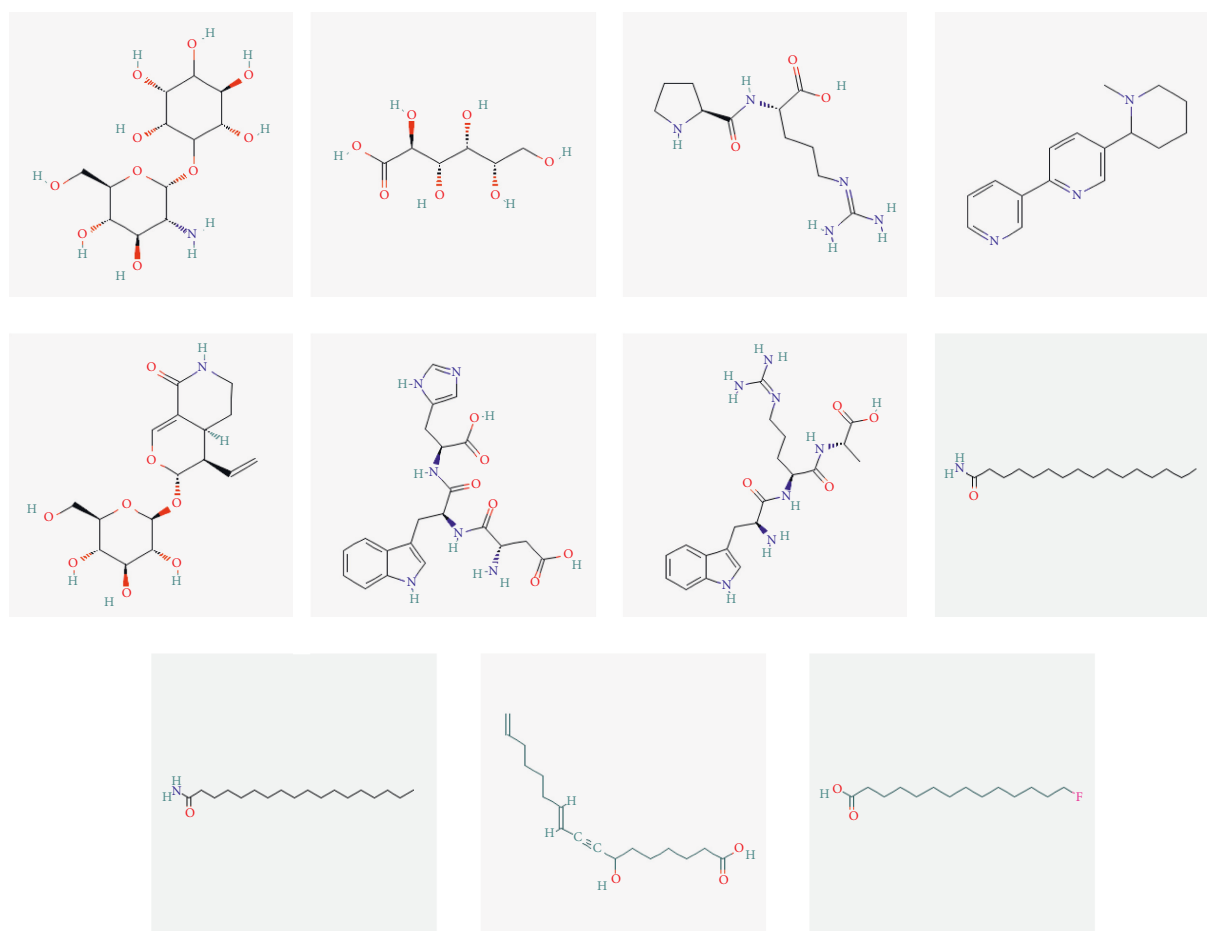


FIGURE 1: Chemical structure of eleven phytochemical compounds and small peptides identified in *Acacia* honey by using HR-LCMS technique.

evaluated bacteria was obtained when honey was used at 100% concentration. At this concentration, *S. aureus* (clinical strain), *E. coli* (clinical strain 217), and *S. epidermidis* ATCC 12228 were revealed as the most sensitive strains, with the corresponding mGIZ values of approximately

40.67 ± 0.57 mm, 50.33 ± 0.57 mm, and 40.33 ± 0.57 mm, respectively (Figure 2).

The most resistant bacterial strains were *A. baumannii* (clinical strain, 146), which exhibited an mGIZ value of approximately 6.00 ± 0 mm. The evaluated AH could not better

TABLE 2: Growth inhibition zone values expressed in mm of *Acacia* honey tested against bacteria, yeast, and molds strains using well-diffusion assay.

Bacteria tested	Dilution tested				Ampicillin (10 mg/ml) GIZ ± SD
	25% GIZ ± SD*	50% GIZ ± SD	75% GIZ ± SD	100% GIZ ± SD	
<i>P. aeruginosa</i> (clinical strain, SP-40)	9.67 ± 0.58f	11.00 ± 1.00h	12.67 ± 0.58f	14.00 ± 100f	6.00 ± 0.00h
<i>S. aureus</i> ATCC 29213	20.67 ± 0.58d	24.33 ± 1.53d	26.00 ± 2.65d	31.33 ± 1.15c	31.00 ± 1.00c
<i>S. epidermidis</i> ATCC 12228	23.33 ± 1.15c	27.00 ± 1.00c	30.00 ± 2.00c	39.33 ± 1.15b	27.33 ± 1.15e
<i>E. coli</i> ATCC 10536	9.33 ± 1.15f	12.00 ± 1.00h	14.33 ± 0.58f	14.33 ± 1.15f	28.67 ± 1.15d
<i>K. pneumoniae</i> (clinical strain, 140)	9.33 ± 0.58f	13.33 ± 1.15g	14.00 ± 1.00f	15.33 ± 1.15e	6.00 ± 0.00h
<i>E. coli</i> (clinical strain, 217)	29.00 ± 1.00b	32.67 ± 2.08b	37.33 ± 1.15b	38.33 ± 1.53b	31.67 ± 0.58c
<i>S. aureus</i> (clinical strain)	31.33 ± 1.15a	35.00 ± 1.00a	43.00 ± 1.00a	48.33 ± 1.53a	39.33 ± 1.154b
<i>S. sciuri</i> (environmental strain)	15.00 ± 1.00e	18.33 ± 1.53f	25.33 ± 1.15d	31.00 ± 1.00c	50.67 ± 1.154a
<i>S. marcescens</i> (clinical strain)	7.67 ± 0.58g	9.33 ± 1.15i	14.00 ± 1.00f	13.00 ± 1.00f	6.67 ± 0.58h
<i>A. baumannii</i> (clinical strain, 146)	6.00 ± 0.00h	6.00 ± 0.00j	6.00 ± 0.00g	6.00 ± 0.00g	21.00 ± 1.00f
<i>E. cloacae</i> (clinical strain, 155)	6.00 ± 0.00h	13.00 ± 1.00g	14.67 ± 1.15f	17.00 ± 1.00d	12.67 ± 0.58g
<i>S. aureus</i> MR (clinical strain, 136)	14.00 ± 1.00e	20.67 ± 0.58e	23.00 ± 1.00e	29.67 ± 1.53c	26.00 ± 1.00e

Yeasts and molds tested	Dilution tested				Amphotericin B (10 mg/ml) GIZ ± SD
	25% GIZ ± SD	50% GIZ ± SD	75% GIZ ± SD	100% GIZ ± SD	
<i>C. albicans</i> ATCC 20402	6.00 ± 0.00a	6.00 ± 0.00a	6.00 ± 0.00b	6.00 ± 0.00b	14.00 ± 0.00a
<i>S. cerevisiae</i> (instant yeast)	6.00 ± 0.00a	6.00 ± 0.00a	14.00 ± 1.00a	18.67 ± 1.15a	7.67 ± 1.54d
<i>C. guilliermondii</i> ATCC 6260	6.00 ± 0.00a	6.00 ± 0.00a	6.00 ± 0.00b	6.00 ± 0.00b	13.00 ± 1.00a
<i>C. tropicalis</i> ATCC 1362	6.00 ± 0.00a	6.00 ± 0.00a	6.00 ± 0.00b	6.00 ± 0.00b	12.00 ± 1.00b
<i>C. vaginalis</i> (clinical strain, 136)	6.00 ± 0.00a	6.00 ± 0.00a	6.00 ± 0.00b	6.00 ± 0.00b	7.33 ± 0.57d
<i>A. fumigatus</i> ATCC 204305	6.00 ± 0.00a	6.00 ± 0.00a	6.00 ± 0.00b	6.00 ± 0.00b	11.00 ± 0.00c
<i>A. niger</i>	6.00 ± 0.00a	6.00 ± 0.00a	6.00 ± 0.00b	6.00 ± 0.00b	6.00 ± 0.00e

*: growth inhibition zone ± standard deviation (expressed in mm); the letters (a–h) indicate a significant difference according to the Duncan test ($p < 0.05$).

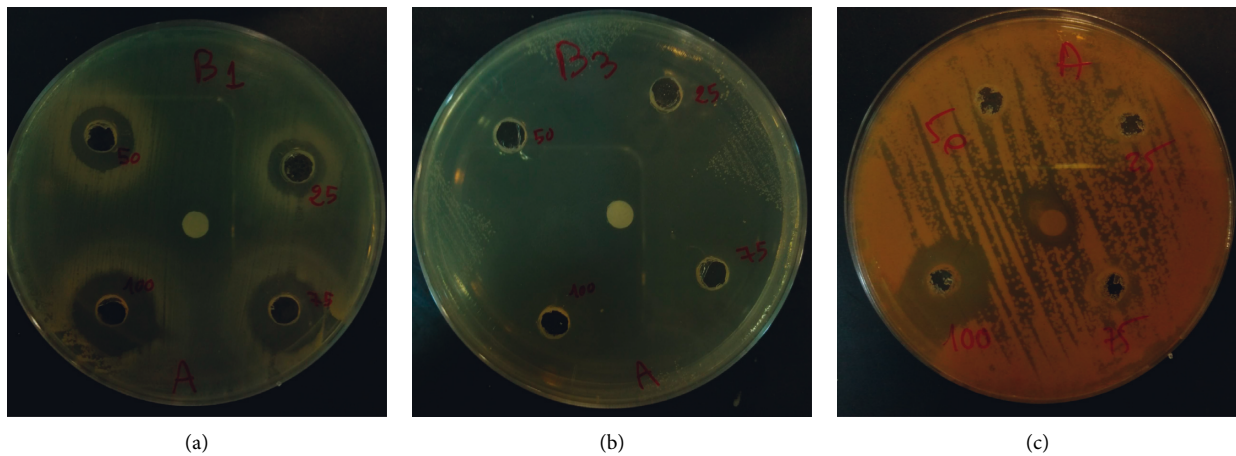


FIGURE 2: Antimicrobial activity of *Acacia* honey. (a) *P. aeruginosa* (clinical strain, SP-40), (b) *S. epidermidis* ATCC 12228 as compared to ampicillin (10 mg/ml), and (c) *S. cerevisiae* as compared to amphotericin B (10 mg/ml).

inhibit the growth of any of the selected yeasts and molds compared to the reference antifungal drug (amphotericin B), except for the growth of the *S. cerevisiae* strain, for which the mGIZ values ranged from 15.00 ± 0 mm at 75% of AH to 20.00 ± 0 mm when pure AH (100%) was used (Figure 2).

The findings of the microdilution method revealed that the lowest MIC values of 75 mg/mL were obtained against the staphylococcal species (*S. aureus*, *S. epidermidis*, and *S. sciuri*) and *S. marcescens*. On the other hand, 300 mg/mL of AH was required to inhibit the growth of methicillin-resistant

S. aureus strain. The MIC values of the fungal strains ranged from 150 mg/mL to 300 mg/mL. Higher concentrations of AH were required to completely kill the bacteria in all evaluated strains (the MBC values ranged from 300 mg/mL to 600 mg/mL). In addition, AH concentrations higher than 600 mg/mL were required to reproduce a fungicidal action against *Candida* and *Saccharomyces* strains. The results obtained using the scheme proposed by Gatsing et al. [19] revealed that AH exhibited bactericidal activity against most Gram-positive and Gram-negative bacteria, with the

TABLE 3: MICs, MBCs/MFCs expressed in mg/ml, and MBCs/MIC, MFC/MIC ratio of *Acacia* honey tested against bacteria, yeast, and molds using microdilution assay.

Test systems	<i>Acacia</i> honey		(BHT)	(AA)
Tested microorganisms	<i>Acacia</i> honey		MBC	MBC/MIC ratio
	MIC			
<i>P. aeruginosa</i> (clinical strain SP-40)	150		300	2
<i>S. aureus</i> ATCC 29213	75		600	8
<i>S. epidermidis</i> ATCC 12228	75		600	8
<i>E. coli</i> ATCC 10536	150		300	2
<i>K. pneumoniae</i> (clinical strain 140)	75		300	4
<i>E. coli</i> (clinical strain 217)	150		300	2
<i>S. aureus</i> (clinical strain)	150		300	2
<i>S. sciuri</i> (environmental strain)	75		600	8
<i>Se. marcescens</i> (clinical strain)	75		300	4
<i>A. baumannii</i> (clinical strain 146)	300		600	2
<i>Enterobacter cloacae</i> (clinical strain 155)	150		>600	>4
<i>S. aureus</i> MR (clinical strain 136)	300		600	2
Tested microorganisms	<i>Acacia</i> honey		MFC	MFC/MIC ratio
	MIC			
<i>C. albicans</i> ATCC 20402	150		600	4
<i>S. cerevisiae</i> (instant yeast)	150		>600	>4
<i>C. vaginalis</i> (clinical strain 136)	300		>600	>2
<i>C. guilliermondii</i> ATCC 6260	150		>600	>4
<i>C. tropicalis</i> ATCC 1362	150		>600	>4

corresponding MBC/MIC ratios of ≤ 4 . Similarly, the evaluated honey samples exhibited fungistatic activity against the selected yeast, with an MFC/MIC ratio of ≤ 4 . All the above data are provided in Table 3.

3.3. Antioxidant Potential of Acacia Honey. The total phenolics, flavonoid, and tannin contents in the AH samples are listed in Table 4. Among the three different approaches used to assess the antioxidant activity of AH, the highest scavenging activity was observed using the DPPH assay, which revealed an IC_{50} value of 0.670 mg/mL, followed by the ABTS and β -carotene assays, which revealed the IC_{50} values of 1.065 mg/mL and >5 mg/mL, respectively.

3.4. Anticancer Activity of Acacia Honey. The results of the cytotoxicity evaluation of AH against breast cancer (MCF-7), lung cancer (A549), and colon cancer (HCT-116) cell lines are summarized in Figure 3. AH exhibited promising anticancer activity against the selected cancer cell lines, with the corresponding IC_{50} values of 5.053 μ g/mL, 5.382 μ g/mL, and 6.728 μ g/mL against the breast, colon, and lung cancer cell lines.

3.5. The in silico Analysis. In order to better understand the mechanistic effects underlying the biological effects of the compounds identified in AH, the binding affinities and molecular interactions of several receptors involved in these biological activities were assessed. The selection of the reported positions was based on the best binding score and RMSD equal to zero, as is commonly reported in the existing literature [22–24]. As presented in Table 5, while all the constituent compounds of AH exhibited negative binding energies (ranging from -3.8 to -11 kcal/mol) with the

different targeted receptors, the best scores were obtained for the complex compound no. 1 and the JIJ receptor. The number of conventional hydrogen bonds, the number of the closest interacting residues, and the closest distance during the ligand-receptor complex formation are presented in Table 6. It was predicted that compound no. 5 established 12 conventional hydrogen bonds with the TyrRS for *S. aureus* tyro-syl-tRNA synthetase (IJIJ). This was the highest number of H-bonds revealed in this study. Interestingly, 12 closest interacting residues were also observed in the same complex (Figures 4 and 5), among which Asp195 was the closest (2.037 Å). Moreover, it was predicted that compound no. 6 established 11 conventional H-bonds with IJNX and evolved 8 closest interacting residues. The distance to Arg1753 was just 2.020 Å, which confirmed that the compound was deeply embedded. Overall, the tripeptides (compound nos. 5 and 6) and aminocyclitol glycoside (compound no. 1) appeared to exhibit better activities toward the different targeted receptors compared to the other classes of compounds. This was particularly true for the tripeptides (Asp-Trp-His and Trp-Arg-Ala) (Figures 4 and 5) (see Figure 6).

4. Discussion

The present study reports eight dominant phytochemicals and three small peptide-like proteins identified in AH using the LC-MS technique. Several phytochemicals have been reported previously in AH [25–28]. The techniques such as liquid chromatography together with UV detection and liquid chromatography-electrochemical detection (LC-ECD) are often employed to determine the contents of phenolic acids in honey samples [26, 29–31]. In 2014, Wang and colleagues demonstrated that the AH collected from

TABLE 4: Antioxidant activities of *Acacia* honey sample as compared to butylated hydroxytoluene (BHT) and ascorbic acid (AA).

Test systems	<i>Acacia</i> honey	(BHT)	(AA)
Total flavonoids content (mg QE/g) extract)	0.400 ± 0.053c	—	—
Total tannins content (mg TAE/g) extract)	5.352 ± 0.964 b	—	—
Total phenols content (mg GAE/g) extract)	6.546 ± 0.876a	—	—
DPPH IC ₅₀ (mg/ml)	0.670 ± 0.015c	0.023 ± 3 × 10 ⁻⁴	0.022 ± 5 × 10 ⁻⁴
ABTS-IC ₅₀ (mg/ml)	1.065 ± 0.116c	0.018 ± 4 × 10 ⁻⁴	0.021 ± 0.001
β-carotene IC ₅₀ (mg/ml)	5b	0.042 ± 3.5 × 10 ⁻³	0.017 ± 0.001

The letters (a–c) indicate a significant difference between the different antioxidant methods according to the Duncan test ($p < 0.05$). Data are presented as mean ± SD.

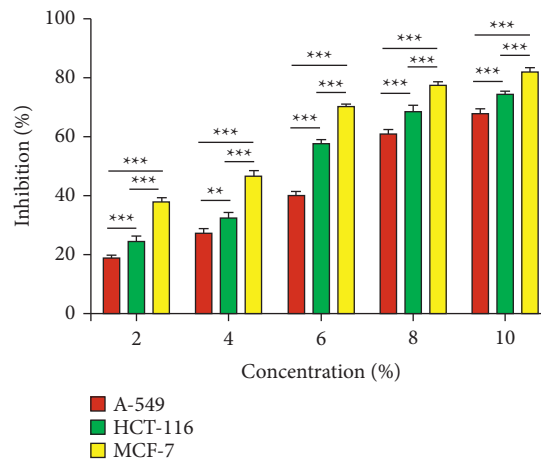


FIGURE 3: Effect of the *Acacia* honey cytotoxicity on breast (MCF-7), lung (A549), and colon (HCT-116) cancer cell lines according to concentration variation. Error bars indicate SEM (standard error of the mean) of three independent experiments. Significance; ns > 0.05, * $p < 0.05$, ** $p < 0.005$, *** $p < 0.0005$.

TABLE 5: Binding affinity of the identified compounds in honey (1–11) with the different targeted receptors (1JIJ, 2XCT, 2QZW, 1HD2, 4UYA, 1JNX, and 4BBG).

No	Compounds	Binding affinity (kcal × mol ⁻¹)						
		1JIJ	2XCT	2QZW	1HD2	4UYA	1JNX	4BBG
1	6-(alpha-D-Glucosaminyl)-1D-myo-inositol	-11.0	-7.7	-8.0	-7.7	-7.9	-7.1	-7.8
2	L-Gulonate	-7.8	-5.6	-6.5	-5.6	-6.3	-5.8	-7.3
3	Pro-Arg	-8.1	-6.7	-7.3	-6.0	-6.8	-6.1	-6.4
4	Anabasamine	-9.4	-6.6	-7.9	-6.4	-6.9	-6.2	-6.3
5	Bakankoside	-9.0	-7.0	-8.7	-6.6	-6.8	-6.5	-7.6
6	Asp-Trp-His	-8.9	-6.8	-8.2	-6.4	-7.4	-6.1	-7.7
7	Trp-Arg-Ala	-5.7	-4.4	-5.2	-4.0	-4.4	-4.5	-4.1
8	Palmitic amide	-6.7	-5.3	-6.0	-5.3	-5.0	-4.4	-4.9
9	Stearamide	-6.5	-4.3	-5.1	-4.9	-4.7	-4.5	-6.0
10	10,16-Heptadecadien-8-ynoic acid, 7-hydroxy, (E)	-6.8	-5.3	-5.9	-5.1	-5.6	-4.0	-4.4
11	14-Fluoro-myristic acid	-5.9	-4.7	-4.8	-4.5	-4.5	-3.8	-4.2

beekeepers in the region of Shaanxi (China) was rich in chlorogenic acid, p-hydroxybenzoic acid, ellagic acid, gallic acid, syringic acid, rosmarinic acid, and protocatechuic acid [26]. Kaempferol rhamnosides and rhamnosyl glucosides have been reported as the markers for AH [32, 33]. In the present study, a pyridine alkaloid compound named anabasamine was isolated, which has also been reported previously in the chemical composition analysis of *Anabasis aphylla* L. [34, 35]. Anabasamine is reported to possess weak

anti-acetylcholinesterase and anti-inflammatory properties [36, 37]. Three small peptide-like proteins (two tripeptides and one dipeptide) were also identified in the present study. Previously, Al Aerjani and colleagues have also used the same technique (LC-MS) and reported identifying short and cyclic peptides in the *A. hamulosa* honey with high medicinal effects, including antioxidant, antimicrobial, and antitumor effects. These peptides were also reported as potential weight loss-inducing peptides [31]. The small

TABLE 6: Conventional hydrogen-bonding, the number of closest interacting residues and distance to closest interacting residue (Å) of the compound with best scores (1, 5, and 6) with the different targeted receptors (1JIJ, 2XCT, 2QZW, 1HD2, 4UYA, 1JNX, and 4BBG).

No.	Chemical structure	Receptor	Conventional H-bonds	No. closest interacting residues	Closest interacting residue	
					Residue	Distance (Å)
1		1JIJ	4	6	Thr75	1.864
		2XCT	4	6	Met1113	2.617
		2QZW	5	6	Arg192	2.088
		1HD2	7	4	Arg86	2.139
		4UYA	7	7	Gly346	1.987
		1JNX	6	6	Glu1836	2.028
		4BBG	5	6	Arg221	2.154
5		1JIJ	12	12	Asp195	2.037
		2XCT	6	9	Ser1098	2.334
		2QZW	9	7	Thr222	2.179
		1HD2	9	7	Asn76	1.818
		4UYA	4	5	Asp289	1.877
		1JNX	7	5	Gly1710	2.079
		4BBG	8	8	Ser235	2.180
6		1JIJ	9	11	Asp177	1.891
		2XCT	11	5	Gly1111	1.912
		2QZW	10	12	Thr222	1.840
		1HD2	9	5	Leu140	2.072
		4UYA	7	6	Phe290	2.422
		1JNX	11	8	Arg1753	2.020
		4BBG	10	11	Ala218	1.956

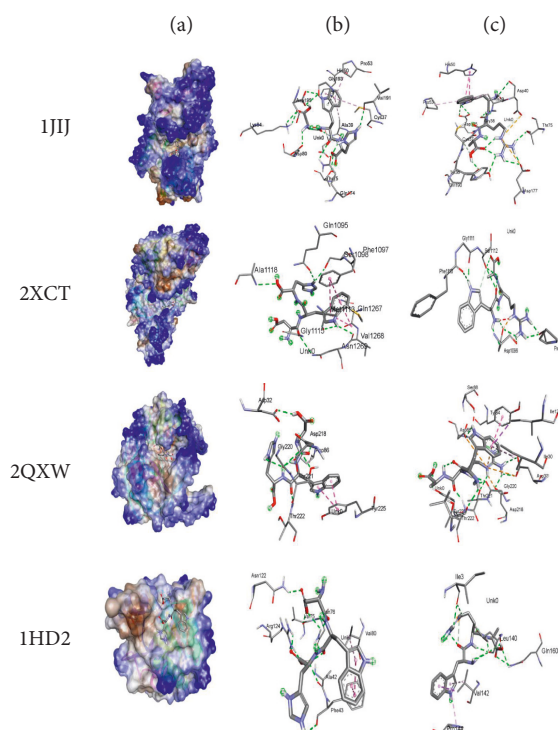


FIGURE 4: 3D illustrations of the selected honey compounds (5 and 6), which possessed the highest binding scores and the targeted receptors (a); the corresponding closest 3D interactions for compounds nos. 5 (b) and 6 (c).

peptide-like proteins identified in the honey samples in the present study were two tripeptides (Asp-Trp-His and Trp-Arg-Ala) and a dipeptide (Pro-Arg). Previous studies have demonstrated that peptides containing tyrosine, arginine,

tryptophan, methionine, lysine, cysteine, and histidine residues exhibit higher antioxidant activities [38]. Recently, it was demonstrated that tripeptides (Asn-Asn-Asn, His-Phe-Gln, Gln-His-Phe, Thr-Leu-Trp, and Gln-Phe-Tyr)

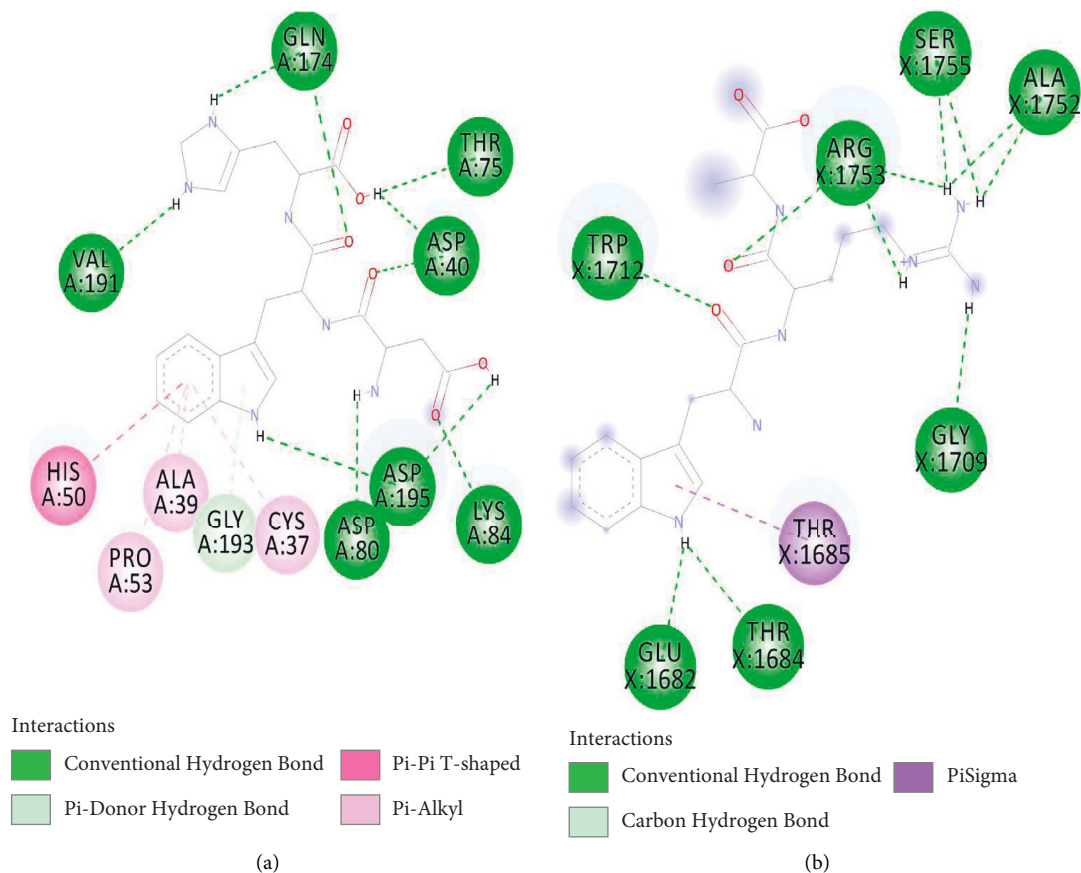


FIGURE 5: 2D diagrams of the closest interactions exhibited by the complexes compound 5-1JJJ (a) and compound 6-1JNX (b), which showed the most significant molecular interactions.

identified in the aqueous and methanolic extracts of *Allium subhirsutum* L. (bulbs) interacted with the structural and nonstructural proteins of SARS-CoV-2 with high binding energy [39].

Several studies have highlighted that honey exhibits antimicrobial potential, particularly against a wide spectrum of pathogenic bacteria, including both Gram-positive and Gram-negative bacteria [40–43]. The emergence of novel drug-resistance bacterial strains has instigated the search for novel phytochemicals with antimicrobial potential. The complexity of the chemical composition of honey and its intrinsic characteristics contribute to the valuable antimicrobial properties that honey exhibits [40]. Several mechanisms and target bacterial sites could be responsible for this antimicrobial property of honey, rendering honey resistance a rare event [41]. The honey that has been most commonly investigated for its antimicrobial potential is Manuka honey. The antimicrobial potential of this honey has mainly been associated with the high value of methylglyoxal (MGO) [42]. A comparative analysis of the antibacterial effects of Manuka honey and AH revealed a valuable result in favor of AH [43]. In addition, AH from various geographical regions has been

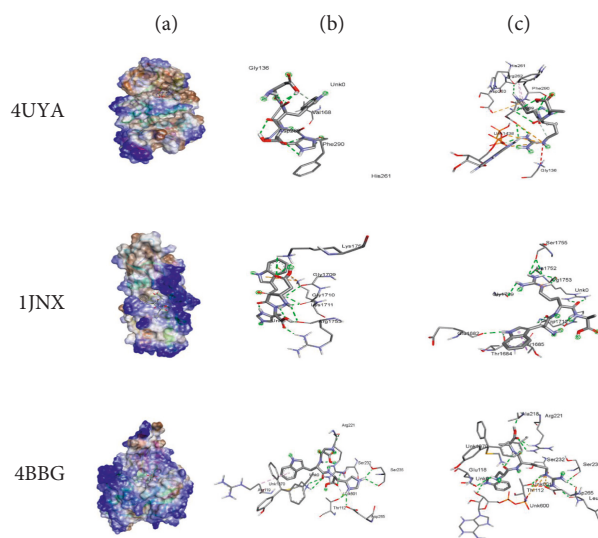


FIGURE 6: 3D illustrations of the selected honey compounds (5 and 6), which possessed the highest binding scores and the targeted receptors (a); the corresponding closest 3D interactions for compounds nos. 5 (b) and 6 (c).

demonstrated to exhibit interesting antimicrobial potentials in several studies [5]. The studies exploring the proprieties of honey samples from Saudi Arabia have revealed significant variation in their physicochemical characteristics, total phenolic contents, pigments, hydrogen peroxide levels, and dicarbonyl compounds with the botanical origin, climate, and altitudes, particularly for the AH samples from this region [7, 44, 45].

In the present study, the antibacterial activity of AH was observed to vary in a dose-dependent manner, with higher antibacterial activities achieved at 100% AH concentration. At this concentration, the efficiency of AH was higher, with the highest mGIZ value obtained against *S. aureus* (clinical strain), *E. coli* (clinical strain 217), and *S. epidermidis* ATCC 12228 (mGIZ values: 40.67 ± 0.57 mm, 50.33 ± 0.57 mm, and 40.33 ± 0.57 mm, respectively). These results were interesting when compared to the mGIZ values observed for ampicillin, which was used as a reference. A recent study on different kinds of honey from Saudi Arabia revealed that AH exhibited a more potent antibacterial effect against several microbial strains, with higher mGIZ values obtained against Gram-positive bacteria compared to when using other kinds of honey [46]. Moreover, *B. cereus*, *S. aureus*, *E. coli*, and *Salmonella enteritidis* were reported as the most sensitive bacterial species [5, 46]. These findings were consistent with the results of the present study, particularly those obtained for *S. aureus* and *E. coli*. The present study also revealed that the antimicrobial potential of AH was dose-dependent, with the highest activity observed when pure honey was used. In another study, the authors concluded that the antimicrobial activity increased when water-diluted honey (33% w/v) was used rather than non-diluted honey [46]. This could be due to the difference in the honey moisture rate. The most resistant bacteria were *A. baumannii* (clinical strain 146), with the mGIZ value of approximately 6.00 ± 0 mm. A recent study investigating the novel nano-composite hydrogels comprising silver nanoparticles (AgNPs) and AH revealed that these hydrogels exhibited strong bactericidal activity against standard nosocomial strains, while *A. baumannii* exhibited a notable resistance [47]. Therefore, it was inferred that *A. baumannii* could exhibit resistance against AH, although this must be confirmed through further investigation.

Furthermore, the activity of AH against the yeast and molds was almost negligible, except for a moderate activity exhibited against *S. cerevisiae* with an mGIZ value of 20 ± 0 mm, which was higher than the corresponding mGIZ value obtained for amphotericin (7.33 ± 0.57 mm). Mracevic et al. [48] evaluated 20 kinds of honey collected from different regions of Serbia, including AH, against *C. albicans* and reported that none exhibited any potency. Another study evaluated several honey samples, including AH, and reported resistance in 9 fungal strains (*F. oxysporum*, *A. brasiliensis*, *A. alternata*, *D. stemonitis*, *T. longibrachiatum*, *T. harzianum*, *P. canescens*, *P. cyclopium*, and *C. albicans*) [49]. These findings are consistent with the results obtained in the present study, indicating that most fungal strains could be resistant to honey. The mechanism of this resistance should, however, be deciphered through further investigation.

The microdilution assay performed for twelve bacteria revealed a significant bactericidal activity of AH against *P. aeruginosa* (clinical strain SP-40), *E. coli* ATCC 10536, *E. coli* (clinical strain 217), *S. aureus* (clinical strain), *A. baumannii* (clinical strain 146), and *S. aureus* MR (clinical strain 136) strains, with the obtained MBC/MIC ratio of 2. In the case of the yeast and fungi, fungistatic effects were observed mainly, with the MFC/MIC ratio of ≥ 4 , which could be the reason for the fungal resistance to AH. Previous studies on the antimicrobial effects of the AH obtained from different regions against a wide variety of bacteria, yeast, and mold strains have reported that the corresponding MIC and MBC/MFC values vary with the chemical composition of the honey sample evaluated. Stojkowska and colleagues [47] reported that AH collected from Serbia in 2018 exhibited antimicrobial activity against a huge collection of Gram-positive and Gram-negative bacteria, and also against certain fungal strains. These authors reported MIC values ranging from 25 mg/mL for *B. cereus* ATCC 10876 strain to >100 mg/mL for *E. coli* ATCC 25922, *P. aeruginosa* ATCC 10145, *S. typhimrium* ATCC 14028, *S. epidermidis* ATCC 12228, *K. pneumoniae* ATCC 70063, *B. subtilis* ATCC 6633, *E. faecalis* ATCC 29212, and *Micrococcus lysodeikticus* ATCC 4698. The AH from Serbia also exhibited anti-*C. albicans* activity with an MFC value of >100 mg/mL [49]. Moreover, Yousaf and colleagues [50] reported that the AH collected from Malaysia exhibited activity against *S. aureus*, *E. coli*, *S. typhimrium*, *P. aeruginosa*, *Listeria monocytogenes*, *Clostridium jejuni* ATCC 29428, and *B. cereus*, with the MIC values ranging from 25% to 50%, while the MBC values ranged from 50% to $>50\%$. A comparison of the results obtained in the present study with the findings of previous studies revealed that AH exhibits an efficient antimicrobial activity against most bacterial strains, particularly the Gram-positive bacteria [51, 52]. The variation in the antimicrobial effect of AH observed in several studies could be attributed mainly to the variations in the composition and constituent phytochemical compounds of AH, which are, in turn, influenced by the botanical origin and the physicochemical properties (osmotic effect, pH, and the presence of undefined molecules with antimicrobial effect) of the honey sample [52–54]. Therefore, AH could be a valuable alternative treatment option for the pathologies associated with drug-resistant bacterial strains. However, the incomplete knowledge regarding the constituent bioactive phytochemicals and their mechanisms of action creates another level of complexity in the use of AH for the treatment of infections. Such reasons have limited the application of honey in conventional medicine in the absence of standardization of antibacterial activity [55, 56].

Since honey is derived from plants, it contains several phytochemicals that confer antioxidant properties to honey. The antioxidant potential of honey is due to the presence of bioactive compounds, such as phenols, flavonoids, and tannins, which are capable of inactivating the free radicals generated during diverse cellular processes. Accumulation of free radicals could have a cytotoxic effect or maybe potentially carcinogenic. In the present study, the free radical-scavenging activity of AH

was investigated using three approaches: DPPH radical-scavenging activity, ABTS radical-scavenging activity, and β -carotene/linoleic acid method. These three methods revealed IC_{50} values of 0.670 mg/mL, 1.065 mg/mL, and >5 mg/mL, respectively, with the highest scavenging activity observed in the DPPH assay. These results were comparable to those obtained for butylated hydroxytoluene (BHT) and ascorbic acid (AA), which were used as references. Therefore, it was inferred that AH derived from the Hail region exhibited significant antioxidant potency. In addition, the total phenolics content (TPC, 6.546 mg GAE/g), total flavonoid contents (TFC, 0.400 mg QE/g), and tannin contents (5.352 mg TAE/g) obtained were interesting. According to a previous report, the AH from Ordu in Turkey exhibited an IC_{50} value of 24.53 ± 1.26 mg/mL when using the DPPH approach, with the estimated total phenol content of 51.91 ± 1.32 mg/100 g GAE [57]. In another study, the AH from central Serbia exhibited an antioxidant potential with $IC_{50} = 8.36 \pm 0.42$ mg Trolox/kg honey, total phenolics content = 68.48 ± 5.53 mg GAE/kg honey, and flavonoid content = 18.59 ± 1.71 mg QUE/kg honey [49]. The AH from the Hail region used in the present study, comparatively, exhibited a higher antioxidant activity. On the contrary, the total phenolics content (TPC) and total flavonoid content (TFC) observed for Malaysian AH were relatively higher (79.08 mg GAE/1 mg and 20.98 mg CE/1 mg, respectively) compared to the AH used in the present study, indicating that the antioxidant properties of the former would enable inhibiting the growth of breast cancer cells through apoptosis [58]. However, even though the AH from the Hail region contained lower levels of TPC and TFC compared to Malaysian AH, higher anticancer activity was observed for this AH in the MTT assay. The TPC and TFC contents may vary with the geographical and botanical origins of the honey samples. A strong antioxidant capacity of AH may, therefore, not be related to the phenolics, flavonoid, or tannin contents only. The phytochemical profiling in the present study revealed the presence of various chemical compounds, such as polypeptides, in the AH, and the synergies among these compounds could also be involved in the mechanism underlying the antioxidant activity of this honey.

Several *in vitro* and *in vivo* studies have demonstrated the anticancer activity of various kinds of honey against different types of cancers. Raw honey contains high levels of polyphenols and flavonoids, which are considered the main factors contributing to antioxidant and anticancer effects. Studies have also demonstrated the efficiency of honey as a chemo-protectant or an adjuvant in cancer treatment [59]. In addition, certain phytochemicals derived from honey exert a therapeutic effect for the treatment of various types of cancer and are, therefore, to be considered prominent chemo-preventive agents [60]. There could be several mechanisms underlying the anticancer effect of honey, including cell cycle arrest, induction of apoptosis, modulation of the mitochondrial pathway, membrane permeabilization, and anti-inflammatory and immunomodulatory effects [2]. AH is considered a potential therapeutic candidate for both the prevention and treatment of cancer. This potential of AH, however, varies in the degree of effectiveness with the floral source of AH and/or the geographical regions from which the AH samples are derived [61].

In the present study, the anticancer potential of the AH from the Hail region of Saudi Arabia was evaluated based on the MTT assay using 3 cancer cell lines: breast cancer (MCF-7), lung cancer (A549), and colon cancer (HCT-116) cell lines. All three cell lines were treated with different concentrations of AH, and it was observed that the proliferation of cancer cell lines was inhibited in a dose-dependent manner. The IC_{50} values obtained for AH against the breast, colon, and lung cancer cell lines were $5.053 \mu\text{g/mL}$, $5.382 \mu\text{g/mL}$, and $6.728 \mu\text{g/mL}$, respectively. These results demonstrated a cytotoxic effect of the AH from the Hail region against cancer cells. In a previous investigation, doxorubicin was reported to exhibit an IC_{50} value of $1.2 \pm 0.036 \mu\text{g/mL}$ for the HCT-116 cell line and $1.09 \pm 0.044 \mu\text{g/mL}$ for the MCF-7 cell line [7]. Another study investigating the AH from the Asir region (southwest of Saudi Arabia) reported a notable cytotoxic effect against HCT-116, MCF-7, and HepG2 cell lines. The authors also reported that the AH from different altitudes of this region exerted different degrees of *in vitro* effects on the cancer cell lines [7]. The high-altitude AH exhibited higher activity against human cancer cell lines compared to that exhibited by the low-altitude AH, and there was a noticeable difference in the total phenolics and flavonoid contents as well. In the present study, AH exhibited a higher anticancer activity against HCT-116 and MCF-7 cancer cell lines, which could be attributed to the differences in the composition of AH from the Hail region and that from the Asir region.

Previous studies have also highlighted that AH from Malaysia inhibits the growth of breast cancer cell line MCF-7 via apoptosis. The induction of apoptosis occurred after 2 h, while the formation of the apoptotic bodies could be detected within 6 h of the AH treatment [58]. The IC_{50} value of AH from Malaysia was $5.49 \mu\text{g/mL}$ after 72 h, while that of the AH used in the present study was $5.053 \mu\text{g/mL}$ after just 24 h of treatment, indicating the higher cytotoxic activity of the latter.

Another study targeting the lung cell cancer line NCI-H460 revealed that AH could inhibit cancer cell proliferation and cause cell cycle arrest at G0/G1 phase. In addition, it was demonstrated that AH might induce the downregulation of bcl-2 and p53 genes [62]. This cytotoxic effect was also observed in the present study against the lung cancer cell line A549.

Recently, studies have revealed that generating silver (Ag) nanoparticles in the presence of AH (Abha, Saudi Arabia) and the plant extract of *Calotropis procera* produces exhibit a synergic effect with prominent anticancer potentials through the inhibition of the liver cancer cell line HepG2 growth with good immunostimulatory effect [63]. Earlier studies have reported that the anticancer potential of honey may vary with the subtype of honey, even when the same honey from different geographical regions is used. This variation is attributed to the variations in the constituents of the honey samples [64]. The anticancer properties of honey have been attributed mainly to the phytochemicals present in the honey, particularly the flavonoids and phenolic acids. These phytochemicals confer cancer prevention and treatment abilities by interfering in several cellular pathways [65]. In the present study, interesting anticancer activities were

demonstrated by AH against three cancer cell lines. In addition to attributing this anticancer activity to the quantitative evaluation of flavonoids and phenolic acids, we should also consider other bioactive compounds that might be contributing to the qualitative constitution of honey. In the present study, tripeptides and aminocyclitol glycoside present in the AH from the Hail region were observed to contribute to enhancing the biological potency of honey.

Furthermore, the binding affinities and molecular interactions of the constituents of honey were assessed against several receptors involved in the studied biological activities (Figure S1). One of these receptors is 1JII, which is a *S. aureus* tyrosyl-tRNA synthetase and is commonly recognized to provide a structural basis for designing novel antimicrobial agents [66, 67]. Another one is 2×ct, which is a type IIA topoisomerase that cleaves and then ligates DNA strands to regulate the DNA topology. Type IIA topoisomerases represent a major class of antibacterial and anticancer drug targets [68]. The receptor 2QZW is an aspartic proteinase Sap 1 secreted from *Candida albicans*, which reportedly plays a key role in superficial *Candida* infections [69]. The human peroxiredoxin 5, 1hd2, reduces hydrogen- and alkyl hydroperoxides and is implicated in the antioxidant protective mechanisms and cellular signal transduction [70]. The MLK4 kinase domain 4uya regulates the JNK, p38, and ERK kinase signaling pathways. Mutations in MLK4 have been detected in several cancers [71]. The receptor 1JNX is the C-terminal BRCT region of BRCA1 and is essential for DNA repair, tumor suppressor functions, and transcriptional regulation [72]. The receptor 4bbg is the mitotic kinesin Eg5 and is critical for the assembly of the mitotic spindle and a promising chemotherapy target [73]. All the compounds present in honey exhibited negative binding energies (ranging from -3.8 to -11 kcal/mol) with the different targeted receptors. As reported in several studies, the variation in the binding affinity could mainly be attributed to the chemical structure of the compound [22, 74, 75]. Usually, there is a strong relationship between the structure and the activity of a compound, which explains the importance of SAR and QSAR analyses. In the present study, the best binding score was obtained for the 1JII-aminocyclitol glycoside complex. The tripeptide Asp-Trp-H is formed 12 conventional H bonds with the TyrRS in the *S. aureus* tyrosyl-tRNA synthetase (1JII). The closest molecular interactions included 12 residues in the active site. Aminocyclitol glycoside was deeply embedded in the active site of the different targeted receptors (1.864–2.617 Å) and was at a distance of only 2.037 Å from the Asp195 residue in 1JII, for which the highest binding affinity was reported. The closely related ligand-amino acids/protein complexes could explain the biological activity [21–24]. The compound 6 (Asp-Trp-His) was predicted to form 11 conventional H-bonds with 1JNX and evolve 8 closest interacting residues. It was at a distance of only 2.020 Å from Arg1753, which satisfactorily explained the potential biological activity. Furthermore, the molecular interactions of the different complexes usually included certain key residues associated with the pharmacological effects [67, 74, 75]. Overall, the biological effects of the phytochemical

compounds in honey appeared to be thermodynamically feasible, particularly those of the tripeptides and aminocyclitol glycoside. These computational results in parallel with the findings of *in vitro* analysis could explain the promising effects of AH and its ethnopharmaceutical use worldwide, particularly in the Middle East region. Owing to the complexity of the composition of AH, there is incomplete knowledge regarding its constituent phytochemicals and their mechanisms of action, which is the main reason for the limited application of honey in conventional medicine in the absence of standardization of biological activities. Therefore, further studies are required to isolate and characterize each compound for a better understanding of the involved mechanism of action.

5. Conclusions

The present study reports the potential biological activities of the AH from the Hail region of Saudi Arabia. A broad-range bactericidal effect of AH against a wide spectrum of clinically relevant bacterial strains was observed. On the other hand, only fungistatic activity was observed for the yeast and the molds. A notable cytotoxic effect of AH was observed on the three cancer cell lines evaluated. Among the identified phytochemicals, the tripeptides and aminocyclitol glycoside exhibited considerable biological effects of enhancing the antimicrobial, anticancer, and antioxidant potentials of AH. In addition, huge amounts of polyphenols and flavonoids were detected in the evaluated honey samples. Nonetheless, further studies on the isolation, characterization, and assessment of these biological activities of the compounds in AH in the present study should be conducted to support the above-stated findings. The findings of the present study demonstrate the potential of AH as a source of natural bioactive compounds that could be used for therapeutic purposes.

Data Availability

The data used to support the findings of this study are available from the corresponding author upon request.

Conflicts of Interest

The authors declare no conflicts of interest.

Acknowledgments

This research has been funded by Scientific Research Deanship at the University of Hail, Hail, Saudi Arabia through project number RG-21 109.

Supplementary Materials

Figure S1: The 2D diagrams of the closest interactions exhibited by AH major identified compounds complexed with the different targeted receptors displaying the most significant molecular interactions. (*Supplementary Materials*)

References

- [1] F. El-Gamal, A. Bajubair, A. Hejji, A. Jarwan, and J. N. Salah, "Complementary and alternative medicine practice and perceptions of Saudi subjects in western region of Saudi Arabia," *Middle East Journal of Family Medicine*, vol. 7, no. 10, p. 88, 2022.
- [2] M. Waheed, M. B. Hussain, A. Javed et al., "Honey and cancer: a mechanistic review," *Clinical Nutrition*, vol. 38, no. 6, pp. 2499–2503, 2019.
- [3] G. Cebrero, O. Sanhueza, M. Pezoa et al., "Relationship among the minor constituents, antibacterial activity and geographical origin of honey: a multifactor perspective," *Food Chemistry*, vol. 315, Article ID 126296, 2020.
- [4] I. A. Alotibi, S. M. Harakeh, M. Al-Mamary et al., "Floral markers and biological activity of Saudi honey," *Saudi Journal of Biological Sciences*, vol. 25, no. 7, pp. 1369–1374, 2018.
- [5] A. G. Hegazi, F. M. Al Guthami, A. F. M. Al Gethami, A. A. Saleh, and E. A. Fouad, "Potential antibacterial activity of some Saudi Arabia honey," *Veterinary World*, vol. 10, no. 2, pp. 233–237, 2017.
- [6] H. A. Ghramh, K. A. Khan, and A. M. A. Alshehri, "Antibacterial potential of some Saudi honeys from Asir region against selected pathogenic bacteria," *Saudi Journal of Biological Sciences*, vol. 26, no. 6, pp. 1278–1284, 2019.
- [7] M. E. A. Mohammed, A. A. Shati, M. Y. Alfaifi et al., "Acacia honey from different altitudes: total phenols and flavonoids, laser-induced fluorescence (LIF) spectra, and anticancer activity," *Journal of International Medical Research*, vol. 48, no. 8, Article ID 030006052094345, 2020.
- [8] A. A. Al-Ghamdi, *Comprehensive Study for Current Bee-keeping Industry of Imported and Native Honeybee in Kingdom of Saudi Arabia*, Final Report King Abdulaziz City for Science and Technology General Administration of Grant Program King Saud University, Riyadh, Saudi Arabia, 2010.
- [9] L. A. Marghitas, D. S. Dezmirean, C. B. Pocol, I. L. E. A. Marioara, O. Bobis, and I. Gergen, "The development of a biochemical profile of *Acacia* honey by identifying biochemical determinants of its quality," *Notulae Botanicae Horti Agrobotanici Cluj-Napoca*, vol. 38, no. 2, pp. 84–90, 2010.
- [10] M. Adnan, A. J. Siddiqui, W. S. Hamadou et al., "Phytochemistry, bioactivities, pharmacokinetics and toxicity prediction of *Selaginella repanda* with its anticancer potential against human lung, breast and colorectal carcinoma cell lines," *Molecules*, vol. 26, no. 3, p. 768, 2021.
- [11] F. Haddaji, A. Papetti, E. Noumi et al., "Bioactivities and in silico study of *Pergularia tomentosa* L. phytochemicals as potent antimicrobial agents targeting type IIA topoisomerase, TyrRS, and Sap1 virulence proteins," *Environmental Science and Pollution Research*, vol. 28, no. 20, pp. 25349–25367, 2021.
- [12] E. Noumi, M. Snoussi, E. H. Anouar et al., "HR-LCMS-based metabolite profiling, antioxidant, and anticancer properties of *Teucrium polium* L. methanolic extract: computational and *in vitro* study," *Antioxidants*, vol. 9, no. 11, p. 1089, 2020.
- [13] K. Mseddi, F. Alimi, E. Noumi et al., "*Thymus musilii* Velen. as a promising source of potent bioactive compounds with its pharmacological properties: in vitro and in silico analysis," *Arabian Journal of Chemistry*, vol. 13, no. 8, pp. 6782–6801, 2020.
- [14] K. Aouadi, H. Hajlaoui, S. Arraouadi, S. Ghannay, M. Snoussi, and A. Kadri, "HPLC/MS phytochemical profiling with antioxidant activities of *Echium humile* desf. extracts: ADMET prediction and computational study targeting human peroxiredoxin 5 receptor," *Agronomy*, vol. 11, no. 11, p. 2165, 2021.
- [15] E. H. K. Ikram, K. H. Eng, A. M. M. Jalil et al., "Antioxidant capacity and total phenolic content of Malaysian underutilized fruits," *Journal of Food Composition and Analysis*, vol. 22, no. 5, pp. 388–393, 2009.
- [16] M. Alreshidi, E. Noumi, L. Bouslama et al., "Phytochemical screening, antibacterial, antifungal, antiviral, cytotoxic, and anti-quorum-sensing properties of *Teucrium polium* L. aerial parts methanolic extract," *Plants*, vol. 9, no. 11, p. 1418, 2020.
- [17] H. Hajlaoui, M. Snoussi, E. Noumi, S. Zanetti, R. Ksour, and A. Bakhrouf, "Chemical composition, antioxidant and antibacterial activities of the essential oils of five Tunisian aromatic plants," *Italian Journal of Food Science*, vol. 22, pp. 320–329, 2010.
- [18] D. Gatsing, J. A. Mbah, and I. H. Garba, "An antisalmonella agent from the leaves of *Glossocalyx brevipes* benth (*Monimiaceae*)," *Pakistan Journal of Biological Sciences*, vol. 9, no. 1, 2006.
- [19] D. Gatsing, V. Tchakoute, D. Ngamga et al., "In vitro antibacterial activity of *Crinum purpurascens* herb leaf extract against the *salmonella* species causing typhoid fever and its toxicological evaluation," *Iranian Journal of Medical Sciences*, vol. 34, no. 2, 2009.
- [20] M. Adnan, A. J. Siddiqui, W. S. Hamadou et al., "Deciphering the molecular mechanism responsible for efficiently inhibiting metastasis of human non-small cell lung and colorectal cancer cells targeting the matrix metalloproteinases by *Selaginella repanda*," *Plants*, vol. 10, no. 5, p. 979, 2021.
- [21] A. Akacha, R. Badraoui, T. Rebai, and L. Zourgui, "Effect of *Opuntia ficus indica* extract on methotrexate-induced testicular injury: a biochemical, docking and histological study," *Journal of Biomolecular Structure and Dynamics*, vol. 40, no. 10, pp. 4341–4351, 2020.
- [22] R. Badraoui, M. Adnan, F. Bardakci, and M. M. Alreshidi, "Chloroquine and hydroxychloroquine interact differently with ACE2 domains reported to bind with the coronavirus spike protein: mediation by ACE2 polymorphism," *Molecules*, vol. 26, no. 3, p. 673, 2021.
- [23] K. Hchicha, M. Korb, R. Badraoui, and H. Naili, "A novel sulfate-bridged binuclear copper (II) complex: structure, optical, ADMET and in vivo approach in a murine model of bone metastasis," *New Journal of Chemistry*, vol. 45, no. 31, Article ID 13784, 2021.
- [24] N. Zammel, M. Saeed, N. Bouali et al., "Antioxidant and anti-inflammatory effects of *Zingiber officinale* roscoe and *Allium subhirsutum*: in silico, biochemical and histological study," *Foods*, vol. 10, no. 6, p. 1383, 2021.
- [25] M. Biesaga and K. Pyrzyńska, "Stability of bioactive polyphenols from honey during different extraction methods," *Food Chemistry*, vol. 136, no. 1, pp. 46–54, 2013.
- [26] J. Wang, X. Xue, X. Du et al., "Identification of *Acacia* honey adulteration with rape honey using liquid chromatography-electrochemical detection and chemometrics," *Food Analytical Methods*, vol. 7, no. 10, pp. 2003–2012, 2014.
- [27] N. Czipa, C. J. C. Phillips, and B. Kovács, "Composition of *Acacia* honeys following processing, storage and adulteration," *Journal of Food Science & Technology*, vol. 56, no. 3, pp. 1245–1255, 2019.
- [28] N. M. Mădaş, L. A. Mărghitas, D. S. Dezmirean et al., "Volatile profile and physico-chemical analysis of *Acacia* honey for geographical origin and nutritional value determination," *Foods*, vol. 8, no. 10, p. 445, 2019.

- [29] Y. Liang, W. Cao, W. J. Chen, X. H. Xiao, and J. B. Zheng, "Simultaneous determination of four phenolic components in *Citrus* honey by high performance liquid chromatography using electrochemical detection," *Food Chemistry*, vol. 114, no. 4, pp. 1537–1541, 2009.
- [30] T. Istasse, N. Jacquet, T. Berchem, E. Haubruge, B. K. Nguyen, and A. Richel, "Extraction of honey polyphenols: method development and evidence of *cis* isomerization ubertas academica," *Analytical Chemistry Insights*, vol. 11, Article ID ACI.S39739, 2016.
- [31] W. M. A. Al Aerjani, S. A. Abu-Melha, K. A. Khan et al., "Presence of short and cyclic peptides in *Acacia* and *Ziziphus* honeys may potentiate their medicinal values," *Open Chemistry*, vol. 19, no. 1, pp. 1162–1173, 2021.
- [32] I. Martos, M. Cossentini, F. Ferreres, and F. A. Tomás-Barberán, "Flavonoid composition of Tunisian honeys and propolis," *Journal of Agricultural and Food Chemistry*, vol. 45, no. 8, pp. 2824–2829, 1997.
- [33] O. Escuredo, L. R. Silva, P. Valentão, M. C. Seijo, and P. B. Andrade, "Assessing *Rubus* honey value: pollen and phenolic compounds content and antibacterial capacity," *Food Chemistry*, vol. 130, no. 3, pp. 671–678, 2012.
- [34] S. Z. Mukhamedzhanov, K. A. Aslanov, A. S. Sadykov, V. B. Leont'ev, and V. K. Kiryukhin, "Structure of anabasamine," *Chemistry of Natural Compounds*, vol. 4, no. 3, pp. 136–138, 1968.
- [35] S. X. Lin, M. A. Curtis, and J. Sperry, "Pyridine alkaloids with activity in the central nervous system," *Bioorganic & Medicinal Chemistry*, vol. 28, no. 24, Article ID 115820, 2020.
- [36] A. Panthong, D. Kanjanapothi, Y. Thitiponpunt, T. Taesotikul, and D. Arbain, "Anti-inflammatory activity of the alkaloid anabasamine," *Doklady Akademii Nauk UzSSR*, vol. 198, pp. 45–47, 1984.
- [37] Z. Tilyabaev and A. A. Abduvakhobov, "Alkaloids of *Anabasis aphylla* and their cholinergic activities," *Chemistry of Natural Compounds*, vol. 34, no. 3, pp. 295–297, 1998.
- [38] H. Guo, Y. Kouzuma, and M. Yonekura, "Structures and properties of antioxidative peptides derived from royal jelly protein," *Food Chemistry*, vol. 113, no. 1, pp. 238–245, 2009.
- [39] M. Snoussi, E. Noumi, A. Mosbah et al., "Tripeptides from *Allium subhirsutum* L. extracts: pharmacokinetics properties, toxicity prediction and in silico study against SARS-CoV-2 enzymes and pro-inflammatory proteins," *Cellular and Molecular Biology*, vol. 67, no. 4, pp. 143–162, 2022.
- [40] S. B. Almasaudi, A. A. Al-Nahari, E. S. M. Abd El-Ghany et al., "Antimicrobial effect of different types of honey on *Staphylococcus aureus*," *Saudi Journal of Biological Sciences*, vol. 24, no. 6, pp. 1255–1261, 2017.
- [41] P. Combarros-Fuertes, J. M. Fresno, M. M. Estevinho, M. Sousa-Pimenta, M. E. Tornadijo, and L. M. Estevinho, "Honey: another alternative in the fight against antibiotic-resistant bacteria?" *Antibiotics*, vol. 9, no. 11, p. 774, 2020.
- [42] J. A. Lane, J. Calonne, H. Slattery, and R. M. Hickey, "Oligosaccharides isolated from MGO™ manuka honey inhibit the adhesion of *Pseudomonas aeruginosa*, *Escherichia coli* O157:H7 and *Staphylococcus aureus* to human HT-29 cells," *Foods*, vol. 8, no. 10, 2019.
- [43] K. Vesna, G. Bojan, and I. Tanja, "Agrores 2020," in *Proceedings of the International Symposium on Agricultural Sciences*, Banja Luka, Bosnia and Herzegovina, 2020.
- [44] M. E. A. Mohammed, W. Alargani, M. A. Suleiman, and H. A. Al-Graham, "Hydrogen peroxide and dicarbonyl compounds concentration in honey samples from different botanical origins and altitudes in the south of Saudi Arabia," *Current Research in Nutrition and Food Science Journal*, vol. 7, no. 1, pp. 150–160, 2019.
- [45] A. S. Alqarni, A. A. Owayss, and A. A. Mahmoud, "Physicochemical characteristics, total phenols and pigments of national and international honeys in Saudi Arabia," *Arabian Journal of Chemistry*, vol. 9, no. 1, pp. 114–120, 2016.
- [46] A. A. Owayss, K. Elbanna, J. Iqbal et al., "In vitro antimicrobial activities of Saudi honeys originating from *Ziziphus spina-christi* L. and *Acacia gerrardii* Benth. trees," *Food science & nutrition*, vol. 8, no. 1, pp. 390–401, 2019.
- [47] J. Stojkowska, P. Petrovic, I. Jancic, M. T. Milenkovic, and B. Obradovic, "Novel nano-composite hydrogels with honey effective against multi-resistant clinical strains of *Acinetobacter baumannii* and *Pseudomonas aeruginosa*," *Applied Microbiology and Biotechnology*, vol. 103, no. 20, pp. 8529–8543, 2019.
- [48] S. D. Mračević, M. Krstic, A. Lolic, and S. Razic, "Comparative study of the chemical composition and biological potential of honey from different regions of Serbia," *Microchemical Journal*, vol. 152, Article ID 104420, 2020.
- [49] N. Z. Srećković, V. B. Mihailović, and J. S. Katanić-Stanković, "Physico-chemical, antioxidant and antimicrobial properties of three different types of honey from central Serbia," *Kragujevac Journal of Science*, vol. 41, pp. 53–68, 2019.
- [50] K. Yousof, N. K. Mar, N. H. Za, and M. R. I. Fitry, "Antibacterial properties of tualang, acacia and yemeni sumur honey against selected food spoilage bacteria and foodborne pathogens," *Food Research*, vol. 5, no. 1, pp. 448–460, 2021.
- [51] N. A. Albaridi, "Antibacterial potency of honey," *International Journal of Microbiology*, vol. 2019, Article ID 2464507, 10 pages, 2019.
- [52] J. M. Alvarez-Suarez, S. Tulipani, D. Díaz et al., "Antioxidant and antimicrobial capacity of several monofloral cuban honeys and their correlation with color, polyphenol content and other chemical compounds," *Food and Chemical Toxicology*, vol. 48, no. 8-9, pp. 2490–2499, 2010.
- [53] P. Combarros-Fuertes, L. M. Estevinho, L. G. Dias et al., "Bioactive components and antioxidant and antibacterial activities of different varieties of honey: a screening prior to clinical application," *Journal of Agricultural and Food Chemistry*, vol. 67, no. 2, pp. 688–698, 2019.
- [54] A. Jeddar, A. Kharsany, U. G. Ramsaroop, A. Bhamjee, I. E. Haffejee, and A. Moosa, "The antibacterial action of honey. An in vitro study," *South African Medical Journal*, vol. 67, no. 7, pp. 257–258, 1985.
- [55] P. H. S. Kwakman, A. A. Te Velde, L. de Boer, C. M. J. E. Vandenbroucke-Grauls, and S. A. J. Zaat, "Two major medicinal honeys have different mechanisms of bactericidal activity," *PLoS One*, vol. 6, no. 3, Article ID e17709, 2011.
- [56] R. Jenkins, A. Roberts, and H. L. Brown, "On the antibacterial effects of manuka honey: mechanistic insights," *Research and Reports in Biology*, vol. 6, pp. 215–224, 2015.
- [57] A. Gül and T. Pehlivan, "Antioxidant activities of some monofloral honey types produced across Turkey," *Saudi Journal of Biological Sciences*, vol. 25, no. 6, pp. 1056–1065, 2018.
- [58] M. A. Mohd Salleh, Z. Eshak, and W. I. Wan Ismail, "Acacia honey induces apoptosis in human breast adenocarcinoma cell lines (MCF-7)," *Jurnal Teknologi*, vol. 79, no. 4, 2017.
- [59] A. P. Sponghini, D. Rondonotti, F. Platini et al., "A Simon's two-stage design trial evaluating the potential role of a kind of honey in preventing chemotherapy-hematopoietic toxicities,"

- Journal of traditional and complementary medicine*, vol. 11, no. 5, pp. 466–469, 2021.
- [60] M. Badolato, G. Carullo, E. Cione, F. Aiello, and M. C. Caroleo, “From the hive: honey, a novel weapon against cancer,” *European Journal of Medicinal Chemistry*, vol. 142, pp. 290–299, 2017.
- [61] A. Muhammad, O. A. Odunola, M. A. Ibrahim et al., “Potential biological activity of acacia honey,” *Frontiers in Bioscience*, vol. 8, no. 2, pp. 771–357, 2016.
- [62] M. Aliyu, O. A. Odunola, A. D. Farooq et al., “Molecular mechanism of antiproliferation potential of *Acacia* honey on NCI-H460 cell line,” *Nutrition and Cancer*, vol. 65, no. 2, pp. 296–304, 2013.
- [63] H. A. Ghramh, E. H. Ibrahim, and Z. Ahmad, “Antimicrobial, immunomodulatory and cytotoxic activities of green synthesized nanoparticles from *Acacia* honey and *Calotropis procera*,” *Saudi Journal of Biological Sciences*, vol. 28, no. 6, pp. 3367–3373, 2021.
- [64] R. Farooq, S. Majid, A. Hanif, A. Ashraf, and A. Khan, “Different types of honey and their properties,” *Therapeutic Applications of Honey and its Phytochemicals*, Springer, New York, NY, USA, 2020.
- [65] A. Rouamba, M. Compaoré, and M. Kiendrebeogo, “Molecular targets of honey bee’s products in cancer prevention and treatment,” *Journal of Herbmed Pharmacology*, vol. 8, no. 4, pp. 261–268, 2019.
- [66] X. Qiu, C. A. Janson, W. W. Smith et al., “Crystal structure of *Staphylococcus aureus* tyrosyl-tRNA synthetase in complex with a class of potent and specific inhibitors,” *Protein Science*, vol. 10, pp. 2008–2016, 2001.
- [67] I. M. M. Othman, M. A. M. Gad-Elkareem, H. A. Radwan et al., “Synthesis, structure-activity relationship and in silico studies of novel pyrazolothiazole and thiazolopyridine derivatives as prospective antimicrobial and anticancer agents,” *ChemistrySelect*, vol. 6, no. 31, pp. 7860–7872, 2021.
- [68] B. D. Bax, P. F. Chan, D. S. Eggleston et al., “Type IIa topoisomerase inhibition by a new class of antibacterial agents,” *Nature*, vol. 466, no. 7309, pp. 935–940, 2010.
- [69] C. Borelli, E. Ruge, J. H. Lee et al., “X-ray structures of Sap1 and Sap5: structural comparison of the secreted aspartic proteinases from *Candida albicans*,” *Proteins*, vol. 72, no. 4, pp. 1308–1319, 2008.
- [70] J. P. Declercq, C. Evrard, A. Clippe, D. V. Stricht, A. Bernard, and B. Knoops, “Crystal structure of human peroxiredoxin 5, a novel type of mammalian peroxiredoxin at 1.5 Å resolution,” *Journal of Molecular Biology*, vol. 311, no. 4, pp. 751–759, 2001.
- [71] A. A. Marusiak, N. L. Stephenson, H. Baik et al., “Recurrent *Mlk4* loss-of-function mutations suppress *jnk* signaling to promote colon tumorigenesis,” *Cancer Research*, vol. 76, no. 3, pp. 724–735, 2016.
- [72] R. S. Williams, R. Green, and J. N. Glover, “Crystal structure of the BRCT repeat region from the breast cancer-associated protein BRCA1,” *Nature Structural Biology*, vol. 8, no. 10, pp. 838–842, 2001.
- [73] J. A. D. Good, F. Wang, O. Rath et al., “Optimized S-trityl-L-cysteine-based inhibitors of kinesin spindle protein with potent in vivo antitumor activity in lung cancer xenograft models,” *Journal of Medicinal Chemistry*, vol. 56, no. 5, pp. 1878–1893, 2013.
- [74] R. Badraoui, M. Saeed, N. Bouali et al., “Expression profiling of selected immune genes and trabecular microarchitecture in breast cancer skeletal metastases model: effect of α -tocopherol acetate supplementation,” *Calcified Tissue International*, vol. 110, no. 4, pp. 475–488, 2022.
- [75] R. Badraoui, M. Saoudi, W. S. Hamadou et al., “Antiviral effects of artemisinin and its derivatives against SARS-CoV-2 main protease: computational evidences and interactions with ACE2 allelic variants,” *Pharmaceuticals*, vol. 15, no. 2, p. 129, 2022.

Research Article

Cytotoxic Activity, Cell Cycle Inhibition, and Apoptosis-Inducing Potential of *Athyrium hohenackerianum* (Lady Fern) with Its Phytochemical Profiling

Abdelbaset Mohamed Elsbali ^{1,2}, Waleed Abu Al-Soud ³, Ziad H. Al-Oanzi ³,
Husam Qanash ^{4,5}, Bandar Alharbi ⁴, Naif K. Binsaleh ⁴, Mousa Alreshidi ^{5,6},
Mitesh Patel ⁷ and Mohd Adnan ⁶

¹Clinical Laboratory Science, College of Applied Sciences-Qurayyat, Jouf University, Sakaka, Saudi Arabia

²Department of Pathology, Faculty of Medicine, University of Benghazi, Benghazi, Libya

³Department of Clinical Laboratory Sciences, College of Applied Medical Sciences, Jouf University, Sakaka, Saudi Arabia

⁴Department of Medical Laboratory Science, College of Applied Medical Sciences, University of Ha'il, Ha'il 55476, Saudi Arabia

⁵Molecular Diagnostics and Personalized Therapeutics Unit, University of Hail, Ha'il 55476, Saudi Arabia

⁶Department of Biology, College of Science, University of Hail, Ha'il 2440, Saudi Arabia

⁷Department of Biotechnology, Parul Institute of Applied Sciences and Centre of Research for Development, Parul University, Vadodara 391760, Gujarat, India

Correspondence should be addressed to Abdelbaset Mohamed Elsbali; aelasbali@ju.edu.sa and Mohd Adnan; drmohdadnan@gmail.com

Received 14 March 2022; Revised 10 April 2022; Accepted 12 May 2022; Published 2 June 2022

Academic Editor: Mohammed El-Maghd

Copyright © 2022 Abdelbaset Mohamed Elsbali et al. This is an open access article distributed under the Creative Commons Attribution License, which permits unrestricted use, distribution, and reproduction in any medium, provided the original work is properly cited.

In the present study, we investigated the cytotoxic effects of *Athyrium hohenackerianum* ethanolic extract (AHEE) on the proliferation of breast, lung, and colon cancer cells. The AHEE was tested for its effect on the progression of the cell cycle, followed by induction of apoptosis determination by flow cytometry. Real-time qRT-PCR was also utilized to observe the initiation of apoptosis. In addition, GC-MS was performed in order to identify the active phytochemicals present in the AHEE. A cytotoxic activity with an IC_{50} value of 123.90 $\mu\text{g}/\text{mL}$ against HCT-116 colon cancer cells was exhibited by AHEE. Following propidium iodide staining, annexin-V/PI, and clonogenic assays, AHEE treatment results in cell arrest in the S phase, causing an increase in the early and late phases of apoptosis and displaying antiproliferative potential, respectively. The morphological alterations were further monitored using acridine orange/ethidium bromide (AO/EB) staining. When compared with the control cells, features of apoptotic cell death, including nuclear fragmentation, in the AHEE-treated cells were noticed. The apoptosis was also confirmed by detecting the increased expression of *p53* and caspase-3 along with the downregulation of *Bcl-2*. GC-MS analysis revealed that trans-linalool oxide, loliolide, phytol, 4,8,12,16-tetramethylheptadecan-4-olide, and gamma-sitosterol were the major phytochemical constituents. Based on these findings, it can be suggested that AHEE causes cellular death via apoptosis, which should be further explored for the identification of active compounds responsible for these observed effects. Therefore, AHEE can be used in the pharmaceutical development of anticancer agents for cancer therapeutics.

1. Introduction

Around the globe, cancer-related deaths are increasing as the incidence of cancer continues to rise [1]. As per the World Health Organization (WHO), colorectal cancer, lung cancer, and breast cancer are the three most frequently diagnosed cancers globally and remain the foremost reason of cancer-

related deaths throughout the world [2]. Conventional cancer treatments are still the most common form of treatment, despite being mainly unsuccessful and causing many deaths due to side effects. In contrast, developing new cancer treatments derived from natural sources with fewer side effects has become an exciting field of research [3]. Plants are regarded as a potential repository of novel

chemical compounds for cancer research [4]. Many well-known anticancer compounds such as paclitaxel and camptothecin have been reported from plants [5]. India, a biogeographically different region, provides a remarkably rich source of different medicinal plants with anticancer properties [6].

Athyrium Roth, commonly known as the lady fern, is one of the cosmopolitan genera in the Athyriaceae family, containing about 300 species distributed around the world. The plants are terrestrial or epilithic, with erect or ascending rhizomes. In diverse areas of the globe, different species of *Athyrium* are used as traditional medicine. There is a tradition that *A. filix-femina* (L.) Roth is utilized with honey for cough treatment in Italy, Province of Salerno, Campania region [7], and its decoction has been used for antiparasitic and antihelminthic purposes [8, 9]. Rhizomes are also used as antiparasitic and antihelminthic agents in Iran as well [10]. *A. pectinatum* (Wall. ex Mett.) T. Moore was used by the Rajasthan Bhils (Indian tribe) as an antihelminthic [11, 12]. Fresh leaf juice of *A. asperum* (Blume) Milde was used as an antihelminthic as well as a carminative in the Mymensingh district of Bangladesh [13]. In Madhya Pradesh (India), *A. falcatum* Bedd. has been used as an antihelminthic [14]. In South India, its roots and fronds were utilized in traditional medicine by the people of the Palani Hills (Western Ghats). As an example, young fronds were consumed as a treatment for cancer and roots were consumed as an antihelminthic [15]. During childbirth, the roots of *A. lanceum* T. Moore are used to relieve pain, particularly breast pain. Besides enhancing milk flow, it is also effective on sores when applied topically [15]. Furthermore, it is used in Malaysia to treat ascariasis, burns, and intestinal fever [16], as well as burns and scalds. The *Athyrium* plant is used to treat sores in New Guinea [17]. In traditional Chinese medicine, *A. multidentatum* has been used as a tranquilizer, antihypertensive, and diuretic [18–20].

A. hohenackerianum T. Moore is native to India and Sri Lanka (Figure 1). In India, it is found in different states such as Goa, Gujarat, Jharkhand, Himachal Pradesh, Karnataka, Kerala, Maharashtra, Madhya Pradesh, Odisha, Rajasthan, and Tamil Nadu. In India, the rhizome and fronds of *A. hohenackerianum* are used as a decoction for rheumatic pain and as an antihelminthic. The rhizome paste is also used against scorpion stings [21]. To our knowledge, there are no reports regarding any biological activity or phytochemistry of *A. hohenackerianum*. Thus, this study is the initial and first report documenting the anticancer potential and phytoconstituents analysis of *A. hohenackerianum* grown in India.

2. Materials and Methods

2.1. Collection of Plant Material and Extraction. The collection of *A. hohenackerianum* whole plants was carried out in the South Gujarat region of Gujarat state, India, in September 2020. The voucher specimen (BVBRC042) was deposited at Bapalal Vaidya Botanical Garden, Department of Biosciences, Veer Narmad South Gujarat University, Surat, Gujarat, India. The collected plant material was washed with tap water, and then, deionized water was used

to rinse. Thereafter, it was dried under shade at room temperature for 7 days. Upon drying, the samples were ground into powder and were then passed through a sieve that had a mesh size of 20 (sieve size 0.85 mm). 25 g powder of the whole plant of *A. hohenackerianum* was macerated in 85% ethanol in an electric shaker at the room temperature for 6 h. After filtering through Whatman filter paper No. 1, the extract solution was evaporated in a water bath at 60°C for 2 h. A total of 3.40 g of the extract was recovered, which was brown in color, solid in appearance, and bristle in texture.

2.2. Cytotoxicity by MTT Assay. The AHEE was tested against human lung (A549), breast (MCF-7), and colon (HCT-116) cancer cells. The National Centre for Cell Science (NCCS), Pune, India, provided cell lines for use in this study. Cancer cell lines were cultured in flasks (25 cm²) with 10% fetal bovine serum (FBS) (MP Biomedicals, Germany) in Dulbecco's Modified Eagle's Medium (DMEM) (MP Biomedicals, Germany) and 10,000 U/mL penicillin and 5 mg/mL streptomycin antibiotic solution (Hi-Media, India) at 37°C in a humidified atmosphere with 5% CO₂. Upon reaching 80% confluence, the cells were seeded at a density of greater than 1 × 10⁵ cells per well in 96-well plates and incubated in the same conditions as above. Trypan Blue (Hi-Media, India) (0.4%) was used to stain the cells, and a hemocytometer was used to determine the viability. Afterward, cells were treated with AHEE at different concentrations (1.56–200 µg/mL) for 48 h. The plate was removed from the incubator, and the media containing AHEE was aspirated. Then, 200 µL of medium containing 10% MTT reagent (MP Biomedicals, Germany) was added to each well to get a final concentration of 0.5 mg/mL, and the plates were incubated for a further 3 h at 37°C in a humidified atmosphere with 5% CO₂. This was then followed by the removal of the medium and the addition of 100 µL DMSO (Merck, Germany) to dissolve the formazan crystals. Using the ELISA reader (EL10 A, Biobase, China), the absorbance of the amount of formazan crystal was measured at 570 nm and 630 nm. The percentage growth inhibition was calculated after subtracting the background and the blank, and the concentration of the test drug needed to inhibit cell growth by 50% (IC₅₀) was calculated from the dose-response curve for the respective cell line. As a positive control, cisplatin was used [22].

2.3. Cell Cycle Analysis. The flow cytometer was used to evaluate the cell cycle using propidium iodide (PI) staining. In a six-well culture plate, HCT-116 cells were plated at 5 × 10⁴ cells per 2 mL and incubated in a CO₂ incubator for 24 h at 37°C. After incubation, the spent medium was aspirated and washed with 1 mL of 1X PBS. Cells were treated with AHEE (IC₅₀) concentration in 2 mL of the culture medium and further incubated for 24 h. One well was left blank as untreated, which was considered as a negative control. The floating and attached cells were collected and washed with chilled PBS. Following permeabilization, the cells were fixed for 1 h at 4°C in ice cold 70% ethanol. A staining solution (50 µg/mL PI and 20 µg/mL RNase A in

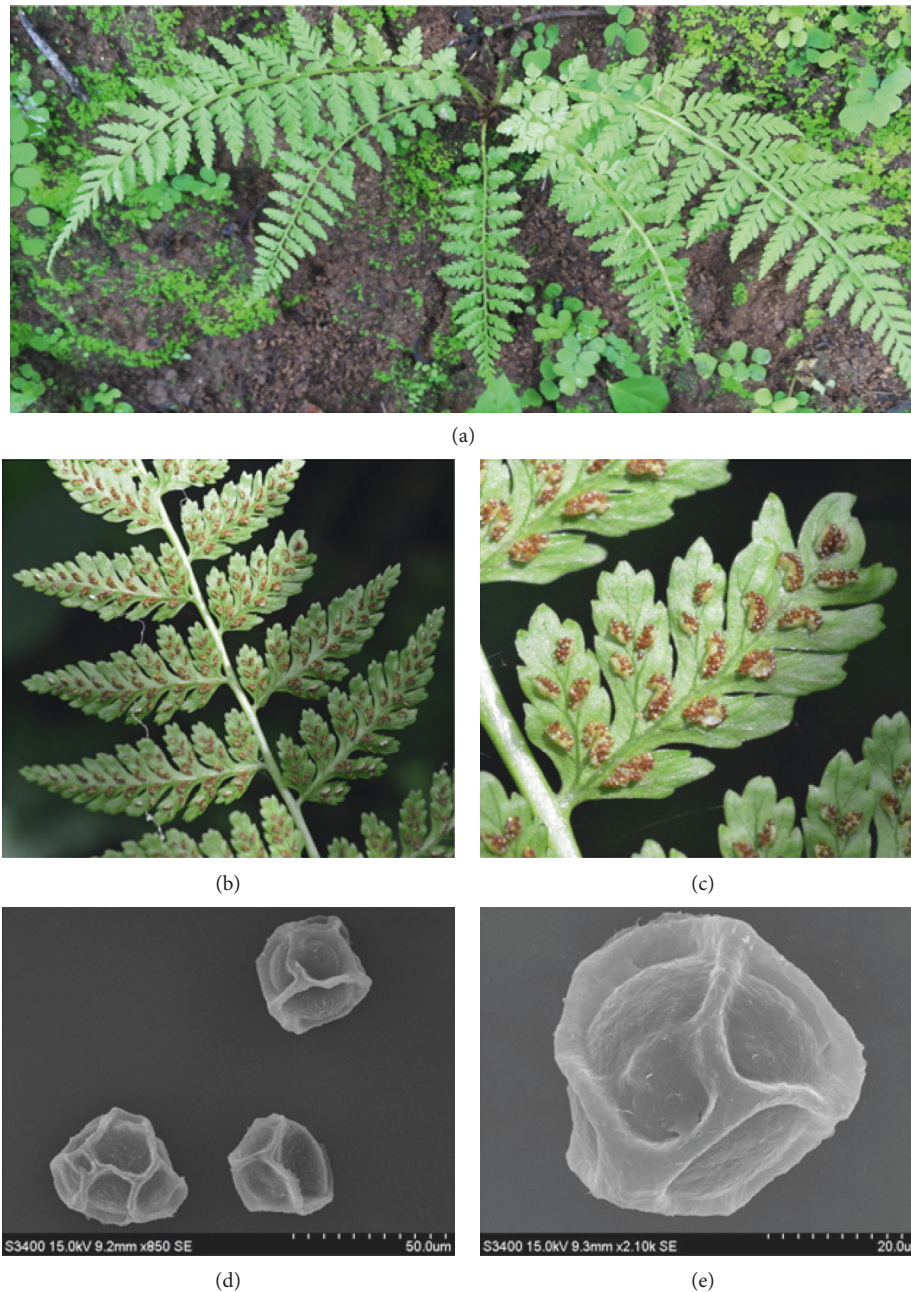


FIGURE 1: *A. hohenackerianum*. (a) Habit, (b) abaxial side of pinnae showing the distribution of sori, (c) close view of sori, (d) and (e) structure of spores under the scanning electron microscope (SEM).

PBS) was then added to the cells for 15 min at 37°C. Samples were mixed well and analyzed with the Cytomics FC500 Flow cytometer, Beckman Coulter, USA [23].

2.4. Fluorescent Double Staining with Acridine Orange/Ethidium Bromide (AO/EB). The cells were plated at a density of 3×10^5 cells/2 mL in 6-well plates and incubated at 37°C for 24 h in a CO₂ incubator. After aspirating the spent medium, 1 mL of PBS was added. The cells were treated with AHEE (IC₅₀) and further incubated for 24 h. For the second time, the medium was removed after incubation and washed in cold

PBS. After that, the cells were suspended in 500 μL of AO/EB staining solution (10 μL of acridine orange (2 mg/mL) and 10 μL of ethidium bromide (2 mg/mL) in 1 mL of PBS), mixed thoroughly, and then incubated for 5 min. In the end, cells were washed with PBS bovine serum albumin three times, and images were taken immediately under a fluorescent microscope (XDFL series, Sunny Instruments, China) [24].

2.5. Colony Formation Assay. In order to determine the antineoplastic effects on *in vitro* cell proliferation, the clonogenic assay was performed as described previously with

minor modifications [25]. In brief, the cells were cultured for 24 h in T-25 tissue culture flasks and exposed to AHEE (IC₅₀) for 24 h. Afterward, trypsinization was performed on the cells; the cells were counted and seeded into a 6-well plate (200 cells/2 mL medium per well) and cultured for 8 days. Methanol was used to fix the colonies. Crystal violet (0.4 g/L) was used to stain the colonies, which were photographed, analyzed, and counted using ImageJ (v1.48) software. The formula for calculating the surviving cell fraction was

$$\text{plating efficiency (PE)} = \frac{\text{no. of cells plated}}{\text{no. of colonies counted}} \times 100,$$

$$\text{surviving fraction (SF)} = \frac{\text{PE of treated sample}}{\text{PE of control sample}}. \quad (1)$$

2.6. Annexin-V Apoptosis Assay. A 6-well plate was seeded with HCT-116 cells at a density of 3×10^5 cells/2 mL and incubated in a CO₂ incubator at 37°C for 24 h. After removal of the spent medium, 1 mL of PBS was added. The cells were treated with AHEE (IC₅₀) in 2 mL of the culture medium and incubated for 12–16 h. An untreated well served as a negative control. At the end of incubation, the medium was removed from all the wells and transferred into 5 mL centrifuge tubes, which were then washed with 500 μ L PBS. PBS was removed from the sample, and 200 μ L of trypsin-EDTA solution was added and incubated for 3–4 min at 37°C. Afterward, the culture medium was transferred into the respective wells again and cells were harvested into the centrifuge tubes. The tubes were then centrifuged for 5 min at $300 \times g$ at 25°C. The supernatant was then removed and washed twice with PBS. The PBS was completely removed, and cells were resuspended in 1X binding buffer at a concentration of 1×10^6 cells/mL. Following this, 100 μ L of the solution (1×10^5 cells) was transferred to a 5 mL culture tube and 5 μ L of AbFlour 488 Annexin V was added. The cells were gently vortexed and incubated for 15 min at 25°C in the dark. At the end, 2 μ L of PI and 400 μ L of 1X binding buffer were added to each tube and vortexed gently. Analyses of the samples were carried out by flow cytometry immediately after the addition of PI [26].

2.7. Gene Expression Analysis. Tri-Pure Isolation Reagent (Sigma-Aldrich®, India, 11667157001) was used to isolate the cellular RNA according to the manufacturer's instructions, and it was quantified with a nanodrop UV spectrophotometric analyzer (P 300, IMPLLEN, USA). The RT-first strand synthesis kit (Qiagen, CA, USA, 330401) was used to reverse transcribe 1 μ g of isolated RNA. SYBR green qRT-PCR (Applied Biosystems® 7500 Fast Real-Time PCR machine, CA, USA) was used to measure the gene expression levels relative to control. The $2^{-\Delta\Delta C_t}$ method was used for the analysis, with values expressed as fold changes over the control value. Each primer pair (Table 1) was used separately. The following conditions were used to determine the relative gene expression: reverse transcription was

TABLE 1: List of forward and reverse primers for apoptosis regulatory genes.

Primer	Sequence	Reference
<i>p53</i> '	Forward- 5'AGAGTCTATAGGCCACCC3'	[27]
	Reverse- 5'GCTCGCACGCTAGGATCTGAC3'	
<i>Bcl-2</i>	Forward- 5'TTCGATCAGGAAGGCTAGAGTT3'	[27]
	Reverse- 5'TCGGTCTCCTAAAAGCAGGC3'	
Caspase-3	Forward- 5'TGCGTCTGCTCTGCCTTCT3'	[27]
	Reverse- 5'CCATGGGTAGCAGCTCCTTC3'	
GAPDH'	Forward- 5'CATGGGGAAGGTGAAGGTCGA3'	[27]
	Reverse- 5'TTGGCTCCCCCTGCAAATGAG3'	

performed at 45°C for 45 minutes as a starting point, initial denaturation at 95°C with 10 min hold, followed by 40 cycles of 95°C for 15 sec, and 60°C for 60 sec [28].

2.8. GC-MS Analysis of *A. hohenackerianum* Crude Extract. Shimadzu Nexis GC-2030 equipped with a QP2020 NX mass spectrometer was used for the GC-MS analysis of AHEE. Helium was used as a carrier gas, which flowed at a rate of 1 mL/min. The GC-MS spectral detection method was based on electron ionization energy ionized at 70 eV, a scanning time of 0.2 s, and fragment masses in the range of 40 to 600 m/z. A volume of 1 μ L and a temperature of 250°C were used for injection. Initially, a temperature of 50°C was set for 3 min in the column oven, then increased by 10°C per min to 280°C, and finally was set to 300°C for 10 min. A comparison of the phytochemicals present in the test samples with a library of authentic compounds maintained by the National Institute of Standards and Technology (NIST) revealed the presence of these compounds based on their mass spectral patterns, retention time (min), peak, area, and height [29].

2.9. Statistical Analysis. All experiments were carried out in triplicate. Results are presented as the mean \pm SD of the number of experiments performed. The significance of the results was determined among the treatments using one-way ANOVA followed by Tukey's post hoc test and Student's *t*-test at $p < 0.05$. The analyses were carried out using GraphPad Prism 5.0 software.

3. Results

3.1. Cytotoxic Activity of *A. hohenackerianum* Crude Extract. To determine the cytotoxic activity, various concentrations of AHEE (1.56–200 μ g/mL) were applied to A549, MCF-7, and HCT-116 cancer cells and then the IC₅₀ values were determined. A dose-response inhibition curve was used to determine the values after 48 hours. Figure 2 illustrates the dose-response curve of exposure of cancer cell lines to the

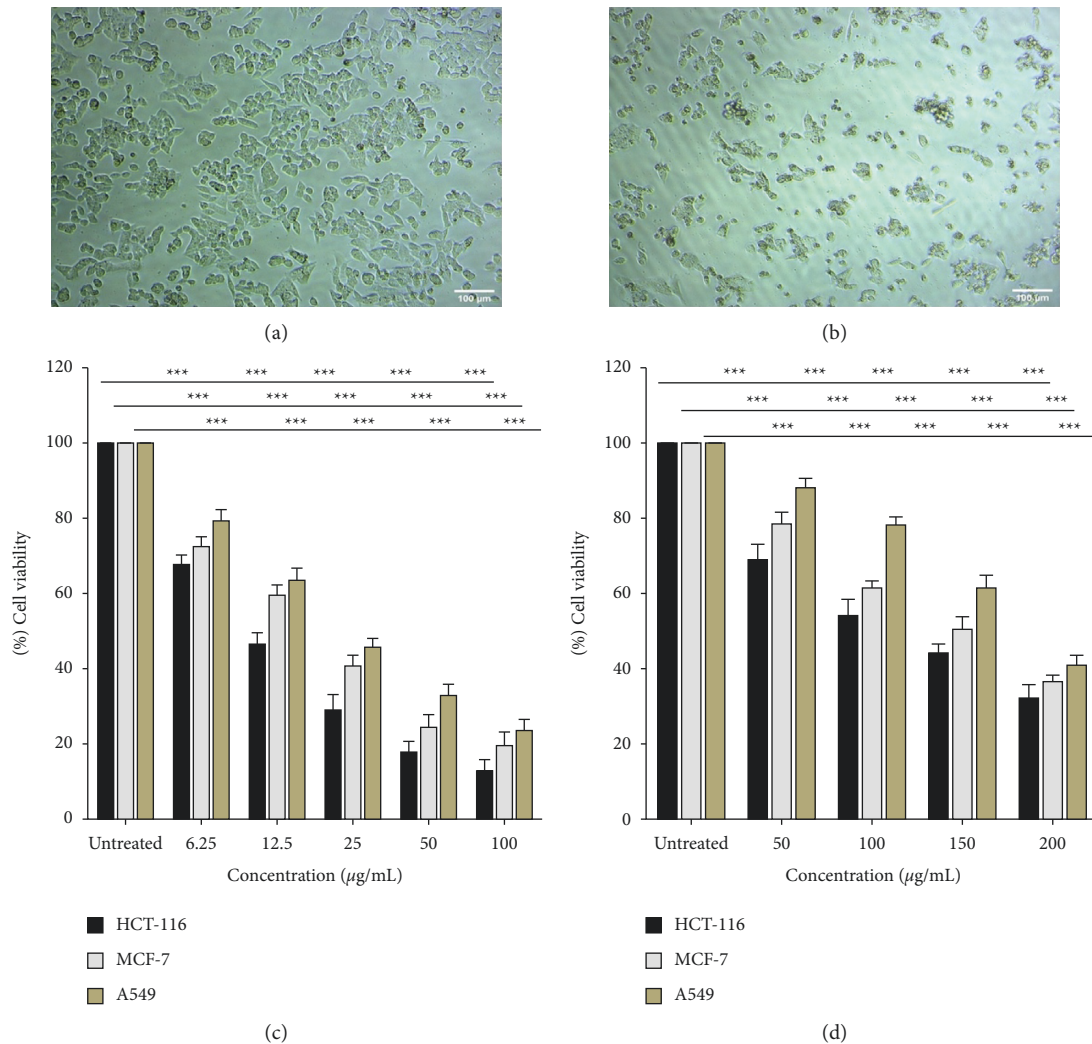


FIGURE 2: Cytotoxic activity of AHEE and standard cisplatin drug against various human cancer cell lines (A549, MCF-7, and HCT-116). (a) Untreated HCT-116 cells. (b) Treated HCT-116 cells with AHEE. (c) Cytotoxicity of cisplatin against A549, MCF-7, and HCT-116. (d) Cytotoxicity of AHEE against A549, MCF-7, and HCT-116. Error bars indicate the SD (standard deviation) of three independent experiments. Significance: ns > 0.05, * $p < 0.05$, ** $p < 0.01$, and *** $p < 0.001$.

crude extract. All tested cell lines were sensitive to the crude extract, among which the most sensitive cells were HCT-116 colon cancer cells ($IC_{50} = 123.90 \mu\text{g/mL}$), more sensitive than MCF-7 breast cancer cells ($IC_{50} = 149.92 \mu\text{g/mL}$) and lung cancer cells ($IC_{50} = 179.74 \mu\text{g/mL}$). Therefore, the remaining assays were conducted on the HCT-116 cells. Cisplatin also showed dose-dependent inhibition of HCT-116 colon cancer cells ($IC_{50} = 25.95 \mu\text{g/mL}$), MCF-7 breast cancer cells ($IC_{50} = 36.33 \mu\text{g/mL}$), and lung cancer cells ($IC_{50} = 43.54 \mu\text{g/mL}$).

3.2. S Phase Cell Accumulation. A flow cytometry assay was conducted to determine how AHEE affected the cell cycle of HCT-116 cells. An increase was observed in the percentage of cells that are in the S phase (40.30 ± 1.35) of the cell cycle in the cells treated with IC_{50} of AHEE with a decline in the percentage of cells in G₀/G₁ (33.50 ± 1.19) and G₂/M (19.80 ± 1.50) phases in comparison with the untreated

control cells. This suggests that the treated cells are arrested in the S phase of the cell cycle (Figure 3).

3.3. Morphological Changes in HCT-116 Cells. To explore the morphological alterations caused by AHEE, HCT-116 cells were monitored using AO/EB staining. As compared with the control cells, the features of apoptotic cell death, including nuclear fragmentation, in the AHEE-treated cells were noticed (Figure 4). These results elucidated that the inhibition of AHEE on HCT-116 cell growth is linked with its induction of apoptosis.

3.4. Antiproliferative Potential of AHEE. The AHEE was examined for its effect on colony-forming ability in HCT-116 cells. Using AHEE, clonogenic assays were conducted to test the differences between untreated and treated cells in terms of reproductive viability. The colonies formed after 8 days were compared between cancer cells seeded with and

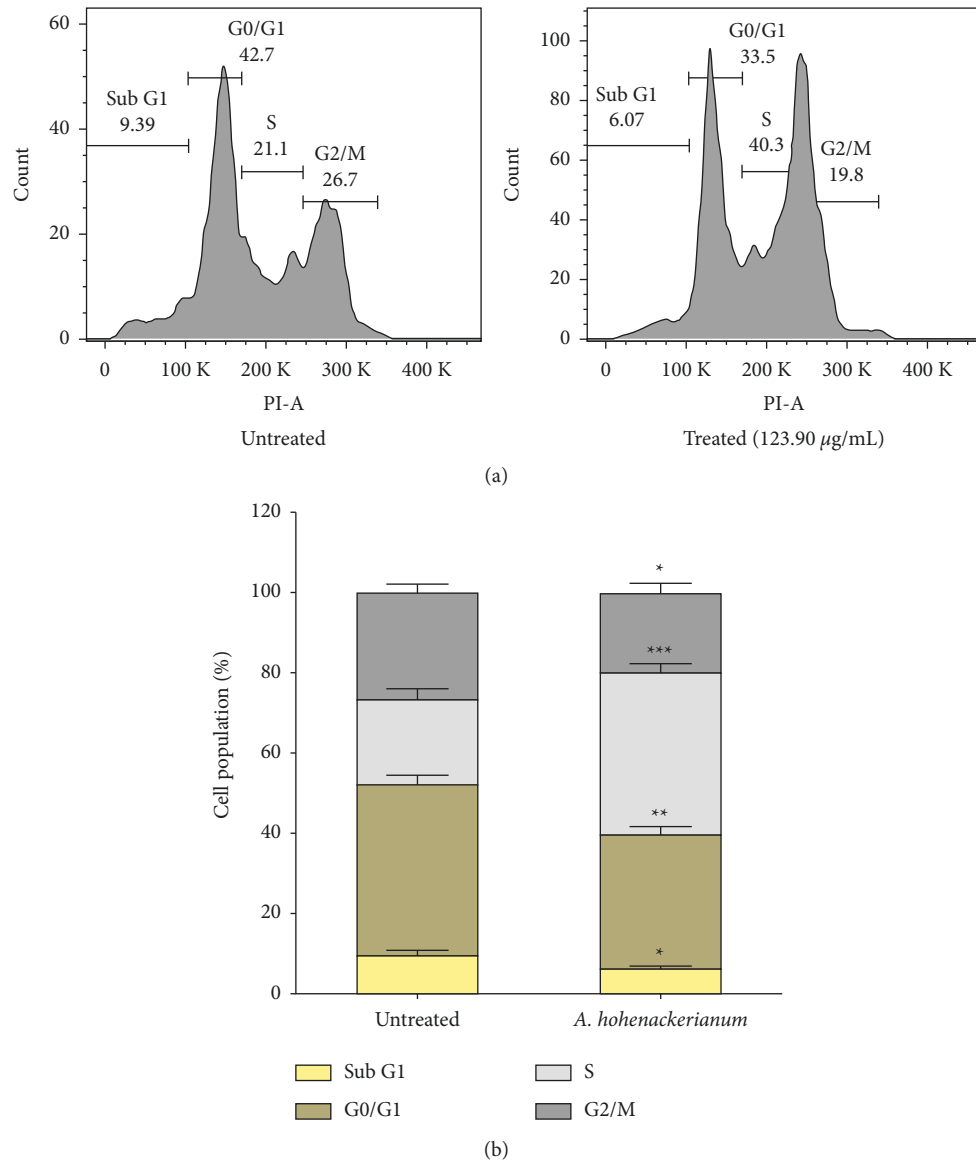


FIGURE 3: Cell cycle phase distribution in control and treated HCT-116 cells. (a) HCT-116 cell cycle phase distribution of control and after being treated with an IC_{50} concentration of AHEE when analyzed using flow cytometry. (b) Bar graph of the average percentage of cells in different phases of the cell cycle in each treatment and control group. Error bars indicate the SD (standard deviation) of three independent experiments. Significance: * $p < 0.05$, ** $p < 0.01$, and *** $p < 0.001$.

without AHEE. A significant reduction in the number of colonies was observed in AHEE (Figure 5).

3.5. Quantification of Apoptotic Cell Death of AHEE-Treated Cells. The apoptosis induction by AHEE on HCT-116 cells was further confirmed using the Annexin-V and propidium iodide staining methods. The results of this experiment are shown in Figure 6. After treatment with IC_{50} , there was a significant increase from $0.51 \pm 0.30\%$ to $9.52 \pm 0.92\%$ and $2.80 \pm 0.38\%$ to $22.3 \pm 1.23\%$ of early and late apoptotic/necrotic cells, respectively.

3.6. Expression of Genes Related to Apoptosis. Real-time PCR was used to detect the expression level of the apoptotic genes

p53, *Bcl-2*, and caspase-3 in HCT-116 cells treated with AHEE. Compared to untreated cells, expression levels of caspase-3 and *p53* were significantly increased, whereas the expression levels of *Bcl-2* were significantly decreased in AHEE-treated cells (Figure 7).

3.7. Identification of *A. hohenackerianum* Compounds by GC-MS. The AHEE was analyzed by GC-MS, and different classes of compounds were identified (Table 2). Among the main constituents are butanoic acid, 2,4,6-trimethyloctane, trans-linalool oxide, hexadecane, 1,10-decanediol, loliolide, n-hexadecanoic acid, n-nonadecanol-1, heneicosanoic acid-methyl ester, 10-nonadecanone, phytol, octacosanol, propanoic acid, 2-(benzoylamino)-3-phenyl-m, methyl (Z)-5,11,14,17-

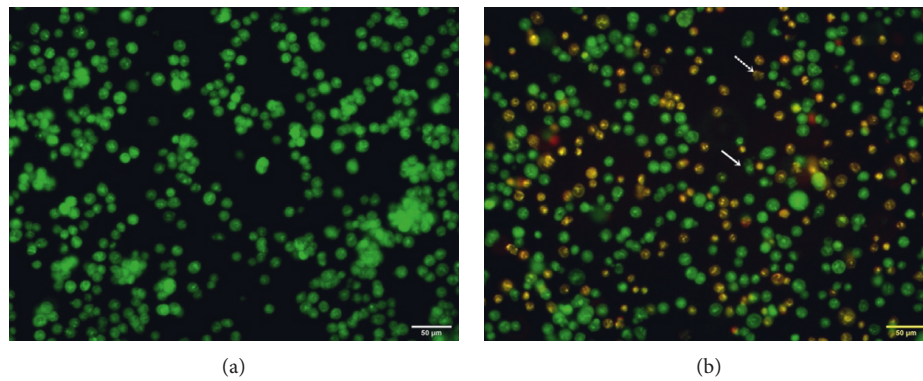


FIGURE 4: Dual acridine orange/ethidium bromide staining of HCT-116 cells. (a) Control: untreated cells. (b) Cells treated with an IC_{50} concentration of AHEE. The solid arrow indicates early apoptotic cells, and the dashed arrow indicates late apoptotic cells. The images were taken with a fluorescence microscope at 40x. Live cells are exclusively green, whereas apoptotic cells appear with orange or yellowish-orange nuclei.

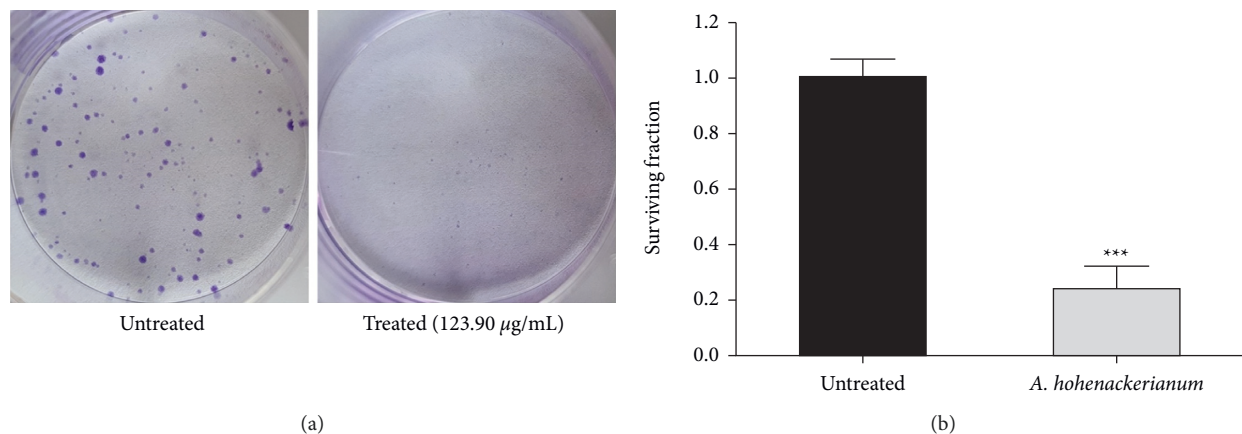


FIGURE 5: Clonogenic assay (crystal violet staining) in HCT-116 cells exposed to the IC_{50} concentration of AHEE. (a) Treatment well represents a decrease in the number and size of colonies in comparison to the untreated well and was observed at 10x. (b) A bar graph representing the surviving fraction of HCT-116 cells in the absence and presence of AHEE. Error bars indicate the SD (standard deviation) of three independent experiments. Significance: *** $p < 0.001$.

eicosatetraenoate, 4,8,12,16-tetramethylheptadecan-4-olide, gamma-sitosterol, hexadecanoic acid-2-hydroxy-1-(hydroxymethyl), octadecanoic acid, 2,3-dihydroxypropyl ester, and androsta-1,4-diene-3,17-dione (Figure 8).

4. Discussion

Medicinal plants have been the known source of medicines for the treatment of various ailments since ancient times. People around the globe have implemented the usage of botanicals for millennia. Although angiosperms and other higher plants have been extensively studied for their medicinal and economic value, ferns and fern-allies have been completely overlooked. There is a strong emphasis on its use in Ayurvedic (Sushruta, Charka, and Samhita), Unani, Homeopathic, and other systems of medicine. People use them in the treatment of different kinds of illnesses like burns, colds, ascarid diseases, bleeding due to trauma, and diarrhea [30]. Preliminary screening on different sorts of bioactivities of traditional medicinal ferns has been reported

[31–36]. However, no in-depth studies on any biological activities of these plants exist.

A. hohenackerianum contains a wide array of phytochemical constituents, making it one of the most valuable medicinal plants [37]. In this study, *A. hohenackerianum* was extracted using ethanol to obtain the largest amount of bioactive phytochemicals. Based on the results of this study, we found that the ethanolic extract of *A. hohenackerianum* conferred high cytotoxic activity on a variety of cancer cells, with good efficacy against human colon cancer cells HCT-116. In addition, we showed that the ethanolic extract of *A. hohenackerianum* arrests the cell cycle at the S phase and specifically induces apoptosis. This fact has been supported by numerous experiments, including labeling with Annexin V-/PI and activation of apoptosis signaling molecules. This study's findings are consistent with a prior study that found other species of *Athyrium* extracts have antiproliferative agents against several cancer cells. It has been reported that *A. multidentatum* shows cytotoxic activity against hepatocellular carcinoma (HepG2 cells) with IC_{50} values of 220 $\mu\text{g}/$

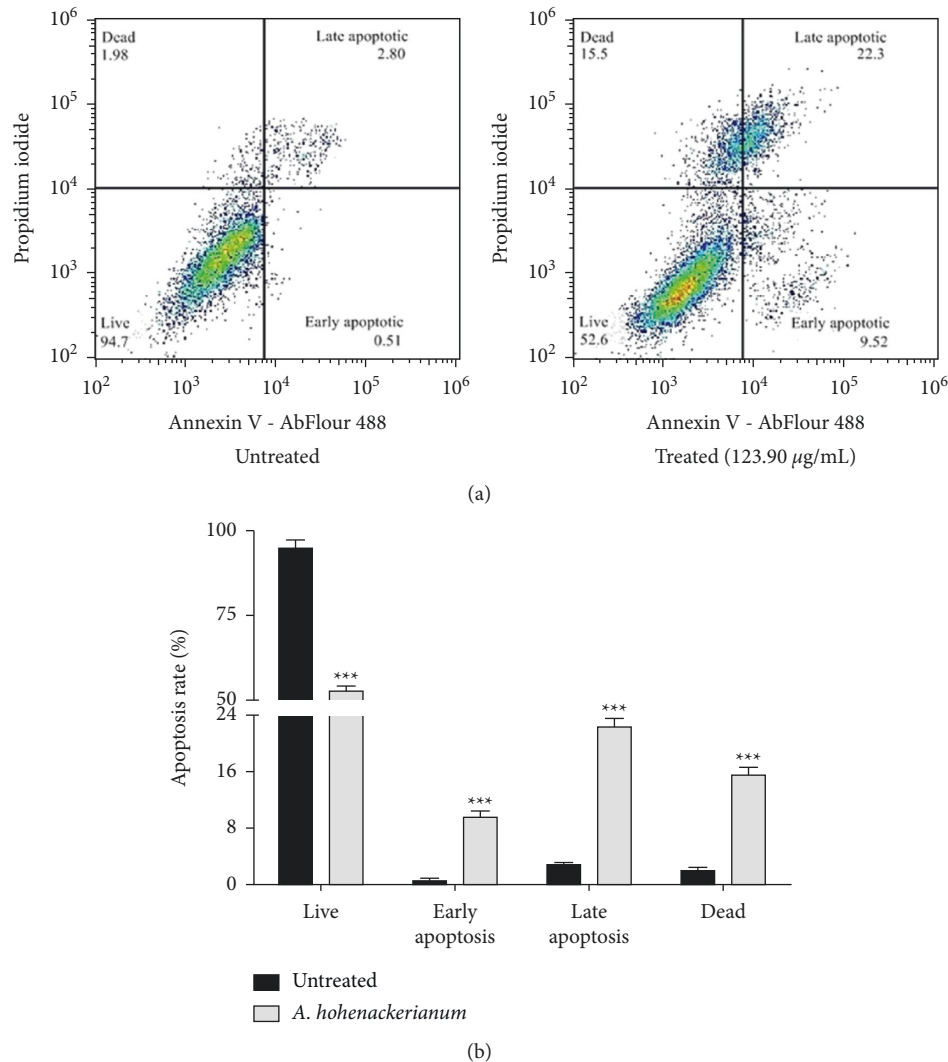


FIGURE 6: Annexin-V/PI apoptosis assay of treated HCT-116 cells. (a) Distribution of HCT-116 cells without treatment and treatment with IC₅₀ concentration of AHEE. (b) A bar graph of cell distribution in control and treated HCT-116 cells, analyzed using flow cytometry. Error bars indicate the SD (standard deviation) of three independent experiments. Significance: *** $p < 0.001$.

mL and 114 µg/mL after 24 h and 48 h, respectively [38]. It was also reported that *A. multidentatum* crude extract causes cytotoxicity in HL-7702 liver cells with IC₅₀ values of 332 µg/mL and 304 µg/mL after 24 h and 48 h, respectively [39]. The butenolide derivative Striatisorolide A of *A. multidentatum* exhibits potent cytotoxic activity against human lung cancer cells (A549) with an IC₅₀ of 7.75 µg/mL [39].

To investigate the mechanisms involved in the growth inhibition of HCT-116 cells treated with *A. hohenackerianum*, the cell cycle distribution was analyzed. In the present study, it was found that cells treated with *A. hohenackerianum* accumulated at the S phase of cells, and therefore, this suggests that HCT-116 cells undergo apoptosis since accumulation of cells at this phase is considered a biomarker for DNA damage as well as an indicator of cell death by apoptosis [40]. As part of the confirmation of apoptosis induction, the Annexin-V/PI apoptosis detection assay was used, which is widely used to distinguish both early and late stages of apoptosis [41]. The apoptotic cell death

mode of *A. hohenackerianum* was confirmed by a shift toward early and late apoptotic cell populations, suggesting the extract exerted an apoptotic effect. The dual staining of Annexin-V/PI and the cells accumulated in the S phase, as well as the morphological changes that occurred during the cell death evident with AO/EB after treatment with *A. hohenackerianum* crude extract, strongly indicate that the cells are undergoing apoptosis. It is well known that intact plasma membrane integrity can be used as a major indicator of apoptotic cells morphologically [42, 43]. In contrast to apoptosis, necrosis is characterized by a loss of integrity in the cell membrane [42]. The dual AO/EB fluorescent staining method is convenient for detecting changes in cell membranes caused by apoptosis. The AO binds to DNA in intact cells and emits green fluorescence. In damaged cells, EB penetrates the membrane and binds to the DNA and fluorescence of orange-red is emitted [44]. Therefore, AO allows the staining of apoptotic cells as well as live cells, and EB permits the staining of both necrotic and late apoptotic cells.

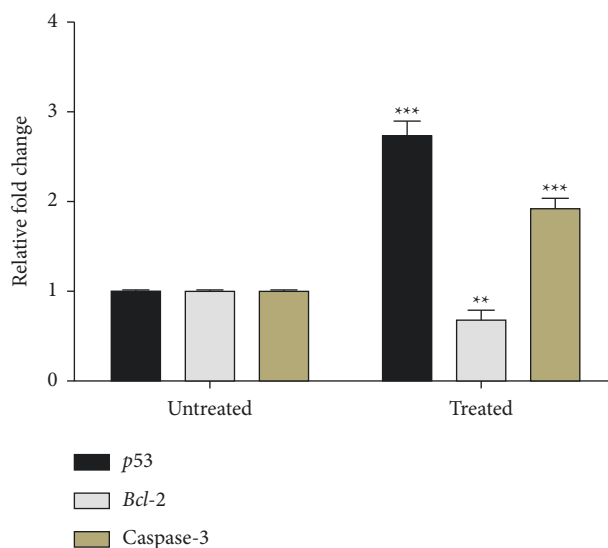


FIGURE 7: Gene expression levels in HCT-116 cells treated with the IC₅₀ concentration of AHEE. The expression level of apoptosis-related genes was determined via quantitative real-time PCR. *GAPDH* was used as an internal control. Error bars indicate the SD (standard deviation) of three independent experiments. Significance: ** $p < 0.01$ and *** $p < 0.001$.

TABLE 2: Identified phytocompounds from the AHEE via GC-MS.

Compound name	Class	Chemical formula	Molecular weight (g/mol)	RT (min)	Area (%)
Butanoic acid	Fatty ester	C ₄ H ₈ O ₂	88.11	2.848	0.22
2,4,6-Trimethyloctane	Fatty acyl	C ₁₁ H ₂₄	156.31	5.781	0.27
trans-Linalool oxide	Terpene alcohol	C ₁₀ H ₁₈ O ₂	170.25	8.870	0.17
Hexadecane	Fatty acyl	C ₁₆ H ₃₄	226.41	8.935	0.24
1,10-Decanediol	Fatty alcohol	C ₁₀ H ₂₂ O ₂	174.28	9.949	0.26
Loliolide	Monoterpene alkaloid	C ₁₁ H ₁₆ O ₃	196.24	11.127	0.95
<i>n</i> -Hexadecanoic acid	Fatty acid	C ₁₆ H ₃₂ O ₂	256.42	12.143	3.26
<i>n</i> -Nonadecanol-1	Fatty alcohol	C ₁₉ H ₄₀ O	284.5	12.329	0.35
Heneicosanoic acid, methyl ester	Fatty acid	C ₂₂ H ₄₄ O ₂	340.6	12.476	0.07
10-Nonadecanone	Fatty acyl	C ₁₉ H ₃₈ O	282.5	12.732	0.17
Phytol	Diterpene alcohol	C ₂₀ H ₄₀ O	296.5	12.900	2.04
Octacosanol	Fatty alcohol	C ₂₈ H ₅₈ O	410.76	13.269	0.13
Propanoic acid, 2-(benzoylamino)-3-phenyl-, m	Fatty acid	C ₂₃ H ₂₁ NO ₃	359.4	13.727	1.03
Methyl (Z)-5,11,14,17-eicosatetraenoate	Fatty acid	C ₂₁ H ₃₄ O ₂	318.5	13.877	0.10
4,8,12,16-Tetramethylheptadecan-4-olide	Terpenoid	C ₂₁ H ₄₀ O ₂	324.5	14.021	0.88
Gamma-sitosterol	Phytosterol	C ₂₉ H ₅₂ O ₂	432.7	14.247	4.17
Hexadecanoic acid, 2-hydroxy-1-(hydroxymethyl)	Glycerolipid	C ₁₉ H ₃₈ O ₄	330.5	14.845	2.43
Octadecanoic acid, 2,3-dihydroxypropyl ester	Fatty acid	C ₂₁ H ₄₂ O ₄	358.55	16.293	1.25
Androsta-1,4-diene-3,17-dione	Steroid	C ₁₉ H ₂₄ O ₂	284.39	16.432	0.20

Furthermore, we also performed a more prolonged clonogenic survival test and found that *A. hohenackerianum* inhibited the survival of HCT-116 cells for a longer period of time. As a result, it should be noted that the crude extract of *A. hohenackerianum* has the potential to be used as a treatment or management for colon cancer, since targeting a cell population that is clonogenic/tumor-initiating/stemlike is believed to be essential for success with cancer therapy.

The apoptotic process is regulated by genes such as *p53*, caspase-3, and *Bcl-2* [45]. A qRT-PCR technique was used to analyze the expression of these apoptotic genes to support the

results from the flow cytometry. Compared to the control, treatment with the extracts significantly lowered the anti-apoptotic *Bcl-2* gene and significantly increased the apoptotic *Bax* and caspase-3 genes, indicating that *A. hohenackerianum* acts through caspase-dependent apoptotic pathways. It has been reported that a similar event occurred in many studies in which natural product extracts increased the expression of these genes in different human cancer cells, thus causing them to undergo apoptosis [46–49]. Overall, our study confirms that *A. hohenackerianum* induces apoptosis in HCT-116 cancer cells.

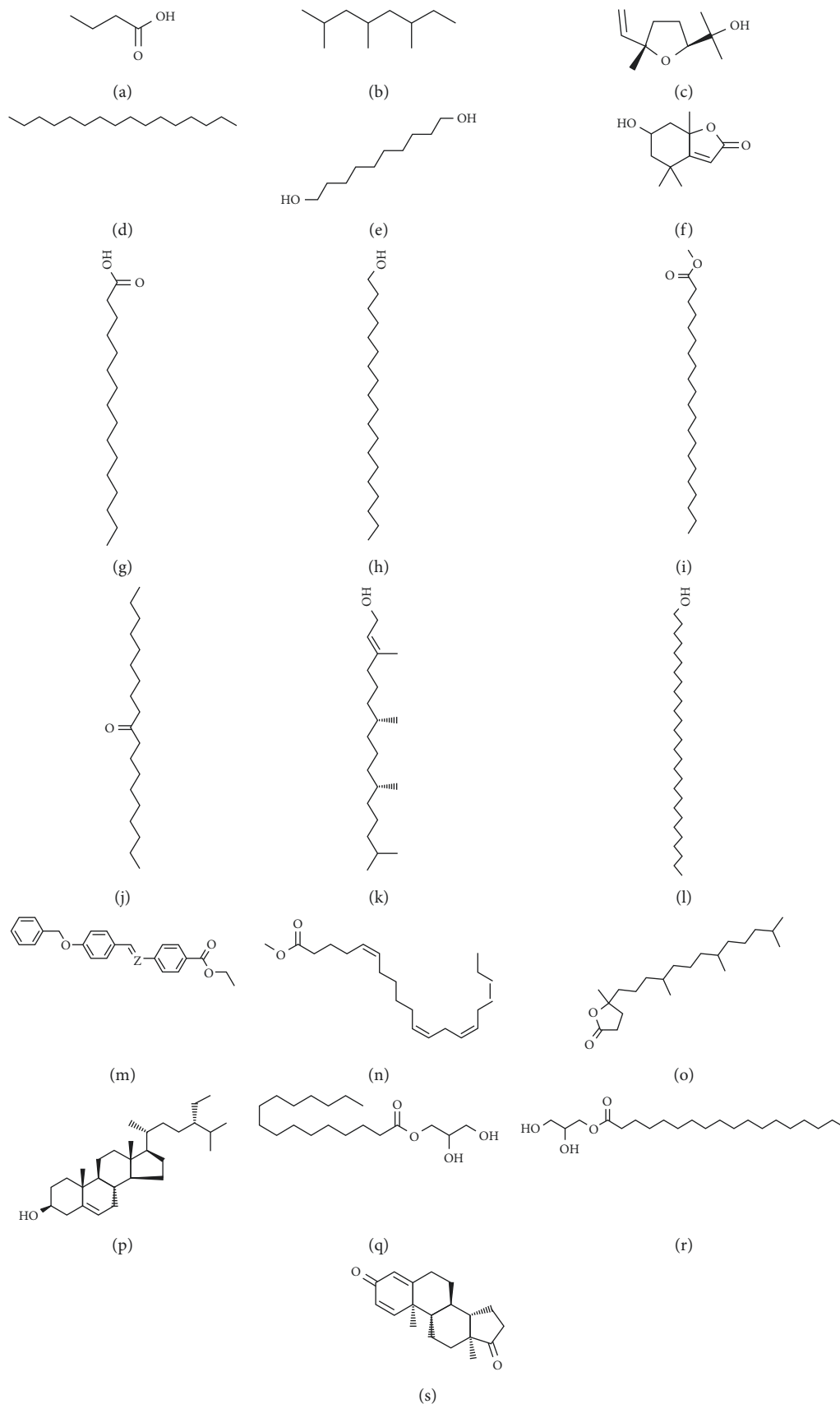


FIGURE 8: Chemical structures of the identified compounds in AHEE via GC-MS analysis. (a) Butanoic acid, (b) 2,4,6-trimethyloctane, (c) trans-linalool oxide, (d) hexadecane, (e) 1,10-decanediol, (f) lolilide, (g) n-hexadecanoic acid, (h) n-nonadecanol-1, (i) heneicosanoic acid-methyl ester, (j) 10-nonadecanone, (k) phytol, (l) octacosanol, (m) propanoic acid, 2-(benzoylamino)-3-phenyl-m, (n) methyl (Z)-5,11,14,17-eicosatetraenoate, (o) 4,8,12,16-tetramethylheptadecan-4-olide, (p) gamma-sitosterol, (q) hexadecanoic acid-2-hydroxy-1-(hydroxymethyl), (r) octadecanoic acid, 2,3-dihydroxypropyl ester, and (s) androsta-1,4-diene-3,17-dione.

The medicinal properties of plant extracts are largely due to the secondary products that act in synergism rather than as a single compound [50–52]. GC/MS is a useful and dependable method for identifying complex plant extracts in an efficient and timely manner [53]. This study identified different classes of phytochemical constituents of *A. hohenackerianum* as having an inhibitory effect on colorectal cancer cells' growth [54], suggesting that these compounds may play a role in the observed activity against HCT-116 colon cancer cells. The natural compound butyric acid is found in food. The anticancer activity of butyric acid has been reported against acute myeloid leukemia, Lewis lung carcinoma cells, and colorectal carcinoma cells [55]. Linalool showed the strongest activity against a broad range of cancers, such as carcinoma of the cervix, stomach, skin, lung, and bone with IC_{50} ranging from 82.3 to 113.6 $\mu\text{g}/\text{mL}$ [56]. Phytol is a substance found in chlorophyll and has been shown to be cytoprotective against oxidative stress. The anticancer and immune-enhancing properties of phytol are well-documented. By regulating macrophage function, phytol not only enhances natural killer cells that remove cancer cells but also strengthens immunity. There is evidence that phytol has an anticancer effect against breast, prostate, cervical, colorectal, lung, and skin cancers, with IC_{50} values ranging from 15.51 to 69.67 μM [57]. Gamma-sitosterol is a compound that belongs to the stigmastanes and derivatives family of organic compounds. It has also anticancer effects against several types of cancer including, breast, lung, hepatocellular, and colorectal cancer [58]. Therefore, it can be concluded that the anticancer effects seen in the extract could be due to the presence of these compounds.

5. Conclusion

The ethanolic extract of *A. hohenackerianum* inhibited the proliferation of various cancer cells. In particular, we demonstrated that the *A. hohenackerianum* extract inhibits the growth of HCT-116 colon cancer cells by apoptosis by inducing cell arrest in the S phase and causing dose-dependent rises in early and late apoptotic cell populations. Moreover, upregulation of apoptosis gene markers in HCT-116 cells confirmed the initiation of apoptosis by *A. hohenackerianum*. Based on preliminary findings, *A. hohenackerianum* has the potential to be a new natural source of anticancer compound(s) that can trigger apoptotic cell death. However, despite the numerous advantages, toxicity concerns are always present with the variety of plants and can be unsafe for the sensitive populations. Therefore, *in vivo* toxicological assessment is a mandatory requirement and must be done prior to the drug development, which is a limitation in this study. Furthermore, certain assays such as migration assay, angiogenesis assay, and protein expression by Western blotting can also be performed to confirm the efficacy of *A. hohenackerianum* and identify the possible cellular and molecular mechanisms involved in the anticancer activity.

Data Availability

All data generated or analyzed during this study are included in this article.

Conflicts of Interest

The authors declare that they have no conflicts of interest.

Authors' Contributions

Abdelbaset Mohamed Elsbali was responsible for conceptualization, original draft preparation, data curation, investigation, and methodology. Waleed Abu Al-Soud involved in data analysis, validation, and visualization. Ziad H. Al-Oanzi participated in formal analysis, investigation, and validation. Husam Qanash and Alharbi Bandar performed formal analysis, investigation, and validation. Naif K Binsaleh took part in data curation, validation, review, and editing. Mousa Alreshidi was responsible for data curation, validation, review, and editing. Mitesh Patel performed methodology, review, and editing. Mohd. Adnan contributed to conceptualization, data analysis, validation, project administration, review, and editing.

Acknowledgments

The authors extend their appreciation to the Deputyship for Research and Innovation, Ministry of Education in Saudi Arabia for funding this work through grant no. 1172659343. The authors would like to extend their sincere appreciation to the Central Laboratory at Jouf University for supporting this study.

References

- [1] F. Bray, J. Ferlay, I. Soerjomataram, R. L. Siegel, L. A. Torre, and A. Jemal, "Global cancer statistics 2018: GLOBOCAN estimates of incidence and mortality worldwide for 36 cancers in 185 countries," *CA: A Cancer Journal for Clinicians*, vol. 68, no. 6, pp. 394–424, 2018.
- [2] H. Sung, J. Ferlay, R. L. Siegel et al., "Global Cancer Statistics 2020: GLOBOCAN Estimates of Incidence and Mortality Worldwide for 36 Cancers in 185 Countries," *CA: A Cancer Journal for Clinicians*, vol. 71, no. 3, pp. 209–249, 2021.
- [3] Q. Y. Zhang, F. X. Wang, K. K. Jia, and L. D. Kong, "Natural Product Interventions for Chemotherapy and Radiotherapy-Induced Side Effects," *Frontiers in pharmacology*, vol. 9, p. 1253, 2018.
- [4] J. Iqbal, B. A. Abbasi, T. Mahmood et al., "Plant-derived anticancer agents: a green anticancer approach," *Asian Pacific Journal of Tropical Biomedicine*, vol. 7, no. 12, pp. 1129–1150, 2017.
- [5] A. G. Desai, G. N. Qazi, R. K. Ganju et al., "Medicinal plants and cancer chemoprevention," *Current Drug Metabolism*, vol. 9, no. 7, pp. 581–591, 2008.
- [6] D. Al-Eisawi and S. Al-Ruzayza, "The flora of holy Mecca district, Saudi Arabia," *International Journal of Biodiversity and Conservation*, vol. 7, pp. 173–189, 2015.
- [7] R. Di Novella, N. Di Novella, L. De Martino, E. Mancini, and V. De Feo, "Traditional plant use in the national park of cilento and vallo di Diano, Campania, southern, Italy,"

- Journal of Ethnopharmacology*, vol. 145, no. 1, pp. 328–342, 2013.
- [8] M. Eskandari, B. Riazi, S. Shirzadian, and A. Mazooji, “A study of threatened species of ferns in Gilan province (N Iran) providing a comparison of protective classification of conservation based on IUCN’s factors,” *Rostaniha*, vol. 13, pp. 1–9, 2012.
 - [9] V. A. Mozaffarian, *Identification of Medicinal and Aromatic Plants of Iran*, FarhangeMoaser Press, Tehran, Iran, 2012.
 - [10] M. B. Bahadori, F. M. Kordi, A. A. Ahmadi, S. Bahadori, and H. Valizadeh, “Antibacterial evaluation and preliminary phytochemical screening of selected ferns from Iran,” *Research Journal of Pharmacognosy*, vol. 2, pp. 53–59, 2015.
 - [11] P. Parihar and L. Parihar, “Some pteridophytes of medicinal importance from Rajasthan,” *Natural Product Radiance*, vol. 5, pp. 297–301, 2006.
 - [12] M. S. Vyas and B. D. Sharma, *Today and Tomorrow*, Sprinters and Publishers, Daryaganj, India, 1988.
 - [13] S. K. Sarker and A. B. M. E. Hossain, “Pteridophytes of greater mymensingh district of Bangladesh used as vegetables and medicines,” *Bangladesh Journal of Plant Taxonomy*, vol. 16, pp. 47–56, 2009.
 - [14] B. P. Singh and R. Upadhyay, “Medicinal pteridophytes of Madhya Pradesh,” *Journal of medicinal plants studies*, vol. 2, pp. 65–68, 2014.
 - [15] G. Sathiyaraj, T. Muthukumar, and K. C. Ravindran, “Ethno medicinal importance of fern and fern- allies traditionally used by tribal people of Palani Hills (Kodaikanal), Western Ghats, South India,” *The Journal of Medicinal Herbs and Ethnomedicine*, vol. 1, pp. 4–9, 2015.
 - [16] D. Corrigan, “Medicinal Plants in Folk Tradition—an Ethnobotany of Britain and Ireland By David E. Allen and Gabrielle Hatfield (Natural History Museum, London, and the Royal Botanic Gardens, Kew). Timber Press, Portland, OR. 2004. 431 pp. $9^{1/4} \times 6^{1/4}$ in. \$29.95. ISBN 0-88192-638-8,” *Journal of Natural Products*, vol. 67, no. 12, p. 2154, 2004.
 - [17] J. M. Powell, “Ethnobotany,” *New Guinea Vegetation*, Australian National University Press, Canberra, 1976.
 - [18] Y. Liu, W. Wujisguleng, and C. Long, “Food uses of ferns in China: a review,” *Acta Societatis Botanicorum Poloniae*, vol. 81, no. 4, pp. 263–270, 2012.
 - [19] G. Qi, L. Yang, C. Xiao, J. Shi, Y. Mi, and X. Liu, “Nutrient values and bioactivities of the extracts from three fern species in China: a comparative assessment,” *Food & Function*, vol. 6, no. 9, pp. 2918–2929, 2015.
 - [20] J. W. Sheng, D. M. Liu, Z. J. Li, L. Qi, and W. F. Zhang, “Bioactivity-guided fractionation for antioxidant property of *Athyrium multidentatum* (Doll) Ching. rhizome,” *Journal of Medicinal Plants Research*, vol. 5, pp. 7000–7005, 2011.
 - [21] S. D. Shaikh, V. P. Masal, and A. S. Shaikh, “Ethnomedicinal uses of some pteridophytes from Konkan region of Maharashtra, India,” *International Journal of Pharmaceutical and Chemical Sciences*, vol. 3, pp. 62–65, 2014.
 - [22] M. Adnan, A. J. Siddiqui, W. S. Hamadou et al., “Deciphering the Molecular Mechanism Responsible for Efficiently Inhibiting Metastasis of Human Non-Small Cell Lung and Colorectal Cancer Cells Targeting the Matrix Metalloproteinases by *Selaginella repanda*,” *Plants*, vol. 10, p. 979, 2021.
 - [23] P. Pozarowski and Z. Darzynkiewicz, “Analysis of cell cycle by flow cytometry,” *Methods in Molecular Biology*, vol. 281, pp. 301–311, 2004.
 - [24] R. Shakeri, J. Khorshidi, T. Radjabian, A. Lashkari, and M. Safavi, “Cytotoxic and Antioxidant Activities of *Crocus pallasii* subsp. *haussknechtii* Corms Extracts Compared with *Crocus sativus*,” *Research Journal Pharmacognosy*, vol. 6, pp. 51–59, 2019.
 - [25] N. A. P. Franken, H. M. Rodermond, J. Stap, J. Haveman, and C. van Bree, “Clonogenic assay of cells in vitro,” *Nature Protocols*, vol. 1, no. 5, pp. 2315–2319, 2006.
 - [26] I. Vermes, C. Haanen, and H. Steffens-Nakken, “A novel assay for apoptosis Flow cytometric detection of phosphatidylserine expression on early apoptotic cells using fluorescein labelled Annexin V,” *Journal of Immunological Methods*, vol. 184, no. 1, pp. 39–51, 1995.
 - [27] M. Behbahani, “Evaluation of in vitro anticancer activity of *Ocimum basilicum*, *Alhagi maurorum*, *Calendula officinalis* and their parasite *Cuscuta campestris*,” *PLoS One*, vol. 9, no. 12, Article ID e116049, 2014.
 - [28] N. Abutaha, F. A. Nasr, M. Al-zharani et al., “Effects of hexane root extract of *ferula hermonis* boiss. on human breast and colon cancer cells: an in vitro and in vivo study,” *BioMed Research International*, vol. 2019, Article ID 3079895, 2019.
 - [29] M. Adnan, A. J. Siddiqui, W. S. Hamadou et al., “Functional and structural characterization of pediococcus pentosaceus-derived biosurfactant and its biomedical potential against bacterial adhesion, quorum sensing, and biofilm formation,” *Antibiotics*, vol. 10, no. 11, p. 1371, 2021.
 - [30] A. Benjamin and V. S. Manickam, “Medicinal pteridophytes from the Western Ghats,” *Natural Product Reports*, vol. 6, pp. 611–618, 2007.
 - [31] M. Singh, N. Singh, P. B. Khare, and A. K. S. Rawat, “Antimicrobial activity of some important *Adiantum* species used traditionally in indigenous systems of medicine,” *Journal of Ethnopharmacology*, vol. 115, no. 2, pp. 327–329, 2008.
 - [32] S. L. Shin and C. H. Lee, “Antioxidant effects of the methanol extracts obtained from aerial part and rhizomes of ferns native to Korea,” *Korean Journal of Polar Research*, vol. 23, pp. 38–46, 2010.
 - [33] A. R. McCutcheon, T. E. Roberts, E. Gibbons et al., “Antiviral screening of British Columbian medicinal plants,” *Journal of Ethnopharmacology*, vol. 49, no. 2, pp. 101–110, 1995.
 - [34] C. Punzón, A. Alcaide, and M. Fresno, “In vitro anti-inflammatory activity of *Phlebodium decumanum*. Modulation of tumor necrosis factor and soluble TNF receptors,” *International Immunopharmacology*, vol. 3, no. 9, pp. 1293–1299, 2003.
 - [35] Y. Mizushima, I. Watanabe, H. Togashi et al., “An Ergosterol Peroxide, a natural product that selectively enhances the inhibitory effect of linoleic acid on DNA polymerase .BETA,” *Biological and Pharmaceutical Bulletin*, vol. 21, no. 5, pp. 444–448, 1998.
 - [36] M. Konoshima, H. Chi, and K. Hata, “Coumarins from the root of *Angelica gigas* NAKAI,” *Chemical and Pharmaceutical Bulletin*, vol. 16, no. 6, pp. 1139–1140, 1968.
 - [37] J. Sheng and Y. Sun, “Antioxidant properties of different molecular weight polysaccharides from *Athyrium multidentatum* (Doll.) Ching,” *Carbohydrate Polymers*, vol. 108, pp. 41–45, 2014.
 - [38] G. Qi, Z. Liu, R. Fan et al., “*Athyrium multidentatum* (Doll.) Ching extract induce apoptosis via mitochondrial dysfunction and oxidative stress in HepG2 cells,” *Scientific Reports*, vol. 7, p. 2275, 2017.
 - [39] D. M. Liu, J. W. Sheng, S. H. Wang, W. F. Zhang, W. Zhang, and D. J. Zhang, “Cytoproliferative and cytoprotective effects of *Striatosporolide A* isolated from Rhizomes of *Athyrium multidentatum* (Doell.) ching on human umbilical vein endothelial cells,” *Molecules*, vol. 21, no. 10, p. 1280, 2016.

- [40] C. Riccardi and I. Nicoletti, "Analysis of apoptosis by propidium iodide staining and flow cytometry," *Nature Protocols*, vol. 1, no. 3, pp. 1458–1461, 2006.
- [41] A. P. Demchenko, "Beyond annexin V: fluorescence response of cellular membranes to apoptosis," *Cytotechnology*, vol. 65, no. 2, pp. 157–172, 2013.
- [42] I. Vermes, C. Haanen, and C. Reutelingsperger, "Flow cytometry of apoptotic cell death," *Journal of Immunological Methods*, vol. 243, no. 1-2, pp. 167–190, 2000.
- [43] Y. Zhang, X. Chen, C. Gueydan, and J. Han, "Plasma membrane changes during programmed cell deaths," *Cell Research*, vol. 28, no. 1, pp. 9–21, 2018.
- [44] K. Liu, P. C. Liu, R. Liu, and X. Wu, "Dual AO/EB staining to detect apoptosis in osteosarcoma cells compared with flow cytometry," *Medical science monitor basic research*, vol. 21, pp. 15–20, 2015.
- [45] Y. Kiraz, A. Adan, M. Kartal Yandim, and Y. Baran, "Major apoptotic mechanisms and genes involved in apoptosis," *Tumor Biology*, vol. 37, no. 7, pp. 8471–8486, 2016.
- [46] E. Chamani, Z. Rezaei, K. Dastjerdi, S. Javanshir, K. Khorsandi, and G. A. Mohammadi, "Evaluation of some genes and proteins involved in apoptosis on human chronic myeloid leukemia cells (K562 cells) by *datura innoxia* leaves aqueous extract," *Journal of Biomolecular Structure and Dynamics*, vol. 38, no. 16, pp. 4838–4849, 2020.
- [47] A. M. G. Zedan, M. I. Sakran, O. Bahattab et al., "Oriental Hornet (*Vespa orientalis*) larval extracts induce anti-proliferative, antioxidant, anti-inflammatory, and anti-migratory effects on MCF7 Cells," *Molecules*, vol. 26, no. 11, p. 3303, 2021.
- [48] G. H. Mansour, M. A. El-Magd, D. H. Mahfouz et al., "Bee venom and its active component Melittin synergistically potentiate the anticancer effect of Sorafenib against HepG2 cells," *Bioorganic Chemistry*, vol. 116, Article ID 105329, 2021.
- [49] N. M. Selim, A. A. Elgazar, N. M. Abdel-Hamid et al., "Chrysophanol, physcion, hesperidin and curcumin modulate the gene expression of pro-inflammatory mediators induced by LPS in HepG2: In silico and molecular studies," *Antioxidants*, vol. 8, no. 9, p. 371, 2019.
- [50] P. Jigna, N. Rathish, and C. Sumitra, "Preliminary screening of some folklore medicinal plants from western India for potential antimicrobial activity," *Indian Journal of Pharmacology*, vol. 37, pp. 408–409, 2005.
- [51] A. Badawy, H. Hassanean, A. K. Ibrahim, E. S. Habib, M. A. El-Magd, and S. A. Ahmed, "Isolates from *Thymelaea Hirsuta* inhibit progression of Hepatocellular Carcinoma *in vitro* and *in vivo*," *Natural Product Research*, vol. 35, no. 11, pp. 1799–1807, 2021.
- [52] A. A. A. Khamis, E. M. M. Ali, M. A. A. El-Moneim, M. M. Abd-Alhaseeb, M. A. El-Magd, and E. I. Salim, "Hesperidin, piperine and bee venom synergistically potentiate the anticancer effect of tamoxifen against breast cancer cells," *Biomedicine & pharmacotherapy*, vol. 105, pp. 1335–1343, 2018.
- [53] A. Iordache, M. Culea, C. Gherman, and O. Cozar, "Characterization of some plant extracts by GC-MS," *Nuclear Instruments and Methods in Physics Research Section B: Beam Interactions with Materials and Atom*, vol. 267, no. 2, pp. 338–342, 2009.
- [54] R. Sankaranarayanan, C. K. Valiveti, R. Dachineni, D. R. Kumar, T. Lick, and G. J. Bhat, "Aspirin metabolites 2,3-DHBA and 2,5-DHBA inhibit cancer cell growth: Implications in colorectal cancer prevention," *Molecular Medicine Reports*, vol. 21, pp. 20–34, 2020.
- [55] L. Pattayil and H. T. Balakrishnan-Saraswathi, "In vitro evaluation of apoptotic induction of butyric acid derivatives in colorectal carcinoma cells," *Anticancer Research*, vol. 39, no. 7, pp. 3795–3801, 2019.
- [56] G. P. P. Kamatou and A. M. Viljoen, "Linalool—A review of a biologically active compound of commercial importance," *Natural Product Communications*, vol. 3, no. 7, 2008.
- [57] B. Pejin, V. Kojic, and G. Bogdanovic, "An insight into the cytotoxic activity of phytol at in vitro conditions," *Natural Product Research*, vol. 28, no. 22, pp. 2053–2056, 2014.
- [58] S. Sundarraj, R. Thangam, V. Sreevani et al., " γ -Sitosterol from *Acacia nilotica* L. induces G2/M cell cycle arrest and apoptosis through c-Myc suppression in MCF-7 and A549 cells," *Journal of Ethnopharmacology*, vol. 141, no. 3, pp. 803–809, 2012.